CLEARY, MICHAEL TERENCE

THE EFFECT OF SUBSTITUTION AT THE 9 POSITION ON THE ELECTROCHEMICAL OXIDATION OF XANTHINE

The University of Oklahoma PH.D. 1980

PLEASE NOTE:

In all cases this material has been filmed in the best possible way from the available copy. Problems encountered with this document have been identified here with a check mark ✓.

1. Glossy photographs _____
2. Colored illustrations _____
3. Photographs with dark background _____
4. Illustrations are poor copy _____
5. Print shows through as there is text on both sides of page _____
6. Indistinct, broken or small print on several pages _____ throughout ✓
7. Tightly bound copy with print lost in spine _____
8. Computer printout pages with indistinct print _____
9. Page(s) _____ lacking when material received, and not available from school or author _____
10. Page(s) _____ seem to be missing in numbering only as text follows _____
11. Poor carbon copy _____
12. Not original copy, several pages with blurred type _____
13. Appendix pages are poor copy _____
14. Original copy with light type _____
15. Curling and wrinkled pages _____
16. Other _____

THE UNIVERSITY OF OKLAHOMA

GRADUATE COLLEGE

THE EFFECT OF SUBSTITUTION AT THE 9 POSITION ON THE ELECTROCHEMICAL OXIDATION OF XANTHINE

A DISSERTATION

SUBMITTED TO THE GRADUATE FACULTY

in partial fulfillment of the requirements for the

degree of

DOCTOR OF PHILOSOPHY

BY

MICHAEL TERENCE CLEARY

Norman, Oklahoma

1980

THE EFFECT OF SUBSTITUTION AT THE 9 POSITION ON THE ELECTRO-CHEMICAL OXIDATION OF XANTHINE

APPROVED BY

DISSERTATION COMMITTEE

ACKNOWLEDGEMENTS

The author wishes to express his gratitude to Dr. Glenn Dryhurst for convincing the author to pursue a Ph. D. degree. Dr. Dryhurst is also to be thanked for the guidance and many helpful suggestions he provided during this work.

Financial assistance in the form of research assistantships from Dr. Glenn Dryhurst and teaching assistantships from the Chemistry Department of the University of Oklahoma is acknowledged. Appreciation is also extended to Gulf Oil Corporation for further financial support through a one year fellowship.

It is impossible to adequately thank James L. Owens and Barbara M. Owens who patiently guided my early laboratory efforts in electrochemistry. Many helpful discussions with faculty members, post-doctoral fellows, and fellow graduate students are acknowledged. Special thanks are accorded Deniz Ege-Serpkenci, James L. Owens, Henry A. Marsh, Jr., Arnold C. Conway and Suleiman Sasa who made graduate study much easier by their friendship.

The ability and inspiration of my high school chemistry teacher, John Davik, provided my initial interest in chemistry. To him, I express my sincerest thanks.

I can never adequately thank my parents for all they

have done for me. I am most indebted to them for their love and understanding, and their encouragement given me in all my endeavors.

Most importantly, I would like to thank my wife, Jane. Without her understanding, love, patience, and encouragement this work would not been brought to completion.

TABLE OF CONTENTS

TABLE OF CONTENTS (continued)

LIST OF TABLES

LIST OF TABLES (continued)

LIST OF TABLES (continued)

LIST OF ILLUSTRATIONS

LIST OF ILLUSTRATIONS (continued)

LIST OF ILLUSTRATIONS (continued)

LIST OF ILLUSTRATIONS (continued)

LIST OF ILLUSTRATIONS (continued)

LIST OF ILLUSTRATIONS (continued)

LIST OF ILLUSTRATIONS (continued)

LIST OF ILLUSTRATIONS (continued)

LIST OF ILLUSTRATIONS (continued)

LIST OF ILLUSTRATIONS (continued)

LIST OF ILLUSTRATIONS (continued)

Figure Page

LIST OF ILLUSTRATIONS (continued)

LIST OF ILLUSTRATIONS (continued)

LIST OF ILLUSTRATIONS (continued)

LIST OF ILLUSTRATIONS (continued)

THE EFFECTS OF SUBSTITUTION AT THE 9 POSITION ON THE ELECTROCHEMICAL OXIDATION OF XANTHINE

PART I

LIQUID CHROMATOGRAPHIC SEPARATION OF ELECTROCHEMICAL OXIDATION PRODUCTS OF BIOLOGICALLY IMPORTANT PURINES

CHAPTER I

INTRODUCTION

Over the past several years work from this laboratory has been concerned with the electrochemical oxidation of biologically important purine derivatives and the relationship between the electrochemical reaction mechanisms and products and the biological reactions of these molecules. It has been shown that many purine derivatives give similiar electrochemical oxidation products[1,2]. A major difficulty in the electrochemical studies has been the separation and identification of these reaction products. Previous studies have employed thin-layer chromatography, polarography, and spectrophotometric methods for both qualitative and quantita-

tive analysis of reaction product mixtures. Many of these techniques applied to complex mixtures are subject to a variety of uncertainties and errors. Ongoing research in this laboratory is concerned with the electrochemical oxidation of nucleoside and nucleotide derivatives of purines where the complexity of the reaction product mixtures is such that the latter analytical techniques could not be utilized with any confidence.

Accordingly, it became necessary to develop a technique for separation of milligram quantities of relatively complex reaction mixtures such that sufficient pure product could be isolated for mass spectral, i. r., and other studies. In addition, a technique was required which could be used to provide quantitative information on the yields of these reaction products.

The simplest and most straightforward purine electro-oxidation is observed with uric acid[3], where at low pH alloxan, urea, and carbon dioxide are the major products, while at pH 2-7 allantoin, urea, and carbon dioxide are the major products. At some pH values parabanic acid is a minor product. In order to devise a suitable analytical technique for our purposes it was decided to attempt to develop a method which could separate all of the above organic materials simultaneously. In addition, oxaluric acid, which has also been observed in some purine electro-oxidations[4] and D-ribose, a likely product from purine

nucleoside electrooxidations, were also added to the mixture. Thus, a six component mixture composed of D-ribose, urea, alloxan, parabanic acid, allantoin, and oxaluric acid was thought to contain the basic structural functionalities of products which might be expected from other purine electro-oxidations. A technique which could satisfactorily separate and quantitate this mixture on a milligram sacle should provide a basic method for separation of other more complex reaction mixtures obtained from electrooxidations of purine nucleosides and nucleotiedes.

The technique which was developed for this separation is based on a combination of gel permeation, ion exchange, and adsorption column chromatography.

CHAPTER II

CHROMATOGRAPHIC THEORY

As mentioned in the introduction, a combination of gel permeation, adsorption, and ion-exchange chromatography was required to separate D-ribose, urea, alloxan, allantoin, parabanic acid, and oxaluric acid. A brief review of the basic theory of each of these chromatographic processes will be presented below.

Gel Permeation Chromatography

The following names all refer to essentially this same process: gel filtration, molecular sieve filtration, exclusion chromatography, and gel chromatography.

Basically, this method of separation employs a column packed with a porous separating medium. A solvent is continuously passed through the column. Usually as a solution in the same solvent that is flowing through the column, a small amount of material to be separated is introduced at the head of the column. In the work reported here a Sephadex G-10 packing was used which is a bead-formed, dextran gel. The G-10 term refers to a highly crosslinked polymer.

For this work, the most important chromatographic parameter is the retention volume. It can be expressed in the following manner:

$$V_R = V_M + KV_S$$

The mobile-phase volume (V_M) and the stationary-phase volume (V_S) are the void volume and total pore volume of the packing material, respectively.

K is the distribution constant and depends on the molecular weight of the sample and the pore size of the gel[5]. Molecules larger than the largest pores of the gel, i.e. above the exclusion limit, cannot penetrate the resin particles and have a K value equal to zero. Small molecules, however, penetrate the gel particles freely and have K values equal to one. Intermediate-size molecules have K values between zero and one and penetrate the resin particles to a varying extent. Molecules therefore are eluted from the gel matrix in order of decreasing molecular size. Three stages of a gel permeation separation are diagrammed in Figure 1 below.

At this time, the detailed separation mechanism is not clear, however various theories have been suggested to explain how molecular size determines the distribution constant. The two most important of these theories are those based on steric exclusion and restricted diffusion.

In the case of steric exclusion, the separation mechanism has been explained as follows: the pore size of

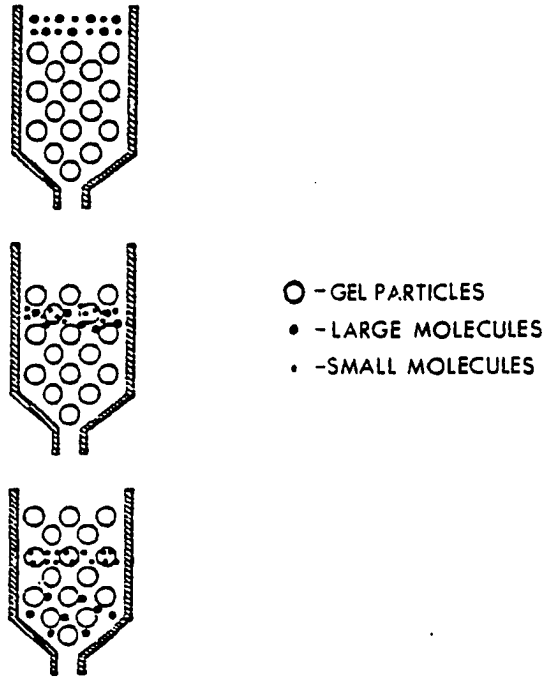

Figure 1. Three stages of a gel permeation separation.

some regions of the packing material are so small that the large molecules cannot diffuse into these regions. By considering the pore size distribution of the column, assigning to each pore size a specific size molecule and assuming that molecules can enter pores larger than their size but not smaller, one can derive a relation between elution volume and molecule shape[6].

The diffusion of the molecule is slowed down by steric hindering and by friction, according to the restricted diffusion theory. Small molecules, because of their higher diffusion coefficients, can diffuse into the pores of the packing material readily and spend more time in the stationary phase than large molecules; hence they have larger elution volumes[7]. However, under equilibrium conditions, it has been shown that the elution volume is insensitive to changes in the flow rate. In the case of nonequilibrium conditions, the differences between the diffusion rates of different-sized molecules have been shown to contribute to the separation[8].

The evidence now available suggests that steric exclusion is the most important separation mechanism. However, the diffusion effect must also play some role in the separation, particularly under nonequilibrium conditions.

Adsorption Chromatography

The molecular sieving properties of various resins have been exploited with enormous success by the use of the

simple gel filtration technique. The reliability of such work is limited in practice by the fact that nonsterical interactions often occur.

Departures from ideal behavior of molecular sieving can be either negative or positive, because non-steric exclusion and adsorption processes can cause a molecule to elute either earlier or later, respectively, than it would in their absence.

Ion exclusion or adsorption processes can be determined in a simple and qualitative manner. Any substance whose gel filtration behavior is solely determined by sterical selection processes must show an elution volume less than the total volume of solvent present in the column. A distribution constant greater than one is unequivocal evidence for the involvement of adsorption[9].

There are two recognized types of adsorption. Physical adsorption resembles phase transformation or mixing processes such as vaporization, melting, and dissolution. The energies involved are generally small, and adsorption and desorption are normally rapid. Van der Waals forces which hold nonionic molecules together in the liquid or solid state are responsible for physical absorption. In chemisorption there is a covalent or an ionic bond formed between adsorbing molecules and the adsorbent surface. The energy of chemisorption is similiar in magnitude to bond formation in a chemical reaction. Adsorption and desorption are frequently slow due to the appreciable

activation energy involved for adsorption. The adsorption energies for organic molecules may be relatively large, with partial electron transfer between adsorbate and adsorbent, yet actual bonding of adsorbate and adsorbent by means of conventional chemical bonds is absent. This phenomena has been defined as polar adsorption, which roughly characterizes such situations[10].

Ion-exchange Chromatography

Ion-exchange chromatography involves the substitution of one ionic species for another without significant change in the structure of the stationary matrix. This matrix, called the ion exchanger, is an insoluble material containing chemically bound charged groups and mobile counter ions.

When the matrix carries positive groups the counter ions will be negative. Such an exchanger is termed an anion exchanger because it will exchange negative ions. When the matrix carries negative groups the counter ions will be positive, and one calls it a cation exchanger. The presence of charged groups is the fundamental property of an ion-exchanger. The group type determines the strength and type of ion-exchanger; also the total number of groups and their accessibility determines the capacity.

In the work presented here, QAE-Sephadex A-25 and SP-Sephadex C-25 were employed. Sephadex ion exchangers are derived from neutral Sephadex G-25 by the introduction of

functional groups attached by ether linkages to the glucose units of the dextran chains. In the case of QAE-Sephadex A-25, the functional group is diethyl-(2-hydroxy propyl) aminoethyl and for SP-Sephadex C-25 the functional group is sulphopropyl.

$$QAE = -C_2H_4N^{\oplus}(C_2H_5)_2CH_2CH(OH)CH_3$$

$$SP = -C_3H_6SO_3^{\ominus}$$

The net result of an ion exchange reaction can be expressed as the following equilibrium:

$$MR + N^{\oplus} = NR + M^{\oplus}$$

where R represents the resin matrix. Here the law of mass action applies, therefore the selectivity coefficient (equilibrium constant) takes the usual form[11]:

$$K = \frac{a_{NR}\, a_{M^{\oplus}}}{a_{MR}\, a_{N^{\oplus}}} = \frac{(NR)(M^{\oplus})}{(MR)(N^{\oplus})} \cdot \frac{\gamma_{NR}}{\gamma_{MR}} \frac{\gamma_{M^{\oplus}}}{\gamma_{N^{\oplus}}}$$

The value of K is constant only when the activities of the various species are used, otherwise it will vary with total and relative concentrations due to changes in activity coefficients. Within the resin, concentrated solutions of

strong electrolytes exist with concentrations on the order of 2 to 8 M. Here there is no adequate theory for treating activity coefficients. The activity coefficient of the resin phase is even more difficult to treat. This leaves one with little choice but to use a psuedo-equilibrium constant, or concentration ratio. Selectivity coefficients are therefore determined empirically and are reasonably constant for given conditions. A number of useful rules have been formulated from experimental observations[12]:

1. As the cross-linking of the matrix is decreased, selectivity coefficients approach unity.
2. The exchange of ions that cause expansion of the resion is favored less than those exchanges that do not; in other words the smaller the ion, the greater the affinity for the resin.
3. There is greater affinity for the resin with greater charge on the ion.
4. The affinity of organic ions and some anionic complexes are unusually high, probably because the electrostatic forces are complimented by short range adsorption (van der Waals) forces.

The extent of dissociation of weak acids is controlled by the pH of the medium. By changing the pH it is possible to increase, decrease, or even reverse the electrical charge on the species. Using this, one has a delicate but powerful means of influencing the distribution ratio, or

of preventing exchange altogether.

At low ionic strength, competition for charged groups on the ion exchanger is at a minimum and substances are bound strongly under these conditions. Increasing the ionic strength increases the competition and thus reduces the interaction between the ion exchanger and the sample substances thus causing their elution. This information can be used to elute components having much different affinities for the ion exchanger. Either continuous or stepwise changes in ionic strength can be set up to cause components to elute. Continuous ionic strength gradients can be prepared by mixing two buffers of different ionic strength. If this volume ratio is changed linearly the ionic strength is changed linearly. Stepwise ionic strength gradients are produced by using buffers of fixed ionic strength. Stepwise elution is technically simpler but it has disadvantages. Substances released by a change of ionic strength are eluted close together. The peaks this technique produces have sharp fronts and pronounced tailing which may lead to the appearance of false peaks if a buffer change is introduced too early. Continuous gradients do not have these problems and cause substances to be eluted in symmetrical peaks with better resolution.

CHAPTER III

RESULTS AND DISCUSSION

Selection of Conditions

Because alloxan, parabanic acid and oxaluric acid are not particularly stable in aqueous solutions; therefore, it was necessary to select conditions where decomposition was held to a minimum. Above pH 4-5 alloxan begins to hydrolyze to alloxanic acid[13,14], this reaction becomes rapid at pH 7-8.

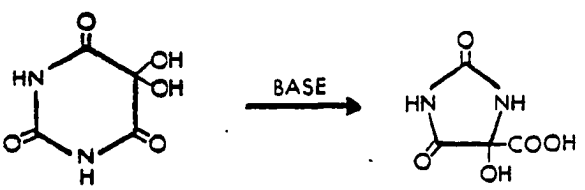

ALLOXAN ALLOXANIC ACID

Parabanic acid also slowly hydrolyses to oxaluric acid at pH 6 and thence to oxalic acid and urea[15]. Accordingly,

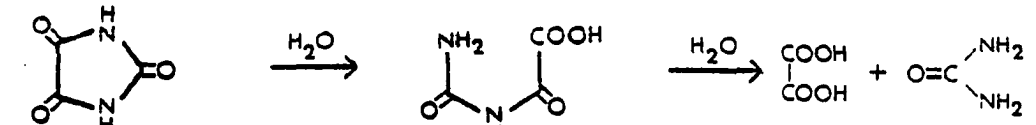

PARABANIC ACID OXALURIC ACID OXALIC ACID UREA

in order to minimize decomposition of alloxan, parabanic acid and oxaluric acid, separations using eluant systems at

pH 2-5 were employed. Within this pH range most of the compounds of interest are either neutral species or partially in their anionic form. Values of reported pK_a values are presented in Table 1.

The monitoring wavelength (199 nm) was selected because many chemical compounds having little or no ultraviolet absorption in the near u. v. region may have fairly strong absorption in the region below about 200 nm. Ribose and urea are such compounds. This phenomenon is commonly referred to as "end absorption," and it is due to $\pi \rightarrow \pi^*$ and $n \rightarrow \sigma^*$ transitions. The presence of auxochromes such as -OH, $-NH_2$, -S, or halogens in a molecule may lead to $n \rightarrow \sigma^*$ transitions that permit detection in the region below 200 nm[18].

Initial attempts to separate a mixture of alloxan, allantoin, parabanic acid, oxaluric acid, D-ribose, and urea utilized various types of ion exchange resins as the column packing. Using a SP-Sephadex C-25 cation exchange resin it was found, using eluants of various ionic strength at pH values between 2-4, that only oxaluric acid could be separated from the other five components which all eluted as a single peak. With only minor differences all chromatograms had the appearance of that shown in Figure 2.

Similarly, using QAE-Sephadex A-25 anion exchange resin and an acetate buffer system similar to that recommended by Pit *et al.*[19], it was found that alloxan, parabanic acid,

TABLE 1

pK_a values for some typical purine electrooxidation products

Compound	Structure	pK_a	Reference
Allantoin	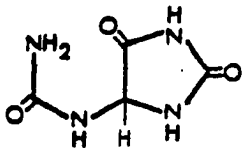	8.96	16
Alloxan monohydrate	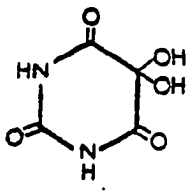	7.20	17
Oxaluric acid	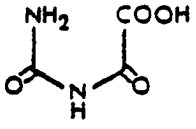	2.00	15
Parabanic acid	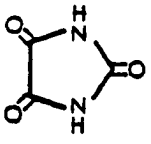	6.10	15
D-Ribose	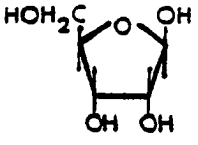	-	-
Urea	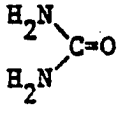	0.10	16

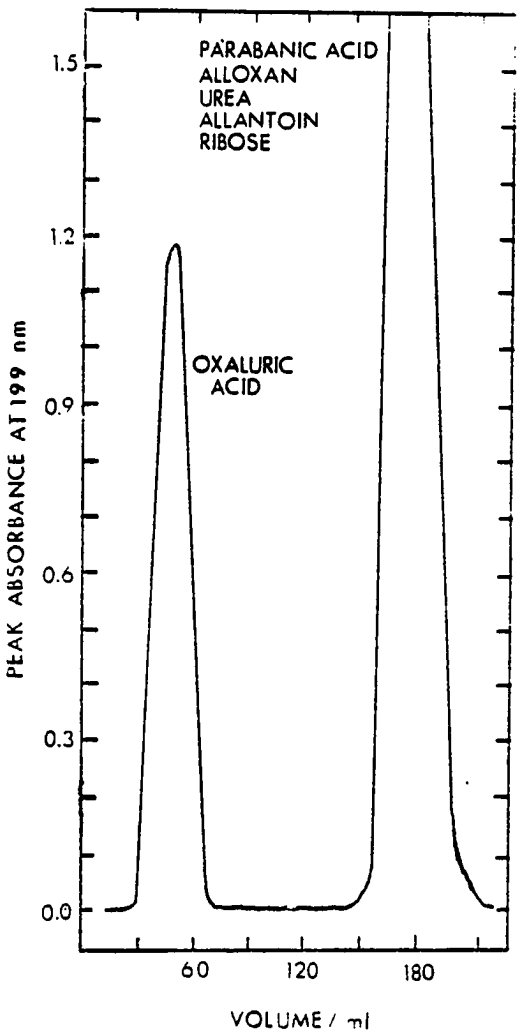

Figure 2. Chromatogram of a mixture of urea (2 mg), D-ribose (20 mg), allantoin (1.3 mg), alloxan (1.3 mg), parabanic acid (1.3 mg), and oxaluric acid (1.3 mg) dissolved in 1 ml of KH_2PO_4/H_3PO_4 pH 2.0 buffer having an ionic strength of 0.05 M. Column: SP-Sephadex C-25, 35 x 2.5 cm. Eluant: Phosphate buffer pH 2.0, ionic strength 0.05 M. Flow rate: 40 mlh^{-1}.

and oxaluric acid could be adequately separated. However, it was not possible to separate alloxan from allantoin or urea and D-ribose even though a variety of ionic strength buffer gradients, column lengths, and flow rates were employed. A typical chromatogram showing the separation of alloxan, parabanic acid, and oxaluric acid is depicted in Figure 3.

Accordingly, the use of Sephadex G-type gel permeation packings was examined. These gels are normally used to fractionate substances according to their molecular dimensions[20]. However, these gels possess other properties which can also be used for certain separations. Sephadex G-type gels reversibly adsorb molecules with π-electron systems[21], provided that their molecular sizes are small enough to permit diffusion into the gel-matrix. The extent of adsorption that will occur with a molecule that contains adsorbable structures thus depends on the amount of gel that is accessible to the solute, the greater the penetration the greater the adsorption[5]. In buffer systems of low pH, organic acids being un-ionized, tend to be adsorbed to the gel either by π-electron interactions or by hydrogen bonding to the gel matrix[22]. Thus, by control of the pH of the eluting medium it is possible to effect separations of acidic organic compounds having different dissociation constants.

Using eluant systems between pH 2-5 having ionic strengths ranging from 0.025 M to 0.500 M attempted separations of the six component mixture of interest were carried out

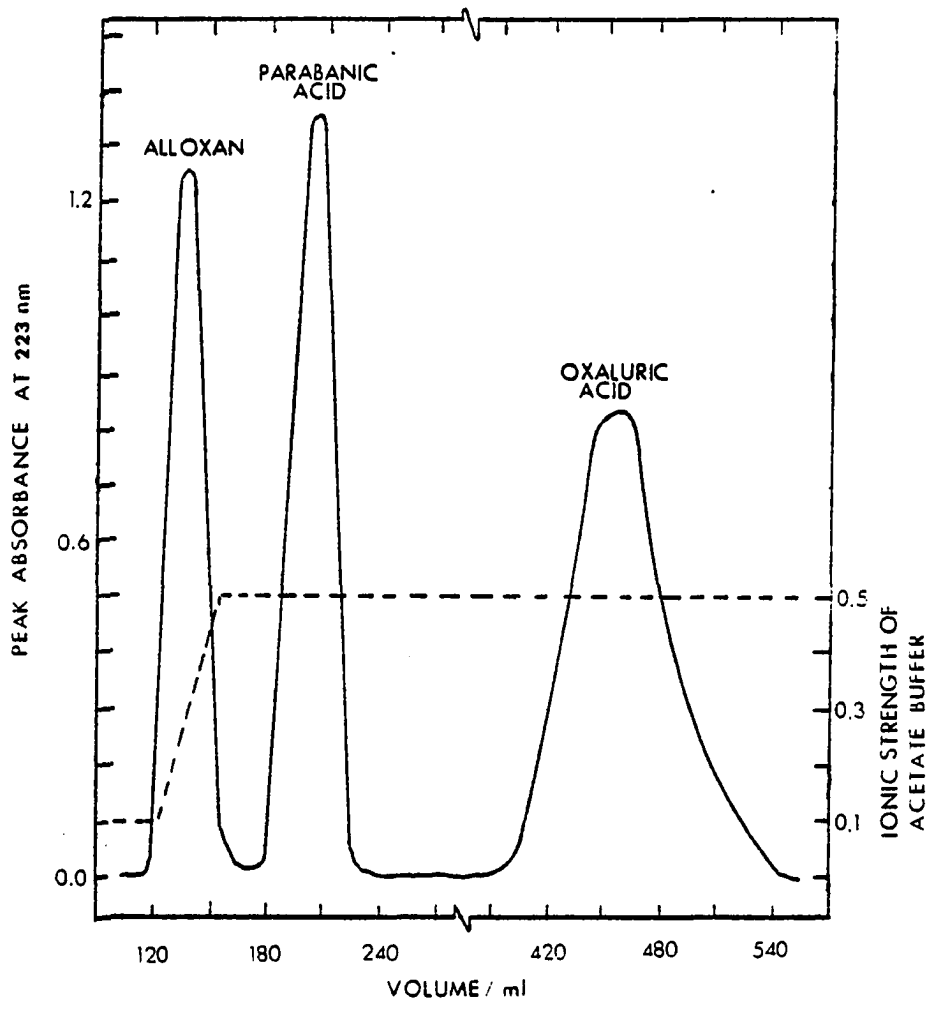

Figure 3. Chromatogram of a mixture of alloxan (1.3 mg), parabanic acid (1.3 mg), and oxaluric acid (1.3 mg) dissolved in 1 ml of KOAc/HOAc pH 4.7 buffer having an ionic strength of 0.1 M. Column: QAE-Sephadex A-25, 25 x 2.5 cm. A step elution method was used where the first two components were eluted with 0.1 M ionic strength KOAc/HOAc buffer and the last component with 0.5 M KOAc/HOAc buffer as the eluant. Flow rate: 40 mlh^{-1}.

using a Sephadex G-10 gel. With only minor differences all chromatograms had the appearance of that shown in Figure 4. Thus, although D-ribose and urea could be separated from the other components, oxaluric acid and allantoin eluted together as did parabanic acid and alloxan. However, previous studies (vide supra) indicated that parabanic acid and alloxan as well as allantoin and oxaluric acid could be separated using a QAE-Sephadex A-25 anion exchange stationary phase. Accordingly, a two column separation using a series combination of Sephadex G-10 gel permeation and QAE-Sephadex A-25 anion exchange resin was investigated. The exact arrangement is shown in Figure 5. It was found, using phosphate buffer pH 4.3 as the eluting medium, that at ionic strengths greater than 0.1 M alloxan and parabanic acid could not be completely resolved. However, using 0.025 M potassium phosphate pH 4.3 as the eluant D-ribose, urea, allantoin, alloxan, and parabanic acid gave well resolved chromatographic peaks although oxaluric acid was not eluted. Experiments revealed that oxaluric acid was in fact strongly retained by the QAE-Sephadex A-25 anion exchange resin and could only be eluted from this column in a reasonable period of time by increasing the ionic strength of the KH_2PO_4 eluant to 0.25 M. Accordingly, a complete separation of all six components could be accomplished by using 0.025 M KH_2PO_4 as the initial eluant through both columns. When the first five components have been eluted the eluant through the anion exchange

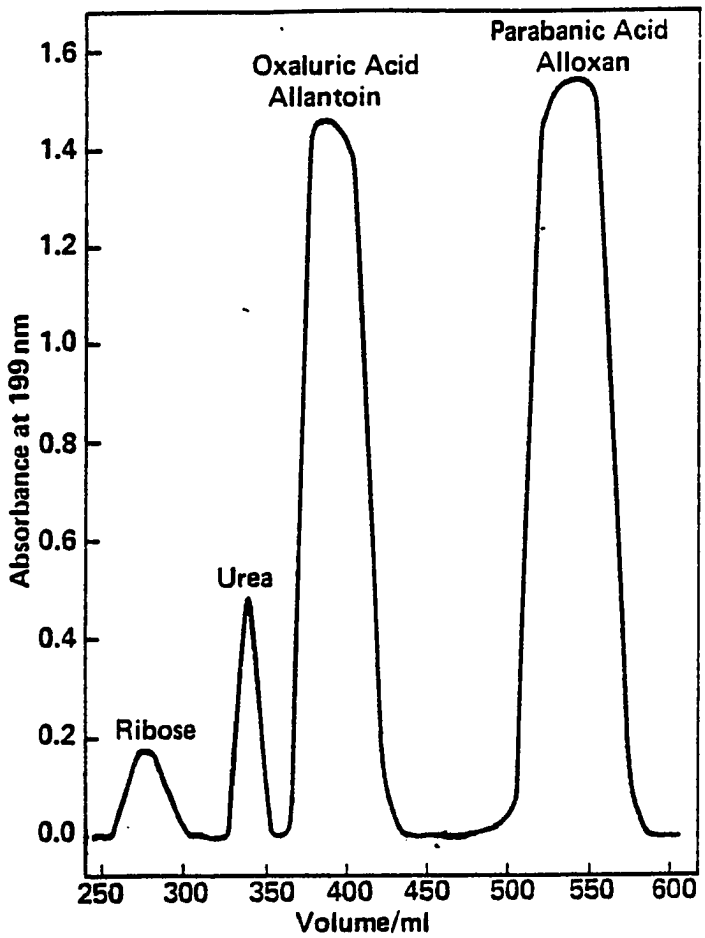

Figure 4. Chromatogram of mixture of urea (2 mg), D-ribose (20 mg), allantoin (1.3 mg), alloxan (1.3 mg), parabanic acid (1.3 mg), and oxaluric acid (1.3 mg) dissolved in 1 ml of KH_2PO_4/H_3PO_4 pH 2.0 buffer having an ionic strength of 0.5 M. Column: Sephadex G-10, 91 x 2.5 cm. Eluant: phosphate buffer pH 2.0, ionic strength 0.5 M. Flow rate: 40 mlh^{-1}.

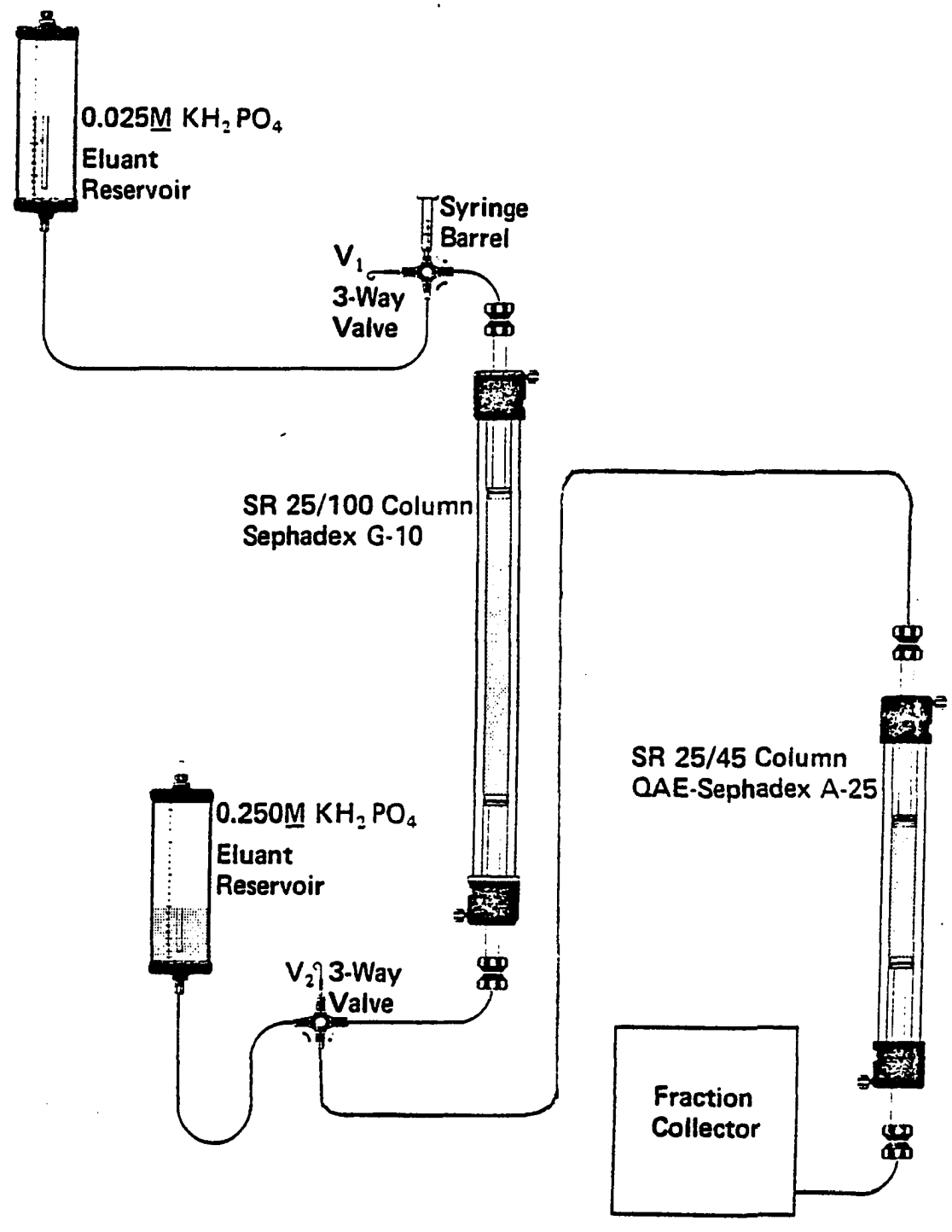

Figure 5. Schematic arrangement for dual column chromatographic system.

column is changed to 0.25 M KH_2PO_4, using the arrangement shown in Figure 5, then oxaluric acid was eluted. A typical chromatogram showing the separation of the six component mixture under these conditions is shown in Figure 6.

Retention Volumes and Sensitivities

From the chromatograms, retention volumes (V_r) may be obtained in the following manner:

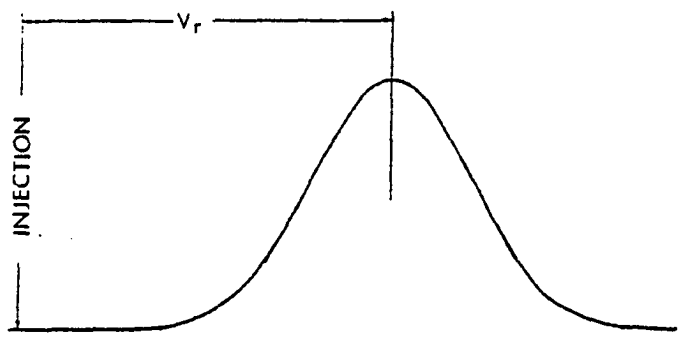

Retention volume data for all six components under optimum chromatographic conditions are presented in Table 2. The retention volumes reported in Taole 2 were the same for chromatograms obtained with only a single component injected onto the columns or with all six components injected simultaneously, i.e., the retention volumes of individual components are not influenced by the presence of other species in the solution. This implies, therefore, that the retention volume data may be used for qualitative identification of

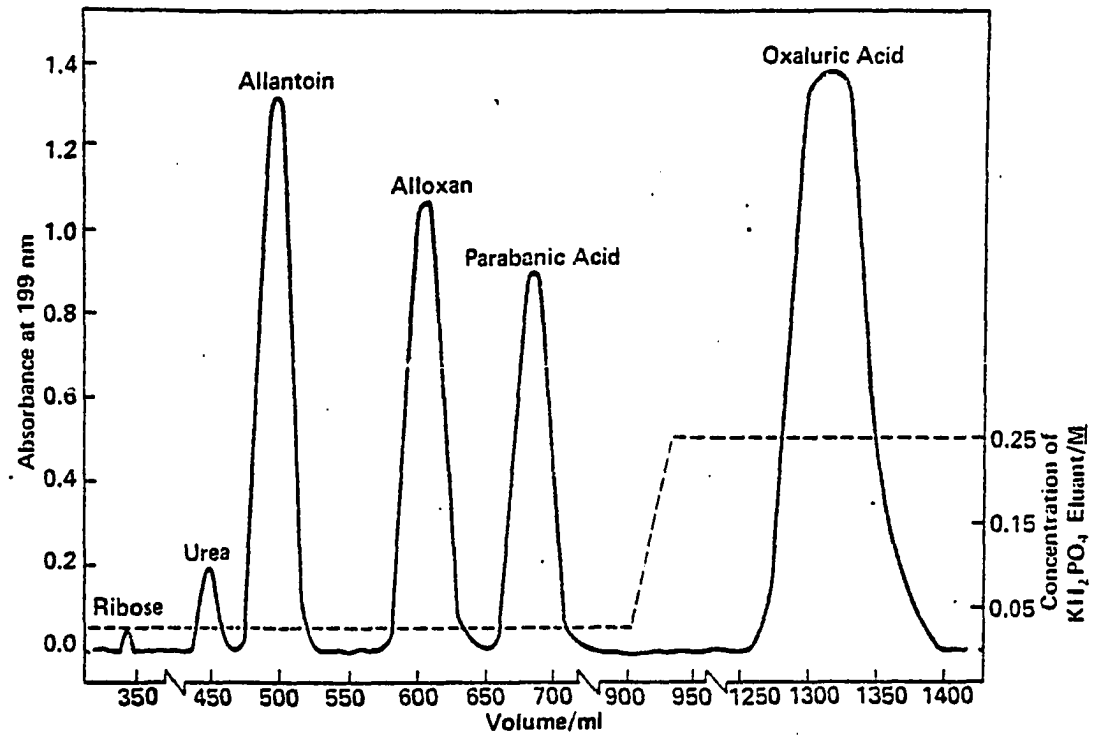

Figure 6. Chromatogram of a mixture of urea (2 mg), D-ribose (13 mg), allantoin (1.3 mg), alloxan (1.3 mg), parabanic acid (1.3 mg), and oxaluric acid (1.3 mg) dissolved in 1 ml of 0.025 M KH_2PO_4 buffer pH 4.3. The arrangement of chromatographic columns is shown in Figure 5. The Sephadex G-10 column has a bed height of 70 cm. and the Sephadex QAE A-25 column has a bed height of 35 cm. A step elution method was used where the first five components were eluted with 0.025 M KH_2PO_4 and the last component with 0.25 M KH_2PO_4 as the eluant through the Sephadex QAE A-25 column. Flow rate 40 mlh^{-1}.

the eluting species. The term relative retention volume, which eliminates deviations in retention volumes due to varying instrumental parameters, is also introduced in Table 2. In these studies allantoin was chosen as the standard, and all retention times reported are relative to it.

The chromatographic sensitivity of each compound was measured for one component solutions. Sensitivity data for oxaluric acid should be suspect. With the change in ionic strength used to elute oxaluric acid and the decrease in the bed height due to the ionic strength change (see experimental), the reproducibility of its peak height and peak area was poor. Sensitivity values were obtained using both peak height and peak area data. In both cases u. v. absorption of three ml aliquots of undiluted eluant was monitored at 199 nm in a one cm path length quartz cell (see experimental). Using peak height data, sensitivities were obtained by dividing the maximum peak absorption by the number of μmoles ml^{-1} in the injected sample. With peak area data, the area of the peak in cm^2 (see legend of Table 2) was divided by the number of μmoles ml^{-1} in the injected sample, to obtain sensitivity values.

Normal chromatographic peaks approximate a triangle, thus the area can be calculated by the triangle formula:

$$A = HW_{\frac{1}{2}}$$

Table 2. Retention volumes and sensitivities for chromatographic separation of typical purine electrooxidation products[a].

Compound	Retention[b] volume/ml	Relative Retention Volume[c]	Sensitivities Peak ht[d]	Peak area[e]
D-Ribose	344	0.69	0.0037	0.0012
Urea	448	0.90	0.2784	0.0252
Allantion	498	1.00	0.1875	1.1875
Alloxan	602	1.21	0.1419	1.1935
Parabanic Acid	682	1.37	0.0795	0.7045
Oxaluric Acid	1314	2.64	0.1527	2.8286

[a]Under conditions outlined in Experimental and Figure 6.

[b]Flow rate 40 ml h^{-1}.

[c]Relative to allantion.

[d] $\frac{\text{Abs.}}{\mu\text{moles ml}^{-1}} = \frac{\text{Detector response}}{\#\ \mu\text{moles ml}^{-1}\ \text{in injected sample}}$

[e] $\frac{\text{cm}^2}{\mu\text{moles ml}^{-1}} = \frac{\text{Area of peak}}{\#\ \mu\text{moles ml}^{-1}\ \text{in injected sample}}$, 0.1 Abs. unit= 1 cm., y-axis; 30 ml = 1 cm, x-axis.

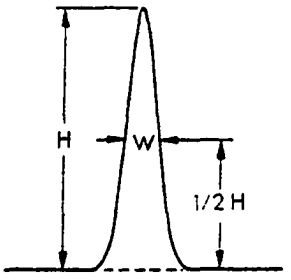

This technique can only be applied to symmetrical peaks or peaks which have similar shapes. The area measured is less than the true area but is proportional to sample size provided the peaks do not distort badly. Thus by using the width at half-height rather than the width at baseline one reduces errors due to tailing and adsorption.

The sensitivities of urea and especially ribose are significantly less than that for alloxan, allantoin, and parabanic acid. Accordingly, their detection in real samples may be difficult and in the case of ribose impossible.

Chromatographic Resolution[5]

The resolution of two adjacent peaks is defined as the distance between the peak maxima divided by the average peak width. Retention volume and peak width were measured in units of ml. Resolution, R_s, is given as:

$$R_s = \frac{2(V_2 - V_1)}{W_1 + W_2}$$

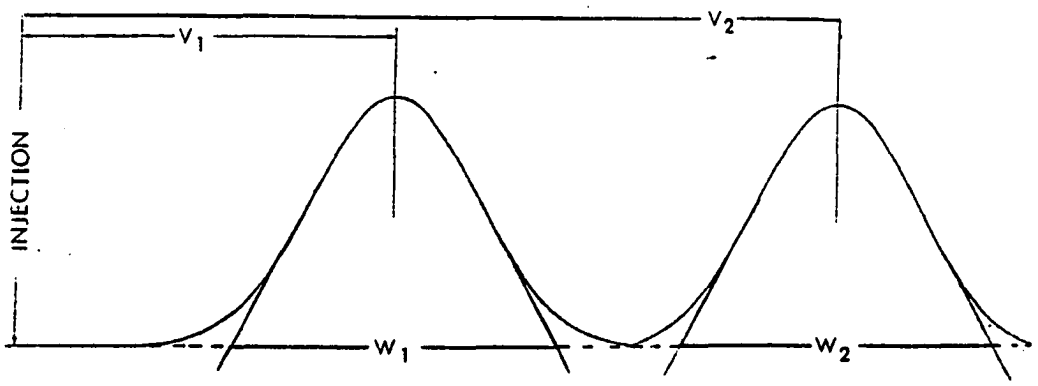

where V_1 and V_2 are the retention volume values of peak 1 and peak 2, and W_1 and W_2 are their baseline peak widths, defined by the tangents to the inflection points of a given curve.

With an R_s value of 1.5, the two peaks are essentially completely separated. This is termed baseline separation. At this value of resolution, the cross contamination of the two peaks is normally much less than 1%, and the observed peak center coincides with the true value in the absence of a second peak. Solute concentration and peak height are proportional in the original sample, and retention time defines the identity of the solute, thus both quantitative and qualitative analyses are possible when the true peak centers coincide with the observed peak centers.

With a resolution of 1, the peaks are readily recognizable over a wide range of relative concentrations. Here the cross contamination of the two peaks is no more than 3%, which is suitable for most purposes. The observed values of peak height and retention time are insignificantly

different from the true values over a wide range of relative concentrations for the two peaks. This means that qualitative and quantitative analyses are not affected. For a resolution of 0.8, two distinct bands are just barely recognizable, and only over a limited ratio of solute concentrations. At lower values of resolution, in most cases, only a single peak is seen. Thus at a resolution of 0.8, qualitative analysis may still be performed, but quantitative analysis, in most cases, is impossible.

The resolution of a mixture of the six compounds of interest was tested using a one ml solution containing 1.3 mg alloxan, 1.3 mg allantoin, 1.3 mg parabanic acid, 1.2 mg oxaluric acid, 2.0 mg urea, and 13.0 mg ribose. Resolutions for all peaks in Figure 6 proved to be 1.50 or better, i.e., baseline separation. However, injection of 1 ml samples containing in excess of 1.3 mg of parabanic acid and alloxan caused the R_s value to decrease. Thus, when the amount of both parabanic acid and alloxan in the 1 ml sample injected was 1.49 mg the R_s value decresase to 1.0. A similar effect was noted for the urea and allantoin peaks when the injected amounts exceeded 2.0 mg and 1.3 mg, respectively. However, the measured retention times for the single component solutions are identical to those for the components in the mixture. Thus, the retention times are not influenced by the presence of other species in the solution and can be used for qualitative and quantitative identification.

Analytical Curves

In order to evaluate the use of chromatograms, such as that shown in Figure 6, for quantitative analysis of the individual components, a series of analytical curves were prepared. In the case of D-ribose the absorbance at 199 nm of even relatively concentrated solutions is so low that useful absorbance *vs.* concentration curves could not be obtained. Oxaluric acid also gave non-reproducible peak height or peak area *vs.* concentration results. This is presumably because of the solvent change required to elute oxaluric acid form the QAE A-25 anion exchange column causing rather distorted chromatographic peaks.

In the case of urea, allantoin, parabanic acid, and alloxan analytical curves based on peak height measurements are shown in Figure 7. With the exception of allantion the compounds give reasonably linear peak height *vs.* concentration curves. Plots of peak area *vs.* concentration gave more reproducible and linear analytical curves (Figure 8). The absorbance of urea at 199 nm is significantly less than that for alloxan, allantoin, and parabanic acid. Accordingly, it would be expected that analyses for urea based on curves such as those in Figures 7 and 8 would be, at best, only semi-quantitative.

When the amount of urea, alloxan, allantoin, and parabanic acid in the 1 ml injected sample exceeded 1.3 mg appreciable peak broadening and distortion occurred with

the result that plots of peak absorbance or peak area vs. concentration become non-linear.

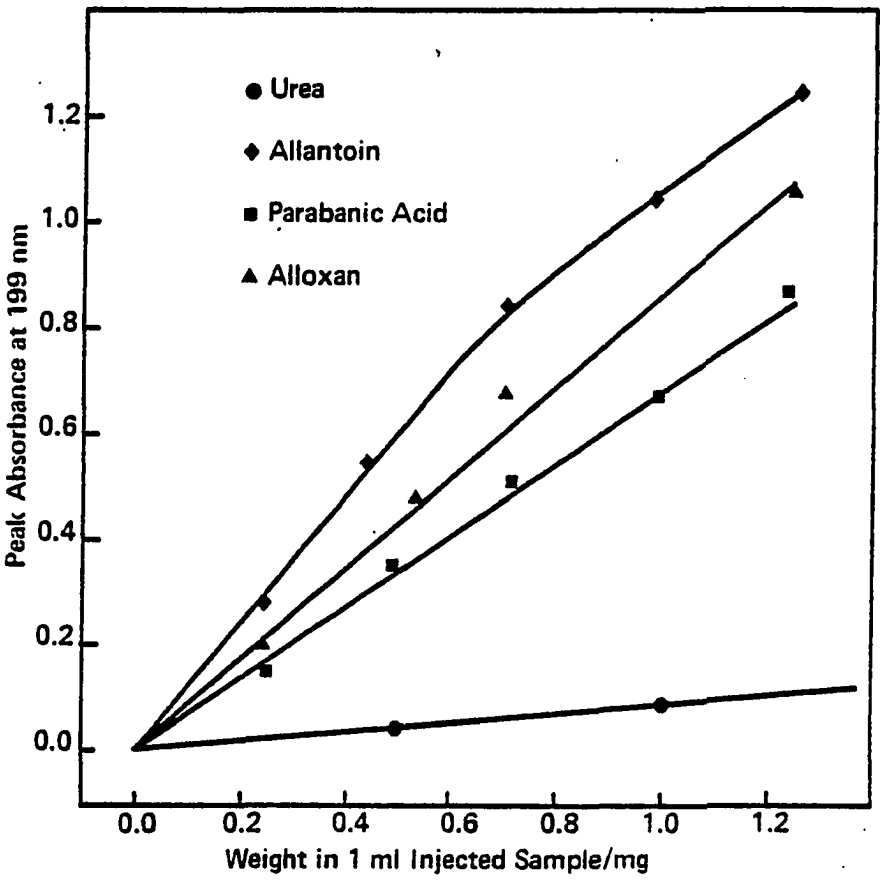

Figure 7. Peak height vs. concentration curves for the chromatographic peaks of urea, allantoin, parabanic acid, and alloxan.
Chromatographic conditions are the same as described in Figure 6.

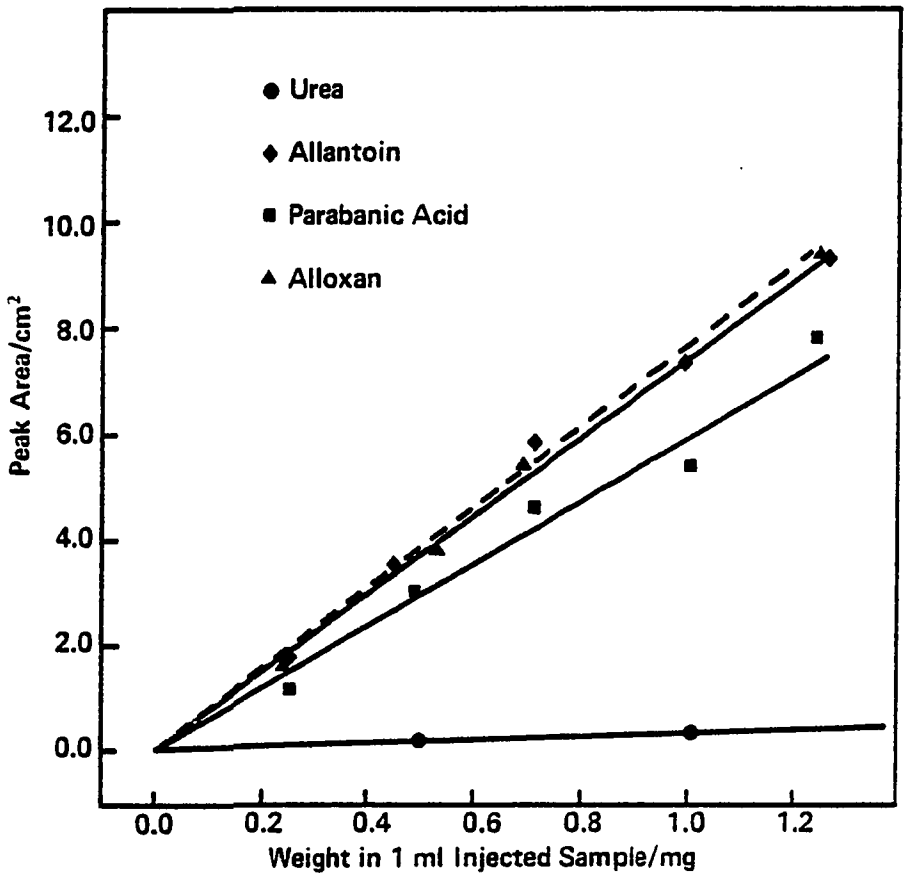

Figure 8. Peak area vs. concentration curves for the chromatographic peaks of urea, allantoin, parabanic acid, and alloxan. Chromatographic conditions are the same as described in Figure 6.

CHAPTER IV

EXPERIMENTAL

Chemicals

Chemicals were obtained from the following sources: alloxan monohydrate and oxaluric acid (Nutritional Biochemicals Corporation); D-ribose (Calbiochem); allantoin and parabanic acid (Eastman Organic Chemicals); urea (Merck Chemical Division). Buffer solutions were prepared from reagent grade chemicals and deionized water. Column chromatography utilized Sephadex G-10, SP-Sephadex C-25, and QAE-Sephadex A-25 (Pharmacia Fine Chemicals, 40-120 μm).

Apparatus

A Buchler Fractomat fraction collector was utilized in column chromatography. U. v. absorption was measured in 4.5 cm x 1.0 cm quartz Beckman cuvettes on a Hitachi Model 124 spectrophotometer. Liquid chromatography was performed in Pharmacia Fine Chemicals Models SR 25/45 (2.5 cm x 45 cm) and SR 25/100 (2.5 cm x 100 cm) columns.

Column Packing and Conditions

Individual Column Separations. Sephadex G-10, QAE

A-25, and SP C-25 resins were allowed to swell in an excess of their respective separation eluants for two days at room temperature with constant gentle stirring. The columns, equipped with adjustable plungers, were mounted vertically using a carpenter's level. Then a plunger was inserted in the bottom of the column and adjusted to a secure position. Eluant was filled in the outlet tubing below the plunger.

After removing excess eluant, the gel was formed into fairly thick slurry; such a thick slurry inhibits bubble formation. An extension tube (eluant reservoir cylinder) was mounted on top of each column to facilitate the addition of all the required gel for each experiment at one time. The outlet tubing from the plunger was adjusted to a height that insured the settling flow rate never exceeded the column operating flow rate. This arrangement is depicted in Figure 9. During the addition of the gel, the outlet tubing was stoppered. As soon as possible the flow was initiated, insuring an even sedimentation. After sedimentation, two column volumes of degassed eluant were passed through each column in order to stabilize and equilibrate the gel bed. Degassing was accomplished by boiling then cooling the water used to make the eluant. Following stabilization, the flow was stopped and a plunger was inserted to approximately 1 cm from the top surface of the gel. The solvent was then eluted through the column with downward flow at a linear rate of 40 mlh^{-1}. When the gel bed ceased to decrease in height,

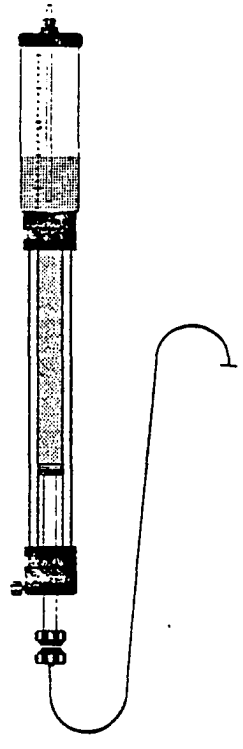

Figure 9. Schematic arrangement of column and eluant reservoir cylinder for gel packing.

the top plunger was adjusted to touch the gel surface and the chromatography experiments were begun. For experiments with SP-Sephadex C-25, the SR 25/45 column was packed to a height of 35 cm. QAE-Sephadex A-25 work was performed using 25 cm of swollen gel packed into the SR 25/45 column. Swollen Sephadex G-10 (91 cm) was packed into the SR 25/100 column for gel permeation work.

Coupled Column System. With this arrangement, the columns were equilibrated and stabilized in the same manner as the individual column separations. For this case, 0.025 M KH_2PO_4 was used as eluant in both columns. A three-way valve (V_2), which also allows the introduction of 0.25 M KH_2PO_4 from a separate reservoir, was used to couple the columns in the order SR 25/100 followed by SR 25/45 with Sephadex G-10 in the former and QAE-Sephadex A-25 in the latter. This set-up is shown in Figure 5. Following equilibration and stabilization the G-10 column was connected to the three-way valve (V_2) through its bottom adaptor. Top adaptors were then inserted into both columns about 1 cm from the top of the gel surfaces and the QAE column was connected to the three-way valve (V_2), through its top adaptor. With the three-way valve (V_2) in the proper setting, eluant was allowed to flow downward through both columns. When the gel beds ceased to decrease in height, the top plungers were both adjusted to touch their respective gel surfaces. During the final adjustment of the top plunger

on the QAE column, the three-way valve (V_2) was rotated to force the eluant between the plunger and gel surface, which was being displaced, into the 0.25 M KH_2PO_4 reservoir. This insured no air bubbles were forced into the bottom of the G-10 column. As far as changing the molarity in the 0.25 M KH_2PO_4 reservoir, the amount of eluant added was insignificant. Chromatography experiments were then begun.

For all preparations and measurements the columns were operated at room temperature.

Separation Procedure

Various amounts of urea, alloxan, allantoin, parabanic acid, oxaluric acid, and ribose were dissolved in five ml of 0.025 M KH_2PO_4. One ml of this solution was then applied, through a syringe barrel attached to a three-way valve (V_2), to the top of the G-10 column. Three ml fractions of eluant were collected in each test tube. The absorbance of the eluant in each test tube was monitored at 199 nm to determine the chromatogram. Ribose, urea, allantoin, alloxan, and parabanic acid were separated using 0.025 M KH_2PO_4. Oxaluric acid was strongly retained on the QAE A-25 resin and was not eluted with 0.025 M KH_2PO_4. After a fifth peak eluted from both columns, the eluant for the QAE A-25 column was changed to 0.025 M KH_2PO_4 using a three-way valve (V_2) and the second eluant reservoir. This permitted the removal of oxaluric acid from the anion exchange column and its eluation as a sixth peak. All determinations were performed at least

in triplicate.

Analytical Studies

Analytical curves were obtained for each component by analyzing a series of solutions in the concentration range 0.25 $mgml^{-1}$ to 1.25 $mgml^{-1}$.

The chromatographic peaks were obtained as plots of absorbance vs volume. Average response was determined in units of absorbance (peak height) and peak area (cm^2). When determining area the parameters used were peak height and the peak width at half-height.

The retention volumes (V_r) were measured as the period from the introduction of sample to the appearance of the peak maximum of each component.

Column Regeneration

It should be noted that when the eluant through the QAE-Sephadex A-25 anion exchange column is changed from 0.025 M KH_2PO_4 to 0.25 M KH_2PO_4 the column packing shrinks by about 2 cm. This results in a very substantial decrease in flow rate through this column and an undesirable amount of dead space at the top of this column, which cannot be corrected by washing in the usual way with 0.025 M KH_2PO_4. Under these circumstances a reverse flow of 0.025 M KH_2PO_4 through the anion exchange column at a flow rate of about 20 $ml.h^{-1}$ for 5 hours serves to restore the column to its original condition.

CHAPTER V

LIQUID CHROMATOGRAPHIC SEPARATION OF THE ELECTROCHEMICAL OXIDATION PRODUCTS OF URIC ACID

Introduction

Following the development of a liquid chromatographic separation for common purine electrooxidation products[23], it became necessary to test this separation using an actual electrochemical oxidation product mixture. Uric acid was chosen as the source of this product mixture because the electrochemical oxidation scheme for uric acid has been throughly studied and is relatively simple and straight forward[3]. As was previously mentioned, this study revealed that at low pH the only products of oxidation are alloxan and urea. With increasing pH the yield of alloxan decrease while that of allantoin increases. At pH 7 the major product is allantoin with smaller amounts of urea and alloxanic acid. Parabanic acid could be detected only in exceedingly small amounts in the products of electrooxidation of uric acid in 1 M HOAc, pH 2.3.

Thus the separation of the electrochemical oxidation

products of uric acid using the technique developed above should provide a good test of the qualitative and quantitive precision of this separation technique.

Results and Discussion

Single-Sweep Peak Voltammetry. Voltammetry may be generally defined as the measurement of current-voltage relationships at an electrode immersed in a solution containing electroactive species. More specifically, it is the determination of the potential of a single electrode during the course of a sustained electron transfer reaction at the electrode surface, i.e., while a net current flows through the electrochemical cell. One considers the electrochemistry of a substance in an unstirred solution containing an excess of background electrolyte. The Nernst equation, shown below, is assumed applicable to the electrode process.

$$E = E^{o} + \frac{RT}{nF} \ln \frac{C_o^e}{C_R^o}$$

where E^{o} = a constant characteristic of a particular half-reaction
R = the gas constant = 8.314 volt coulombs/^{o}K/mole
T = the absolute temperature
n = number of electrons participating in the reaction as defined by the equation describing the half-cell reaction
F = the faraday = 96,493 coulombs
ln = the natural logarithim = 2.303 $\log_{10}$
C_o^e = concentration of oxidized species at electrode
C_R^e = concentration of reduced species at electrode

The voltammogram will normally show a peak (Figure 10).

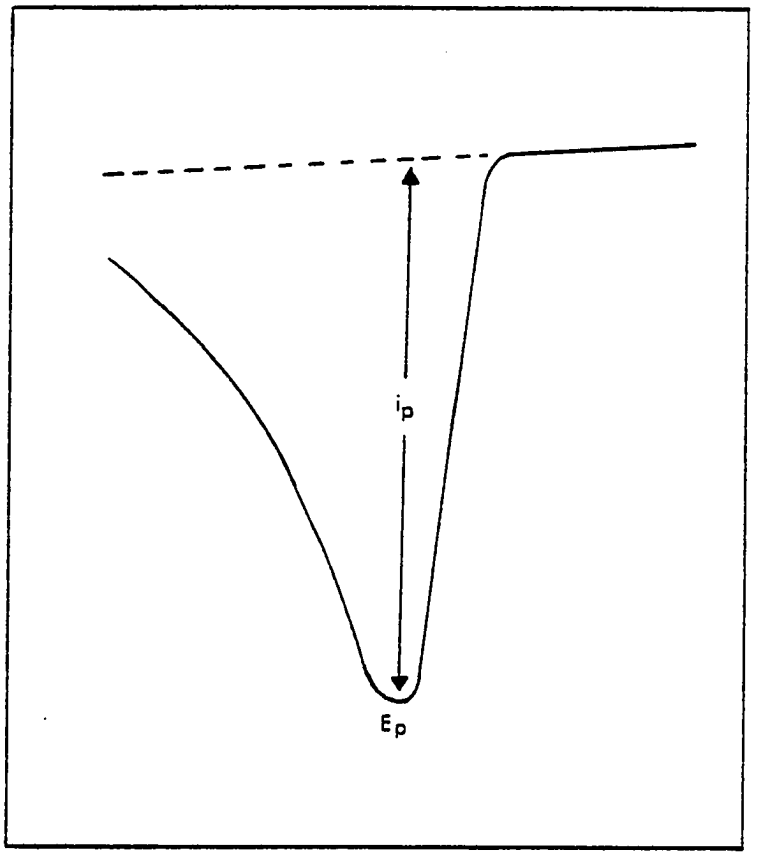

Figure 10. Schematic voltammogram obtained at a stationary microelectrode in quiet solution.

The peak current, ip, is given for a reversible electrode reaction by the Randles-Sevcik[24,25] equation.

$$ip = 2.687 \times 10^5 \, n^{3/2} \, A \, D^{1/2} \, C \, v^{1/2}$$

where ip = peak current, μA
C = bulk concentration of electroactive species, mM
A = electrode area, cm^2
n = electron number
v = scan rate of the applied linear voltage sweep, volts sec^{-1}
D = diffusion coefficient of electroactive species, $cm^2 sec^{-1}$

Clearly, the current depends on the scan rate of the applied voltage sweep. It might appear that with increasing scan rate the peak currents would increase and an extraordinary sensitivity might be attained at very high scan rate. Unfortunately, the charging current increases linearly with scan rate, while the faradaic peak current increases only with $v^{1/2}$. Thus, one can increase the scan rate only up to a limited value without the charging current becoming large in comparison to the faradaic peak current.

Over the pH range 1 to 7, uric acid shows a well-defined oxidation peak at the PGE (Figure 11). The peak potential of this peak shifts linearly more negative with increasing pH; Ep = 0.76 - 0.069 pH (Figure 12).

Controlled Potential Electrolysis and Coulometry. Controlled potential electrolysis is employed for two principle reasons in electrochemistry: first, to prepare sufficient products of the electrode reaction to allow their isolation

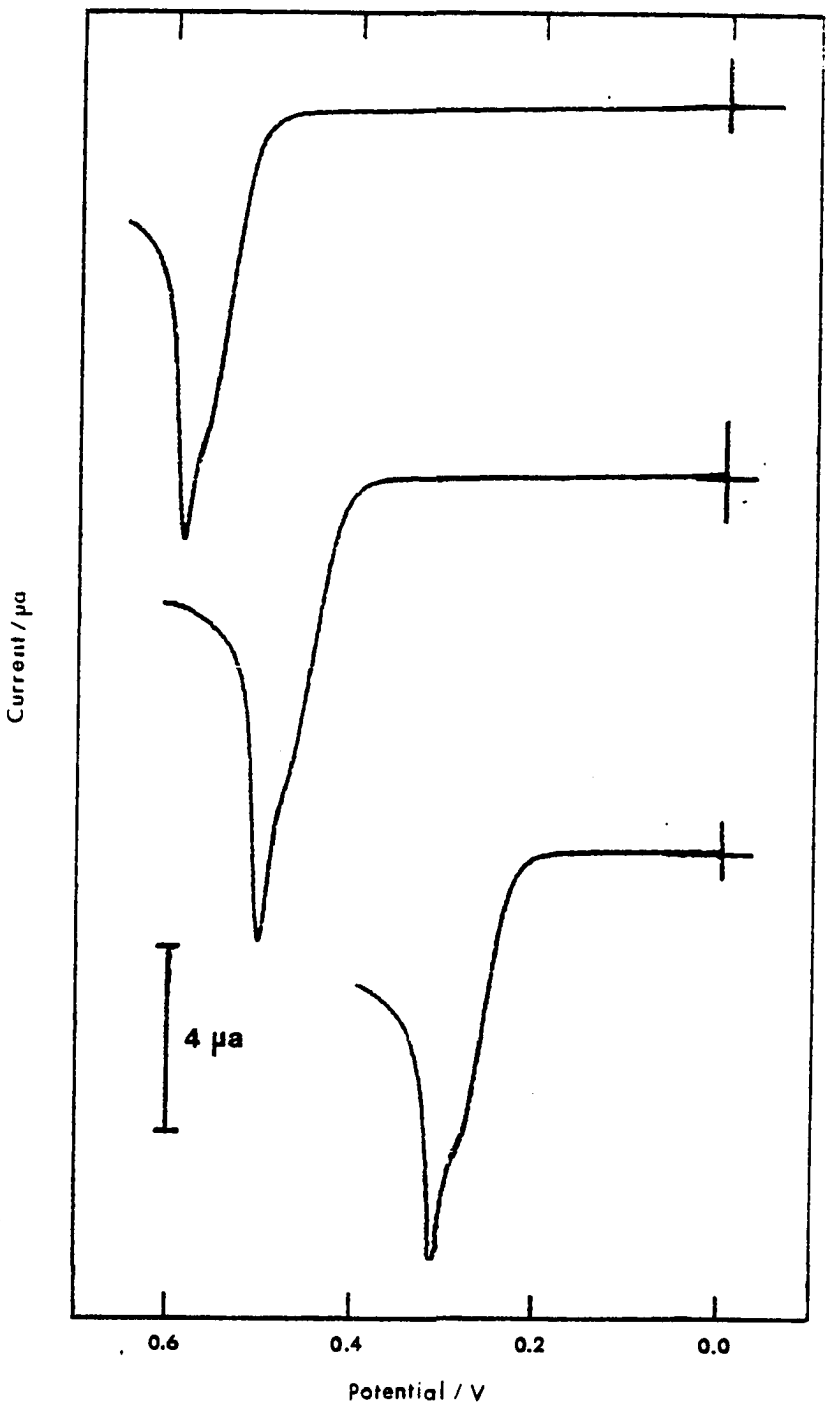

Figure 11. Voltammograms of 1 mM solutions of uric acid at (a) pH 2.3, 1 M HOAc; (b) pH 4.3, 0.025 M KH_2PO_4; (c) pH 7.0, 0.025 M KH_2PO_4/K_2HPO_4. Scan rate: 5 mV sec^{-1}.

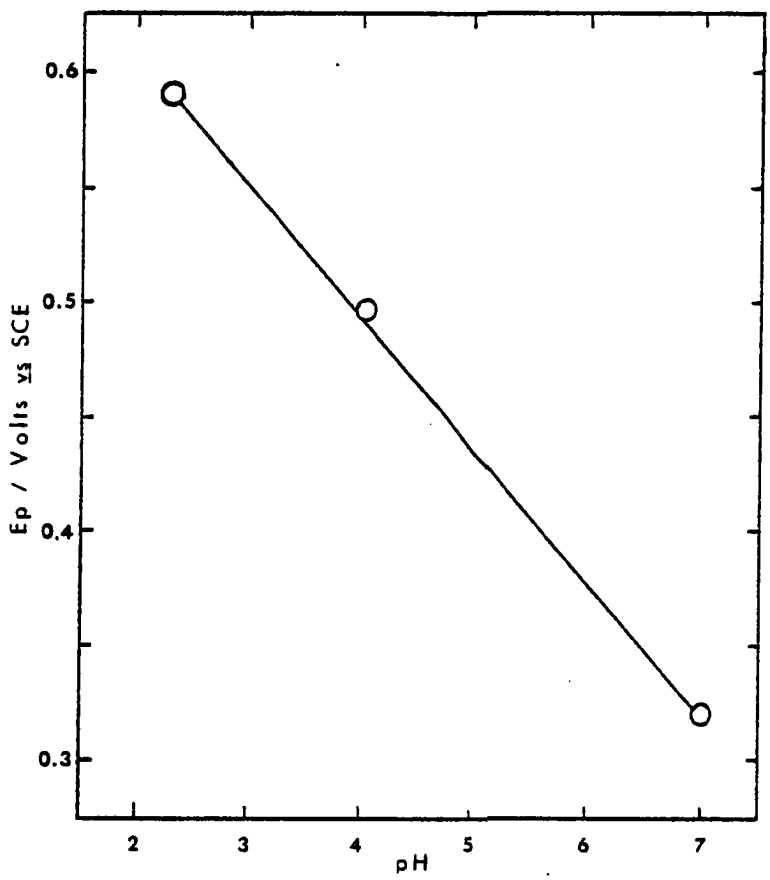

Figure 12. Variation of peak potential with pH for electro-oxidation of uric acid. The values of the slope and y-intercept for this line are identical to work previously published by Dryhurst.[3]

and/or identification and, second, to determine the number of electrons involved in an electrode process.

Coulometry of uric acid was carried out at various pH values between pH 2.3 - 7, the most commonly encountered pH range in biological systems. Typical coulometric data is presented in Table 3 which clearly indicates that at all pH values examined the n value for uric acid is two.

Product Isolation and Characterization. I. Separation and Quantitation. To obtain a sufficient amount of material for characterization, solutions of 0.25 mM to 1.00 mM uric acid concentration were electrolyzed. Qualitative and quantitative analyses of the electrolysis products were carried out from electrooxidations in pH 2.3 acetate, pH 4.3 phosphate, and pH 7.0 phosphate buffer.

Chromatographic separation of electrolysis products was accomplished on Sephadex gel permeation and Sephadex anion exchange resins. After lyophylization, product mixtures were dissolved in 1 ml of water in the phosphate buffer cases and 1 ml of 0.025 M KH_2PO_4 in the acetate buffer cases, then applied to the coupled chromatographic column[23].

At a pH of 2.3 in 1 M HOAc, 3.960 mg of uric acid was oxidized at +0.70 V. vs SCE. Using previously described chromatographic conditions, a separation, whose chromatogram is shown in Figure 13, was obtained. Peak area data gave the following yields, alloxan (0.54 mole), allantoin (0.16 mole), parabanic acid (0.24 mole), and urea (0.78 mole) per

TABLE 3

Coulometric n-values for the controlled potential electrolysis of uric acid at the PGE

pH	Buffer system	Amount[a] electrolyzed (mg)	Applied Potential V *vs.* SCE	n-value
2.3	1*M* HOAc	3.960	0.70	1.95
4.3	Phosphate	3.046	0.55	1.94
7.0	Phosphate	1.445	0.40	1.91

a All electrolyses were continued until all uric acid was oxidized.

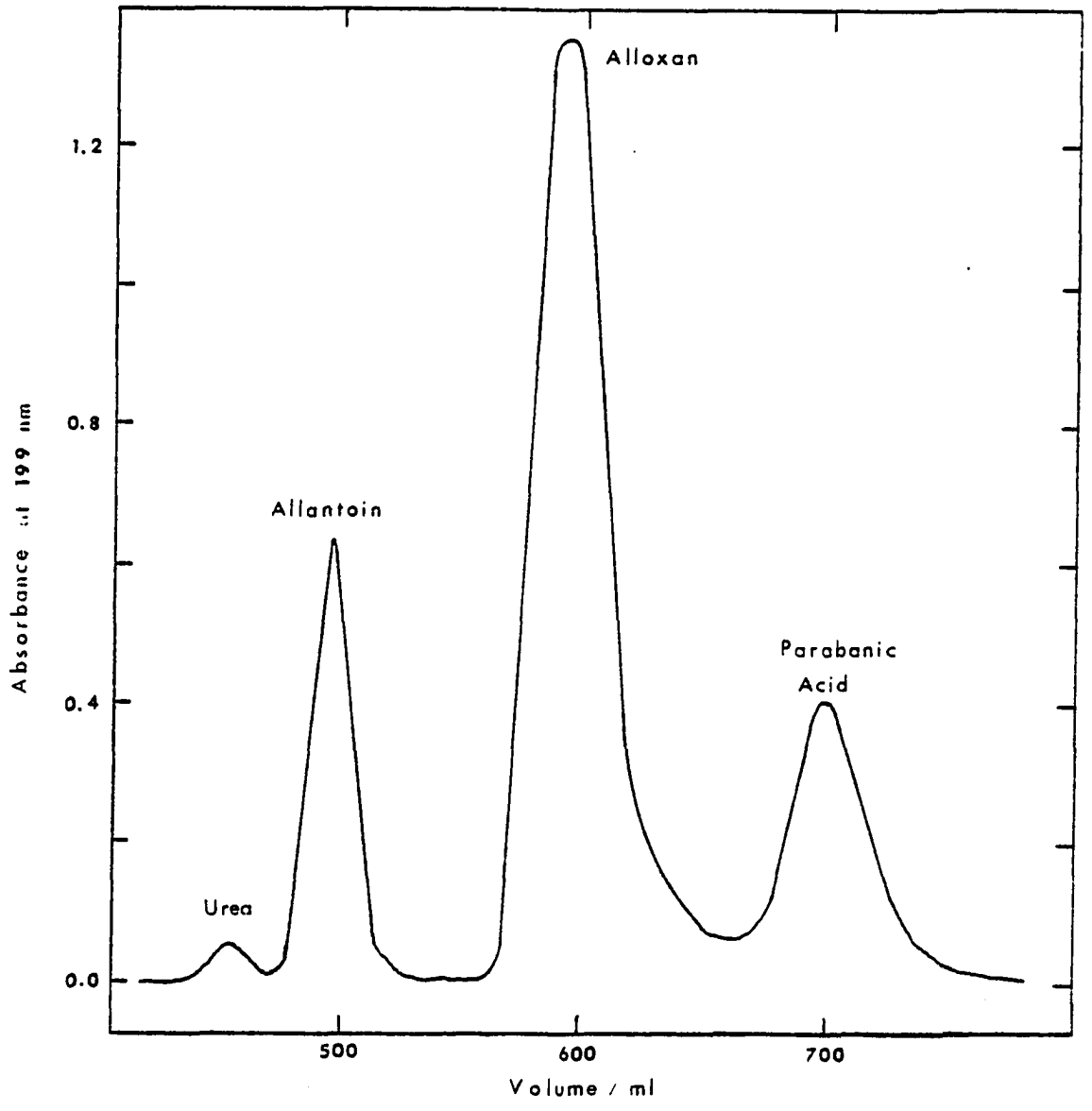

Figure 13. Chromatogram of uric acid (3.9 mg) oxidation products from a 1 M HOAc pH 2.3 solution dissolved in 1 ml of 0.025 M KH_2PO_4. The arrangement of chromatographic columns is shown in Fig. 5. The column conditions are the same as those in Fig. 6.

mole of uric acid oxidized. For both allantoin and urea, the above yields agree favorably with those obtained by Dryhurst[3]. In the cases of alloxan and parabanic acid, above yields show less alloxan and more parabanic acid than the previous study. However, both studies have similar total, alloxan plus parabanic acid, concentrations. Also, the total concentration, alloxan plus parabanic acid, is equal to the urea concentration. This would be expected according to the mechanism proposed by Dryhurst[3].

Uric acid (3.073 mg) was also oxidized at +0.55 V. vs SCE in 0.05 M KH_2PO_4. This solution had a pH of 4.3. A chromatogram of the separated products is shown in Figure 14. Peak area data gave the following yields per mole of uric acid oxidized, allantoin (0.62 mole), urea (0.33 mole), alloxan (0.04 mole), and parabanic acid (0.03 mole). Alloxanic acid was also detected, but not determined quantitatively. Again allantoin and urea were in good agreement with Dryhurst[3]. The yield of alloxan was much lower than that obtained from the previous study. A possible explanation for this discrepancy could be hydrolysis of alloxan while it is moving through the column to alloxanic acid. Additional information, which also lends substance to this explanation, is the broad, severely tailed peak produced by alloxanic acid.

At pH 7.0 in KH_2PO_4/K_2HPO_4 buffer with an ionic strength of 0.1 M, the best correlation between previous and

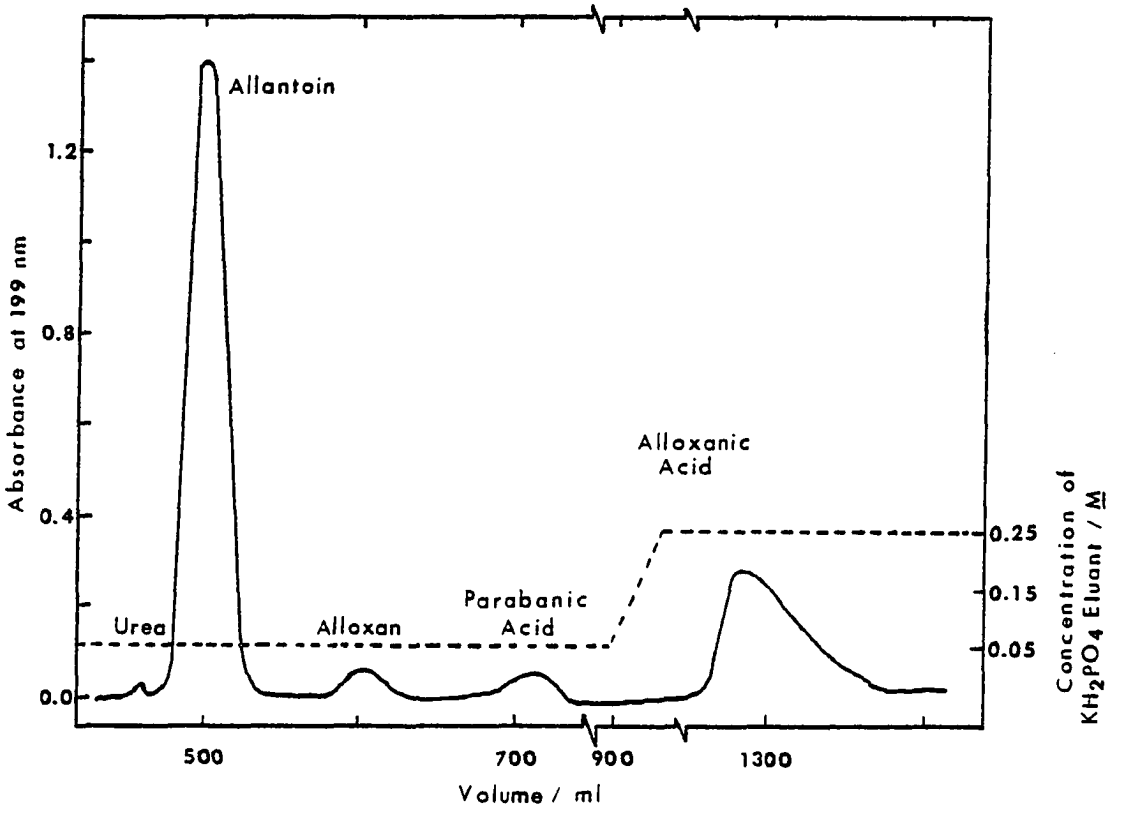

Figure 14. Chromatogram of uric acid (3.07 mg) oxidation products from a 0.025 M KH_2PO_4 pH 4.3 solution dissolved in 1 ml of water. The arrangement of chromatographic columns is shown in Figure 5. The column conditions are the same as those in Figure 6.

present studies was obtained. When 1.445 mg of uric acid was oxidized at +0.4V. vs SCE the following yields of products were obtained, allantoin (0.79 mole) and urea (0.22 mole), per mole of uric acid. Alloxanic acid was also detected, but not analyzed quantitatively. Figure 15 shows a typical pH 7.0 chromatogram.

It should be noted that the relative yields of products obtained at any pH were somewhat variable from one electrolysis to another, the values quoted here are simply typical values. It can also be seen that on occasion the sum of total products does not equal 100% of the initial uric acid. The product yields however can be regarded as equivalent to a complete material balance in view of the analytical accuracy achieved by this chromatographic technique.

Quantitative analytical data, obtained via liquid chromatography, on products of electrochemical oxidation of uric acid at the PGE is presented in Table 4. For comparison, Dryhurst's[3] analytical data is also presented. Overall, there appears to be good correlation between the two sets of data. Any differences may be assumed due to varying analytical techniques. This study, therefore, serves to reinforce the product analysis and mechanism proposed by Dryhurst.

II. Removal of Phosphate. In order to properly identify the products separated by the liquid chromatographic technique it became necessary to remove the aqueous phosphate eluant from each component. This would then allow techniques

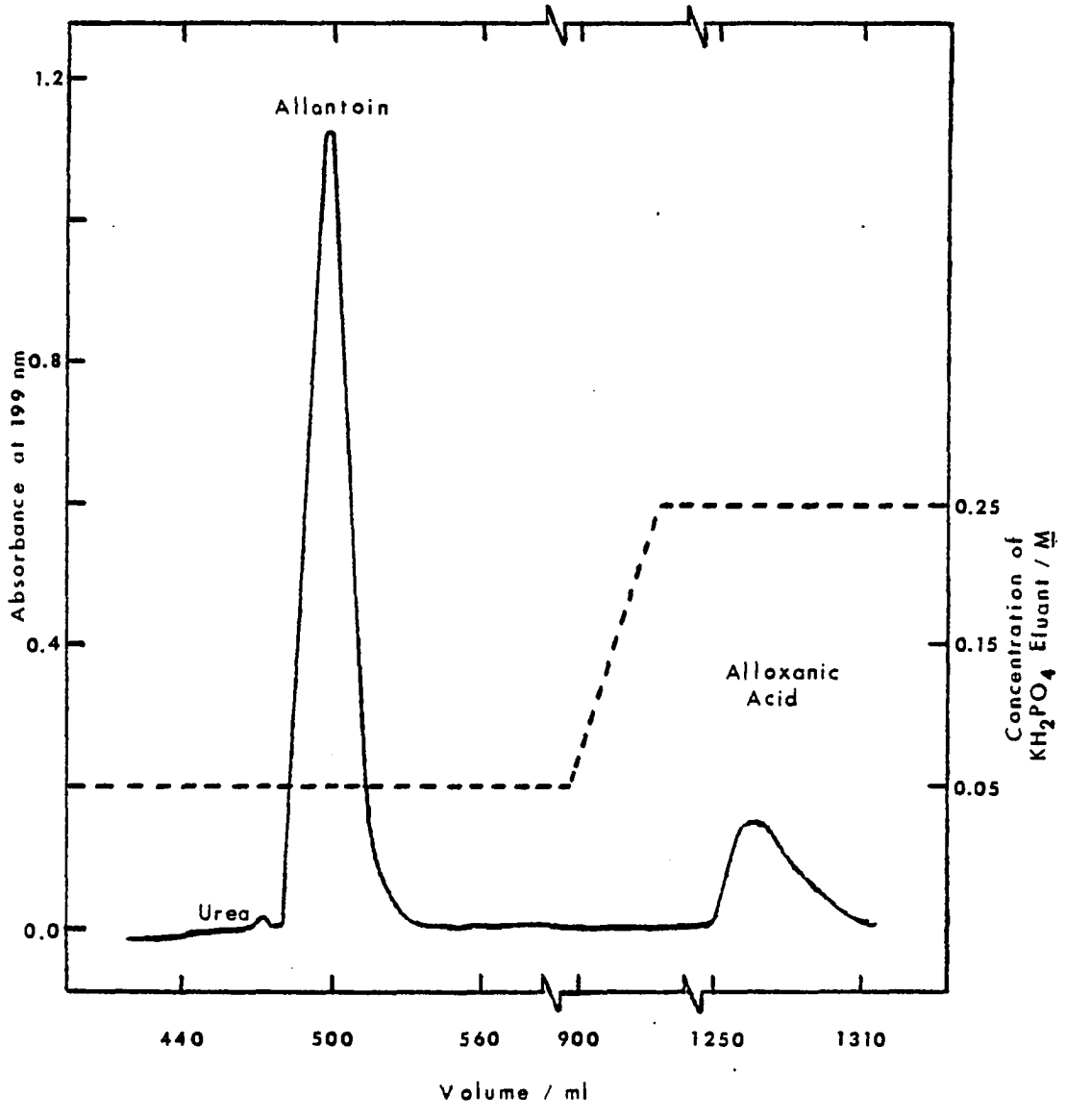

Figure 15. Chromatogram of uric acid (1.4 mg) oxidation products from a 0.025 M KH_2PO_4/K_2HPO_4 pH 7.0 solution dissolved in 1 ml of water. The arrangement of chromatographic columns is shown in Figure 5. The column conditions are the same as those in Figure 6.

TABLE 4

Quantitative analytical data on products of electrochemical oxidation of uric acid via liquid chromatography and past techniques.

pH	Buffer System	Product, mole/mole of uric acid electro-oxidized[a]			
		Alloxan	Urea	Allantoin	Parabanic Acid
		via liquid chromatography			
2.3	1M HOAc	0.54	0.78	0.16	0.24
4.3	phosphate	0.04	0.33	0.62	0.03
7.0	phosphate	ND[b]	0.22	0.79	ND
		via past techniques			
2.3	1M HOAc	0.8	0.8	0.2	0.03
4.7	acetate	0.37	0.37	0.63	ND
7.0	McIlvane	ND	0.18	0.82	ND

[a] Generally, between 1.0-5.0 mg of uric acid in 20 ml of buffer were oxidized.

[b] Not detected.

such as mass and infrared spectroscopy to be used to identify various components. Owens, et al.[26], have developed a chromatographic method to quantitatively separate a number of organic compounds from relatively large excesses of inorganic phosphate. Each component from the separation of uric acid oxidation products was eluted in a volume of about 40-50 ml of 0.025 M KH_2PO_4. By freeze-drying the latter solutions to about 1 ml, each organic component would be present in a solution of ca. 1 M inorganic phosphate.

Some typical chromatograms showing the separation of phosphate and allantoin and urea using Sephadex G-10 resin with water as the eluant are presented in Figure 16. Clearly, a satisfactory separation of the organic component from inorganic phosphate can be achieved. The yield of the organic component was exactly the same as the amount initially added to the column, i.e., a quantitative recovery of the organic component was possible.

For alloxan and parabanic acid under identical conditions it was observed that using water as the eluant a broad, ill-defined peak occurs between the phosphate and alloxan or parabanic acid peaks. The yield of alloxan or parabanic acid that could be recovered after freeze-drying the fractions under their respective peaks was significantly lower than the original amount of these compounds added to the column. The low yields of these compounds and the distorted form of the chromatograms suggested that both alloxan and parabanic

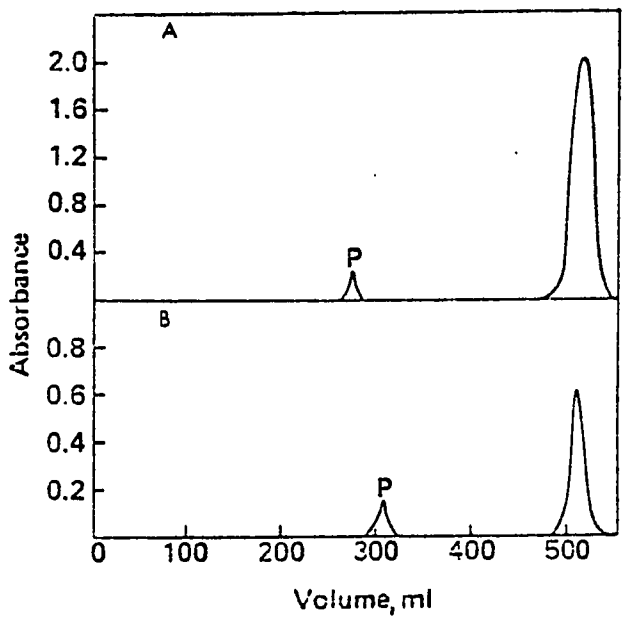

Figure 16. Typical chromatograms obtained for the separation of phosphate from (a) allantoin and (b) urea using water as the eluant. Flow rate was 50 mlh^{-1}. Absorbance monitored at (a) 215 nm and (b) 201 nm. P refers to the peak for phosphate.

decompose to some extent as the separation proceeds. It is well-known that above about pH 4-5 alloxan decomposes to alloxanic acid[27,28]. In addition at neutral pH parabanic acid decomposes to oxaluric acid[29].

In order to satisfactorily elute alloxan or parabanic acid from a Sephadex G-10 column and to separate these compounds from phosphate it was found that the pH of the eluant has to be significantly lowered. This was accomplished by using dilute HCl (0.001 M, pH 3) as the eluting solvent. Hydrochloric acid was used because it is subsequently easily removed from the organic component by freeze-drying. Figure 17 shows chromatograms for alloxan and parabanic acid in mixtures with phosphate using dilute HCl as the eluant. Clearly, in each case, a very good separation between inorganic phosphate and the organic component is noted with no distortion of the chromatographic peaks.

The chromatograms shown in Figures 16 and 17 indicate that the resolution of the phosphate and organic component peaks was excellant. For comparative purposes some peak resolution values (R_s) between each of the four organic components and phosphate are presented in Table 5.

All fractions under component peaks under conditions similar to those shown in Figures 16 and 17 gave no evidence for the presence of any phosphate.

III. Qualitative Characterization. The solid organic components after desalting and freeze-drying were tested for

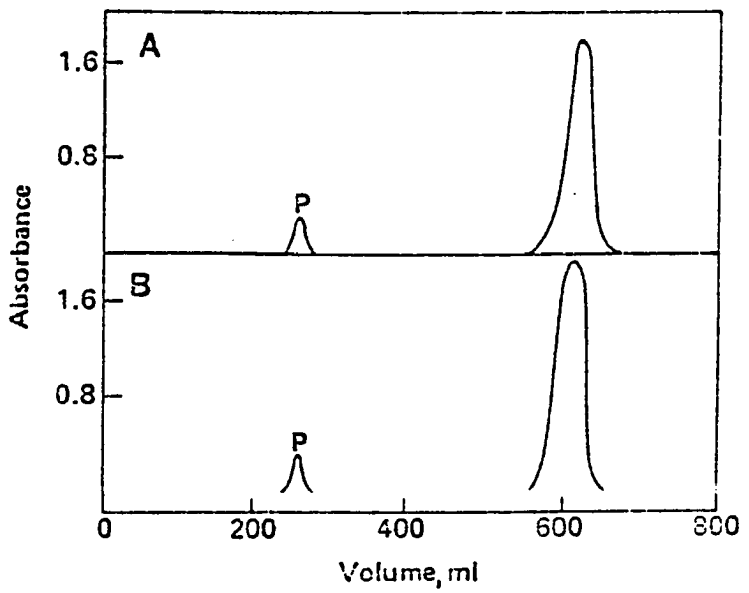

Figure 17. Typical chromatograms obtained for the separation of phosphate from (a) alloxan and (b) parabanic acid using 0.001 M HCl in water as the eluant. Flow rate was 50 mlh^{-1}. Absorbance monitored at (a) 206 nm and (b) 210 nm. P refers to the peak for phosphate.

TABLE 5

Resolution between phosphate and organic component chromatographic peaks on Sephadex G-10 column[a]

Compound	Eluant	Resolution[b]
Allantoin	H_2O	2
Parabanic Acid	Dilute HCl[c]	4.2
Urea	H_2O	4.3
Alloxan	Dilute HCl[c]	4.6

[a] Flow rate 54.0 ml h^{-1}.

[b] See page 26 for definition.

[c] 0.001 M HCl in water.

their authenticity. Typically, i. r. and mass spectra were taken of each component (Figures 18, 19, 20, and 21). These spectra were compared to spectra from authentic compounds. In each case the eluted organic compounds were found to be analytically pure and free from inorganic phosphate.

Experimental

Chemicals. Chemicals were obtained from the sources indicated: parabanic acid and allantoin (Eastman Organic Chemicals); alloxan (Nutritional Biochemicals Corporation); and urea (Merck Chemical Division). Column chromatography utilized Sephadex G-10 and QAE-Sephadex A-25 resins (Pharmacia Fine Chemicals, 40-120 μm).

Apparatus. A Buchler Fractomat fraction collector was utilized in the separation of the oxidation products. An ISCO Golden Retriever or an ISCO Model 1200 fraction collector was utilized for collection of desalted samples. Product separation was performed in Pharmacia Fine Chemicals Models SR 25/45 (2.5 cm x 45 cm) and SR 25/100 (2.5 cm x 100 cm) columns. For desalting, chromatographic columns 75 cm long and 2.75 cm in diameter were used. A Mariotte flask system was utilized to obtain constant and reproducible flow rates.

Column Packing Conditions. The coupled column separation system is the one reported earlier, and its packing is thus the same as described before. For the

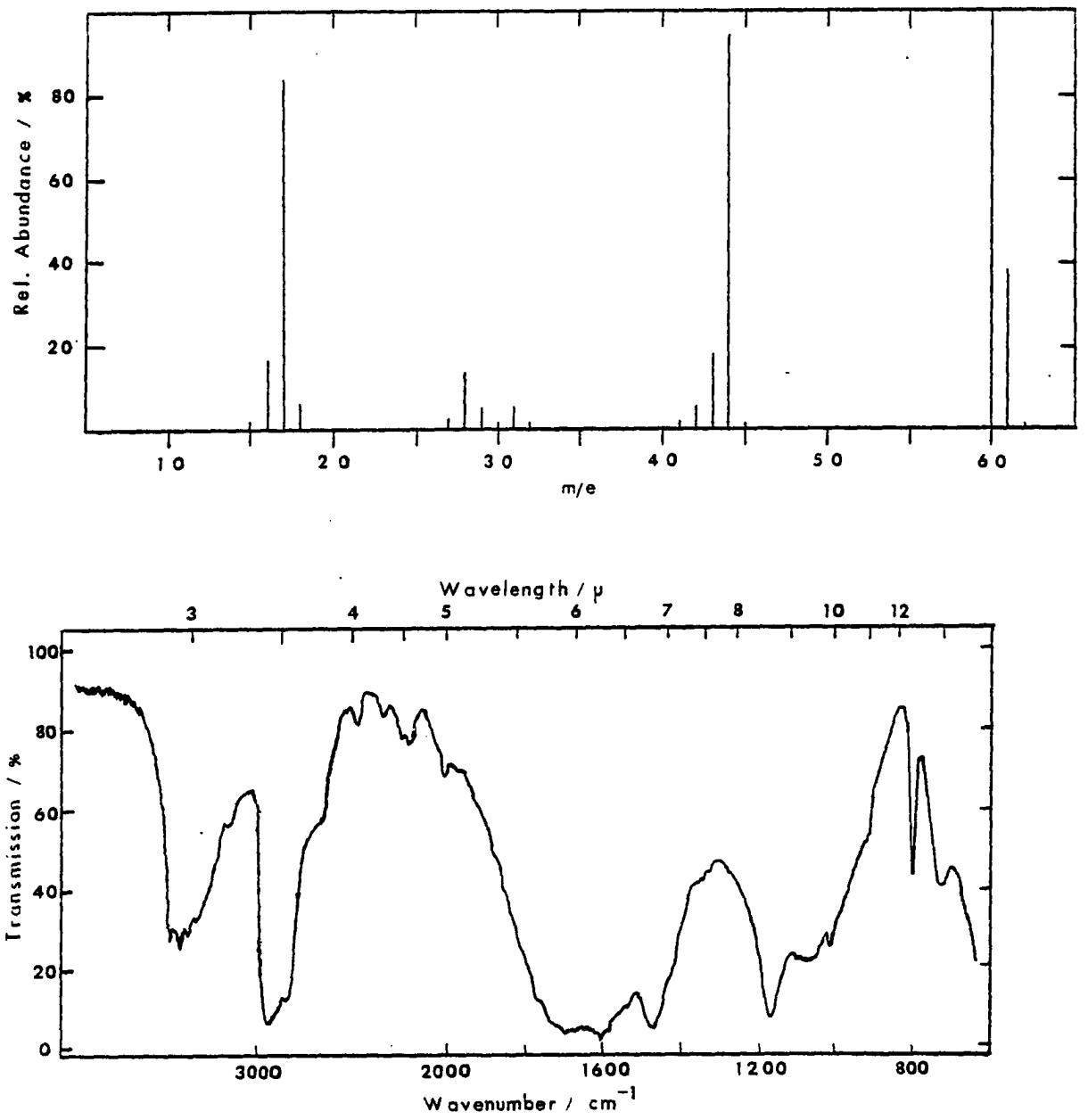

Figure 18. Mass (a) and i. r. (b) spectra of urea. I. r. is of KBr disc.

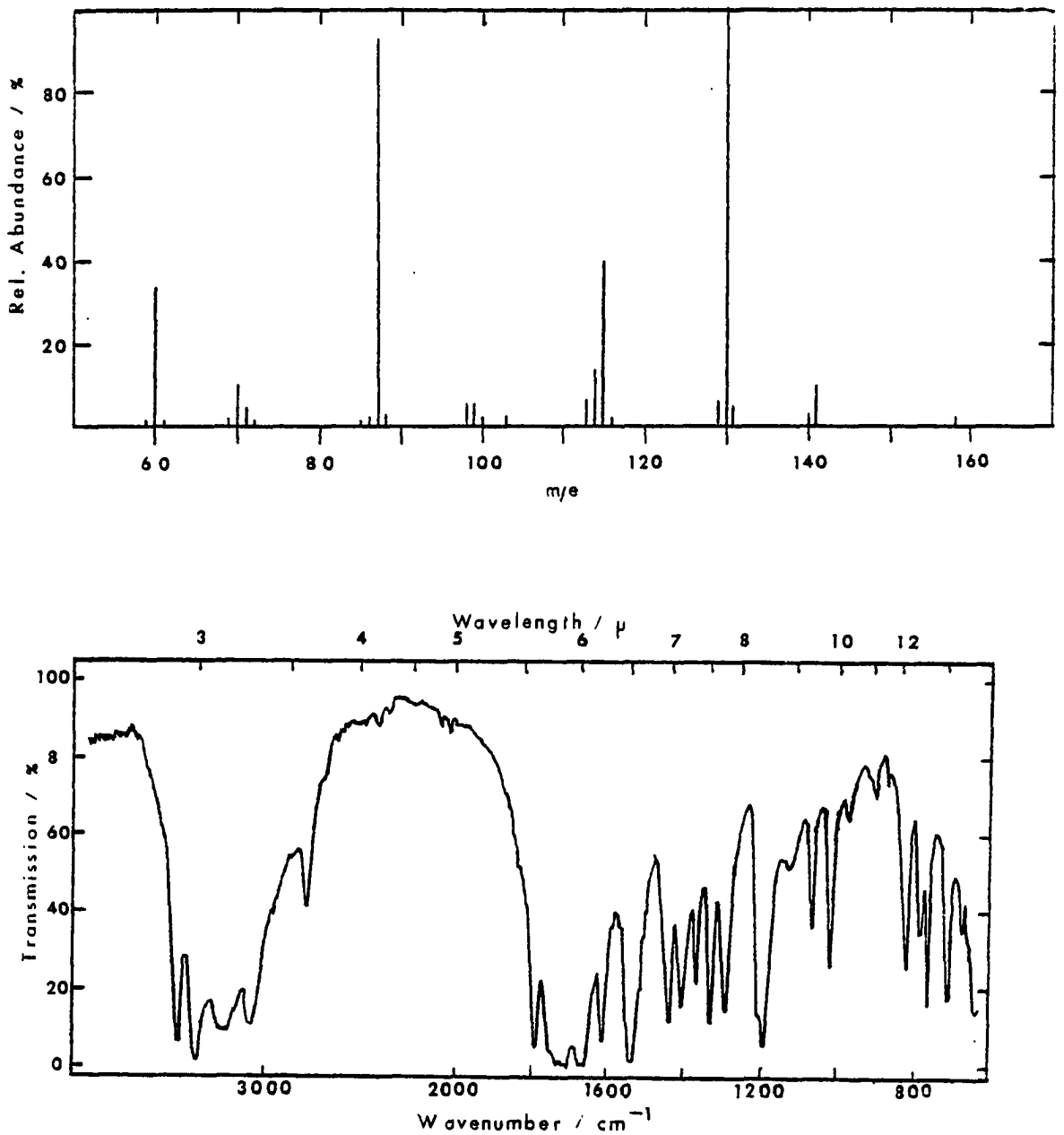

Figure 19. Mass (a) and i. r. (b) spectra of allantoin.
I. r. is of KBr disc.

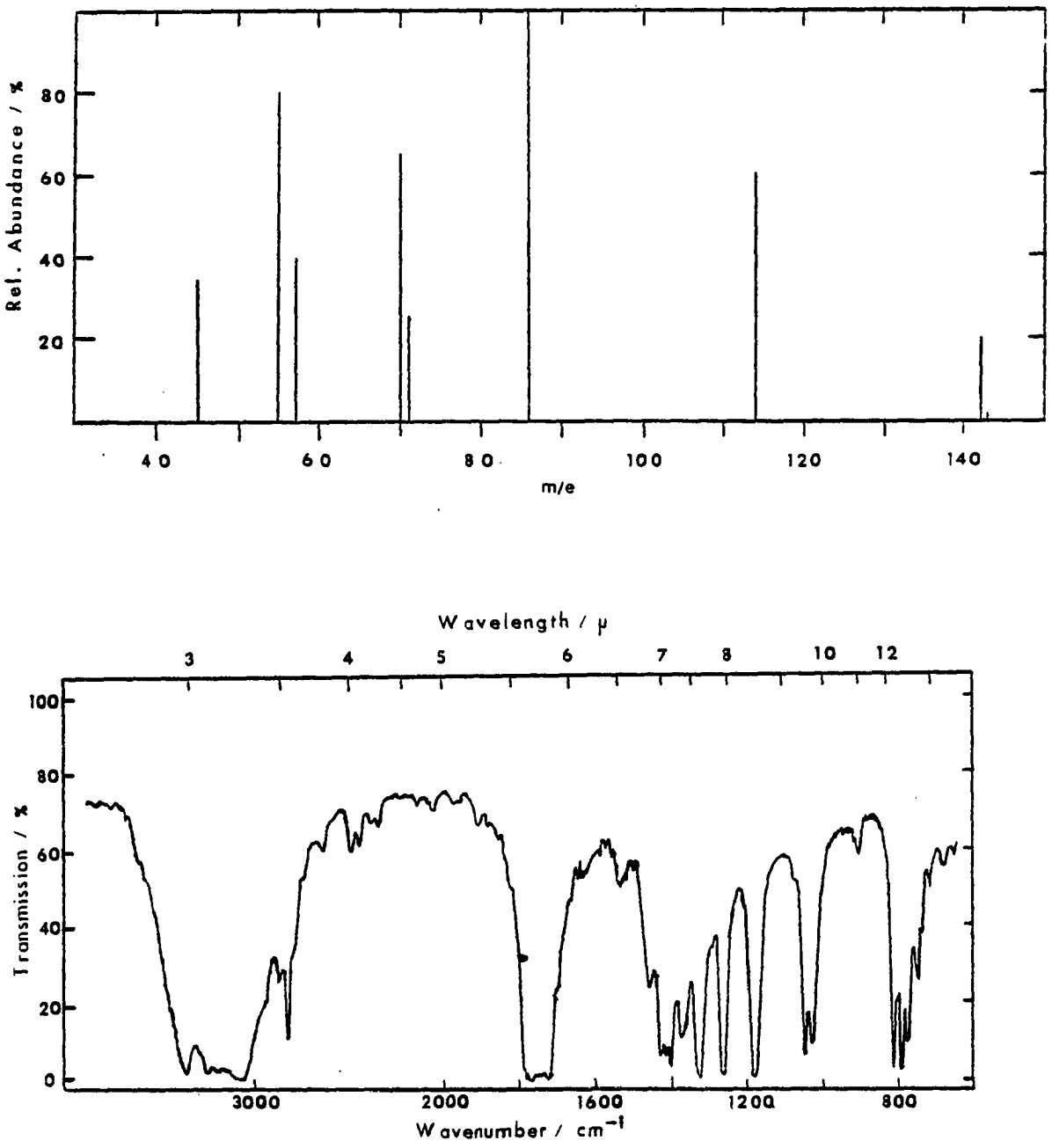

Figure 20. Mass (a) and i. r. (b) spectra of alloxan. I. r. is of KBr disc.

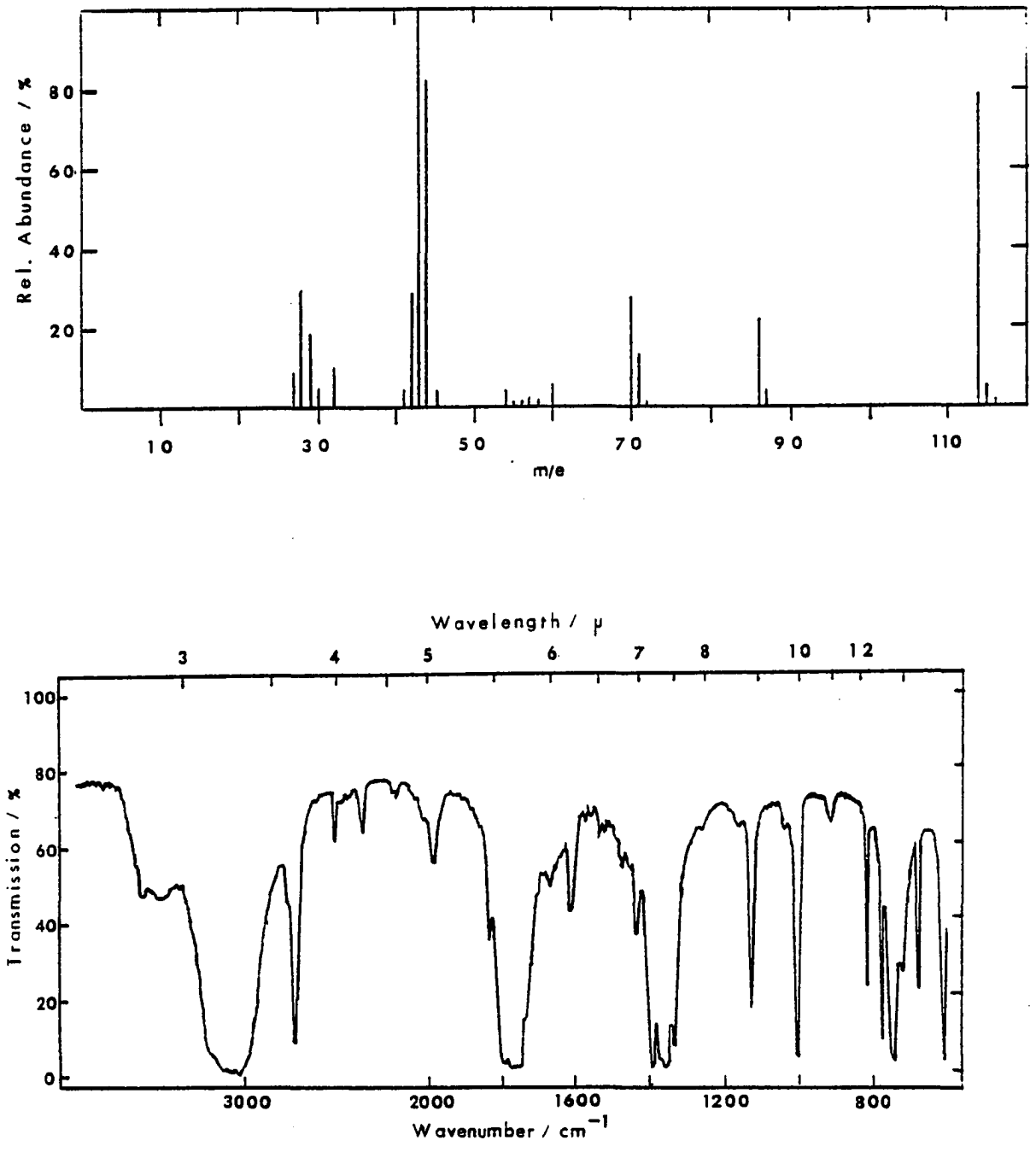

Figure 21. Mass (a) and i. r. (b) spectra of parabanic acid. I. r. is of KBr disc.

desalting columns, two hundred grams of the dry resin were allowed to swell in excess water and dilute HCl, respectfully, by heating on a boiling water bath for at least one hour with constant stirring. The slurry was then allowed to cool to room temperature (ca. 1 1/2 h). Excess water was removed from the gel in order to form a thick slurry. Then, with the aid of a long glass rod, the slurry was carefully poured into the column which contained about 100 ml of water. The column flow was started immediately since this was found to give the most even packing. An extention reservoir was placed on the top of the column so that all the required gel could be added at one time. This also aids in obtaining an evenly packed bed. The G-10 packing filled all but the upper 4-8 cm of the column. This space was filled with the eluant and a Mariotte flask was fitted to ensure a constant flow rate. Serveral bed volumes of eluant were passed through the column in order to stabilize and equilibrate the gel bed. Such columns were operated at room temperature with flow rates of 42.0 - 54.0 $ml h^{-1}$.

pH measurements were made with a Corning Model 10 pH meter. Infrared spectra were recorded on a Beckman AccuLab 3 Spectrophotometer. KBr discs were made with a Barnes Econo-Press. Ultraviolet absorption was measured in 4.5 cm x 1.0 cm quartz Beckman cuvettes on a Hitachi Model 124 spectrophotometer. Mass spectra were recorded on a Hitachi RMU-6E spectrometer. Lyophilization was accomplished using

a Virtis 12-port manifold and a Vactorr 25 vacuum pump. Cooling was provided by a Neslab CryoCool cooling unit.

Voltammograms were obtained with an instrument of conventional operational amplifier design[30], employing a function generator patterned after that of Myers and Shain[31,32]. Voltammograms were recorded on a Hewlett-Packard Model 7001A X-Y Recorder.

The pyrolytic graphite electrodes were machined from small rods of pyrolytic graphite to a diameter of 2mm and length ca. 8mm, and were sealed into lengths of 3mm bore glass tubing with Hysol Epoxi-Patch (Hysol Corp., Olean, N. Y.). The electrodes were ground flush with the end of the glass tube, and were resurfaced before each voltammogram with 600-grit silicon carbide paper (Buehler Ltd., Evanston, Ill.) mounted on a rotating disc. The electrode was then sprayed with a stream of deionized water to remove the graphite powder from the surface, and dried by touching the surface with absorbent tissue paper.

A three-compartment cell with each compartment separated by a medium or fine-porosity sintered glass frit was used. Salt bridges inserted on the counter and reference sides of the frits were prepared by dissolving 4 grams of agar in 90 ml water and then adding 0.5 grams KH_2PO_4. A mercurous chloride reference electrode (SCE) and a platinum foil counter electrode were used.

Controlled potential electrolyses were carried out using

a Princeton Applied Research (PAR) Corporation Model 373 Potentiostat/Galvanostat. Current integration during controlled potential coulometry was performed with a PAR Model 379 Digital Coulometer. Both electrolyses and coulometry were performed in the same three-compartment cell with a platinum gauze counter electrode, SCE reference electrode, and a working compartment volume of 20 ml was used.

Voltammetric Procedure. Test solutions ca. 0.3 mM to 1.5 mM in uric acid were prepared. Test solutions were made up in buffers, using deionized water, yielding ionic strength of 0.05 M.

Coulometric and Electrolysis Procedure. For controlled potential coulometry and electrolysis at the pyrolytic graphite electrode, 20 ml of ca. 0.3 - 1.5 mM solution of uric acid in pH 2.3, 4.3 or 7.0 buffer was placed in the working electrode compartment of the electrochemical cell. The test solution was stirred and deaerated with nitrogen. Deaeration was continued throughout the electrolysis. When the current had decreased to a low, constant value, a reading of the number of coulombs passed was taken. Electrolysis was allowed to continue for 30-60 minutes longer and another coulomb reading taken. The background coulombs were calculated by the formula given below and subtracted from the total coulombs, yielding the net coulombs from which the n-value was determined.

$$\frac{(\text{Coulombs at time}_2 - \text{Coulombs at time}_1)}{\text{time}_2 - \text{time}_1} \times \text{total time}$$

= Background Coulombs

Completion of the oxidation was confirmed by the absence of either the uric acid voltammetric oxidation peak or the absence of uric acid's unltraviolet absorption peaks.

Isolation and Characterization of Electrolysis Products.

I. Separation Procedure. Lyophilization of the electrolysis solution upon complete oxidation of 1-5 mg of uric acid yielded a white residue. This lyophilized residue was dissolved in 1 ml of deionized water when the oxidation was performed in KH_2PO_4 buffer. With a supporting electrolyte of 1 M HOAc for the electrolysis, the lyophilized residue was dissolved in 1 ml of 0.025 M KH_2PO_4. The concentrated electrolysis solution was then applied to the coupled liquid chromatographic separation system. The actual separation procedure was outlined previously.

II. Procedure for removal of phosphate. Separate test tubes containing the products were combined, giving total volumes of ca. 40-60 ml. These solutions were lyophilized. Then each component, dissolved in 1 ml of deionized water, was carefully applied to the top of its respective Sephadex G-10 column after first very carefully draining any eluant above the surface of the column. (The upper surface of the gel bed was protected with a disc of Whatman No. 1 filter

paper.) The sample was carefully absorbed into the top of the column and the column walls and gel surface washed by careful addition of 1-2 ml of eluant. These washings were allowed to drain into the column and one or two identical washings were performed. The column was then filled with eluant and connected to a Mariotte flask. Fractions of 3 ml volume were collected with a fraction collector. In the case of each organic compound, the first peak to be eluted was that of phosphate which at high concentrations gives a readily detectable u. v. absorption. The presence of phosphate in the chromatographic effluent was detected by adding a few drops of 3M nitric acid to ca. 1 ml of test solution followed by 100-200 mg of ammonium molybdate. The resulting solution was gently heated. The presence of phosphate was indicated by formation of a bright yellow precipitate of ammonium phosphomolybdate, $(NH_4)_3PO_4 \cdot 12\ MoO_3$[33].

III. Product identification. Those fractions containing the organic component were combined and freeze-dried. The resulting residue was tested to confirm its identity, usually by i. r. and mass spectrometry (Figs. 18, 19, 20, and 21).

IV. Analytical Studies. Analytical yields were obtained for each component by comparing peak height and peak area data with that in Figs. 7 and 8.

The chromatographic peaks were obtained as plots of absorbance vs. volume. When determining area the parameters

used were peak height and the peak width at half-height.

V. Column Regeneration. It should be noted that after several separations on the dual column apparatus, alloxan and parabanic acid or their hydrolysis products, alloxanic acid and oxaluric acid, begin to adsorb to a noticable extent of the anion exchange resin. In fact, their expected yields were not obtained. To remove these adsorbed substances the anion exchange column was washed with 1000 ml of 0.25 M KH_2PO_4. This should remove any substances bound by ionic forces. Washing in this manner caused a significant shrinkage in the anion resin bed. Under these circumstances a reverse flow of 0.025 M KH_2PO_4 through the anion exchange column at a flow rate of about 20 mlh^{-1} for 5 hours serves to restore the column to its original condition.

VI. Detection of alloxanic acid. Alloxanic acid was prepared by dissolving 5 mg alloxan in 1 liter of pH 8 phosphate buffer (ionic strength 0.1 M) and allowing this solution to stand for 48 hours. Two solvent systems were used in thin layer chromatographic detection of alloxanic acid: 1-BuOH-HOAc-H_2O (12:3:5) and n-PrOH-H_2O (7:3). Prepared compound and the lyophilized electrolysis product were applied to thin layer sheets as very small crystals and were dissolved by repeated addition of water. Two thin layer supports were employed, silica gel with Fluorescent Indicator (Eastman

Chromogram 6060) and cellulose with Fluorescent Indicator (Brinkmann Polygram CEL 300 UV_{254}). r_f values for the electrolysis product using both solvent systems were identical on both supports to prepared alloxanic acid.

CHAPTER VI

SUMMARY

The dual gel permeation-anion exchange column liquid chromatographic method has been shown to be useful for separation of common electrochemical oxidation products of purines. Base-line separations were achieved using milligram quantities of materials sufficient to allow their isolation and identification by conventional chemical and instrumental methods. In the case of urea, alloxan, allantoin, and parabanic acid the height or area of the chromatographic peaks may be used for quantitative analysis of these components in reaction mixtures.

At the values of pH where uric acid electrooxidation was examined, 1 M HOAc, pH 2.3; 0.025 M KH_2PO_4, pH 4.3; and 0.025 M KH_2PO_4/K_2HPO_4, pH 7.0, the products obtained were qualitatively identical and in most cases quantitatively the same as those proposed in earlier work from this laboratory.

The general methodology reported should be applicable to the separation and analysis of the products formed upon electrochemical (and biochemical) oxidation of other more complex purine systems and perhaps for the analysis of the oxidation products of other N-heterocyclic systems.

CHAPTER VII

REFERENCES

1. G. Dryhurst, Electrochemistry of Biological Molecules, Academic Press, New York, 1977.

2. G. Dryhurst, Topics in Current Chemistry, 34, 47(1972).

3. G. Dryhurst, J. Electrochem. Soc., 119, 1559(1972).

4. G. Dryhurst and P. J. Elving, J. Electrochem. Soc., 115, 1014(1968).

5. B. L. Karger, L. R. Snyder, and C. Horvath, An Introduction to Separation Science, Wiley, New York, 1973.

6. M. J. R. Cantow and J. F. Johnson, J. Polymer Sci., Part A-2, 6, 1348(1968).

7. G. K. Ackers, Biochemistry, 3, 723(1964).

8. W. W. Yau and C. P. Malone, J. Polymer Sci., Part B, 5, 663(1969).

9. D. O. Hayward and B. M. W. Trapnell, Chemisorption, Butterworth, London, 1964.

10. L. R. Snyder, The Principles of Adsorption Chromatography, Dekker, New York, 1968.

11. O. Samuelson, Ion Exchange Separation in Analytical Chemistry, 2nd ed., Wiley, New York, 1968.

12. R. L. Pecsok and L. D. Shields, Modern Methods of Chemical Analysis, Wiley, New York, 1968.

13. G. M. Richardson and R. R. Cannon, Biochem. J., 23, 68(1929).

14. D. Seligson and H. Seligson, J. Biol. Chem., 190, 647(1951).

15. J. C. Andrews and I. T. Sell, Arch. Biochem. Biophys., 56, 405(1955).

16. R. C. Weast (Ed.), CRC Handbook of Chemistry and Physics, 1972-1973.

17. W. A. Struck and P. J. Elving, J. Am. Chem. Soc., 86, 1229(1964).

18. D. H. Rodgers, American Lab., 9, 122(1977).

19. W. W. Pit, C. D. Scott, W. F. Johnson, and G. Jones, Clin. Chem., 16, 657(1970).

20. J. Porath and P. Flodin, Nature, 183, 1657(1959).

21. B. Gelotte, J. Chromatog., 3, 330(1960).

22. A. J. W. Brook and S. Housley, J. Chromatography, 42, 112(1969).

23. M. T. Cleary and G. Dryhurst, Anal. Chim. Acta, 94, 343 (1977).

24. J. E. B. Randles, Trans. Faraday Soc., 44, 327(1948).

25. A. Sevcik, Collect Czech, Chem. Commun., 13, 349(1948).

26. J. L. Owens, H. H. Thomas, and G. Dryhurst, Anal. Chim. Acta, 96, 89(1978).

27. G. M. Richardson and R. R. Cannon, Biochem. J., 23, 68(1929).

28. D. Seligson and H. Seligon, J. Biol. Chem., 190, 647(1951).

29. G. Dryhurst, B. H. Hansen, and E. B. Harkins, J. Electroanal. Chem., 27, 375(1970).

30. G. Dryhurst, M. Rosen, and P. J. Elving, Anal. Chim. Acta, 42, 143(1968).

31. R. L. Meyers and I. Shain, Chem. Instr., 2, 203(1969).

32. D. L. Mcallister and G. Dryhurst, Anal. Chim. Acta, 64, 121(1973).

33. C. H. Sorum, Introduction to Semimicro Qualitative Analysis, 3rd ed., Prentice-Hall, Englewood Cliffs, New Jersey, 1960, P. 200.

PART II

THE ELECTROCHEMICAL OXIDATION OF 9-METHYLXANTHINE AND XANTHOSINE

CHAPTER I

INTRODUCTION

Some purines are found in all living cells. Most arise as constituents of macromolecules, however in certain biological systems free purines are indeed found.

First named by Emil Fischer[1], purine (I) consists of fused pyrimidine and imidazole rings.

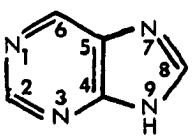

I

The numbering system most widely employed is that of Fischer[2]. A detailed account of the nomenclature of purines has been prepared by Robins[3] as a result of the confusion occurring through the use of trivial as well as typical chemical names in purine chemistry. In order to simplify nomenclature in this text, either trivial names or other nomenclature that more accurately describes the proper structure of the species

will be employed.

Purines are customarily found in biological systems as higher molecular weight derivatives. The carbohydrate derivative called a nucleoside, for example, is one in which the purine is linked through its N-9 position via a β-N-glycoside bond to either D-ribose or 2-deoxy-D-ribose. Thus, there are two types of nucleosides as a result of the two sugar moities: the ribonucleosides and the deoxyribonucleosides. Purine nucleotides are the phosphate esters of the nucleosides with the esterification occurring primarily at the C-5′ hydroxyl group of the ribose or deoxyribose. The purine nucleotides in conjunction with the pyrimidine nucleotides can form highly polymerized structures called nucleic acids.

Generally, purines are a stable class of molecules. Despite their involvement in biological processes many purine derivatives have low solubility in water[4-6]. The infrared spectra of purines have been studied in the solid state and reveal that purines exist predominantly in the keto form[7].

Uric acid and other oxypurines are the principle final products of purine catabolism in man[8,9], although further degradation of the purine molecule takes place in many organisms. Uric acid is found in human urine, blood, milk, spinal fluid, and elsewhere[3]. Xanthine (2,6-dioxypurine) which was discovered as a constituent of bladder stones[10],

has been found in tea, milk, human urine and other miscellaneous biological sources[3]. Hypoxanthine (6-oxypurine) is also found in various animal tissues and fluids. N-Methylated xanthines are widely present in nature. Caffine (1,3,7-trimethylxanthine) was found by Runge[11] in coffee. Woskresensky[12] discovered theobromine (3,7-dimethylxanthine) in cocoa beans, and Kossel[13] extracted theophylline (1,3-dimethylxanthine) from tea leaves. Many of the methylated xanthines possess pharmacological significance. 1,7-dimethylxanthine has marked antithyroid activity[14]. Methylated xanthines are widely used as diuretics[15]. Caffeine, theobromine, and theophylline are noted for their stimulation of the central nervous system[16].

Nitrogen heterocyclic molecules, of which purines are a class, appear chosen to be incorporated in many of the fundamental reactions of nature. Most of the nitrogen heterocyclic molecules observed in living organisms contain extensive delocalized or mobile (π) electron systems. These compounds are usually quite good electron acceptors and/or donors. Very many biologically important nitrogen heterocyclic molecules can be studied by various electrochemical techniques because of this property. The use of modern electrochemical techniques can provide information on the nature of electron transfer processes. Also, under favorable conditions it is possible to detect unstable intermediates and follow-up products. An added advantage to the examination of electron-

transfer reactions electrochemically is the relative ease with which the experimental conditions may be varied. Whereas in most other chemical or biological studies this can not be performed satisfactorily. Accordingly, it is possible to study an electrode reaction over a wide range of pH, in different buffer systems, and to employ a variety of temperatures. The manipulation of these parameters may allow the deduction of the reaction mechanism using electrochemical methods where it would be more difficult or impossible employing in vivo studies.

There are several similarities between enzymatic and electrochemical reactions which make the application of electrochemical investigations to biological systems quite justifiable. Several of these are[17]:

1. Electrochemical and biological oxidation-reduction reactions comprise essentially heterogenous electron-transfer processes. Electrochemically, this process occurs at the electrode-solution interface; biologically, it occurs at an enzyme-solution interface.
2. Both reactions can take place at similar pH and in the presence of similar ionic strengths of inert electrolyte.
3. Both normally take place at similar temperatures.
4. In both cases it is likely that the substrate molecule has to be oriented in a rather specific

manner before the electron transfer can occur.

It is inaccurate to assume these statements are meant to imply that the unique selectivity associated with an enzyme can be duplicated by an electrode. Likewise, no thermodynamically impossible reaction may be caused to proceed by an enzyme; all of the basic principles of chemistry still apply to an enzyme-catalyzed reaction. This is not to say that all electrochemical oxidation reactions of purine derivatives will mimic their biological transformations. Rather, the similarity between electrochemical and biological reactions, which can not be duplicated in other chemical systems warrants the study of the electrochemistry of biologically important molecules.

One of the early purines investigated in our laboratory was uric acid. The reason for this was the behavior of this compound appears to be characteristic of a number of purine bases. Also, there has been extensive work reported on the enzymatic oxidation of this compound. A recent report[18] has proposed that the mechanism of electrooxidation of uric acid (I, Figure 1) proceeds by an initial $2e^{\ominus}$, $2H^{\oplus}$ oxidation to give an unstable diimine species (II, Figure 1) which is then hydrated in two steps to give first an imine-alcohol (III, Figure 1) and then a diol (IV, Figure 1). This latter compound decomposes to a number of ultimate products, depending on the pH of the solution, as indicated in Part I of this dissertation. With the use of a variety

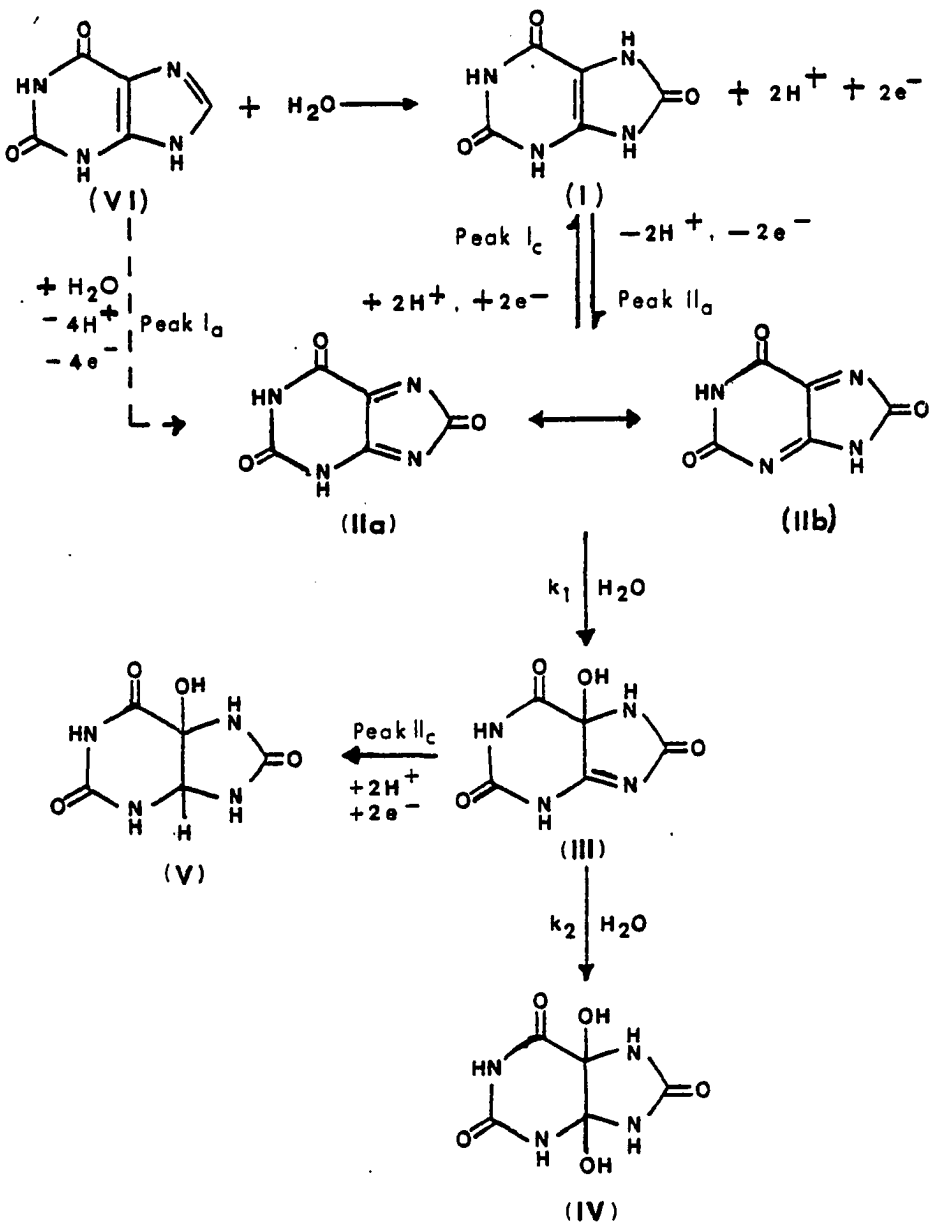

Figure 1. Proposed mechanism for the electrochemical oxidation of uric acid and xanthine at the pyrolytic graphite electrode.

of electroanalytical techniques, it has recently been demonstrated[18] that the primary electrooxidation product, i.e., the proposed diimine (II, Figure 1), is very unstable in solution and is rapidly hydrated to a second intermediate in a first order reaction. A voltammetric peak due to the reduction of the putative diimine may be observed on cyclic voltammetry of uric acid at quite slow sweep rates (e. g., 200 mVs^{-1}), in spite of its instability in homogeneous solution. The proposed imine-alcohol (III, Figure 1) formed by partial hydration of the diimine was observed as a second intermediate which also undergoes first order hydration to uric acid-4,5-diol (IV, Figure 1). It must be noted that the diimine, imine-alcohol, and diol species proposed as intermediates in the electrooxidation of uric acid have not been isolated. However the proposed mechanism has been strongly supported by studies of the electrochemical oxidation of a number of N-methylated uric acid derivatives[19].

The enzymatic oxidation of uric acid has been studied by a number of investigators. In the presence of uricase/O_2[20-22], peroxidase/H_2O[23,24], methemoglobin/H_2O_2[25], and cytochrome c[26] the major organic product at low pH is alloxan while at around pH 7 the major product is allantoin. Paul and Avi-Dor[23] found that the neutral form of 1-methyluric acid is oxidized in the presence of horseradish peroxidase and H_2O_2 via a u. v.-absorbing intermediate which apparently decomposes to alloxan or allantoin in a first order reaction. The mechanism

which they proposed for this reaction was that 1-methyluric acid (I, Figure 2) was oxidized in a $2e^{\ominus}$, $2H^{\oplus}$ reaction to give an intermediate diimine (II, Figure 2); this species being the proposed u. v.-absorbing intermediate. By uptake of two molecules of water the diimine was proposed to give a 4,5-diol derivative of 1-methyluric acid (III, Figure 2) which decomposes to the ultimate products. Canellakis et.al.[24] also proposed that uric acid-4,5-diol is an intermediate species formed upon oxidation of uric acid in the presence of various peroxidase enzymes. Spectral, electroanalytical, and kinetic data reported by Wrona and Dryhurst[27] support the conclusion that for all methylated uric acid derivatives the electrochemical and enzymatic reactions proceed, in a chemical sense, by identical mechanisms.

Xanthine (VI, Figure 1) is electrochemically oxidized by way of a single, pH-dependent voltammetric peak. Coulometry of xanthine in solutions of pH 1-7 reveals that complete oxidation involves four electrons[28]. The first and potential controlling reaction is probably a $2H^{\oplus}$, $2e^{\ominus}$ oxidation of the N-9=C-8 (or C-8=N-7) bond of xanthine to give uric acid (I, Figure 1). Uric acid, which is more readily oxidized than xanthine, immediately oxidizes further in a $2H^{\oplus}$, $2e^{\ominus}$ process to the diimine (II, Figure 1), which then undergoes the same secondary reactions as described previously, so that the same products in about the same yields are obtained from xanthine as are obtained from uric acid[28]. The involvement

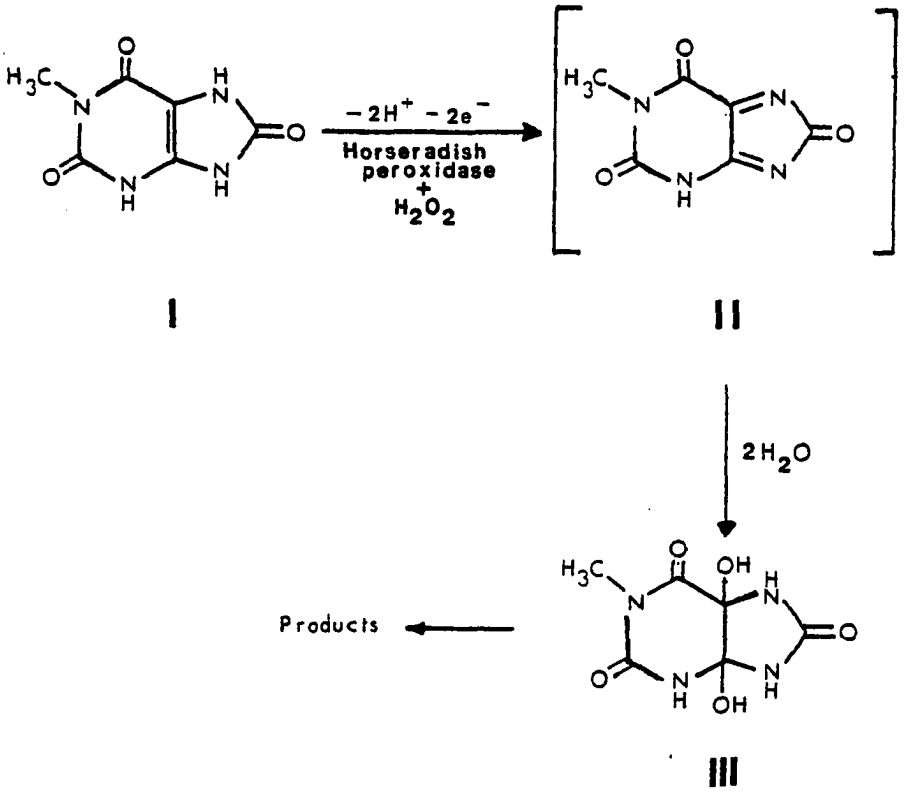

Figure 2. Proposed mechanism for the enzymatic oxidation of 1-methyluric acid in the presence of horseradish peroxidase and H_2O_2.

of uric acid and its diimine in the electrochemical oxidation of xanthine is clearly established from recent work in our laboratory[18]. A cyclic voltammogram for xanthine is shown in Figure 3. The first sweep toward positive potentials shows only a single peak (peak Ia, Figure 3) corresponding to the $4H^{\oplus}$, $4e^{\ominus}$ oxidation of xanthine (VI, Figure 1) to the diimine (II, Figure 1). The diimine can be detected as a reduction peak (peak Ic, Figure 3). Peak Ic corresponds to reduction of the diimine to uric acid (I, Figure 1). On the second positive-going sweep the uric acid formed in the latter reaction is reoxidized to the diimine and gives rise to peak IIa (Figure 3). The more negative, second cathodic peak observed in Figure 3 (peak IIc) has been proposed[19] to be due to reduction of the partially hydrated diimine (III, Figure 1) to compound V (Figure 3).

Studies of the electrochemical oxidation of several N-methylated xanthines[29,30] revealed similar results to xanthine itself with the obvious methylated differences in the observed products. Theophylline (1,3-dimethylxanthine) was an exception to this rule[31]. The products of the electro-oxidation of theophylline differ from those obtained from other xanthines in that a theophylline dimer, 8-(1,3-dimethyl-xanthyl)-1,3-dimethylxanthine is also formed (V, Figure 4). As a result of dimer formation it is obvious that the first two electrons must be removed from theophylline (I, Figure 4) in a stepwise manner, resulting in the formation of a free

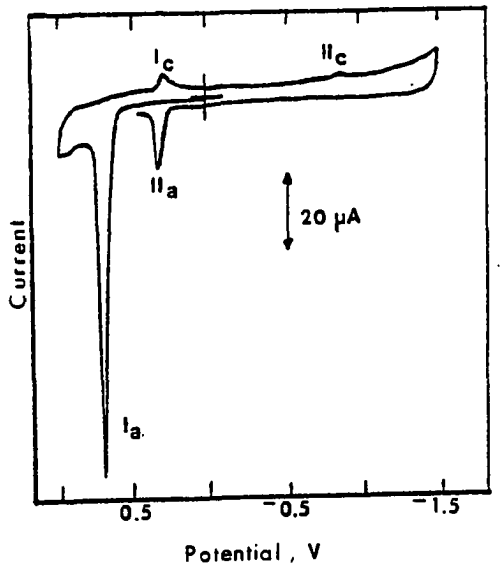

Figure 3. Cyclic voltammogram of xanthine in pH 7 phosphate buffer at a clean PGE. Scan rate, 200 $mVsec^{-1}$.

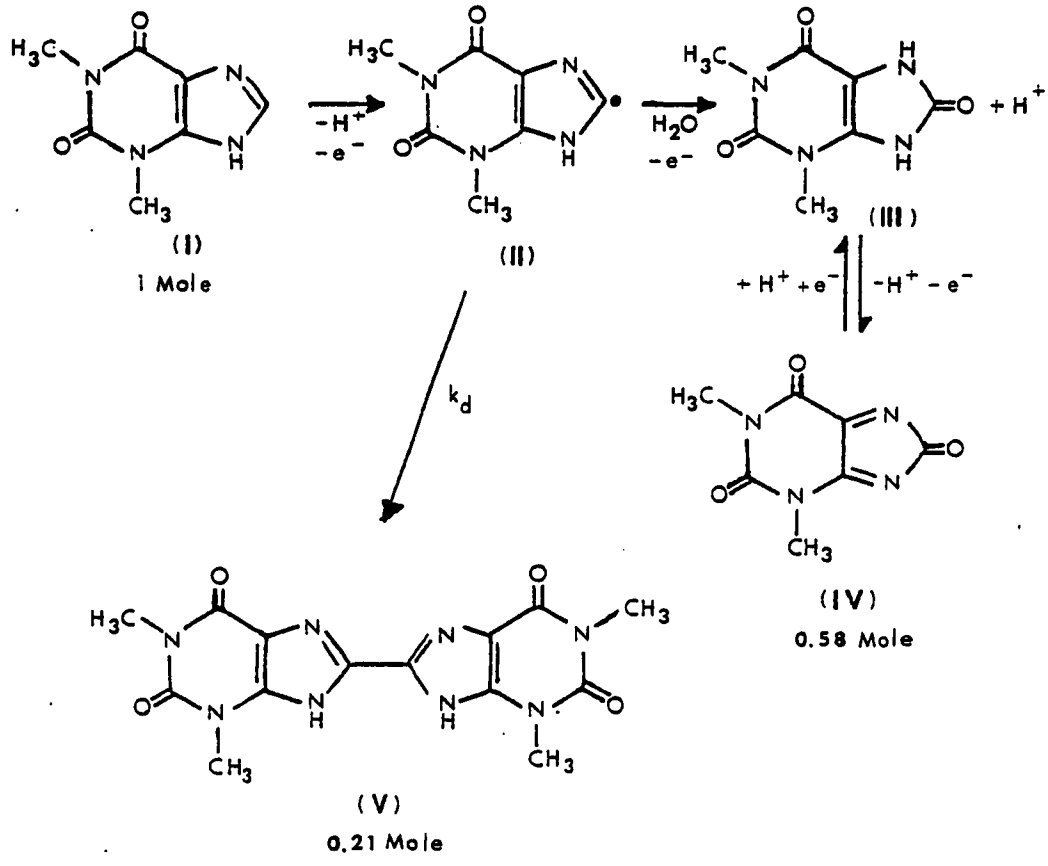

Figure 4. Products and mechanism for the primary electrode processes of the electrochemical oxidation of theophylline at the PGE. Molar amounts of products are those formed in 1M HOAc.

radical (II, Figure 4). About 40% of the free radical dimerizes to give V (Figure 4), while the remainder is further oxidized to 1,3-dimethyluric acid (III, Figure 4). This is then further oxidized to the diimine (IV, Figure 4). This diimine is susceptible to hydrolysis in the normal manner.

The biochemical oxidation of xanthines has centered around the enzyme xanthine oxidase. Xanthine oxidase has been shown to be a rather nonspecific enzyme[8]. Bergmann and Dikstein[32], by examining a large number of purines and their response to xanthine oxidase, found that there were three distinct groups of purines:

1. Those that react with xanthine oxidase at a rate of oxidation comparable to that of xanthine, e.g., 1-methylxanthine, 6.8-dioxypurine, hypoxanthine, and purine.

2. Those that were attacked at one-tenth to one-ten thousandth the rate of xanthine, e.g., 2- and 8-oxypurine and 2,8-dioxypurine.

3. Those that were not attacked at a measurable rate, e.g., 1- and 7-methyhypoxanthine, 3-,7-, and 9-methylxanthine, and caffeine (1,3,7-trimethylxanthine).

Through this and a subsequent study[33], a generalized route for oxidation of purines to uric acids by xanthine oxidase was formulated. It was assumed that purines undergo hydration at one -HC=N- grouping either prior to or simultaneously with a dehydrogenation step. Therefore, the process

would involve either of the two pathways depicted in Figure 5. Pathway a would give a lactim form of the oxidized purine, while b would give the corresponding lactam. It was proposed that, in multistage oxidations, the enzyme-substrate complex dissociates after each individual step to recombine with the newly oxidized purine in a different fashion. This was confirmed by spectrophotometric and chromatographic data.

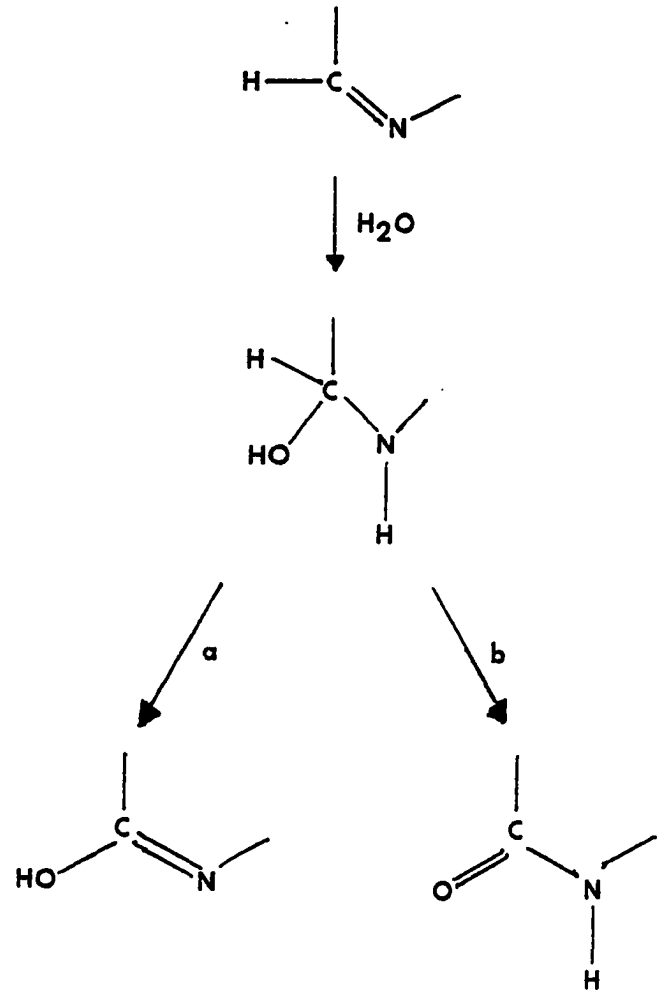

Figure 5. Generalized route for oxidation of purines by xanthine oxidase[33].

CHAPTER II

ELECTROCHEMICAL OXIDATION OF 9-METHYLXANTHINE

Introduction

In order to obtain information relating to the effect of substitution at the 9-position of xanthine which might be applied later to the understanding of the electrochemistry of the more complex, biologically important nucleoside, a detailed study of the electrochemistry of 9-methylxanthine (II) was initiated.

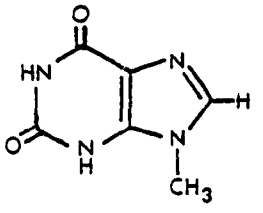

II

Previous work has shown that 9-methylxanthine is electrochemically oxidizable at the PGE[34]. However, the latter work was limited to a study of voltammetry and some spectroelectrochemistry of 9-methylxanthine, and consequently no information is available concerning final products or mechanisms.

The present study was directed toward a detailed examination of the electrochemical oxidation of 9-methylxanthine, including a determination of rate constants,

isolation and identification of reaction products, and elucidation of reaction mechanisms. Experiments revealed that 9-methylxanthine is not electrochemically reducible at the pyrolytic graphite electrode over the pH range 2-9.

Results and Discussion

Physical properties of 9-methylxanthine

Solutions of 9-methylxanthine at a concentration of 1 mM are stable in pH 7 and pH 4 phosphate buffer up to 72 hours as determined by voltammetry of these solutions. The difference in n. m. r. chemical shifts of several xanthines[35] provides results which support the idea that in aqueous solutions of xanthines the lactam form is predominant. U. v. spectra establish the order of anion formation in 9-methylxanthine as position N-3 then position N-1[35], with pK_a values for ionization of 5.9 and ca. 10.5, respectively. Jordan has reported the pK_a for 9-methylxanthine as 6.3[36]. Figure 6 shows the variation of λ_{max} with pH for the two u. v.-absorbing peaks of 9-methylxanthine from data obtained in our laboratory. These results correlate well with those reported in references 35 and 36.

Linear and cyclic sweep voltammetry

Over the pH range 2-9, 9-methylxanthine shows up to four well defined oxidation peaks (peaks Ia, IIa, IIIa, and IVa) at the PGE. Variations of Ep with pH for solutions 0.5 mM in 9-methylxanthine are illustrated in Figures 7-10.

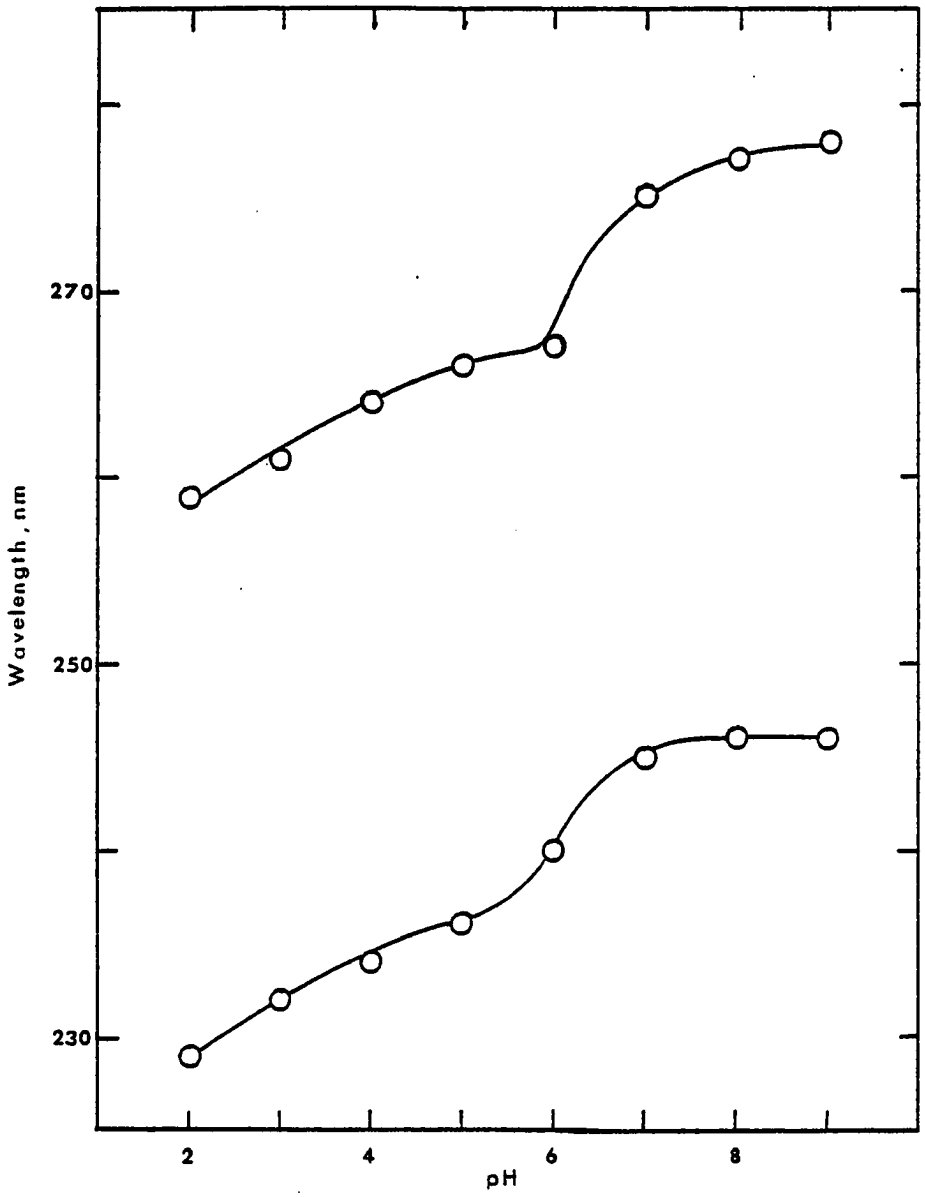

Figure 6. Wavelength versus pH for the two u. v.-adsorbing peaks of 1 m<u>M</u> 9-methylxanthine.

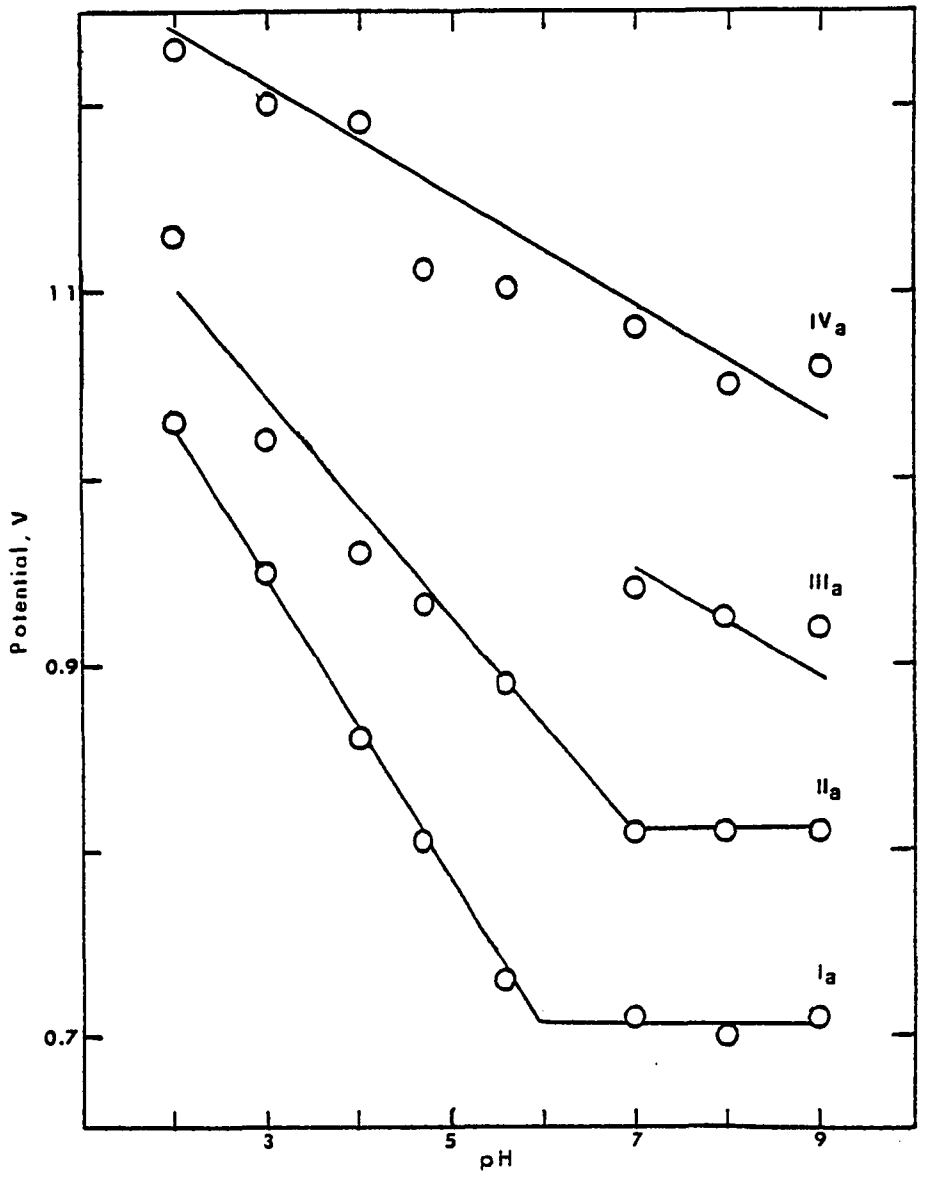

Figure 7. Dependence of Ep on pH for 9-methylxanthine peaks Ia, IIa, IIIa, and IVa. Solutions ca. 0.5 mM. Scan rate 5 $mVsec^{-1}$.

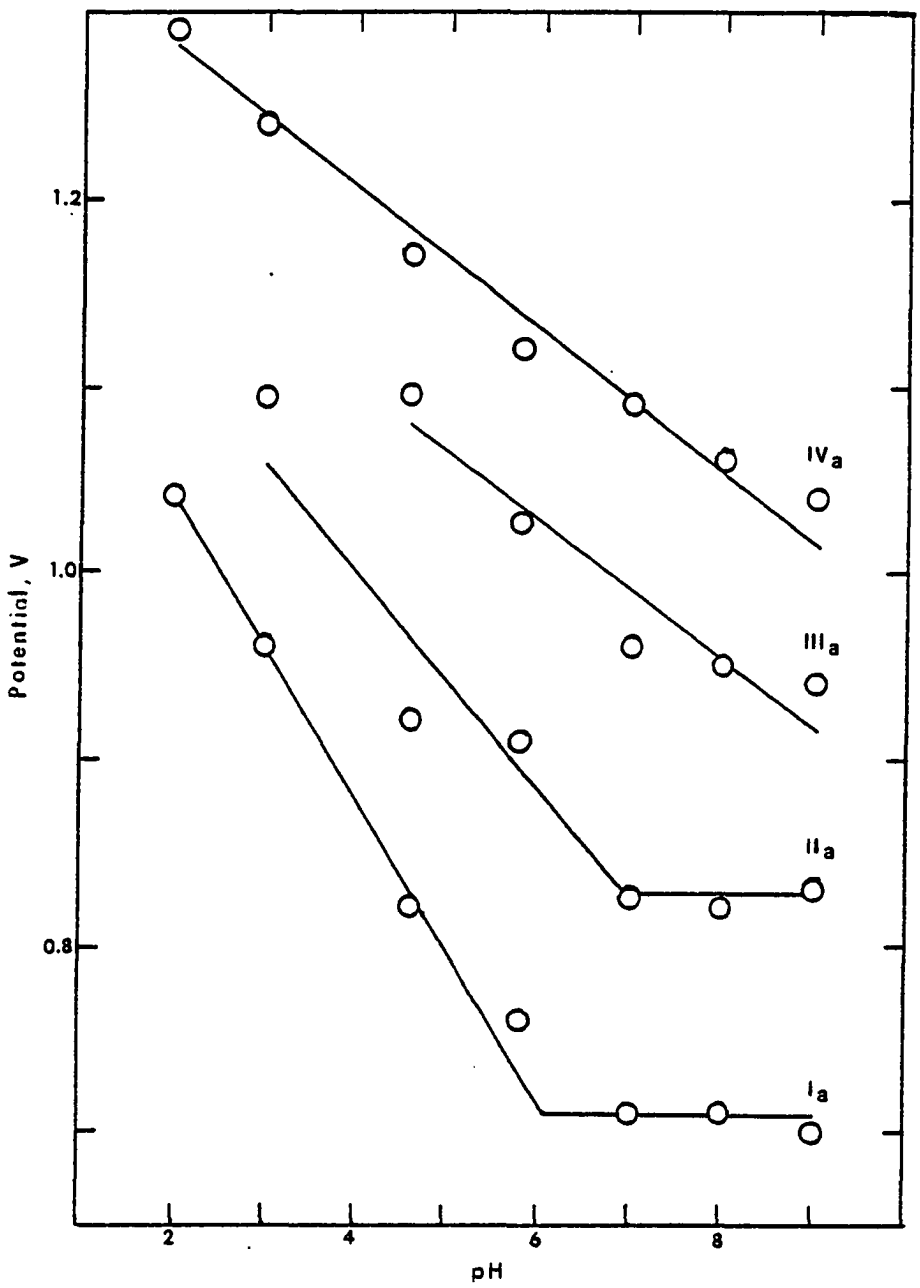

Figure 8. Dependence of Ep on pH for 9-methylxanthine peaks Ia, IIa, IIIa, and IVa. Solutions ca. 0.5 mM. Scan rate 20 $mVsec^{-1}$.

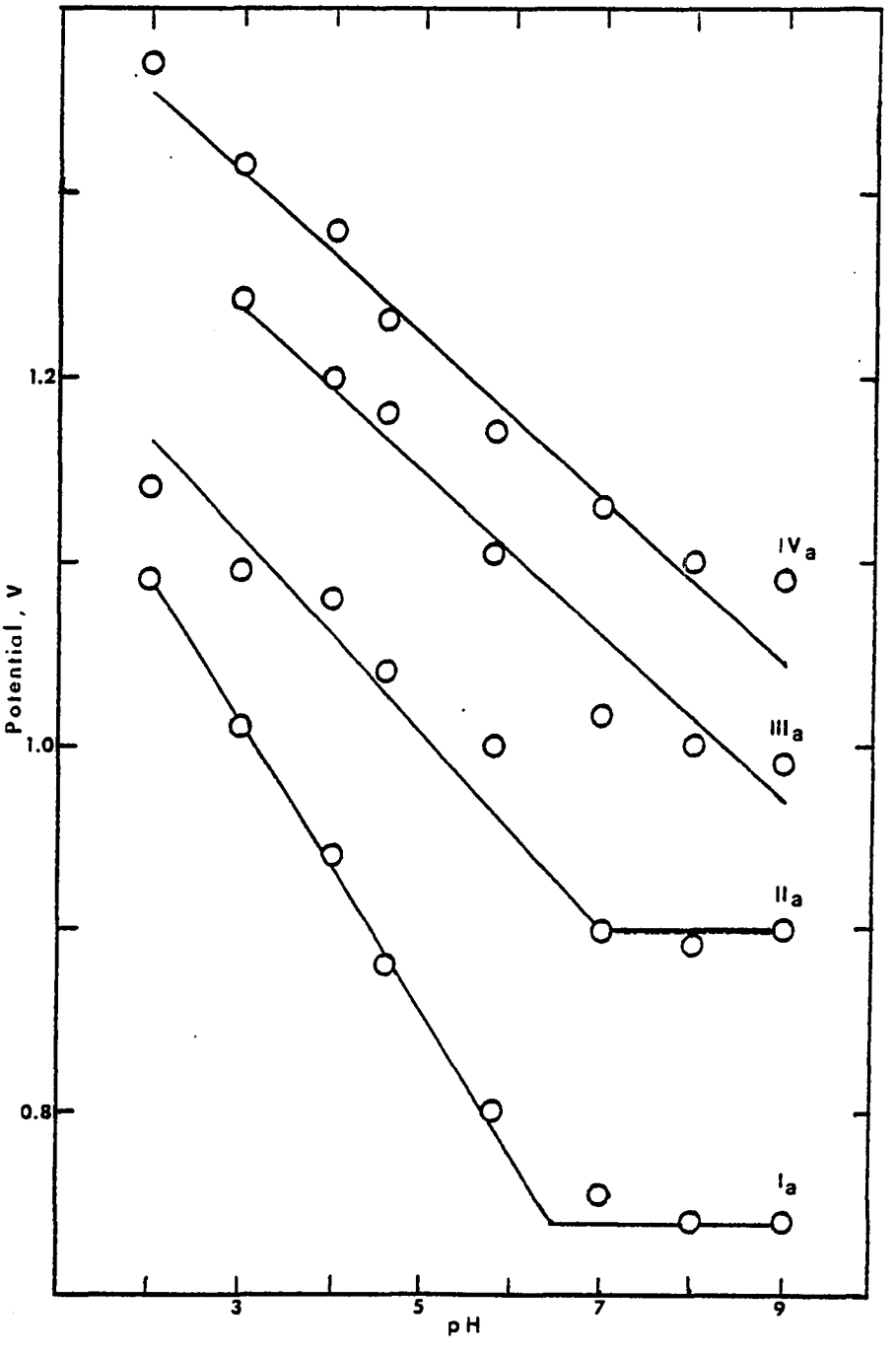

Figure 9. Dependence of Ep on pH for 9-methylxanthine peaks Ia, IIa, IIIa, and IVa. Solutions ca. 0.5 mM. Scan rate 200 $mVsec^{-1}$.

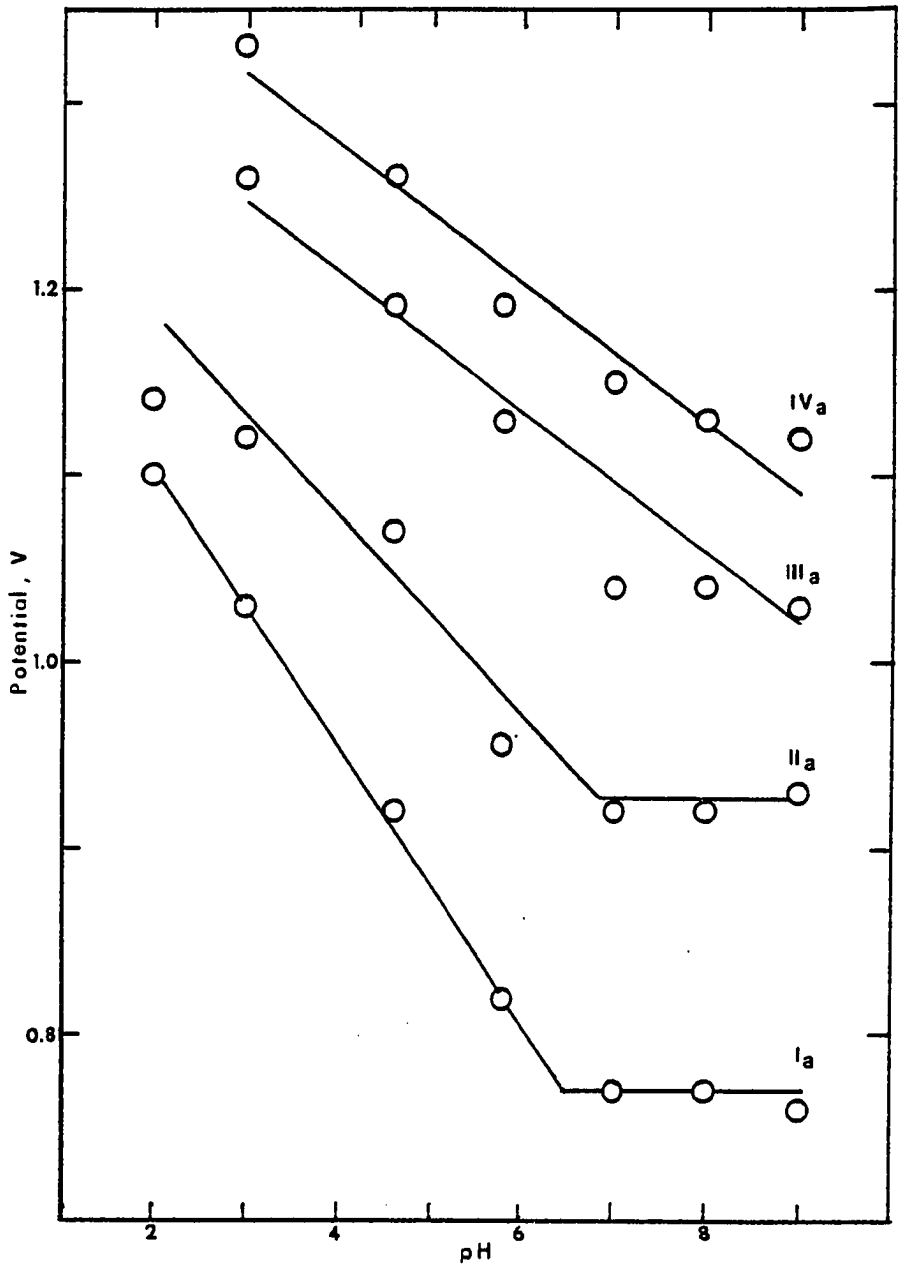

Figure 10. Dependence of Ep on pH for 9-methylxanthine peaks Ia, IIa, IIIa and IVa. Solutions ca. 0.5 mM. Scan rate 500 $mVsec^{-1}$.

The oxidation occurring most easily, i.e., at the lowest positive potentials, first appears in the pH region around 2 and is observed through pH 9. The variation of peak potential with pH for this reaction is as follows:

500 $mVsec^{-1}$; pH 2-6, Ep = (1.25 - 0.073 pH)V
pH 7-9, Ep = 0.77 V

200 $mVsec^{-1}$; pH 2-6, Ep = (1.25 - 0.080 pH)V
pH 7-9, Ep = 0.74 V

20 $mVsec^{-1}$; pH 2-6, Ep = (1.21 - 0.085 pH)V
pH 7-9, Ep = 0.71 V

5 $mVsec^{-1}$; pH 2-6, Ep = (1.20 - 0.085 pH)V
pH 7-9, Ep = 0.71 V

A second process is observed occurring over the entire pH range. At a sweep rate of 5 $mVsec^{-1}$, this second peak is more prominent that the first oxidation peak, but the second process is barely detected at a sweep rate of 500 $mVsec^{-1}$. The variation of peak potential with pH is shown below:

500 $mVsec^{-1}$; pH 2-7, Ep = (1.29 - 0.053 pH)V
pH 7-9, Ep = 0.93 V

200 $mVsec^{-1}$; pH 2-7, Ep = (1.27 - 0.053 pH)V
pH 7-9, Ep = 0.90 V

20 $mVsec^{-1}$; pH 3-7, Ep = (1.23 - 0.058 pH)V
pH 7-9, Ep = 0.83 V

5 $mVsec^{-1}$; pH 2-7, Ep = (1.22 - 0.060 pH)V
pH 7-9, Ep = 0.81 V

A third process is observed over the entire pH range

studied (3-9) for 500 $mVsec^{-1}$ and 200 $mVsec^{-1}$ scan rates. This process occurs over the pH range 5-9 at a scan rate of 20 $mVsec^{-1}$. At a scan rate of 5 $mVsec^{-1}$, the third process is detected only in the pH range 7-9. Equations for variation of peak potential with pH are as follows:

500 $mVsec^{-1}$; pH 3-9, Ep = (1.36 - 0.038 pH)V

200 $mVsec^{-1}$; pH 3-9, Ep = (1.37 - 0.041 pH)V

20 $mVsec^{-1}$; pH 5-9, Ep = (1.25 - 0.032 pH)V

5 $mVsec^{-1}$; pH 7-9, Ep = (1.15 - 0.028 pH)V

A fourth, completely pH dependent electrode process, which occurs at all scan rates, is evident. Its variation in peak potential with pH is as given below:

500 $mVsec^{-1}$; pH 3-9, Ep = (1.42 - 0.036 pH)V

200 $mVsec^{-1}$; pH 2-9, Ep = (1.44 - 0.044 pH)V

20 $mVsec^{-1}$; pH 2-9, Ep = (1.35 - 0.036 pH)V

5 $mVsec^{-1}$; pH 2-9, Ep = (1.28 - 0.027 pH)V

It should be noted that the equations describing the pH dependence of peak potentials at the different sweep rates are very similar for each individual oxidation process.

The theoretical equation of a linear diffusion controlled irreversible peak voltammogram is[42]:

$$(i_p)_{irrev} = 2.98 \times 10^5 \, n \, (\alpha n_a)^{1/2} \, AD^{1/2} v^{1/2} C \qquad (1)$$

where,

$(i_p)_{irrev}$ = total peak current, μA

n = total number of electrons transferred in the electrochemical process

n_a = number of electrons involved in the initial electron transfer process

α = electron transfer coefficient

A = electrode area, cm^2

D = diffusion coefficient of electroactive species, $cm^2\ sec^{-1}$

v = voltage sweep rate, Volts sec^{-1}

C = concentration of electroactive species, mM

According to equation 1, the peak current function, $i_p/ACv^{1/2}$, should remain constant with variation in scan rate and a plot of i_p/C vs C should be linear and parallel to the concentration axis.

Voltammograms of 0.5 mM 9-methylxanthine in solutions of phosphate buffer having an ionic strength of 0.5 (pH 2, 4, 7, and 9) are reproduced in Figure 11 (sweep rate 5 $mVsec^{-1}$) and Figure 12 (sweep rate 200 $mVsec^{-1}$). It is observed that as the scan rate increases the first peak shifts toward more positive potentials at pH values less than 6 (at pH 4, 5 $mVsec^{-1}$, $Ep^{Ia} = {}^{+}0.87$ V vs SCE; at 200 $mVsec^{-1}$, $Ep^{Ia} = {}^{+}0.96$ V vs SCE). Similar effects were noted by Dryhurst[37] in the oxidation of 6-thiopurine at the PGE and are characteristic of an adsorption peak where the product of the electrochemical reaction is adsorbed[38]. The values of the experimental peak Ia peak current function, $i_p/AC\ v^{1/2}$, are presented in Table 1.

The peak currents were measured by first recording

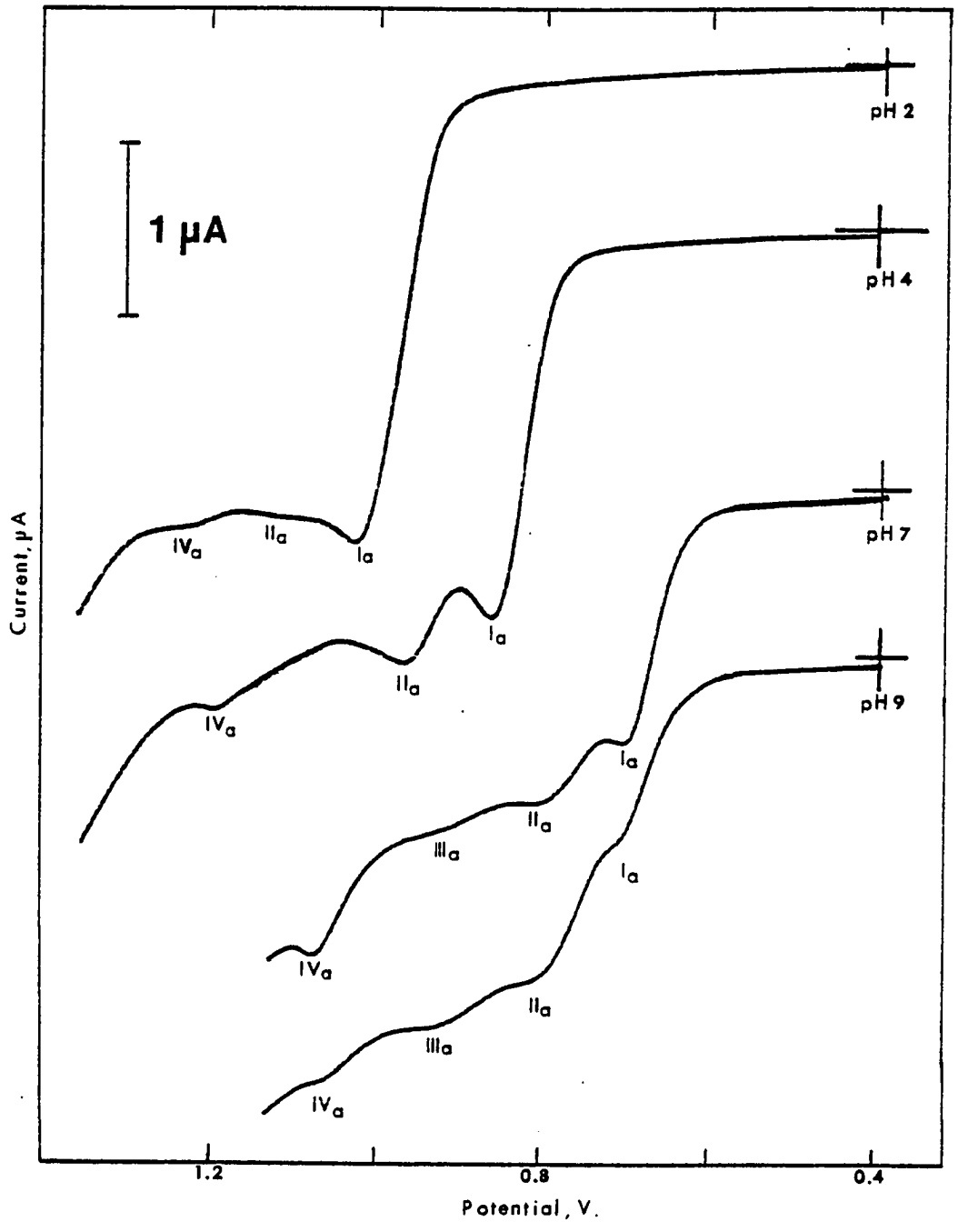

Figure 11. Voltammograms of 0.5 mM 9-methylxanthine in various pH solutions at a scan rate of 5 $mVsec^{-1}$.

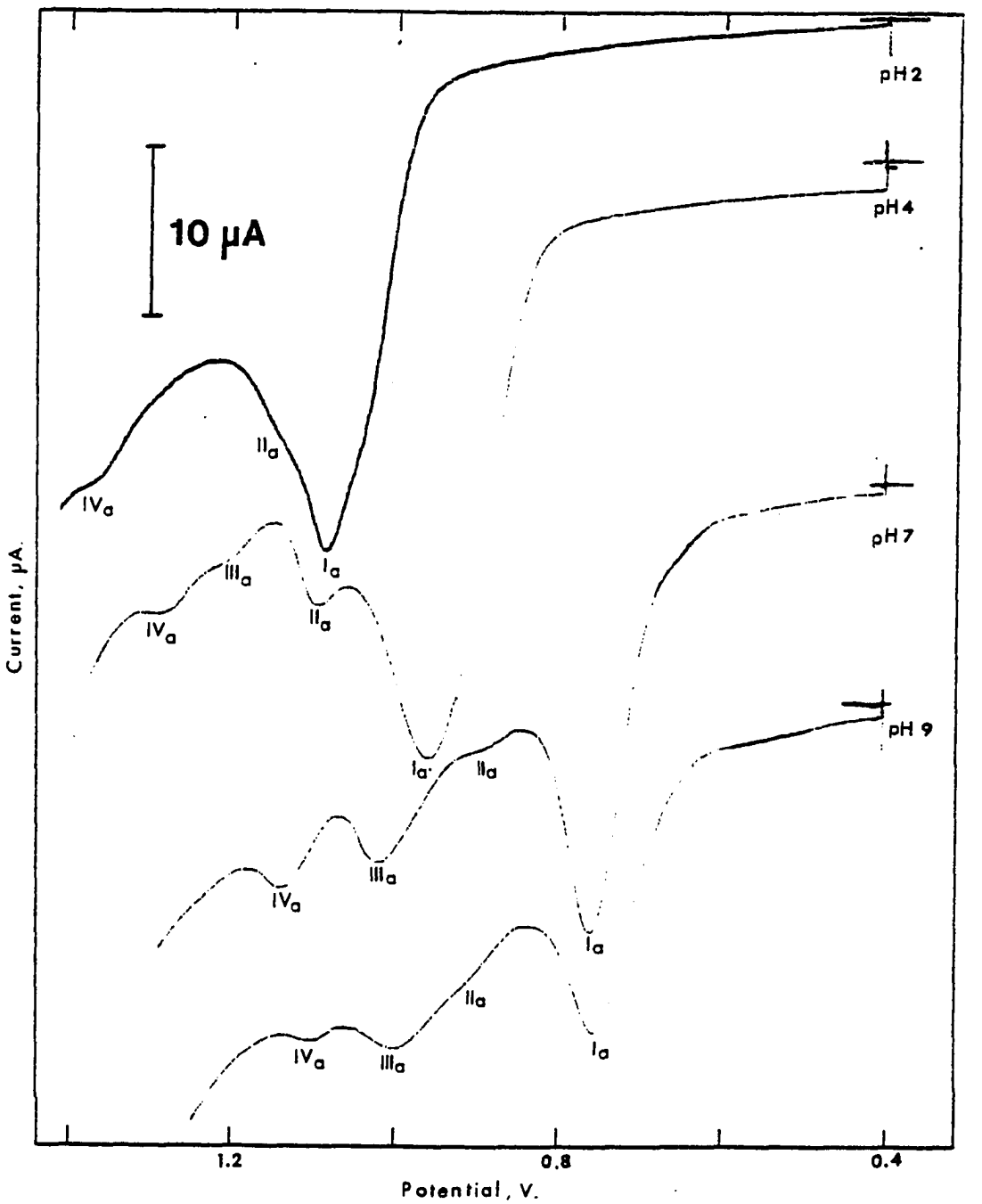

Figure 12. Voltammograms of 0.5 mM 9-methylxanthine in various pH solutions at a scan rate of 200 $mVsec^{-1}$.

TABLE 1

Peak current function values for the oxidation of 9-methylxanthine at the PGE at peak Ia.

pH	i_p [a]	v	$i_p/ACv^{1/2}$
2.0	3.8	0.005	3044
4.0	1.7	0.005	1362
7.0	1.3	0.005	1042
9.0	1.1	0.005	881
2.0	4.8	0.020	3830
4.0	5.0	0.020	2009
7.0	4.2	0.020	1687
9.0	3.2	0.020	1288
2.0	26.5	0.200	3359
4.0	29.0	0.200	3676
7.0	25.0	0.200	3169
9.0	17.0	0.200	2155
2.0	47.0	0.500	3766
4.0	57.5	0.500	4607
7.0	48.0	0.500	3846
9.0	36.0	0.500	2885

a i_p = voltammetric peak current, μA

A = electrode area, cm^2 = 0.0353 cm^2
C = concentration of electroactive species, m$\underline{M}$ = 0.5 m$\underline{M}$
v = voltage sweep rate, $Vsec^{-1}$

a voltammogram of a solution of 9-methylxanthine, then recording a voltammogram of background solution under identical conditions. Peak currents were then taken as the difference in background current and current in the presence of the electroactive compound at the peak potential.

Studies of the dependence of peak current function for peak Ia upon potential scan rate revealed that at pH 4, 7, and 9 an increase in peak current function, $i_p/AC\ v^{1/2}$, with increasing scan rate (Figure 13) was observed. Such behavior is usually indicative of reactant adsorption at the electrode[38]. The fact the peak current function decreases with increasing pH from 2 to 9 is probably related to the increased solubility of 9-methylxanthine in basic solutions. With increasing sweep rate in the pH range 7-9 peak IIa decreases in height relative to peak Ia. This fact made detailed studies of peak IIa as a function of voltage sweep difficult. At pH below 5 peaks IIIa and IVa begin to merge with background discharge making studies of these latter peaks at low pH as a function of voltage sweep impossible. However, voltage sweep rate studies were possible at neutral pH and above. The values of peak IIIa and IVa peak current as a function of scan rate are shown in Table 2.

Studies of the dependence of peak current upon potential scan rate revealed that for peak IIIa at both pH 7 and 9 an increase in $i_p/v^{1/2}$ with increasing scan rate. Whereas, for peak IVa at both pH 7 and 9 the value of $i_p/v^{1/2}$

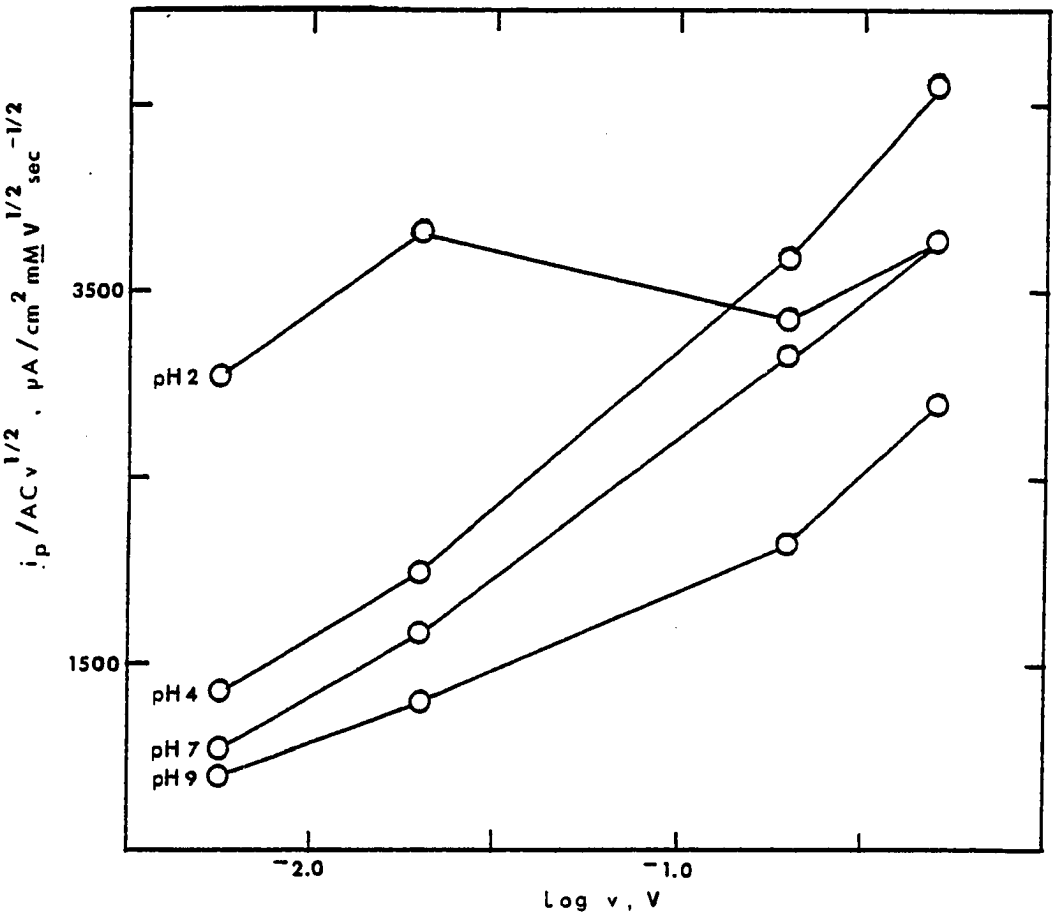

Figure 13. Variation of peak current function for peak Ia with voltage sweep rate at several pH values for 0.5 mM solutions of 9-methylxanthine at the PGE.

TABLE 2

Peak current values for the oxidation of 9-methylxanthine at the PGE for peaks IIIa and IVa.

	v	i_p	$i_p/v^{1/2}$
Peak IIIa			
1. pH 7.0	0.005	1.7	24.04
	0.020	3.8	26.84
	0.200	19.0	42.49
	0.500	34.0	48.08
2. pH 9.1	0.005	1.8	25.46
	0.020	4.2	29.70
	0.200	16.0	35.78
	0.500	28.0	39.60
Peak IVa			
1. pH 7.0	0.005	2.2	31.11
	0.020	3.4	24.04
	0.200	14.0	31.30
	0.500	20.0	28.28
2. pH 9.1	0.005	1.9	26.87
	0.020	3.8	26.87
	0.200	12.0	26.83
	0.500	18.0	25.45

remains essentially constant, which is what one would expect for a diffusion controlled process. Graphs of $i_p/v^{1/2}$ vs log v are shown in Figure 14.

The scan rate is likely the most important experimental parameter for differentiating between the effects due to adsorbed material and those due to material arriving at the electrode by diffusion. This is because the adsorbed material constitutes a fixed amount of material and charge flow, while the amount of material diffusing to the electrode surface is time dependent. At sufficiently fast scan rates, the amount of diffusing material is small relative to the amount of adsorbed material reacting at the electrode surface, while at slow scan rates the reverse is true. In the presence of weakly adsorbed material, stationary electrode voltammograms may exhibit enhancement of the peak current[39,40] because of electron transfer involving the adsorbed material at nearly the same potential as the "normal" electron transfer. On the other hand, if the product or reactant is strongly adsorbed, a separate adsorption peak may occur prior to or after the normal peak[41]. When the electrode reaction involves the strong adsorption of the product, the stationary electrode voltammogram exhibits an adsorption peak prior to the normal diffusion peak[38]. As the scan rate increases, the ratio of the adsorption peak height to the diffusion peak height increases. At low scan rates the behavior approaches that of an uncomplicated oxidation. As the scan rate is increased,

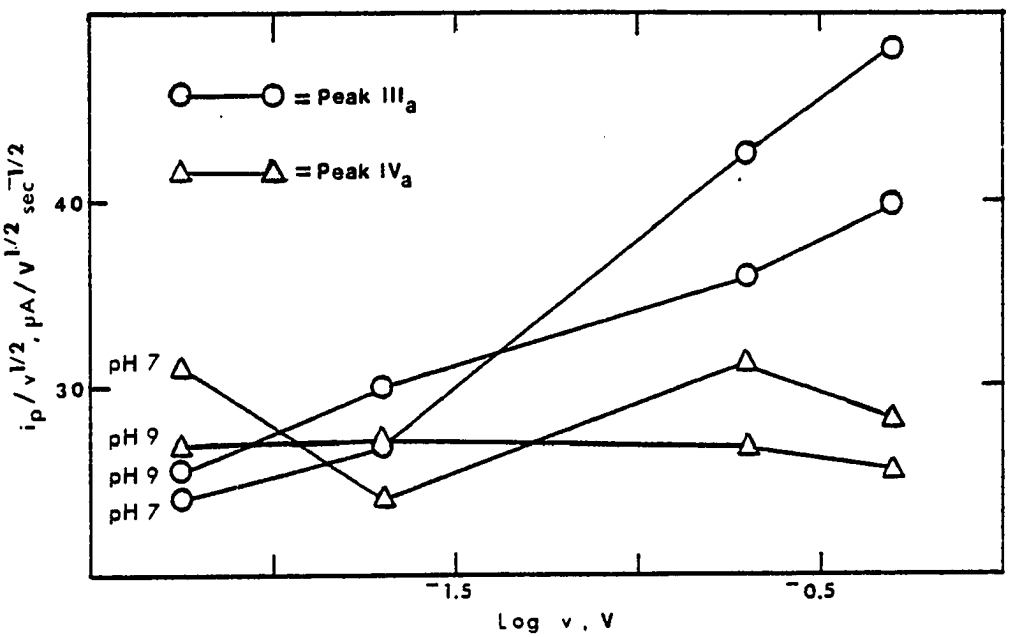

Figure 14. Variation of peak current for peaks IIIa and IVa with voltage sweep rate at pH 7 and 9 for 0.5 mM solutions of 9-methylxanthine at the PGE.

the adsorption peak appears and increases with only a small decrease in the diffusion peak. With further increase of the scan rate, the adsorption peak increases further, and the diffusion peak decreases until only one peak appears at the potential of the adsorption peak. This appears to be the behavior shown by peaks IIIa and IVa at pH 7 and 9 and shown in Figures 15 and 16. Thus peak IIIa could be an adsorption pre-peak for peak IVa, where the product of IVa is strongly adsorbed, or peak IIIa could be due to oxidation of an unstable peak Ia or IIa product so that it is very small at slow sweep rates and much larger at faster sweep rates.

Matsuda and Ayabe[43] examined the relations in peak voltammetry for reversible, quasireversible, and totally irreversible systems. For a totally irreversible peak voltammogram, the product of the transfer coefficient (α) and the number of electrons in the rate-determining step (n_a) can be found from the effective slope of the peak voltammogram:

$$Ep - Ep/2 = \frac{0.048}{\alpha n_a} V \qquad (2)$$

The experimental value of αn_a for peak Ia from the above equation was determined between pH 2 and 9 at 0.02 $Vsec^{-1}$ (Table 3). Using the appropriate value of αn_a and a diffusion coefficient for 9-methylxanthine of 11.13 X 10^{-6} $cm^2 s^{-1}$ (a value obtained from calculated diffusion coefficients of 9-methyluric acid and xanthine, molecules of similar size

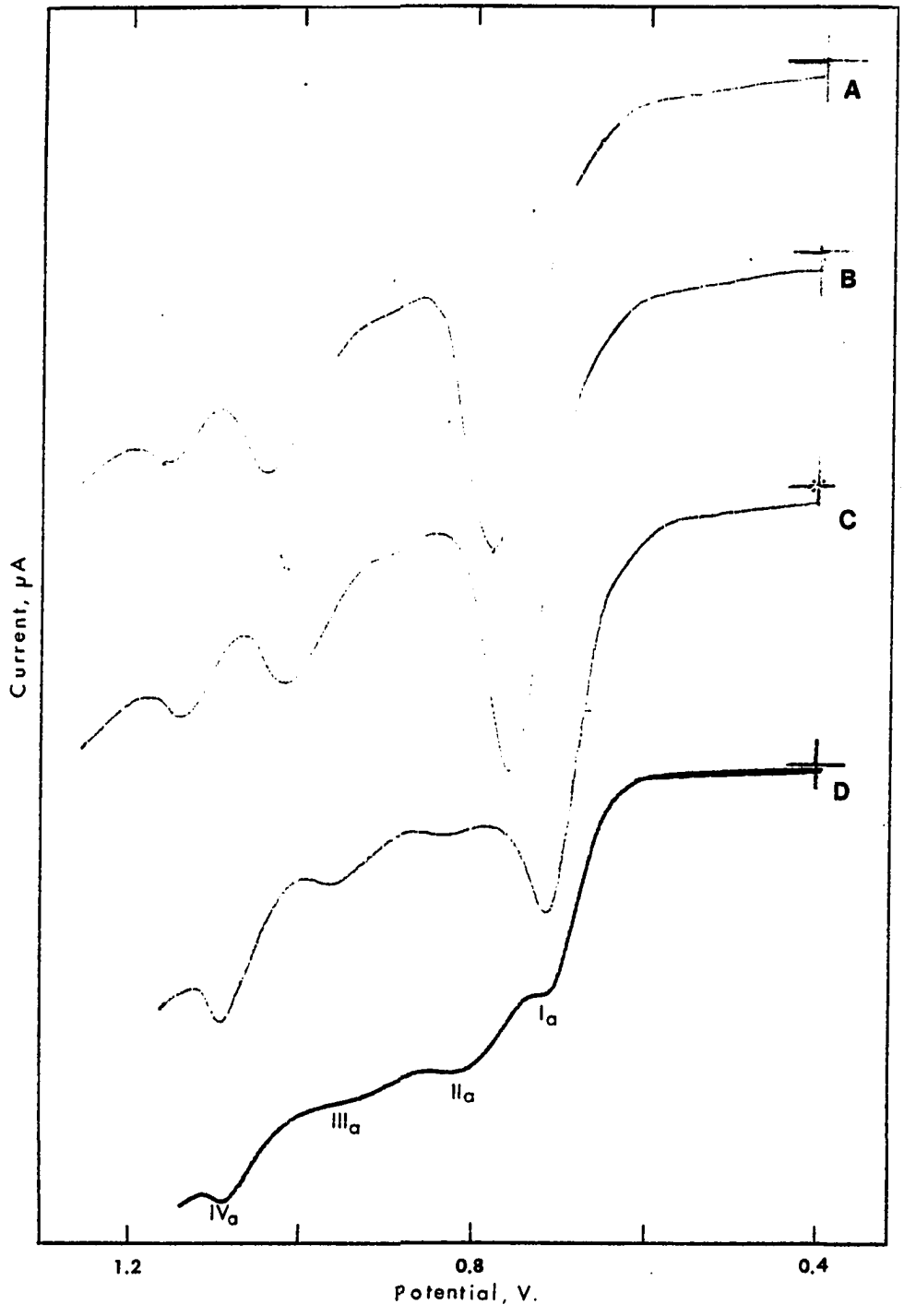

Figure 15. Voltammograms of 0.5 mM 9-methylxanthine in pH 7 phosphate buffer at (A) 500 $mVsec^{-1}$, 20 μAin^{-1}; (B) 200 $mVsec^{-1}$, 10 μAin^{-1}; (C) 20 $mVsec^{-1}$, 2 μAin^{-1}; (D) 5 $mVsec^{-1}$, 1 μAin^{-1}.

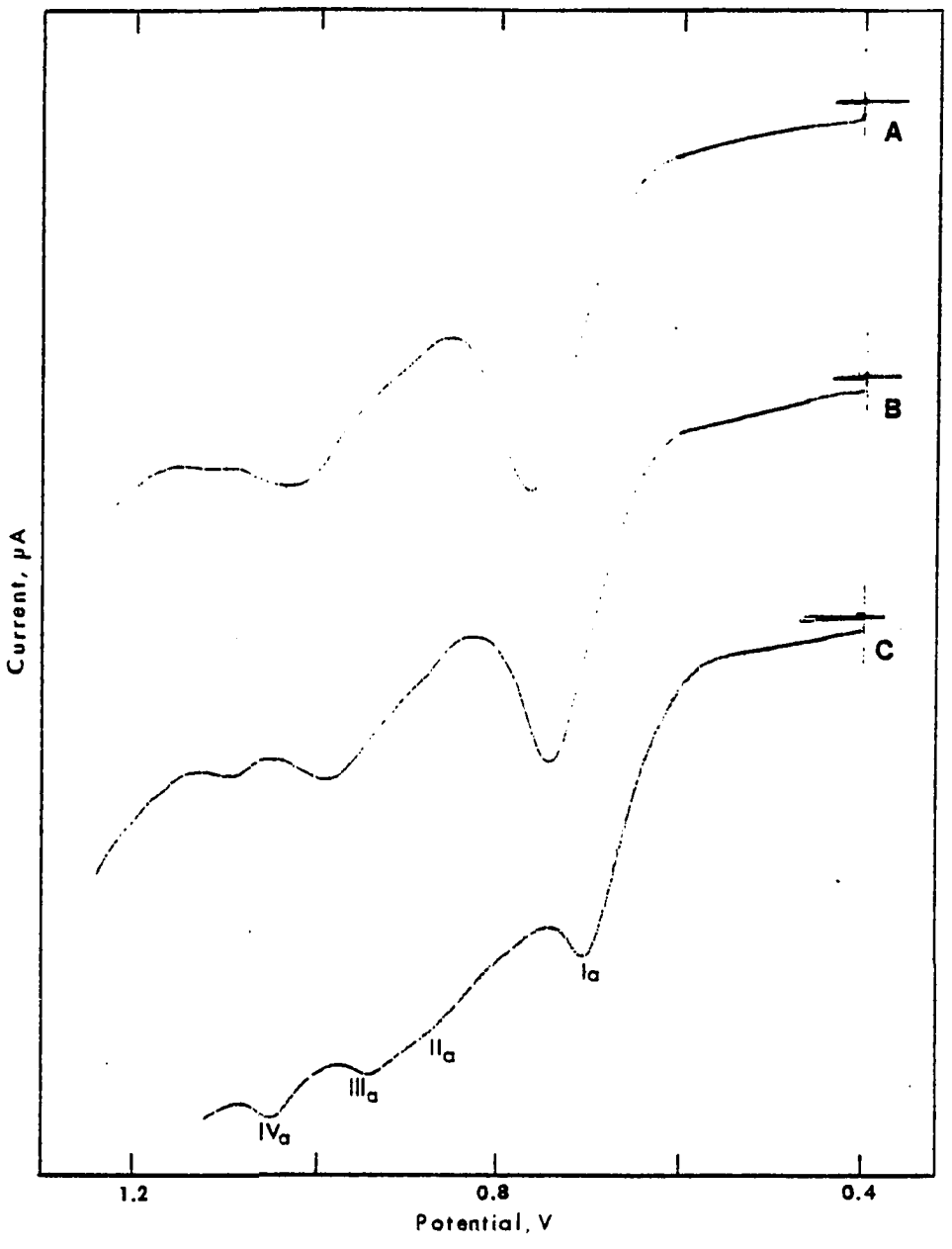

Figure 16. Voltammograms of 0.5 mM 9-methylxanthine in pH 9 phosphate buffer at (A) 500 $mVsec^{-1}$, 20 μAin^{-1}; (B) 200 $mVsec^{-1}$, 10 μAin^{-1}; (C) 20 $mVsec^{-1}$, 2 μAin^{-1}.

TABLE 3

Experimental values of αn_a for peak Ia of 9-methylxanthine

pH	$Ep - Ep_{/2}$	αn_a
2	0.056	0.857
3	0.052	0.923
4	0.049	0.980
5	0.050	0.960
6	0.045	1.07
7	0.042	1.14
8	0.050	0.960
9	0.049	0.980

Scan rate = 0.02 $Vsec^{-1}$

Concentration = 0.5 m$\underline{M}$

and molecular weight), application of equation 1 for a totally irreversible uncomplicated process will allow the determination of n (the total number of electrons involved in the voltammetric reaction). The peak Ia process is clearly not uncomplicated because of adsorption phenomena and a variety of follow-up reactions (vide infra). At a sweep rate of 0.02 $Vsec^{-1}$ and a concentration of 0.5 mM the experimental n-value is 2.08, 2.32, 1.77, and 1.39 at pH 2, 4, 7, and 9 respectively. Enhancement of the peak current by reactant adsorption is least at the highest pH (Figure 13) although still noticably present. In view of this it was concluded that under voltammetric conditions the peak Ia process involves between 1-2 electrons per molecule of 9-methylxanthine.

The dependence of peak current upon concentration at pH 7 for peaks Ia, IIa, IIIa, and IVa of 9-methylxanthine is shown in Figure 17. It is apparent that at a concentration of 1 mM in pH 7 phosphate buffer at a scan rate of 5 $mVsec^{-1}$ only peaks Ia and IVa are prominent. At 0.5 mM, peaks IIa and IIIa are quite visible with peak Ia becoming less salient. With a concentration of 10 mM, peak IIa becomes the most prominent with Ia still visible and IIIa and IVa almost undetectable.

Figure 18 shows that at pH 4 the peak current of all four peaks is also dependent on concentration. At a concentration of 0.1 mM only peaks Ia and IVa are visible as

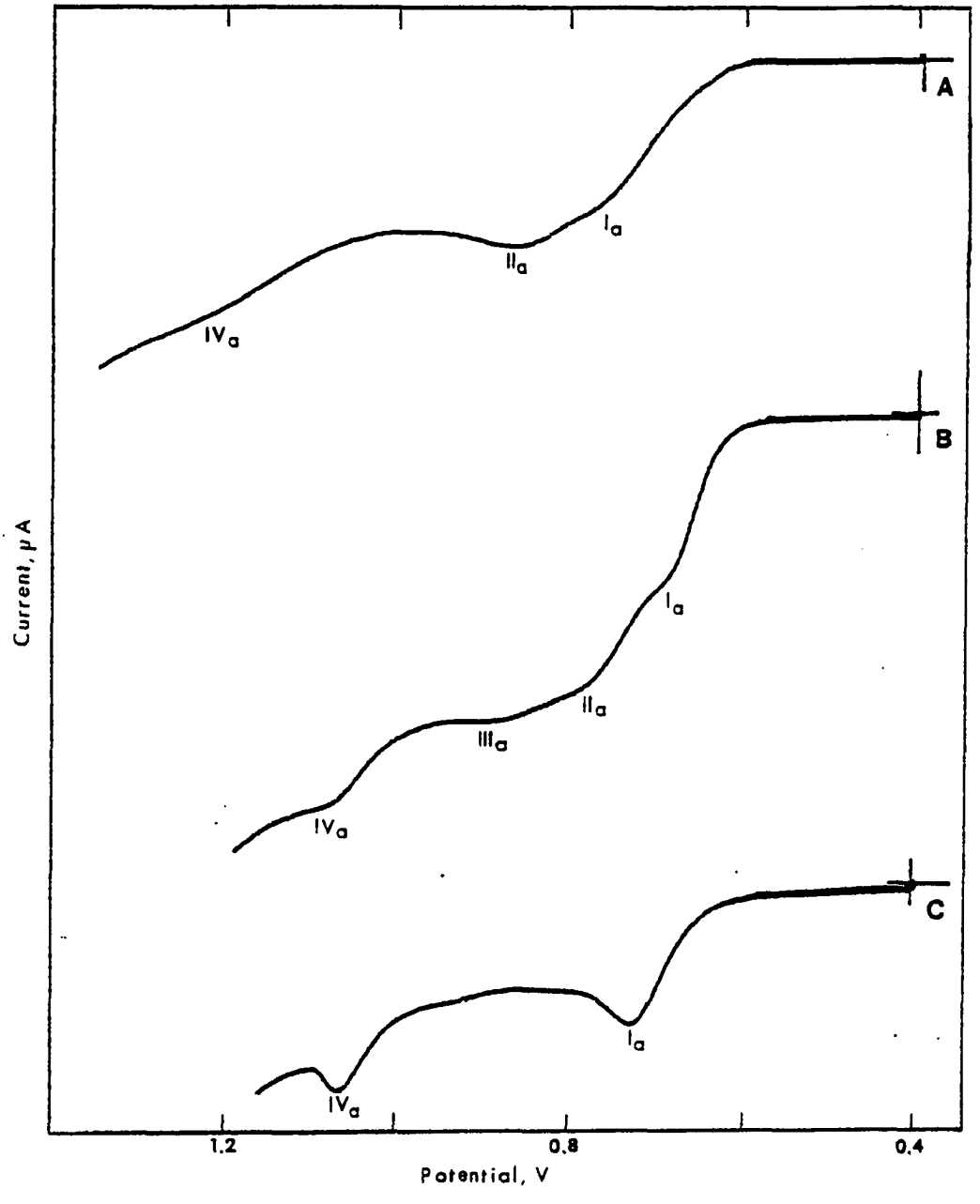

Figure 17. Voltammograms of 9-methylxanthine in pH 7 phosphate buffer at (A) 10 m$\underline{M}$, 20 $\mu A in^{-1}$; (B) 0.5 m$\underline{M}$, 2 $\mu A in^{-1}$; (C) 0.1 m$\underline{M}$, 1 $\mu A in^{-1}$. Scan rate 5 $mV sec^{-1}$.

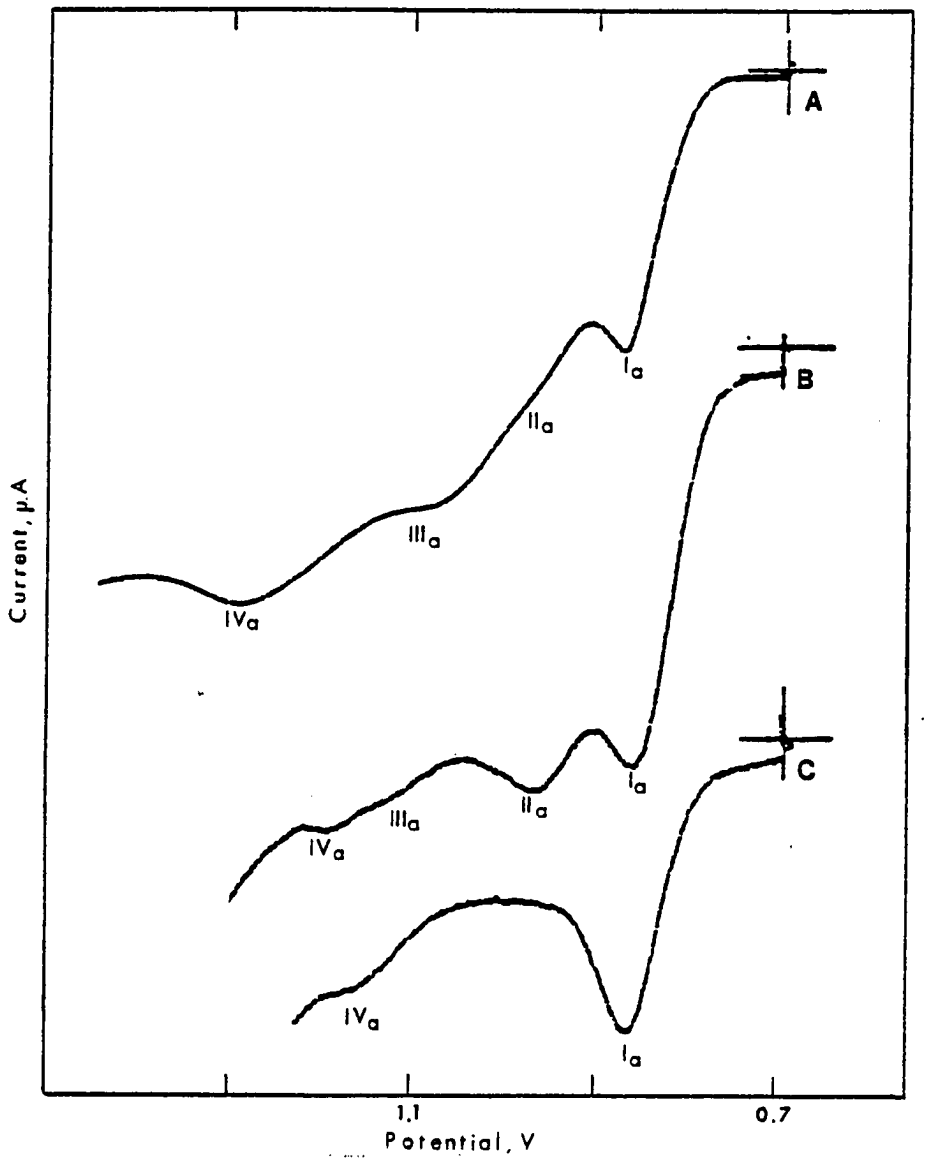

Figure 18. Voltammograms of 9-methylxanthine in pH 4 phosphate buffer at (A) 4 m<u>M</u>, 5 $\mu A in^{-1}$; (B) 0.5 m<u>M</u>, 1 $\mu A in^{-1}$; (C) 0.1 m<u>M</u>, 1 $\mu A in^{-1}$. Scan rate 5 $mV sec^{-1}$.

in pH 7.0 buffer. At 0.5 mM, peaks IIa and IIIa become visible with IIa as prominent as Ia. With a concentration of 4 mM, peaks Ia, IIa, and IVa are the three prominent peaks.

The involvement of adsorption, especially for peaks Ia, IIa, and IIIa, was confirmed by studies of the dependence of peak height upon concentration. From Figure 19 it can be seen that peaks Ia, IIa, and IIIa of 9-methylxanthine exhibit behavior characteristic of adsorption processes. Adsorption at peak IVa is apparently much less extensive; the plot of i_p/C vs C is essentially parallel to the C axis over the concentration range 1-5 mM and the peak current changes only slightly with scan rate (Figure 14, 19).

Cyclic voltammetry employs a triangular wave-form voltage applied to the electrode and the current is recorded as a function of the applied potential as in linear sweep voltammetry. Voltage sweep rates normally range from 5 $mVsec^{-1}$ to 1 $Vsec^{-1}$. Since voltammetry is performed at a stationery electrode in a quiet solution and the time interval between reverse sweeps is relatively short, the products of an oxidation, for example, are still in the vicinity of the electrode surface and thus, available for reduction on the negative-going segment of the voltage sweep. Cyclic voltammetry can thus provide information used for qualitative evalution of electrode processes (e.g., intermediates, follow-up reactions, etc.).

Cyclic voltammetry of 9-methylxanthine at pH 7 shown

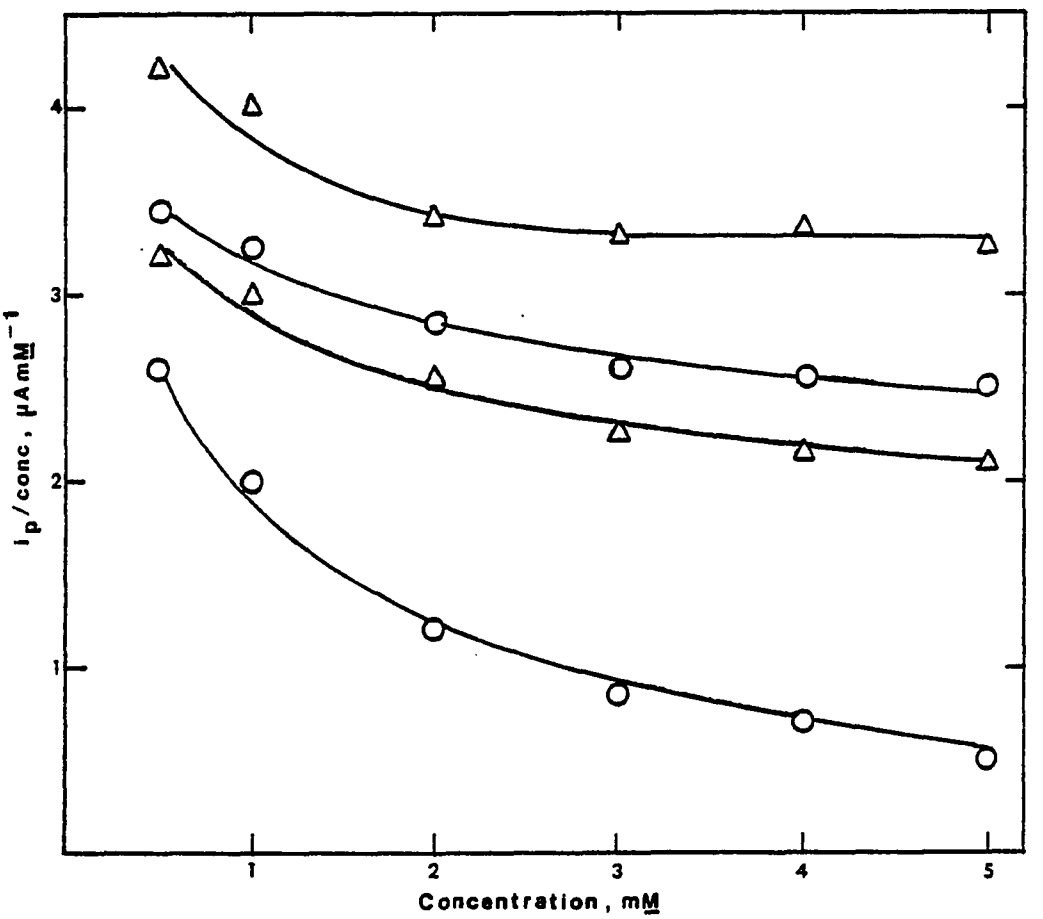

Figure 19. Variation of i_p/C with concentration for 9-methylxanthine at the PGE.

in Figure 20, is significantly different from that observed for xanthine shown in Chapter I. One of the most obvious differences is the presence of the four oxidation peaks on the initial positive-going sweep of 9-methylxanthine. This is in contrast to only one electrooxidation peak for xanthine on the initial positive-going sweep. Another difference noted from switching potential studies (i.e., reversing the sweep from positive to negative-going at different potentials) was the fact that the Ic - Va couple and peak IIc were observed to any significance only after sweeping into the peak IIIa or IVa region as shown in Figure 21. The Ic - Va couple and peak IIc were absent even when the sweep was stopped and held at a potential in the vicinity of peak Ia equal to the time required to sweep to peaks IIIa - IVa and back again. It should be noted that when the potential is reversed in the vicinity of peaks Ia and IIa several small peaks become noticable. These small peaks have been shown to be due to the oxidation of decomposition products from the peak IIa process (vide infra). The peak potentials of the Ic - Va system and peak IIc observed in the voltammetry of 9-methylxanthine are similar to those observed in the voltammetry of uric acid, xanthine, and 9-methyluric acid. A further discussion on the nature of these voltammetric peaks will be presented later.

Cyclic voltammetry at varying concentrations (0.01mM - 20mM) of 9-methylxanthine in pH 7 buffer was performed at

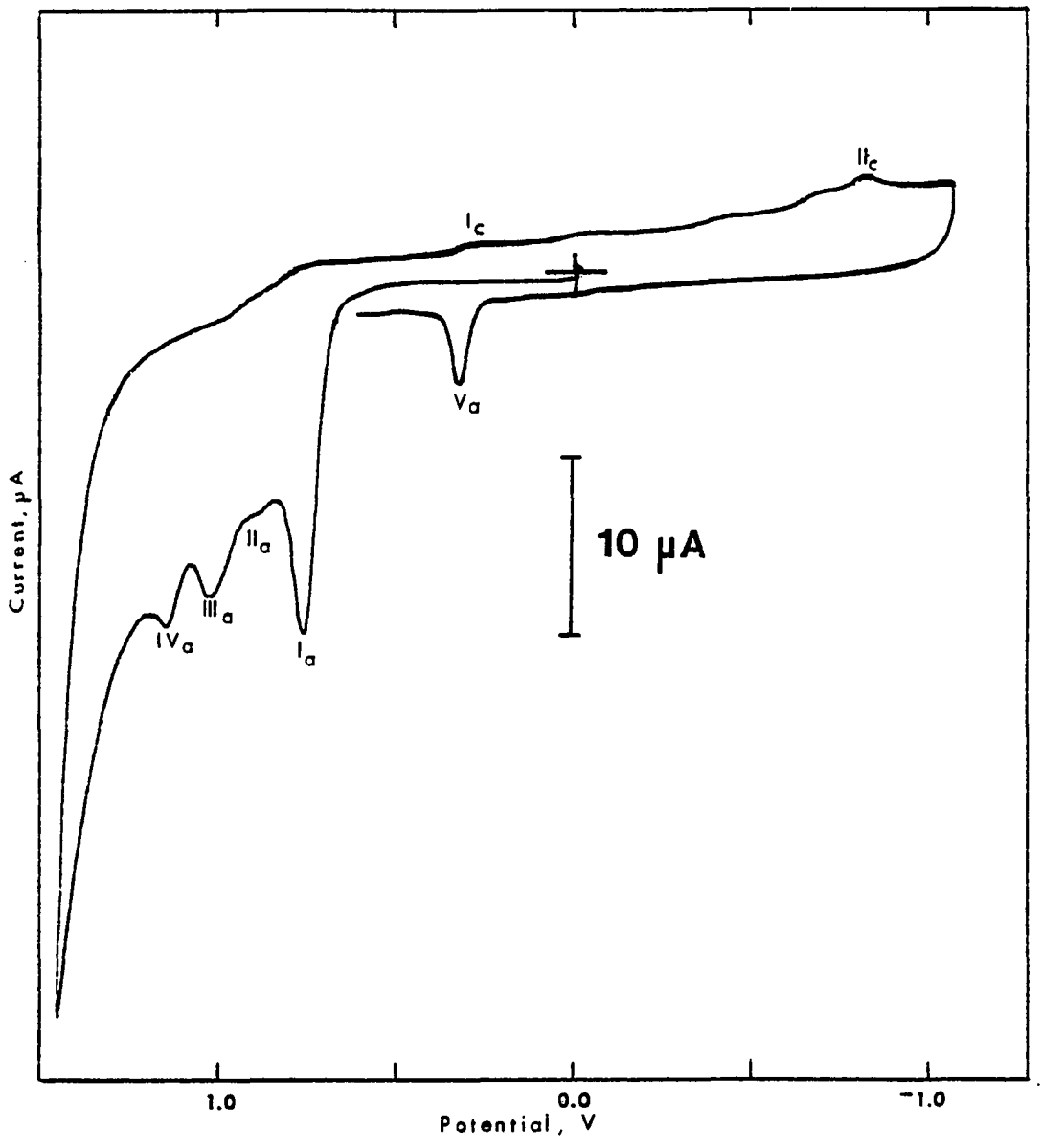

Figure 20. Cyclic voltammogram of 0.5 mM 9-methylxanthine at pH 7 in phosphate buffer. Scan rate 200 $mVsec^{-1}$.

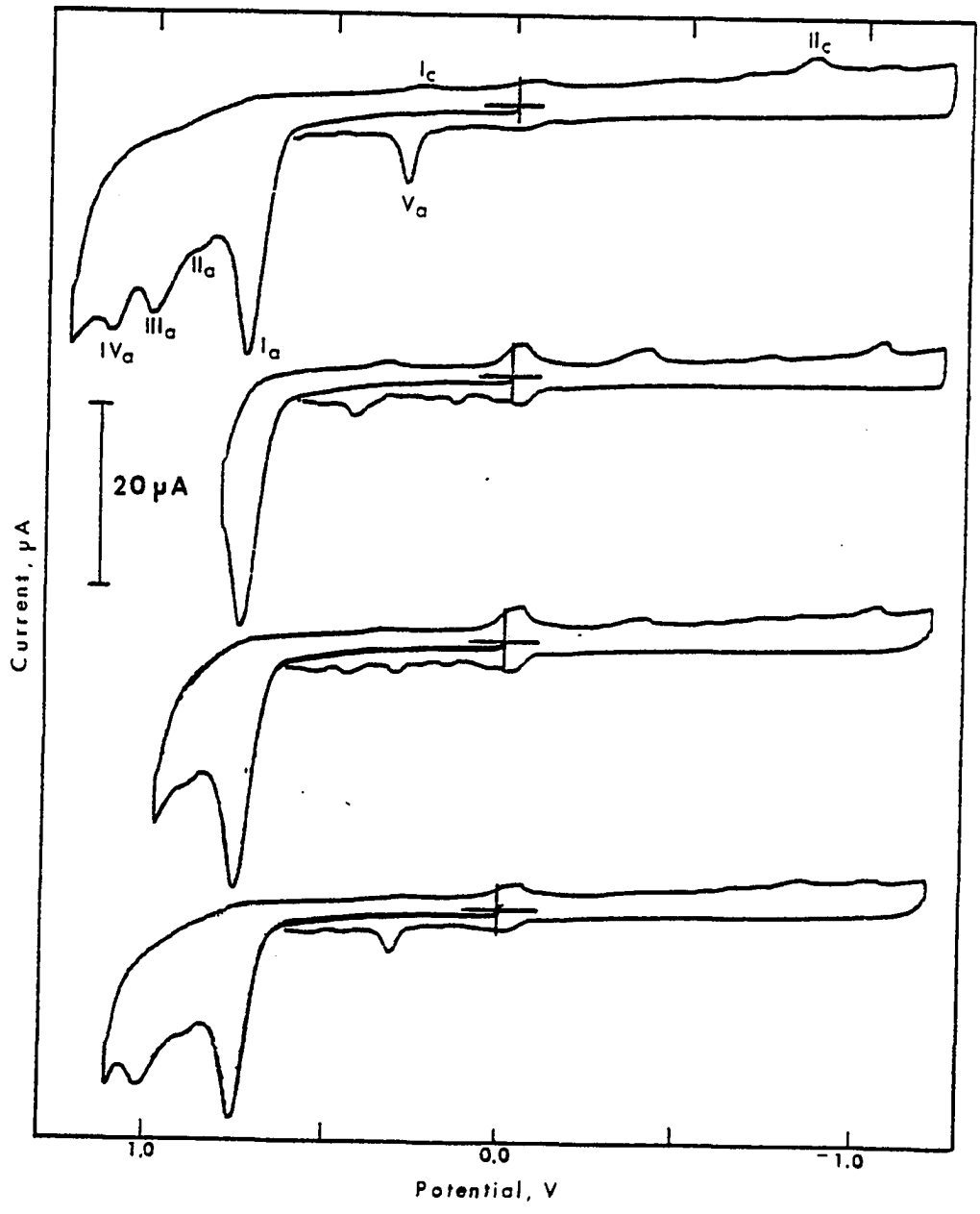

Figure 21. Switching potential study on the cyclic voltammetry of 0.5 mM 9-methylxanthine at pH 7 in phosphate buffer. Scan rate 200 $mVsec^{-1}$.

the PGE. It was observed that as the concentration was lowered below 0.5 mM peak IIa disappeared, while at concentrations greater than 2 mM (example 16 mM, Figure 22) peak IIa became the most prominent peak. Switching potentials studies in the vicinity of peak Ia at the various concentrations revealed that at concentrations below 0.1 mM, oxidation peak Va was present. This was in contrast to switching potential studies in the vicinity of peak Ia at higher concentrations (Figure 21) where peak Va was absent.

Cyclic voltammetry of 9-methylxanthine below its pK_a of approximately 6.3 was very similar to that observed at pH 7. The major difference being that at pH 4 the voltammograms did not change significantly with varying concentrations of 9-methylxanthine. This is shown in Figure 23, where at 0.1 mM, 0.5 mM, and 4.0 mM concentrations all three voltammograms show prominent Ia and IVa peaks on the first positive going scan. Another similarity is noted from switching potential studies undertaken at pH 4. Here, as in studies at pH 7, the Ic - Va couple and peak IIc are observed more significantly when sweeping into the peak IIIa, IVa region. This is shown in Figure 24. It should also be noted from Figure 24, that switching the potential in the vicinity of peak Ia does not entirely eliminate peak Va from the voltammogram.

Again at pH 4, the peak potential of the Ic - Va couple and peak IIc observed in the voltammetry of 9-methyl-

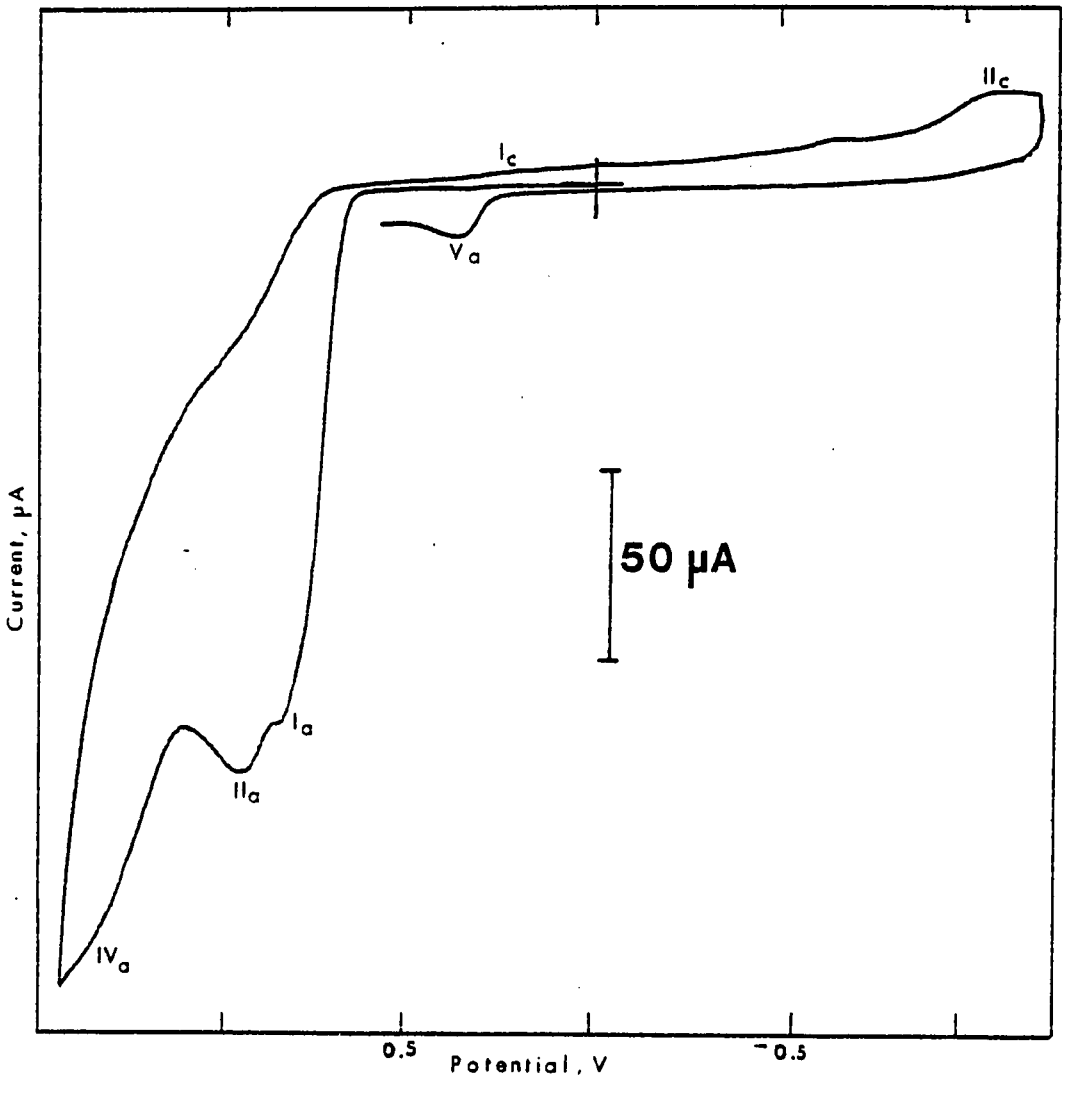

Figure 22. Cyclic voltammogram of 16 mM 9-methylxanthine at pH 7 in phosphate buffer. Scan rate 200 $mVsec^{-1}$.

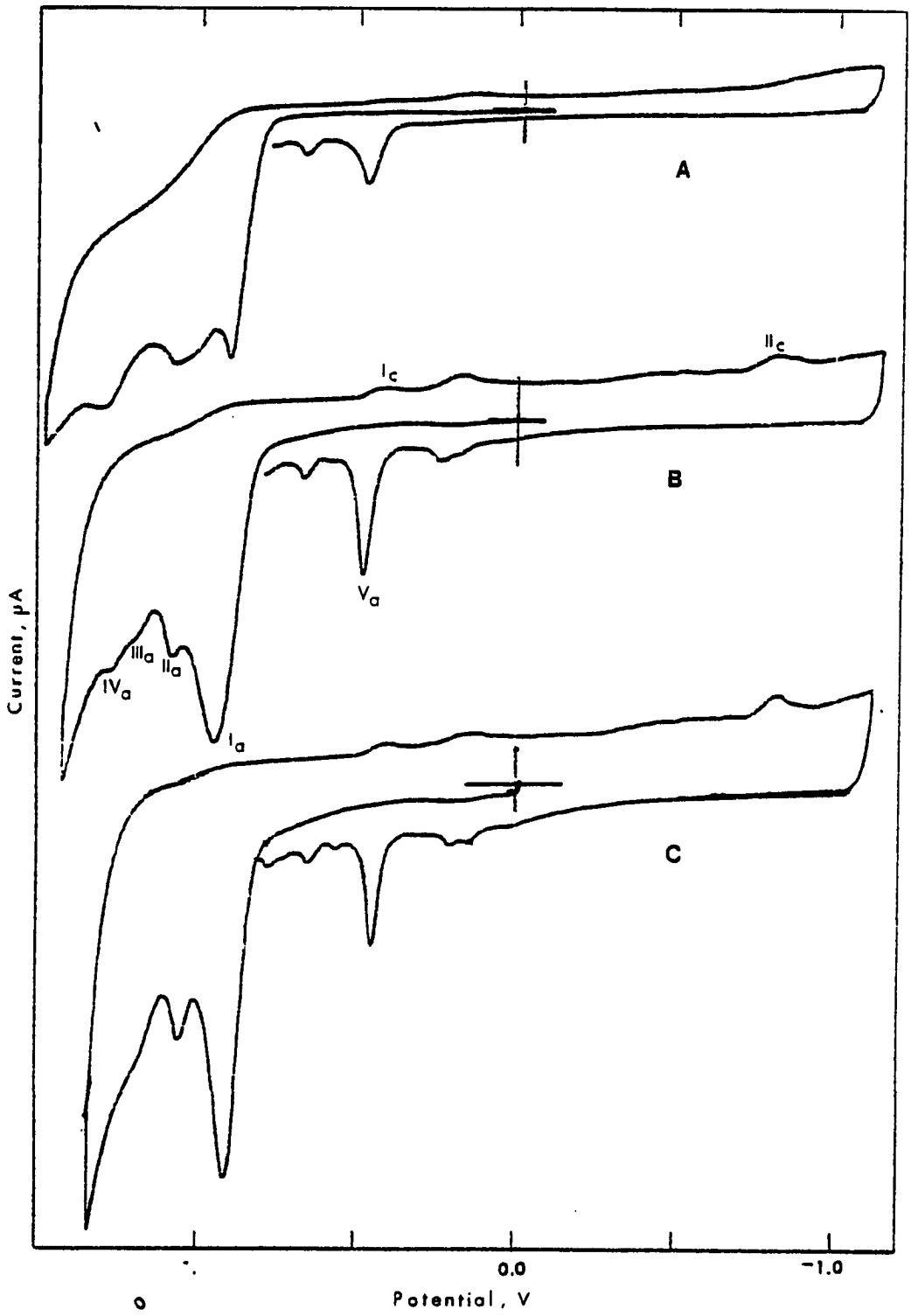

Figure 23. Cyclic voltammograms of 9-methylxanthine at pH 4 in phosphate buffer at (A) 4 m$\underline{M}$, 50 μA; (B) 0.5 m$\underline{M}$, 20 μA; (C) 0.1 m$\underline{M}$, 10 μA. Scan rate 200 mVsec^{-1}.

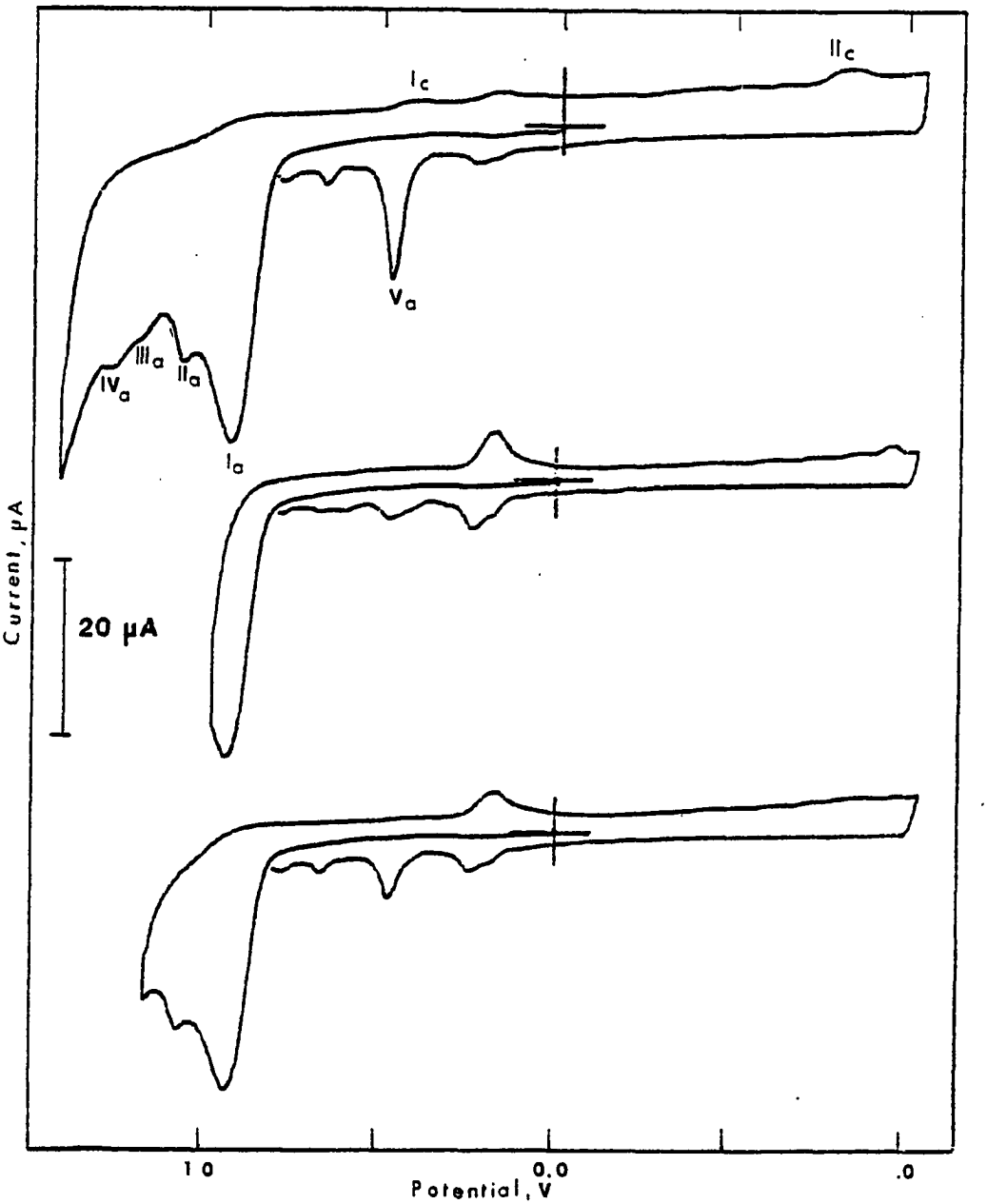

Figure 24. Switching potential study on the cyclic voltammetry of 0.5 mM 9-methylxanthine at pH 4 in phosphate buffer. Scan rate 200 $mVsec^{-1}$.

xanthine match well with those observed in the voltammetry of uric acid, xanthine and 9-methyluric acid at similar pH.

Controlled potential coulometry

Controlled potential coulometry of 9-methylxanthine at the PGE varied with pH, potential, and concentration (Table 4). At potentials in the vicinity of peaks IIIa and IVa, coulometry of 9-methylxanthine yielded a faradaic n-value approaching about 4 at concentrations less than about 1 mM and in solutions of pH greater than the pK_a of 6.3. In higher concentration solutions of similar pH the n-value fell to as low as 2.7. When the applied potential was less positive, e.g., in the vicinity of peaks Ia and IIa for 9-methylxanthine, the observed faradaic n-value ranges from ca. 3.1-3.5 at low concentration to ca. 2.8 at high concentration. In solutions where the pH is less than the pK_a of 6.3, the variation in the faradaic n-value is not as significant with changes in potential and concentration, ranging from 3.6 to 4.1. It was generally found throughout this study that the experimental n-values were rather variable.

It was noted during controlled potential electrolyses of 9-methylxanthine that a yellow-orange color appeared in the solution that was also dependent upon pH, potential, and concentration. No color change was noted in electrolyses of solutions at various applied potentials at pH 2 and 3. With increasing pH but below the pK_a of 6.3 there was a gradual increase in the intensity of the yellow color, but at

TABLE 4

Coulometric[a] n-values for the electrochemical oxidation of 9-methylxanthine at the PGE.

pH[b]	Initial Concentration, mM	Controlled Potential V vs SCE	n-value[c]
4	3.0	1.0 (peaks Ia/IIa)	3.6**
4	3.0	1.3 (peak IVa)	3.7
4	0.5	1.0	3.8
4	0.5	1.3	4.1
4	0.1	1.0	3.9
4	0.1	1.3	4.1
7	3.0	0.8 (peaks Ia/IIa)	2.8*
7	3.0	1.1 (peak IVa)	3.0*
7	0.5	0.8	3.1*
7	0.5	1.1	4.0
7	0.1	0.8	3.5
7	0.1	1.1	3.9
9	3.0	0.8 (peaks Ia/IIa)	2.8*
9	3.0	1.1 (peak IVa)	2.7*
9	0.5	0.8	3.2*
9	0.5	1.1	3.9
9	0.1	0.8	3.3
9	0.1	1.1	3.8

a Electrolyses continued until voltammetry and u. v. spectrum of initial 9-methylxanthine gone

b All buffers made using mixed NaH_2PO_4 and Na_2HPO_4

c Each n-value is the average of at least three experiments

** slight yellow solution after electrolysis

* yellow solution after electrolysis

only high concentrations was it stable for more than approximately 1 hour. In solutions of pH 7-9 at potentials of ca. 1.0-1.2 V (corresponding to peaks IIIa - IVa) with concentrations below approximately 0.5 mM the yellow-orange color appeared in the solution within 10 minutes. The intensity of the yellow-orange solution reached its maximum in about one hour and then gradually faded and completely disappeared within 2-3 hours. When the concentration of 9-methylxanthine was greater than 0.5 mM, the intensity of the yellow-orange solution was greater when it reached its maximum and did not completely fade away when voltammetry indicated that all of the 9-methylxanthine had been oxidized.

It was also discovered that the yellow-orange color appeared when the applied potential corresponded to peaks Ia and IIa of 9-methylxanthine (0.75-0.90 V vs SCE). At these potentials and with a concentration of 3 mM a coincidence of the maximum in intensity of the yellow-orange solution and the completion of the electrolysis (confirmed by voltammetry) was observed. The stability of the material causing the color was studied. The intensity of the yellow-orange color was monitored periodically at 415 nm to check for any decay. Over a period of 12 hours the yellow intensity did not change.

Cyclic voltammetry was also run periodically on controlled potential electrolysis solutions during the course of these experiments. When 9-methylxanthine was

electrolyzed at all potentials, but most notably at those corresponding to peaks Ia and IIa (ca. 0.75-0.90 V vs SCE) in pH 7-9 buffer, peak IIa began to grow significantly (Figure 25) in relation to the other peaks. As the electrolysis progressed, peak IIa continued to grow while peaks Ia, IIIa, IVa, Ic and Va all began to diminish. Finally, as shown in Figure 25 D, only peak IIa is present. This behavior would imply that the peak IIa process is not an oxidation of initially present 9-methylxanthine. To form peak IIa, the electrolysis must first produce the peak Ia product. Therefore, during the initial portion of an electrolysis as more peak Ia product is formed an increase in oxidation peak IIa is observed. Once all of the 9-methylxanthine present is oxidized in the peak Ia process, the peak IIa process becomes dominent. Then peak IIa will begin to diminish and finally disappear. In addition, it was discovered that the growth and disappearance of peak IIa was related to the increase in yellow-orange color intensity.

This behavior is not observed at low pH. At pH values below pK_a (6.3) all oxidation peaks disappeared uniformly as the electrolysis proceeded.

It appears from these data that peaks IIIa and IVa represent oxidation of the initially present 9-methylxanthine. As 9-methylxanthine is consumed in the peak Ia process peaks IIIa and IVa correspondingly disappear at all pH values. However, in the pH range where 9-methylxanthine exists as

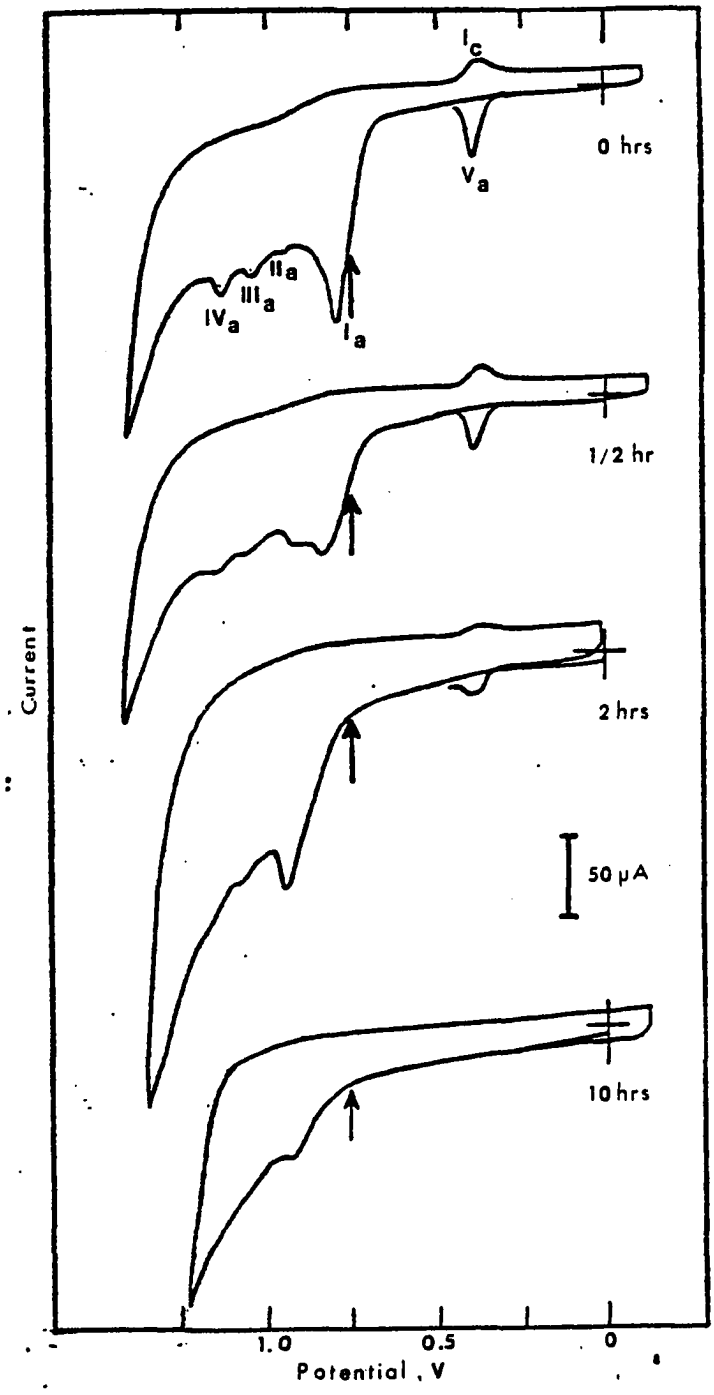

Figure 25. Cyclic voltammograms at various stages during electrolysis of 1 mM 9-methylxanthine at pH 7 at the PGE. Arrow at applied potential (0.75 V). Scan rate 200 $mVsec^{-1}$.

a monoanion, oxidation via the peak Ia process produces a product which is then slowly oxidized in the peak IIa process.

Due to the close proximity of the electrode processes' oxidation peaks it was impossible to isolate and determine an n-value for each individual peak process. Thus interference from neighboring peak processes affects the reported n-values.

A plausible mechanism to explain the observed concentration dependency of the controlled potential coulometric data could have the peak Ia process behave in the following manner:

$$A \rightarrow B + n_1 e \qquad \text{(step 1)}$$

$$2B \rightarrow C \qquad \text{(step 2)}$$

$$B \rightarrow D + n_2 e \qquad \text{(step 3)}$$

In this situation a non-integral value of n would be expected. It would approach $(n_1 + n_2)$ at low concentrations and n_1 at high concentrations, and vary with the initial concentration. At pH 4, where 9-methylxanthine is a neutral species, step 2 above would apparently be negligible as the n-value is similar at all concentrations at pH 4 and close to the values obtained at low concentrations at pH 7. Therefore, A could proceed to D and concentration would not be as important a factor in determining the value of n. This could explain the fact that changes in concentration do not greatly affect the observed n-value of 9-methylxanthine at pH 4 (Table 4). However in the case where 9-methylxanthine is an anion (pH > 6), step 2 could be an important

factor in the determination of the n-value. This may be shown in Table 4, by the decrease in n-value observed with an increase in initial concentration of 9-methylxanthine at both pH 7 and 9.

Potentiostatic studies

To further clarify the nature of the peaks Ia, IIa, IIIa, and IVa processes, potentiostatic current-time curves were measured at pH 4 and pH 7 in 0.5 to 10 mM solutions of 9-methylxanthine at potentials corresponding to all four oxidation peaks. The expression for the instantaneous current at a plane electrode under semiinfinite linear diffusion control is given by the Cottrell equation[44]:

$$i_t = \frac{nFAD^{1/2}C}{\pi^{1/2}t^{1/2}} \qquad (3)$$

where i_t = current at time (t) in amperes

n = total number of electrons

A = electrode area, cm^2

D = diffusion coefficient of electroactive species, $cm^2 sec^{-1}$

C = concentration of electroactive species in moles ml^{-1}

For a particular value of concentration the value of $i_t t^{1/2}$ should remain constant if the system is under diffusion control. In the case of 9-methylxanthine for periods between 0.02 and 4 seconds, the product $i_t t^{1/2}$ does in fact remain essentially constant. Potentiostatic current-time curves were measured in order to obtain n-values for two reasons; (1) controlled potential coulometry proved rather difficult

at high potentials due to rather variable results caused by large background current corrections, and (2) the short time period required to complete potentiostatic studies could separate the inital electrode process from subsequent chemical and electrochemical processes. The values of n determined by potentiostatic methods were found to be both pH and concentration dependent, similar to those observed with controlled potential electrolysis. Typical curves used for obtaining n-values via potentiostatic studies are shown in Figure 26 (pH 4, 3 mM) and Figure 27 (pH 7, 3 mM).

Potentiostatically determined n-values (Table 5) parallel those determined by coulometry (Table 4) in that there is a general increase in the n-value as the potential is also increased. However, potentiostatic experiments do a much better job of isolating the peak Ia process from subsequent peak processes. Also, the implication from potentiostatic data is that the initial peak Ia process for both pH 4 and pH 7 are the same owing to their similar n-values. This was not obvious from controlled potential coulometry experiments. There is clearly no evidence for an ece (coupled electrochemical-chemical-electrochemical) or similar mechanism over the time scale of these experiments since there is no tendency for n to veer from, e.g., 1 to 2, 2 to 4, etc.

Spectroelectrochemistry

The methodology of thin-layer spectroelectrochemistry coupled to a rapid scan spectrometer was first proposed by

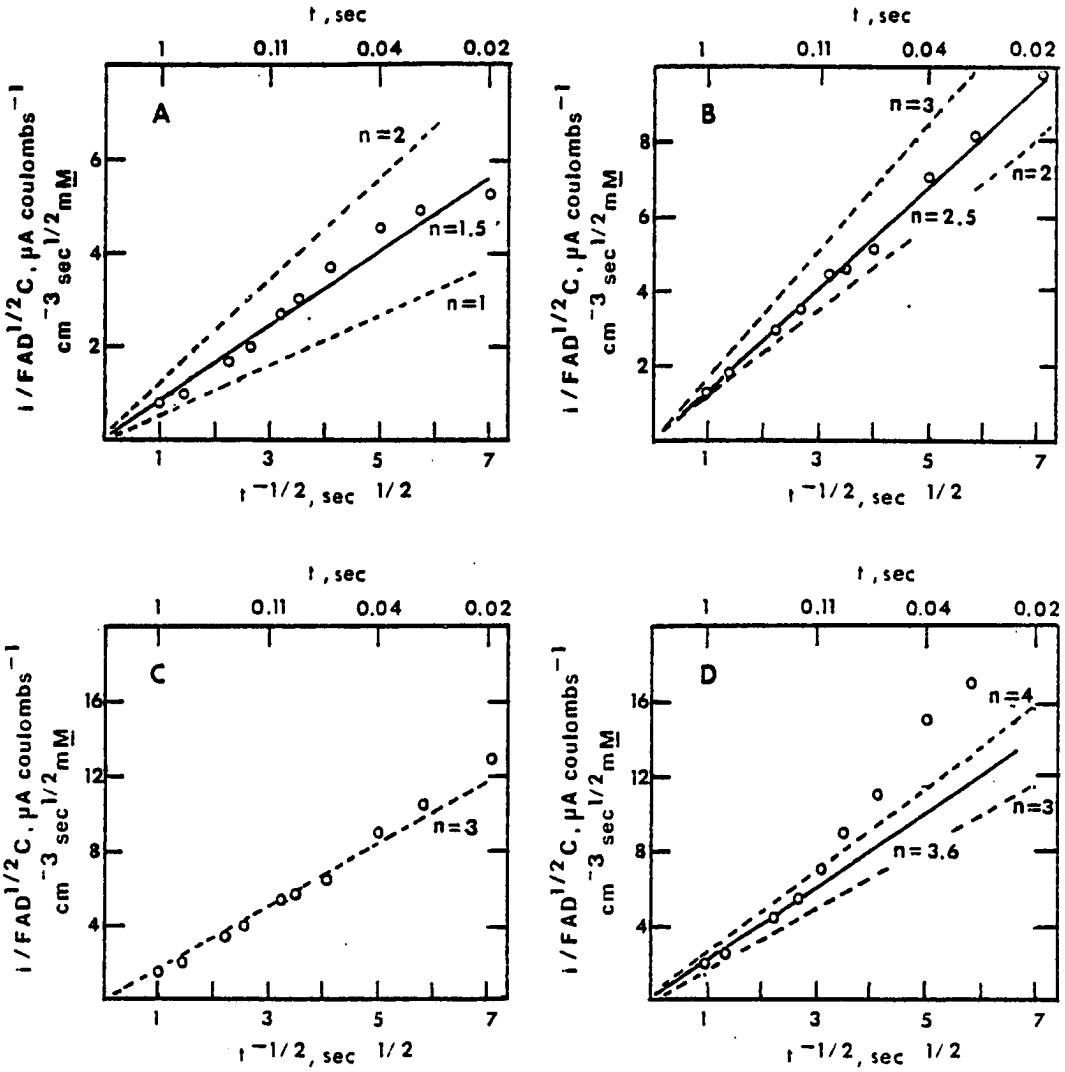

Figure 26. Comparison of experimental with the theoretical normalized current-time curves for the electrochemical oxidation of 9-methylxanthine at the PGE in pH 4; (A) at 0.93 V , peak Ia, (B) 1.04 V , peak IIa, (C) 1.10 V , peak IIIa, and (D) 1.35 V , peak IVa. Circles represent experimental values. Dotted lines represent theoretical curves calculated from the Cottrell equation.

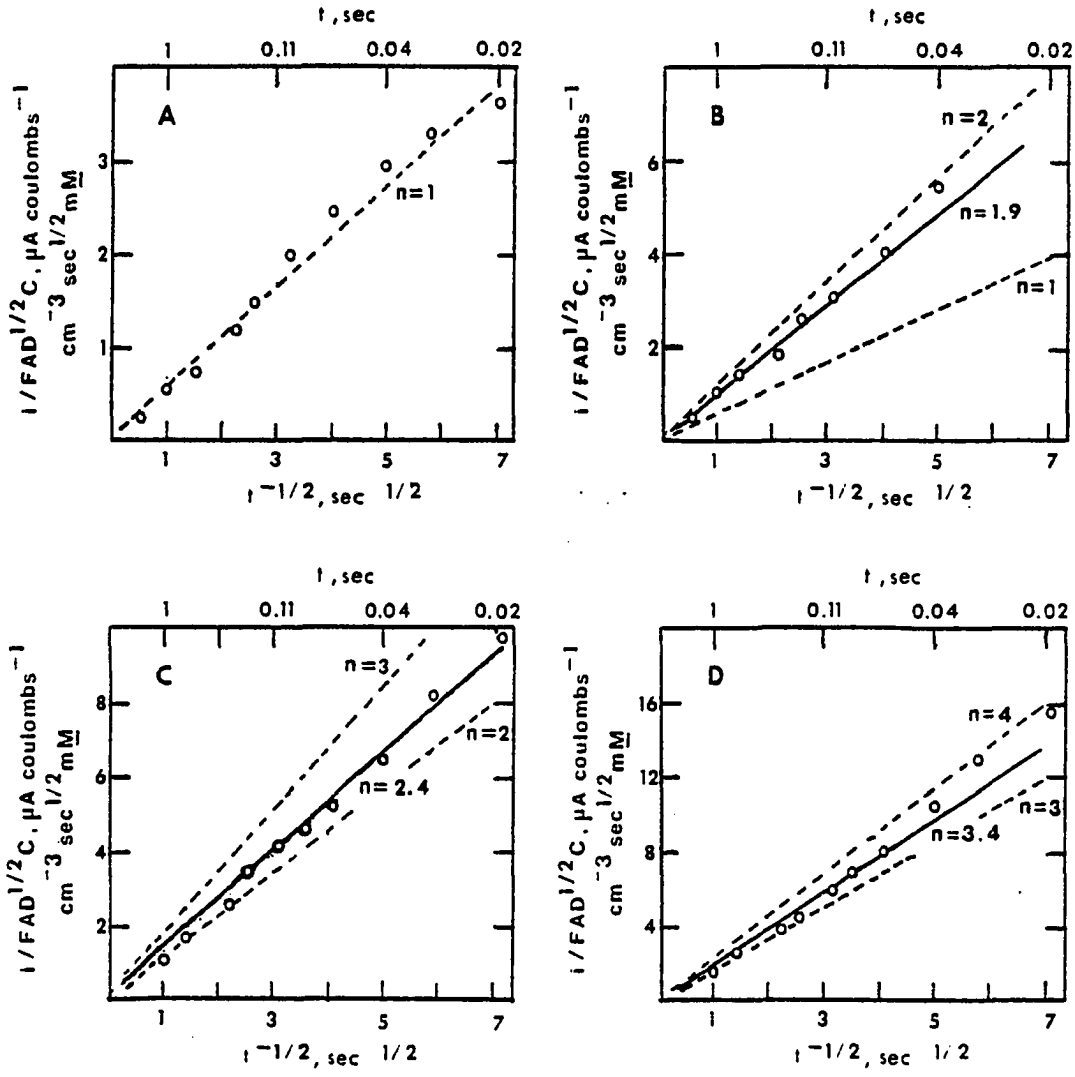

Figure 27. Comparison of experimental with the theoretical normalized current-time curves for the electrochemical oxidation of 9-methylxanthine at the PGE in pH 7; (A) at 0.75 V , peak Ia, (B) 0.90 V , peak IIa, (C) 1.00 V , peak IIIa, and (D) 1.24 V , peak IVa. Circles represent experimental values. Dotted lines represent theoretical curves calculated from the Cottrell equation.

TABLE 5

Potentiostatic n-values for the electrochemical oxidation of 9-methylxanthine at the PGE.

pH	Initial Concentration, mM	Applied Potential V vs SCE	n-value
4	3.0	0.93 (peak Ia)	1.5
4	3.0	1.04 (peak IIa)	2.5
4	3.0	1.10 (peak IIIa)	3.0
4	3.0	1.35 (peak IVa)	3.6
7	0.5	0.75 (peak Ia)	2.1
7	0.5	0.90 (peak IIa)	2.2
7	0.5	1.00 (peak IIIa)	3.0
7	0.5	1.20 (peak IVa)	3.7
7	3.0	0.75 (peak Ia)	1.0
7	3.0	0.90 (peak IIa)	1.9
7	3.0	1.00 (peak IIIa)	2.4
7	3.0	1.25 (peak IVa)	3.4
7	10.0	0.85 (peak Ia)	1.3
7	10.0	1.00 (peak IIa)	1.8
7	10.0	1.40 (peak IVa)	3.0

Murray, et al.[45]. Using this technique the spectrum of an electrolyzing solution is monitored in the hope that any transient but absorbing intermediates might be detected. It was anticipated that this method would allow a more detailed study of any absorbing chemical and electrochemical intermediates.

Most of the thin-layer spectroelectrochemical studies utilized a reticulated vitreous carbon working electrode. Optically transparent thin-layer cells utilizing a reticulated vitreous carbon (RVC) electrode were preferred over thin-layer cells containing optically transparent gold minigrid electrodes because the RVC cell could be made much thicker, giving the cell a longer path length. This permitted solutions of less than 2 mM concentration to give large enough absorbance readings to permit meaningful data acquisition. Gold minigrid electrodes were used with high concentration ($\geq$ 2 mM) solutions of 9-methylxanthine. Solutions at these concentrations in RVC cells gave too large an absorbance signal. Thus, gold minigrid electrodes, with their shorter path length, were used to obtain meaningful data from solutions of 2 mM and higher concentration. An additional reason for using a RVC cell is that at potentials of ca. 1.0 V the positive potential window of the gold electrode is limited by gold oxide formation[46].

It has already been shown[34] by voltammetry and coulometry that the electrochemical behavior of 9-methylxanthine

at a gold electrode parallels that observed at the PGE.

On the basis of extensive thin-layer spectroelectrochemical studies it was found that 9-methylxanthine behaves differently at pH 8 with change in concentration but at pH 4 there is no change in the spectroelectrochemistry of 9-methylxanthine with concentration. A typical u. v. spectrum of 9-methylxanthine obtained prior to electrolysis in pH 8 buffer at a concentration of 10 mM at a gold minigrid electrode is shown in curve 1 of Figure 28. It may be observed that 9-methylxanthine exhibits two absorption bands with λ_{max} values of 283 nm and 250 nm. Upon application of a potential of 1.2 V (which using a gold minigrid electrode corresponds to peak IIa) both u. v. bands begin to decrease with time. However, this effect is more pronounced for the band at longer wavelengths. Simultaneously, new absorption bands, λ_{max} = 340 and 219, respectively, appear and grow. These bands reach maximal values and then they also decrease. Curve 2 in Figure 28 is the spectrum observed when essentially all 9-methylxanthine has been oxidized and the bands having λ_{max} ≈ 340 nm and ≈ 230 nm have reached their maximal values. Curve 3 in Figure 28 is the spectrum of an exhaustively electrolyzed solution of 9-methylxanthine. Both u. v. spectra shown in curves 2 and 3 correlate well with products isolated from mass electrolyses (*vide infra*). Thin-layer spectroelectrochemical studies of 9-methylxanthine between pH 7 and 9 at potentials ranging from 0.9 to 1.2 V over a concentration range of 2-20 mM gave results similar to those shown in

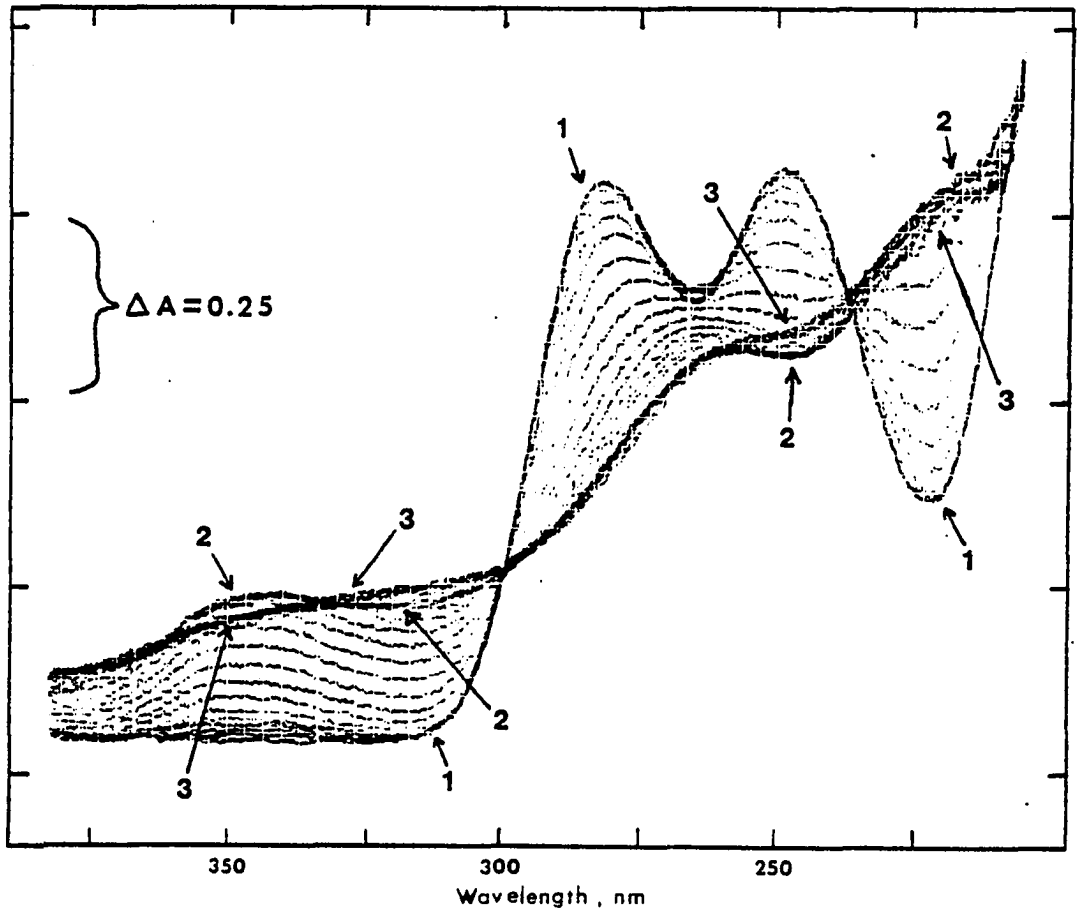

Figure 28. Spectra of 10 mM 9-methylxanthine electrolyzed at 1.2 V (peak IIa) at pH 8 at a gold minigrid electrode in a thin-layer cell. Curve (1) is spectrum before electrolysis. Electroysis when absorption peak with λ_{max} = 340 nm has reached its maximum, curve (2). Curve (3) is spectrum after exhaustive electrolysis. Repetitive scans are 23.5 sec.

Figure 28. However, one important phenomenon was observed. At a concentration of 2 m$\underline{M}$, the maximum absorbance at 340 nm was about 15 per cent of the initial absorbance of 9-methylxanthine at 283 nm; whereas at a concentration of 20 m$\underline{M}$, the maximum absorbance at 340 nm was almost 30 per cent. For concentrations between 2 and 20 m$\underline{M}$ the ratio $(A_{max})_{340}$ / $(A_{initial})_{283}$ increased with increasing concentration. This suggests that 9-methylxanthine forms a primary electrochemical product which may undergo a second-order reaction such as dimerization. The relative extent of dimerization can be greatly increased by employing initial concentrations on the order of those above, as noted by Meites[47]. If the electrolysis is discontinued when the peaks at 340 nm and 230 nm reach their maximum absorbance (curve 2, Figure 28), an absorbance decay is observed in the region 330-360 nm which is different from the decay in that same region when the electrolysis is continued. The decay in the 230 nm region is very small, making it impossible to determine whether discontinuing the electrolysis causes a different decay in this region. The effect on the absorption peaks of discontinuing the electrolysis at the peaks' maximum absorbance is shown in Figure 29. It should be noticed that there is no change in the shape of the absorption peak at 340 nm, only a general decay over the region 330-360 nm.

In the same pH range using a reticulated vitreous carbon working electrode, but over a concentration range of 0.2-1.0 m$\underline{M}$

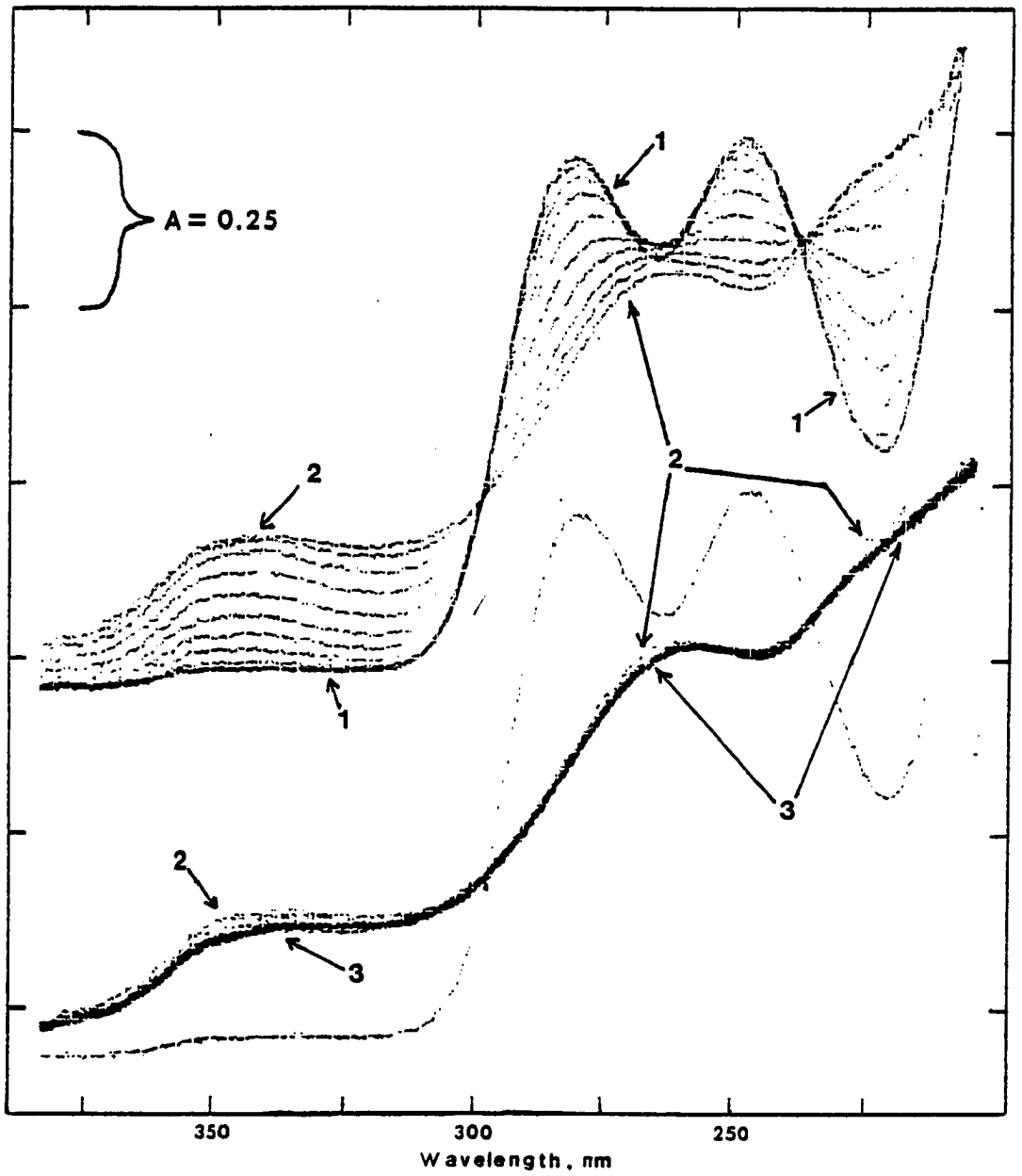

Figure 29. Spectra of 10 mM 9-methylxanthine electrolyzed at 1.2 V (peak IIa) at pH 8 at a gold minigrid electrode in a thin-layer cell. Curve (1) is spectrum before electrolysis. Electrolysis stopped at Curve (2). Curve (3) is spectrum after decay of intermediate. Repetitve scans are 23.5 sec.

at potentials corresponding to all four oxidation peaks no absorption band with a λ_{max} at 340 nm appears similar to that depicted in curve 2 of Figure 29. The electrolysis appears to proceed directly to a spectrum similar to that of curve 3 in Figure 28. Typical behavior is shown in Figure 30. If this electrolysis is discontinued before total decay of the initial absorption peaks take place a different decay is observed, most prominently at ≈230 nm and ≈272 nm, (Figure 31). These are similar wavelength regions to those in Figure 29 where small decays took place. A similar result to that observed for 0.2-1.0 m$\underline{M}$ 9-methylxanthine was also observed for 1.0 m$\underline{M}$ 9-methyluric acid at 1.30 V (slight positive of its oxidation peak Ia[19]). This is shown in Figure 32. These similar spectra for both molecules may imply that at low concentration in the pH range 7-9, 9-methyluric acid and peak IVa of 9-methylxanthine have an identical intermediate.

Studies of the thin-layer spectroelectrochemical oxidation of 9-methylxanthine at low pH (2-5) gave results similar to those shown in Figure 33 over a concentration range of 0.2-2.0 m$\underline{M}$ and a potential span between 1.0-1.4 V (peaks Ia - IVa). Prior to electrolysis in pH 4 buffer at a reticulated vitreous carbon electrode, a typical u. v. spectrum of 9-methylxanthine is shown in curve 1 of Figure 33. Two absorption bands with λ_{max} values of 269 nm and 240 nm are observed for 9-methylxanthine. Upon application of a potential

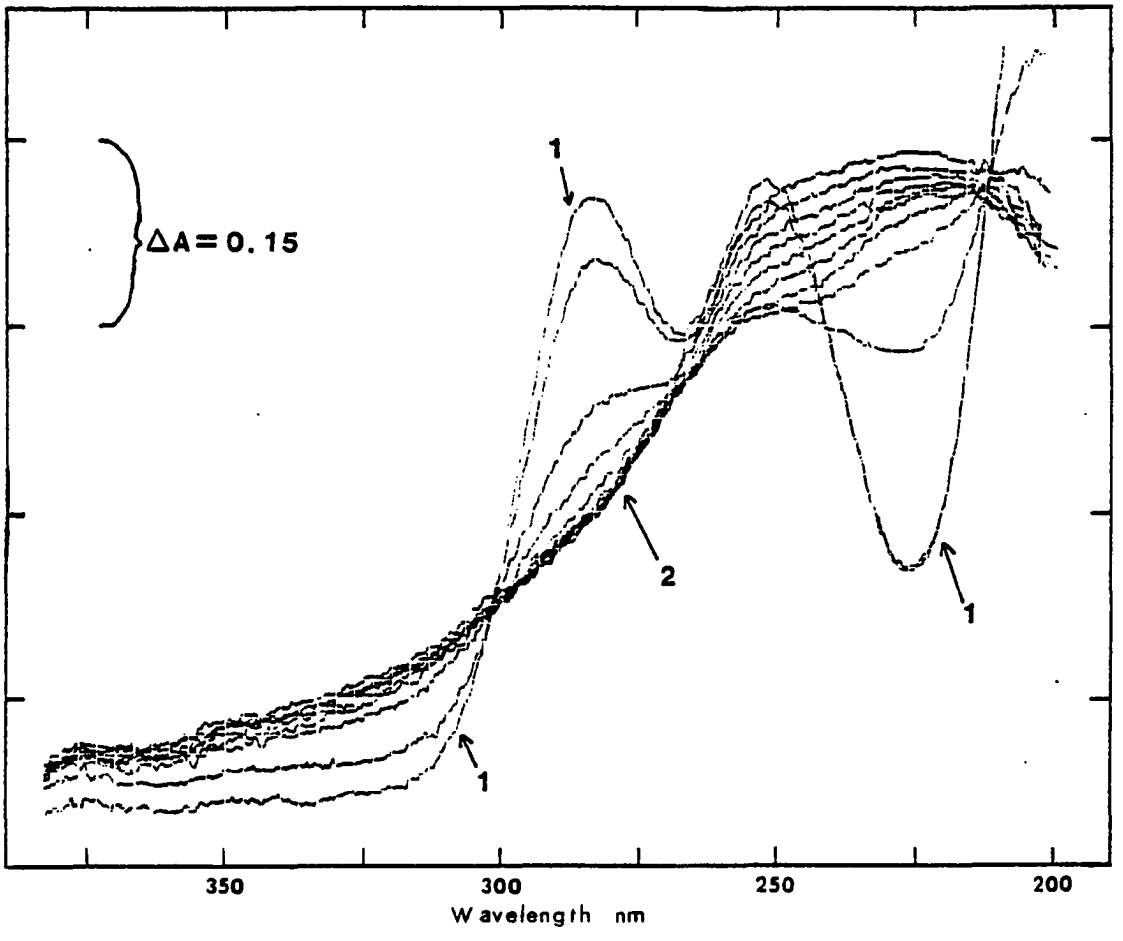

Figure 30. Spectra of 0.5 mM 9-methylxanthine electrolyzed at 1.2 V (peak IVa) at pH 8 at a reticulated vitreous carbon electrode in a thin-layer cell. Curve (1) is spectrum before electrolysis. Curve (2) is spectrum after electrolysis. Repetitive scans are 23.5 sec.

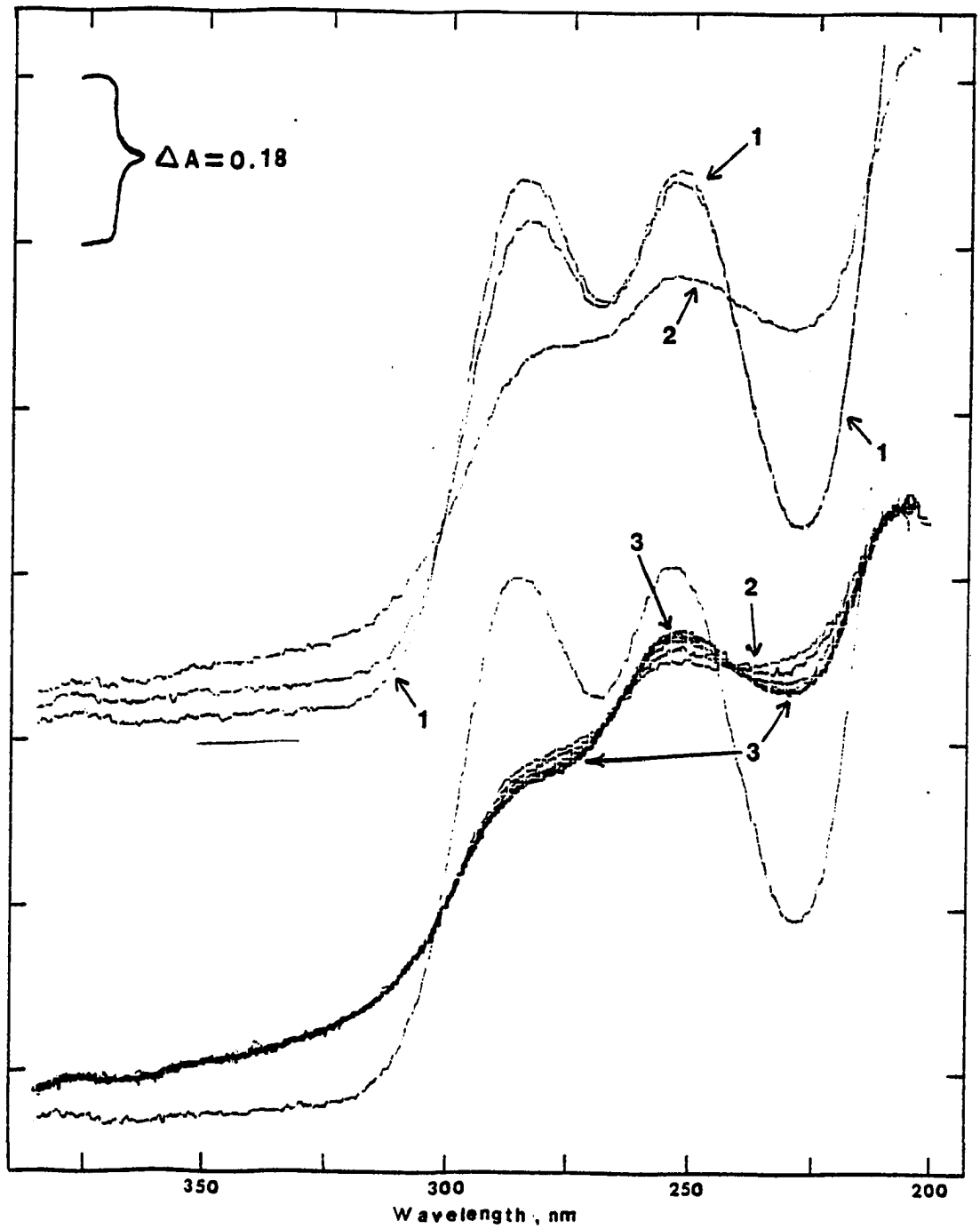

Figure 31. Spectra of 0.5 mM 9-methylxanthine electrolyzed at 1.2 V (peak IVa) at pH 8 at a reticulated vitreous carbon electrode in a thin-layer cell. Curve (1) is spectrum before electrolysis. Electrolysis stopped at Curve (2). Curve (3) is spectrum after decay of intermediate. Repetitive scans are 23.5 sec. for upper spectra and 47 sec. for lower spectra.

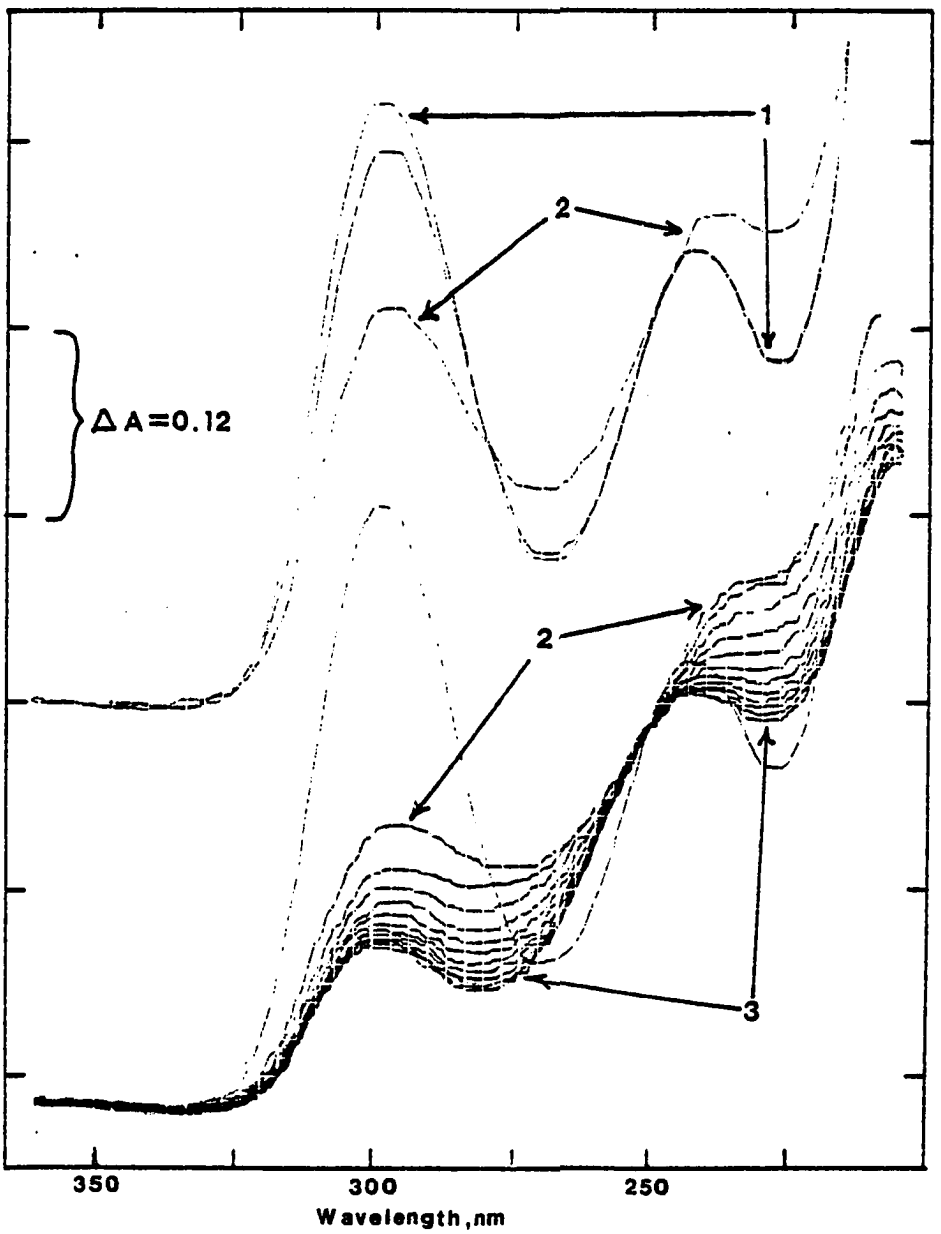

Figure 32. Spectra of 0.5 mM 9-methyluric acid electrolyzed at 1.0 V (the major oxidation peak of 9-MUA) at pH 8 at a reticulated vitreous carbon electrode in a thin-layer cell. Curve (1) is spectrum before electrolysis. Electrolysis stopped at curve (2). Curve (3) is spectrum after decay of intermediate. Repetitive scans are 18.9 sec.

of 1.30 V corresponding to oxidation peak IVa, both u. v. bands begin to decrease with time. Simultaneously, two new absorption bands, one with λ_{max} = 234 nm and the other λ_{max} = 280, appear and grow. These bands reach maximal values and then also decrease and disappear. Curve 2 in Figure 33 is the spectrum observed when essentially all 9-methylxanthine has been oxidized and the bands having λ_{max} ≈ 234 nm and ≈ 280 nm have reached their maximal values. The observed spectroelectrochemical behavior this supports the view that upon electrochemical oxidation of 9-methylxanthine an unstable intermediate is formed which has two absorption peaks at different wavelengths than the absorption peaks for 9-methylxanthine. Curve 3 in Figure 33 is the spectrum of an exhaustively electrolyzed solution of 9-methylxanthine at a time when all of the absorbing intermediate species has disappeared. The decrease of absorbance observed around 234 nm and 280 nm occurred regardless of whether the initial potential applied to the electrode was maintained or turned off as shown in Figure 34. It should be noted that at no potential or concentration did an absorption band with a λ_{max} = 340 nm appear, as in the case of 9-methylxanthine at pH 7-9 and concentrations greater that 1 m<u>M</u>.

Similar thin-layer spectroelectrochemical behavior was observed for the oxidation of 9-methyluric acid (Figure 35) at pH 4 as was observed for 9-methylxanthine.

For reasons detailed below, it is believed that an

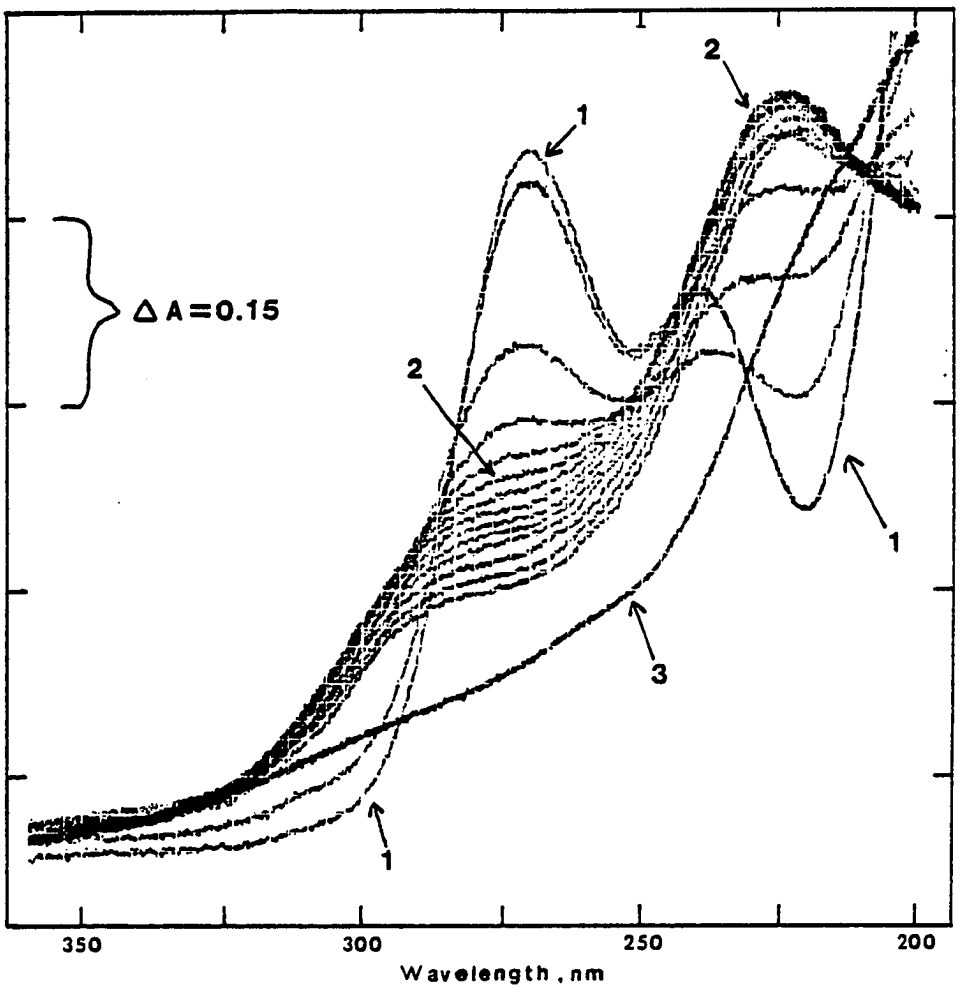

Figure 33. Spectra of 1 mM 9-methylxanthine electrolyzed at 1.4 V (peak IVa) at pH 4 at a reticulated vitreous carbon electrode in a thin-layer cell. Curve (1) is spectrum before electrolysis. Electrolysis when absorption peak with λ_{max} = 234 nm has reached its maximum, curve (2). Curve (3) is spectrum after exhaustive electrolysis. Repetitive scans are 47 sec.

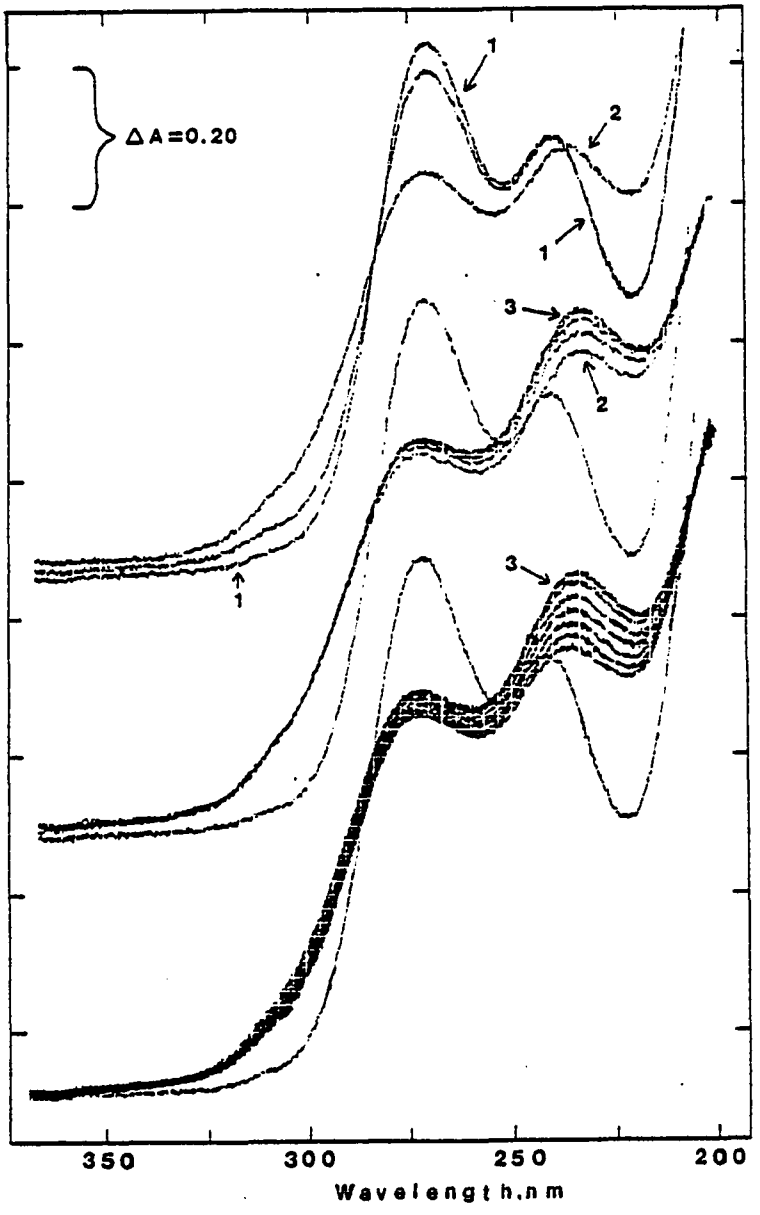

Figure 34. Spectra of 1 mM 9-methylxanthine electrolyzed at 1.4 V (peak IVa) at pH 4 at a reticulated vitreous carbon electrode in a thin-layer cell. Curve (1) is spectrum before electrolysis. Electrolysis stopped at Curve (2). Curve (3) is spectrum when absorption peak with λ_{max} = 234 nm has reached its maximum. This peak subsequently decays. Repetitive scans are 47 sec. for upper two spectra and 94 sec. for lower spectra.

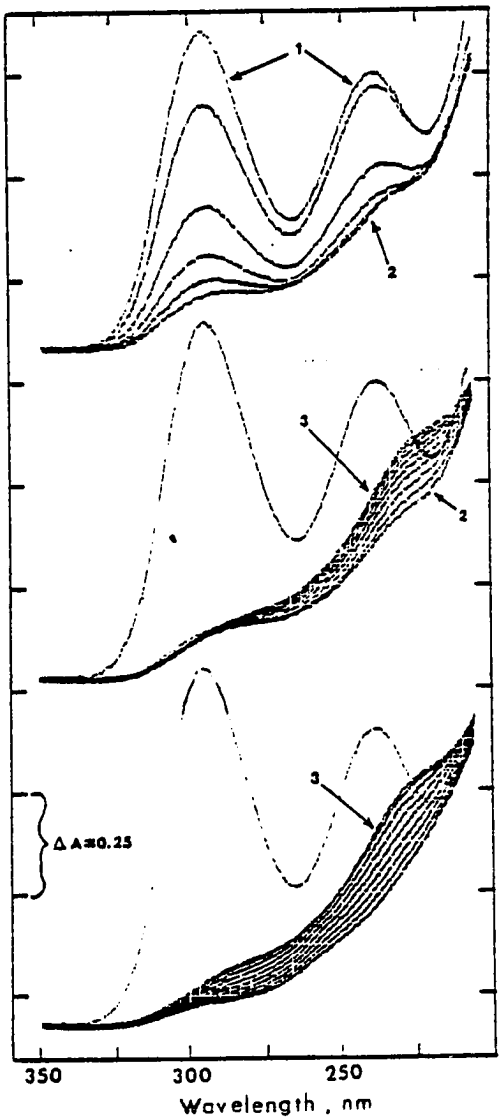

Figure 35. Spectra of 1 mM 9-methyluric acid electrolyzed at 1.2 V (the major oxidation peak of 9-MUA) at pH 4 at a reticulated vitreous carbon electrode in a thin-layer cell. Curve (1) is spectrum before electrolysis. Electrolysis stopped at curve (2). Curve (3) is spectrum when absorption peak with λ_{max} = 234 nm has reached its maximum. This peak subsequently decays. Repetitive scans are 18.9 sec. for upper spectra, 23.5 sec. for middle spectra, and 94 sec. for low spectra.

u. v.-absorbing imine-alcohol intermediate similar to structure III of Figure 1 formed by partial hydration of the diimine primary electrooxidation product of uric acid is also the u. v.-absorbing intermediate species detected by thin-layer spectroelectrochemistry for 9-methylxanthine between pH 7-9, at concentrations below 1 mM. It has been reported[19] that uric acid and its 1- and 7-methyl derivatives give an u. v.-absorbing intermediate with λ_{max} (ca. 310 nm) at longer wavelengths than the parent uric acid whereas all other N-methylated uric acids give an intermediate which absorbs between ca. 230-280 nm. This data suggests a more extensively conjugated structure for the intermediate formed form uric acid and from 1-methyl and 7-methyl uric acids resulting in the observed bathochromic shift. Over the pH range where the u. v.-absorbing intermediate was observed (pH 6-9) uric acid and its 1- and 7-methyl derivatives exist as a monoanion. Thus it would seem reasonable to conclude that the imine-alcohol would also be an anionic species. Clearly the u. v.-

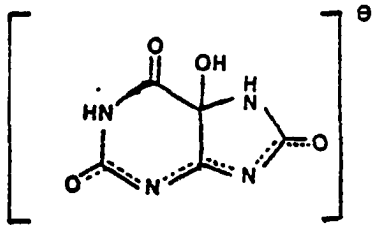

III

absorbing imine-alcohol anion (III) can exist in several resonance forms even if the N(1) and/or N(7) positions are methylated. Such a structure has a more delocalized π-electron

system than even the parent uric acid, hence it would be expected to absorb at longer wavelengths. All other N-methylated uric acids studied by Wrona, et al.[19] which gave an u. v.-absorbing intermediate were substituted at N(3) or N(9) and hence could not form an imine-alcolhol anion having the many resonance forms shown above. Accordingly, they suggested such imine-alcohol intermediates should absorb at shorter wavelengths. The fact that 9-methylxanthine and 9-methyluric acid show similar spectroelectrochemistry and have similar rate constants and products (vide infra) implies similar reaction mechanisms for both molecules. The very short lifetime of the u. v.-absorbing intermediate effectively precludes additional experiments to determine the structures proposed for the imine-alcohol.

That the u. v.-absorbing imine-alcohol intermediate is responsible for reduction peak IIc observed on cyclic voltammetry of 9-methylxanthine was further demonstrated by other thin-layer spectroelectrochemical experiments using a reticulated vitreous carbon working electrode. A solution of 9-methylxanthine at pH 8 was first electrolyzed at a potential slightly positive of peak IVa so that the imine-alcohol was formed and could be observed via its u. v. spectrum. After 50 seconds the electrode potential was switched to a potential negative of reduction peak IIc. Under these conditions the imine-alcohol spectrum disappeared much more rapidly than if no potential was applied, i.e., at potentials corres-

ponding to reduction peak IIc the imine alcohol is electrochemically reduced.

In the case of 9-methylxanthine at low pH (pH 3-5), it is also believed that an u. v.-absorbing imine-alcohol intermediate is the species detected by thin-layer spectroelectrochemistry. The reasoning is similar to that proposed for 9-methylxanthine at pH 7-9 above. The only difference is slower kinetics at low pH.

From data collected by voltammetry, controlled potential coulometry, and u. v. - vis. spectroscopy (vide infra) it is thought that an u. v. and vis. (yellow) absorbing dimer is decaying species detected by thin-layer spectroelectrochemistry in pH 7-9 buffer at concentrations above 1 mM in 9-methylxanthine. The formation of this yellow dimer is the result of further oxidation (peak IIa) of the dimer formed in the peak Ia process (vide infra). The absorbance peak at 340 nm is due to the peak Ia dimer. The yellow dimer also shows u. v. absorption in the wavelength range 330-360 nm. However it displays only a gradual rise in absorbance (no peaks) from longer to shorter wavelength over this range. The yellow dimer, unlike the peak Ia dimer, is only moderately stable in water ultimately decomposing to 1-methylallantoin (vide infra) as determined by i. r. and mass spectroscopy. The fact that the peak Ia dimer is stable (vide infra) and that the relative shape of the absorption peak at 330-360 nm in Figure 29 did not change, but the whole peak decreased,

during the absorbance decay indicates it was not the peak Ia dimer that decayed. A species which had similar absorption over the entire 330-360 nm range, i.e. the yellow dimer, must have decayed. The observed small decays at ≈ 272 nm and ≈ 230 nm, which are at similar wavelengths to the imine-alcohol intermediate of 9-methylxanthine at low concentration in pH 7-9 solutions (Figure 31), may be an imine-alcohol intermediate from the decompostion of the yellow dimer to 1-methylallantoin.

Kinetic measurements

The kinetics of the decomposition reaction of the u. v.-absorbing intermediate species formed by electrooxidation of 9-methylxanthine were studied by thin-layer spectroelectrochemical techniques. The basic procedure employed was to electrolyze the 9-methylxanthine in an optically transparent thin-layer cell. The electrolysis was terminated when most of the 9-methylxanthine had been electrolyzed as indicated by an appropriate decrease of its u. v. absorbance. Then, the absorbance of the intermediate species was monitored as a function of time at a selected wavelength at which interference from the absorption of the starting material was minimal. Selected absorbance vs time graphs are shown in Figures 36-38. Figure 36 is typical of the absorbance at 340 nm vs time graphs obtained for 2-20 mM 9-methylxanthine solutions in pH 7-9 buffer at potentials from 0.9-1.2 V (peaks Ia-IIa). The absorbance at 230 nm vs time graph shown in Figure 37 is representative of 0.2-0.5 mM 9-methylxanthine solutions in

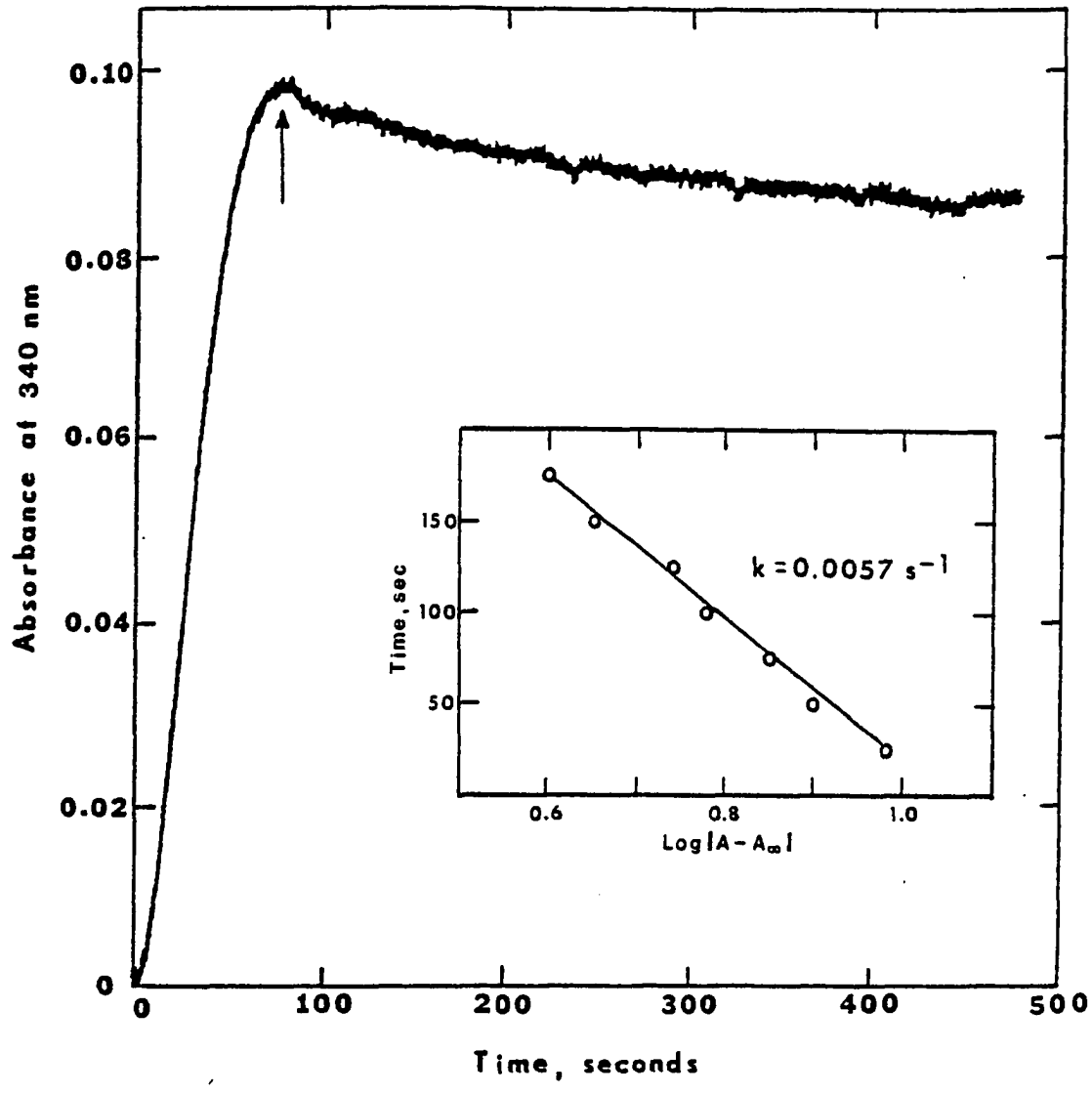

Figure 36. a. Absorbance vs. time for electrooxidation of 10 mM 9-methylxanthine at pH 8 at 340 nm. Electrolysis at 1.2 V (peak IIa) stopped at arrow. b. Time vs. Log $|A - A_\infty|$ at 340 nm of the intermediate species formed on electrooxidation of 10 mM 9-methylxanthine at pH 8.

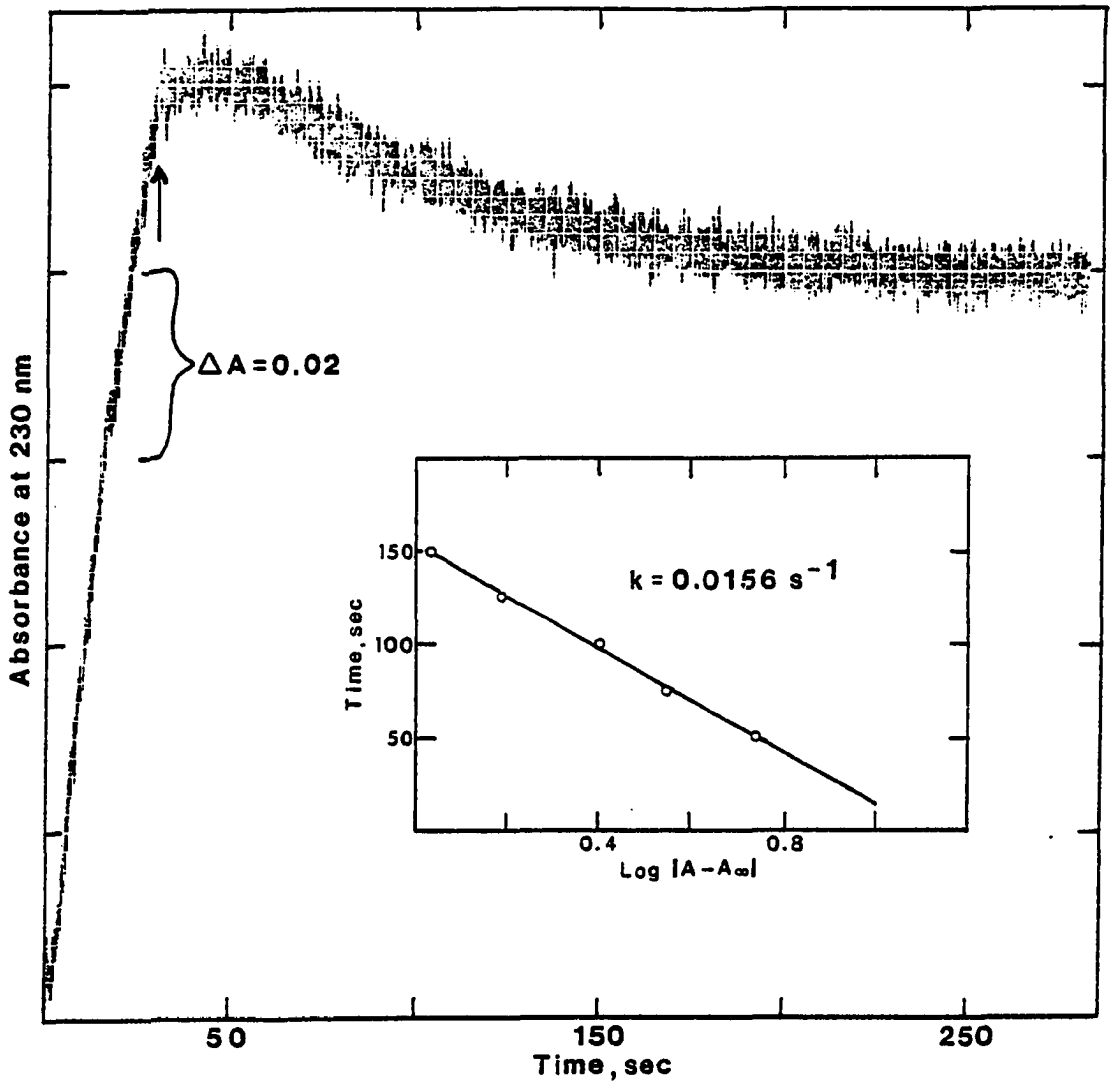

Figure 37. a. Absorbance vs. time for electrooxidation of 0.5 mM 9-methylxanthine at pH 8 at 230 nm. Electrolysis at 1.2 V (peak IVa) stopped at arrow. b. Time vs. Log $|A - A_\infty|$ at 230nm of the intermediate species formed on electro-oxidation of 0.5 mM 9-methylxanthine at pH 8.

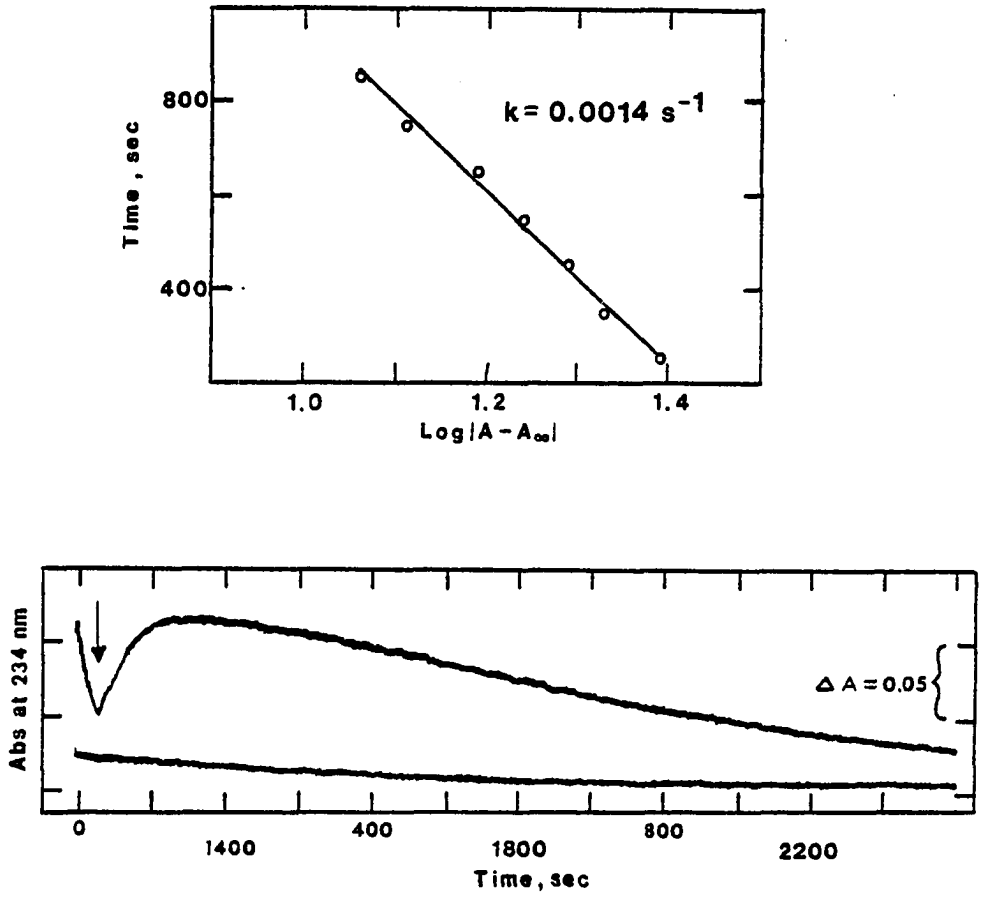

Figure 38. a. Absorbance vs. time for electrooxidation of 1.0 mM 9-methylxanthine at pH 4 at 234 nm. Electrolysis at 1.4 V (peak IVa) stopped at arrow. b. Time vs. log $|A - A_\infty|$ at 234 nm of the intermediate species formed on electrooxidation of 1.0 mM 9-methylxanthine at pH 4.

pH 7-8 buffer at a potential of 1.2 V corresponding to oxidation peak IVa. Solutions of 9-methylxanthine (0.2-2 mM) in pH 3-5 buffer at 1.4 V (peak IVa) gave absorbance at 234 nm vs time graphs similar to that shown in Figure 38. If the rate of these reactions depends only on the first power of the concentration of a single reacting species, they are considered first-order reactions. Representing the concentration of the species by C and if the volume of the system remains essentially constant during the course of the reaction at a given temperature, the first-order rate law can be written as

$$-\frac{dc}{dt} = kc \qquad (4)$$

The rate constant is then a positive quantity and has the units of the reciprocal of time. Thus experimental results are obtained by comparing absorbance, which is related to concentration, at various times. Such data can better be compared with the integrated form of the first-order rate law. If the initial absorption, at time t=0, is A_o and if at some later time t the absorption has fallen to A, the integration gives

$$-\int_{A_o}^{A} \frac{dA}{A} = k\int_{o}^{t} dt \qquad (5)$$

and

$$-\ln \frac{A}{A_o} = \ln \frac{A_o}{A} = kt \qquad (6)$$

or

$$\log \frac{A_o}{A} = \frac{k}{2.303} t \qquad (7)$$

A more convenient form is

$$\log A = -\frac{k}{2.303} t + \log A_o \qquad (8)$$

Thus a reaction can therefore be said to be a first-order reaction if a plot of log A against t gives a straight line. If a straight line is obtained, the slope of the line can be used to give the value of the rate constant k. For 9-methylxanthine under all conditions studied, plots of log $|A-A_\infty|$ vs time were linear, as shown in Figures 36-38 indicating that the decomposition reactions of the u. v. absorbing intermediates follow first-order kinetics. Values of the observed first-order solution rate constants studied at different pH values and concentrations are presented in Table 6. It is clear that the observed first-order rate constants vary as a function of pH over the pH range 3-9. However, the rate constants are generally independent of pH over the shorter ranges 3-5 and 7-9. In addition the rate constants are generally independent of concentration. Below pH 6, the rate constant is independent over the concentration range 0.2-2.0 mM. Above pH 6 there appears to be two distinct rate constants, one at high concentrations (2.0-20 mM) and one at lower concentrations (0.2-1.0 mM). Each proved independent over

TABLE 6

Observed first-order rate constants for reaction of the u.v.-absorbing intermediates formed on electrochemical oxidation of 9-methylxanthine and 9-methyluric acid

Compound Oxidized	λmax for absorption of intermediate, nm	pH	Initial Concentration, mM	k_{obs}, s^{-1}
9-methylxanthine	234	3	1.0	0.0014
9-methylxanthine	234	4	0.2	0.0013
9-methylxanthine	234	4	0.5	0.0014
9-methylxanthine	234	4	1.0	0.0014
9-methylxanthine	234	4	2.0	0.0015
9-methylxanthine	234	5	1.0	0.0016
9-methylxanthine	230	7	0.50	0.0121
9-methylxanthine	230	8	0.20	0.0185
9-methylxanthine	230	8	0.35	0.0151
9-methylxanthine	230	8	0.50	0.0143
9-methylxanthine	340	7	2.0	0.0055
9-methylxanthine	340	8	2.0	0.0058
9-methylxanthine	340	8	5.0	0.0060
9-methylxanthine	340	8	10.0	0.0054
9-methylxanthine	340	8	20.0	0.0059
9-methylxanthine	340	9	2.0	0.0056
9-methyluric acid	234	4	1.0	0.0014
9-methyluric acid	230	8	0.50	0.0130

its own concentration range. The rate constants and the shapes of the absorbance vs. time graphs for 9-methylxanthine at pH 4 are in good agreement with those results obtained for 9-methyluric acid under identical conditions (Figure 39). The shapes of the absorbance vs. time graphs for 9-methylxanthine and 9-methyluric acid above pH 6 and at a concentration below 1 mM are quite similar (Figure 40). However, the values of their rate constants are not in as good agreement as at pH 4. This may be due to influence from the "high concentration" mechanism.

For 9-methylxanthine at pH 4 and at 0.2-0.5 mM concentrations at pH 8, the kinetic curves show similar shape, but significantly different rate constants. This suggests that the imine-alcohol is more stable in the pH 4 region. At both pH 4 and pH 8, the rise in absorbance of the kinetic curves can be hypothesized to be the partial hydration of the diimine to an imine-alcohol. The fact that the intermediate continues to grow after the potential is turned off provides evidence that the observed rise in absorbance is not due to the formation of a primary electrooxidation product (diimine), but rather involves a species in homogeneous solution. Hydration of the imine-alcohol to the 4,5-diol is the hypothesized mechanism for the decreasing portion of the kinetic curves at both pH 4 and pH 8 (0.2-0.5 mM) for 9-methylxanthine. It should be noted that the rate constants reported here at pH 8 for 9-methylxanthine (0.2-0.5 mM, k = 0.015) and 9-methyl-

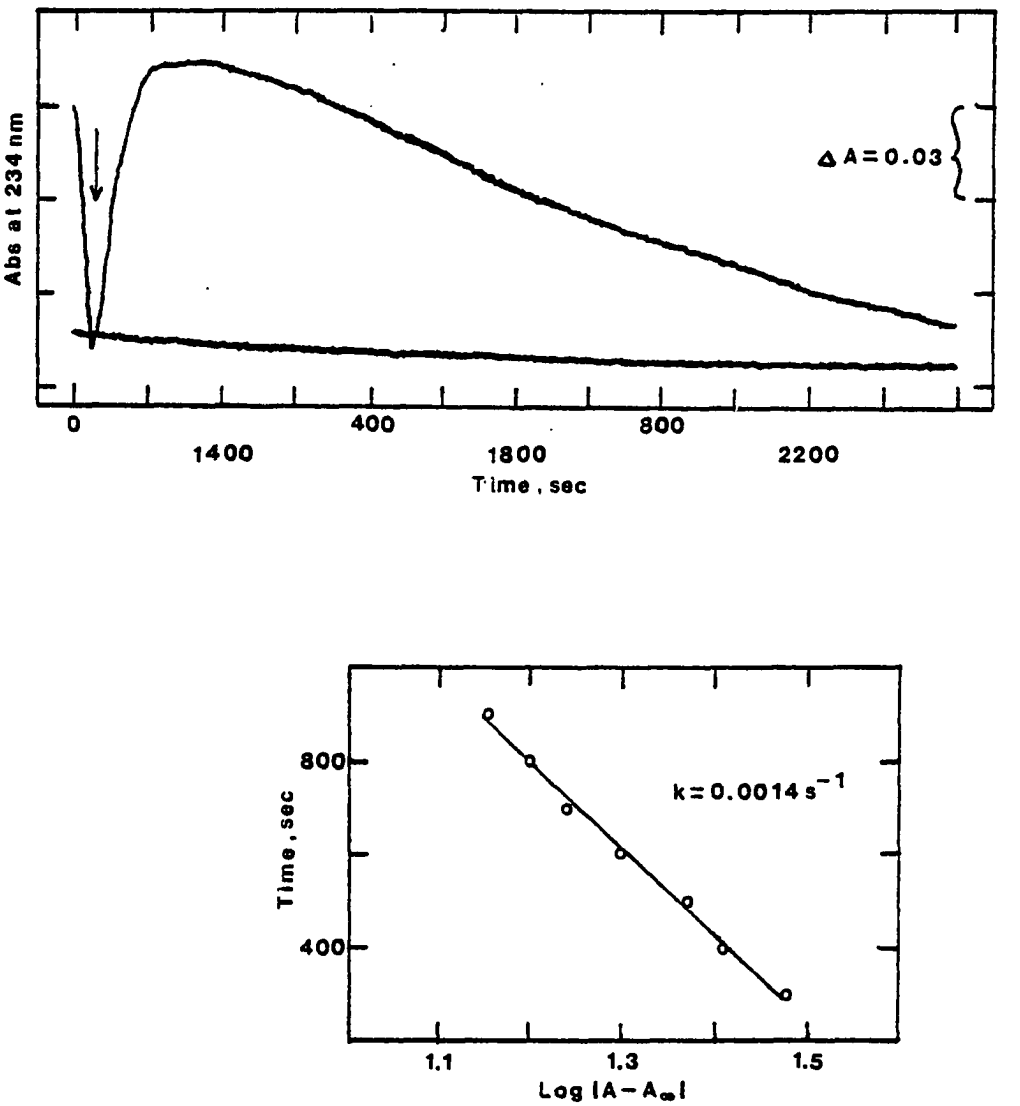

Figure 39. a. Absorbance vs. time for electrooxidation of 1.0 mM 9-methyluric acid at pH 4 at 234 nm. Electrolysis at 1.2 V (the major oxidation peak of 9-MUA) stopped at arrow. b. Time vs. log $|A - A_\infty|$ at 234 nm of the intermediate species formed on electrooxidation of 1.0 mM 9-methyluric acid at pH 4.

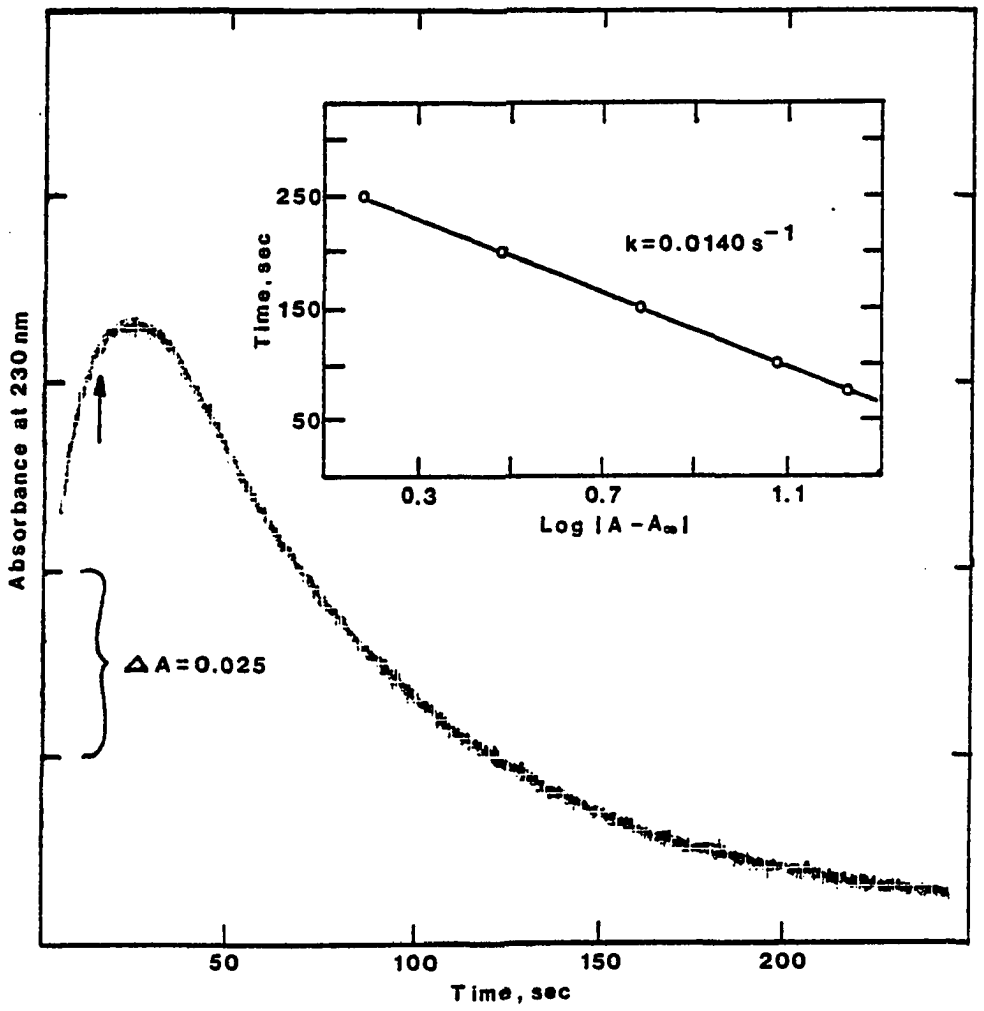

Figure 40. a. Absorbance vs. time for electrooxidation of 0.5 mM 9-methyluric acid at pH 8 at 230 nm. Electrolysis at 1.0 V (the major oxidation peak of 9-MUA) stopped at arrow. b. Time vs. log $|A - A_\infty|$ at 230 nm of the intermediate species formed on electrooxidation of 0.5 mM 9-methyluric acid at pH 8.

uric acid (κ=0.013) are in excellent agreement with that published by Wrona, et al.[19] for 9-methyluric acid (κ=0.014) at the same pH. Their RSS was equipt with a xenon arc lamp (in contrast to the deuterium lamp used in this study) which limited her useful u. v. spectrum to between 380-240 nm. Below 240 nm. her absorbance signal was very noisy and no meaningful data could be obtained. This precluded Wrona from observing the slower kinetics of the imine-alcohol at pH 4 because the largest absorbance changes for this reaction occur at 240 nm and shorter wavelengths. Therefore, no low pH comparison can be made between their work and that reported here on the kinetics of 9-methyluric acid. It is believed for 2.0-20 mM concentrations of 9-methylxanthine at pH 8 the rise in absorbance of the kinetic curve is due to the electrochemical formation of two dimer, one stable and the other only moderately stable (vide infra). This hypothesis is supported by the fact that the rise in absorbance stops and an immediate decay is observed when the potential is turned off. The decreasing portion of the kinetic curve is thought to be due to the hydration of the moderately stable dimer to 1-methylallantoin (vide infra).

Product Isolation and Characterization

To obtain a sufficient amount of material for characterization, solutions of 0.5 to 30 mM 9-methylxanthine concentration were electrolyzed. Based upon voltammetric, coulometric, and thin-layer spectroelectrochemical studies, the electrochemical behavior of 9-methylxanthine in solutions of pH 4

and pH 7 was judged to be representative of the electrochemical tendencies of xanthosine below and above the pK_a (6.3). Thus macroscale electrolyses were conducted exclusively in these media.

Although the definite structures of all the products were not established (primarily because of their instablity), the evidence obtained from mass, i. r. and u. v. spectroscopy plus chromatography and voltammetry allowed conclusions to be drawn regarding the nature of the electrochemical products.

pH 7. Peak Ia. Lyophilization of the solution after oxidation at 0.76 V. for 2 hrs. of 4 mg 9-methylxanthine (1 mM) in 25 ml of phosphate buffer gave a pale yellow residue. This residue was dissolved in ca. 2 ml of doubly distilled water. The resultant solution was separated by liquid chromatography on a gel-permeation resin (Sephadex G-10, 90 cm x 2.5 cm) using pH 7 phosphate having an ionic strength of 0.1M as the eluting solvent at a flow rate of 30 $mlhr^{-1}$. The chromatogram obtained is shown in Figure 41. Three very large peaks (retention volumes 211 ml, 450 ml, and 504 ml) were observed (u. v. detector at 207 nm) along with four additional small peaks (retention volumes 248 ml, 293 ml, 356 ml, and 383 ml). The small chromatographic peaks proved to be oxidation peak IIa products (vide infra). The appearance of these chromatographic peaks from oxidation peak IIa is due to the small potential difference between the peak Ia process and the peak IIa process. The first large chromatographic peak (retention volume 211 ml) is due to phosphate from the electrolysis solution. Attempts

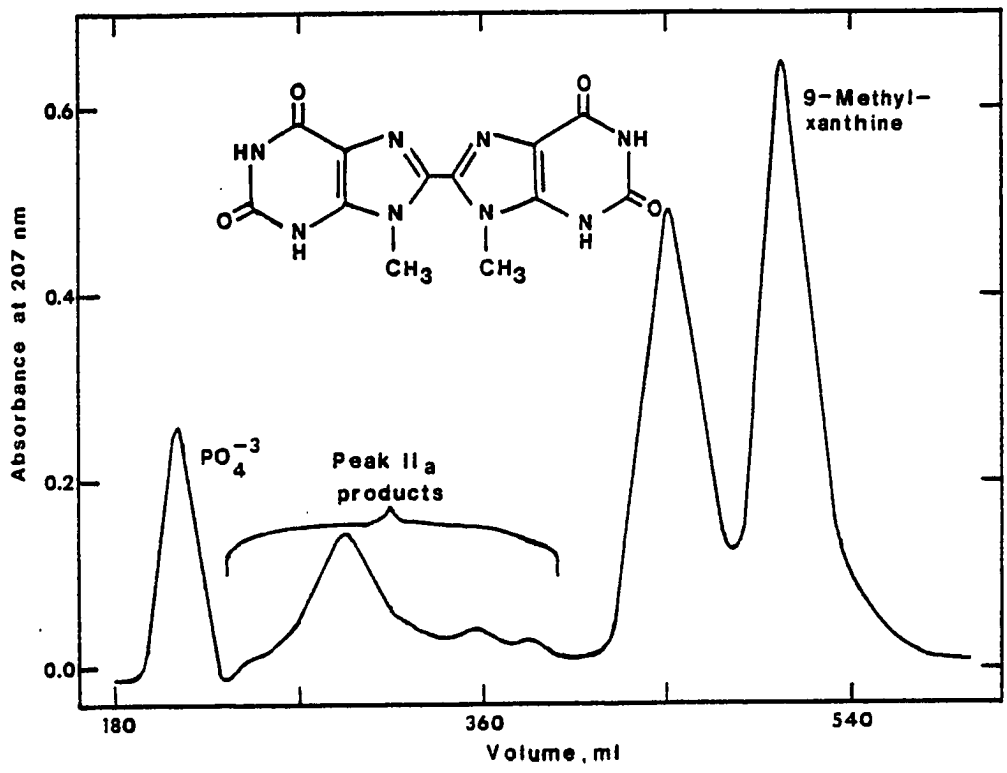

Figure 41. Chromatogram of oxidation peak Ia products using a gel-permeation resin (Sephadex G-10, 90 cm x 2.5 cm). The eluant was pH 7 phosphate buffer, having an ionic strength of 0.1. Flow rate 30 $mlhr^{-1}$.

to desalt[48] the final two large chromatographic peaks were not completely successful. Even though these products could not be purified, u. v., i. r., and field desorption mass spectroscopy plus voltammetry of the crude material yielded information regarding possible structures. Voltammetry and u. v. spectroscopy of the final large chromatographic peak (retention volume 504 ml) proved identical to that for pure 9-methylxanthine.

Regular direct insertion and coupled gas chromatography mass spectroscopy of the chromatographic peak with retention time 450 ml were unsuccessful. However, field desorption mass spectroscopy was useful on this product. The basis for FDMS is the unique properties which arise from the behavior of chemical compounds under high potential fields. When a high field (10^7-10^8 Vcm^{-1}) is applied to an adsorbed organic layer on a metal surface, that surface experiences an electrostatic force. If the metal surface (emitter) has the proper geometry (sharp tip) and is under high vacuum (10^{-6} torr), the electrostatic force can be sufficient to eject particles as positive ions which can be analyzed via a mass spectrometer. The small amount of transferred energy in the FDMS process (≈ 0.1 eV) increases the probability of detecting intact molecular ions. This is the salient feature of FDMS. The attachment of alkali ions (cationization) to adsorbed organic molecules is one method of producing stable quasimolecular ions. The stability of the $(M + C)^+$ ions is due to strong

charge localization at the alkali atom. Thus, the charge shift by rearrangement of the bonding electrons within the ion necessary for decomposition is prevented[49]. The alkali atoms are present because the molecules of interest are applied to the emitter in salt containing solutions. For many organic compounds, the FD mass spectra produced show the molecular ion or molecule-cation complex alone or as the peak of highest relative intensity.

The advantage of cationization can be easily destroyed when large quantities of inorganic salts reach the emitter and surround the organic molecules binding them so strongly that the temperature necessary for field desorption became too high. The optimum temperature for field desorption is achieved when the emitter current is between 5-10 mA. When the temperature becomes too great, the molecules will decompose thermally before molecular ion formation or cationization can take place[49].

The product from the chromatographic peak having a retention time of 450 ml desorbed quite smoothly over the emitter current range 25-30 mA. It appeared to be a mixture of two compounds. For each of these M^+ and $(M + Na)^+$ were observed at m/e 287 and 310, and m/e 330 and 353, respectively. Field desorption mass spectra at 25 and 30 mA are shown in Figure 42. Such mass spectra indicate the presence of a 9-methylxanthine dimer. The large peak at m/e = 287 also appears in the FD mass spectra of the product from oxidation

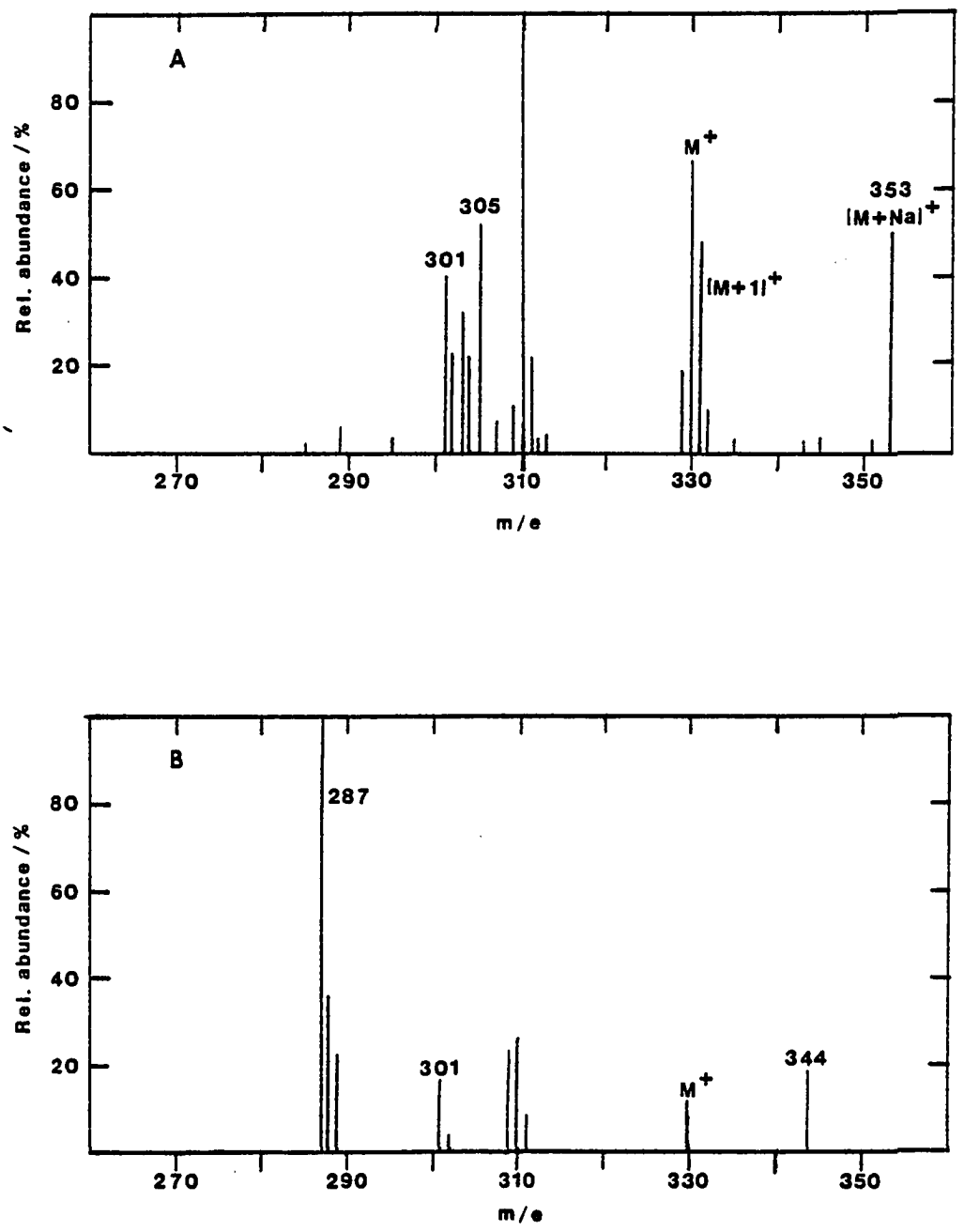

Figure 42. Field desorption mass spectra at (A) 25 mA and (B) 30 mA for oxidation peak Ia product with retention volume of 450 ml.

peak IIa. This may indicate a thermally decomposed product.

The i. r. spectrum of the separated unknown product is reproduced in Figure 43. The u. v. spectrum of the unknown separated product is also reproduced in Figure 43. This u. v. spectrum is very similar to the one reported by Hansen and Dryhurst[31] for the dimer of theophylline.

The molecular weight determination of the molecule is in complete accord with the fact that the separated oxidation product of peak Ia of 9-methylxanthine is a dimer. If N-N dimerization had occurred, there is every reason to believe that the unoxidized C_8 positions would be further oxidized to carbonyl functions. This would result in n-values of about 5, which were never observed. The similarities in the u. v. spectrum (both show an absorption peak at 340 nm) and i. r. spectrum (both show absorption peaks at 1695 cm^{-1}, 1600 cm^{-1}, 1585 cm^{-1}, and 1450 cm^{-1}) of the 9-methylxanthine dimer (Figure 43) and the theophylline dimer[31] imply they have similar structures. It would therefore appear the C-C dimerization at the C_8 position, similar to that observed for the theophylline dimer, has occurred with 9-methylxanthine. Taking into account the determined molecular weight of 330 (Figure 42) two structures for the C-C dimeric species IV and V are possible:

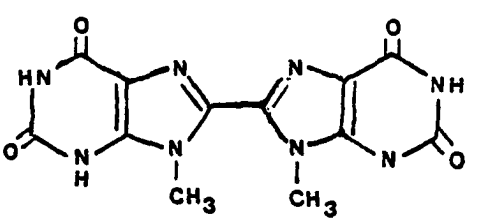

IV

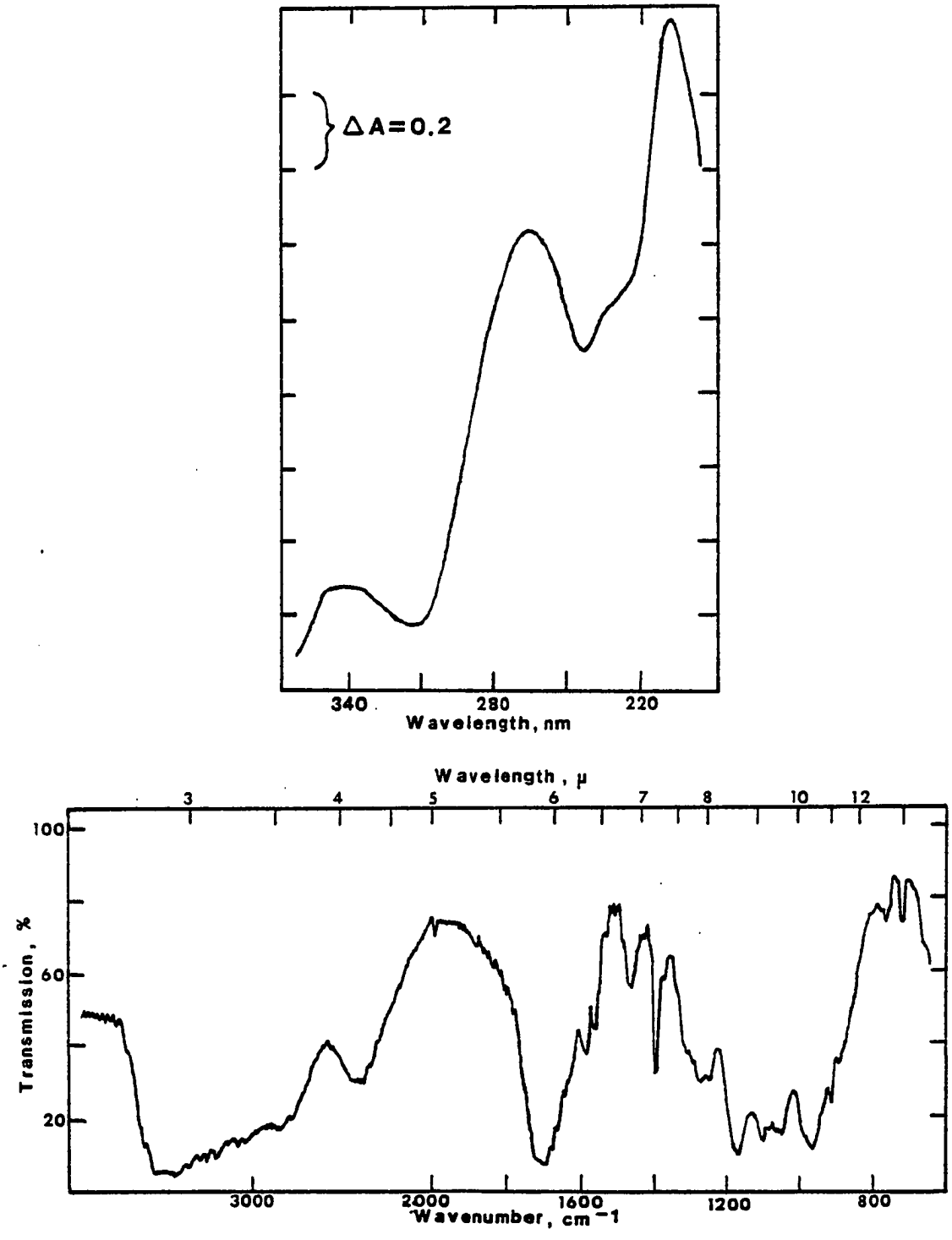

Figure 43. I. r. and u. v. spectra of oxidation peak Ia product with retention volume of 450 ml. I. r. is of a KBr disc.

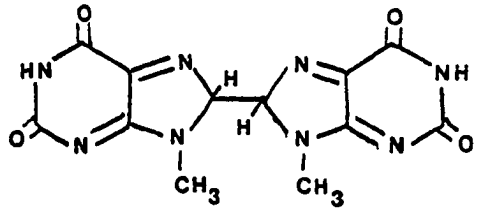

V

Comparison of the i. r. and u. v. spectra (Figure 43) of the dimer with those of analogous structures supports IV as the actual dimeric structure. The i. r. spectrum possesses two peaks which help determine the structure of the dimer. That at 1585 cm^{-1} is due to C=N and that at 1695 cm^{-1} is due to amide carbonyl absorption[50]. I. r. spectra of two compounds having a $N_3-C_4=N_9-C_8-N_7=C_5-$ grouping similar to the $-N_3=C_4-N_9-C_8-N_7=C_5-$ of V namely: 1,3-dimethyl-8,8-pentamethylene-8H-xanthine (VI)[51] and 1,3,8,8-tetramethyl-8H-xanthine (VII)[52] reveal

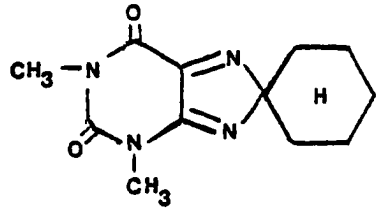

VI

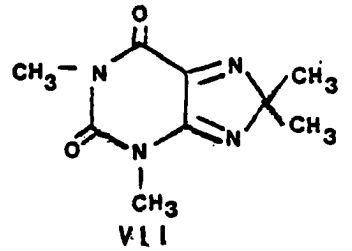

VII

a distinct carbonyl absorption due to C_6 at ca. 1750 cm^{-1} with the C_2 amide carbonyl absorption appearing closer to 1700 cm^{-1}.

Compounds with the $-C_4=C_5-C_6=O$ grouping of IV[50,53] reveal a single carbonyl absorption and that in the 1700 cm^{-1} region since both C_6 and C_2 exist as amide carbonyls. Such is true of 9-methylxanthine and other methylated xanthines[54]. Thus, the absence of the 1750 cm^{-1} related peak in the dimer i. r. is evidence that it does not possess the $C_6-C_5=N_7-$ grouping of V.

The observed u. v. spectrum of the dimer (Figure 43) in phosphate buffer, pH = 7, is also plausible for structure IV. 9-Methylxanthine exhibits a maximum u. v. absorption due to the $-C_4=C_5-C_6=O$ grouping at a wavelength of 283 nm in pH 7 solution[35,55]. A shift in the maximum to 340 nm for the grouping $-C_4=C_5-N_7=C_8-C_8'=N_7'-C_5'=C_4'-$ possessed by IV can be rationalized by considering that extention of an ethylenic bond by a tertiary nitrogen produces a 20 nm bathochromic shift[56] and that the increment for a double bond extending conjugation for enone absorption is given as 30 nm[57]. It is not unlikely therefore that a wavelength maximum at 340 nm at pH 7 is observed for the $-C_4=C_5-N_7=C_8-C_8'=N_7'-C_5'=C_4'-$ grouping in IV.

The fact that 9-methylxanthine was a product obtained by liquid chromatography implies the electrolysis was not allowed to run to completion. All electrolyses at 0.76 V vs SCE to obtain peak Ia oxidation products were terminated

at approximately two hours. At that time the electrolysis solutions began to show a pale yellow color. Voltammetry after two hours of electrolysis at 0.76 V was similar to the voltammogram in Figure 25 after the same amount of time. This voltammogram shows there was still some peak Ia left when the electrolyses were terminated. This was necessary to keep the amount of peak IIa product (yellow product, vide infra) produced to a minimum. Since there was still some peak Ia present when the electrolyses were stopped, all of the 9-methylxanthine initially present was not oxidized and it appeared in the chromatography.

pH 7. Peak IIa. After oxidation at 0.90 V (until no voltammetric peaks remain) of a solution containing 4 mg of 9-methylxanthine (1 mM) in 25 ml of phosphate buffer, lyophilization gave a bright yellow residue. This residue was dissolved in ca. 2 ml of doubly distilled water. Attempts to separate this resultant solution using various liquid chromatographic techniques (vide supra) were for the most part unsuccessful. Using a chromatographic set-up similar to that used to separate the products from oxidation peak Ia a chromatogram was obtained which was similar to that for oxidation peak Ia. The difference being the minor chromatographic peaks with retention volumes 248 ml, 293 ml, 356 ml, and 383 ml were the major chromatographic peaks. It was noted however that none of these four chromatographic peaks upon lyophilization produced a product with the intensity of

yellow color that the crude electrolysis product possessed. The one chromatographic peak which did show a yellow product had an intensity of color similar to that shown by the oxidation peak Ia crude electrolysis product after it was lyophilized. It is quite apparent that in the time frame required for separation the yellow product underwent decomposition. This decomposition takes place upon dilution or continued application of potential after voltammetry shows no oxidation peak IIa left. As was noted in the coulometry section (vide supra) the intensity of the yellow color was stable when the potential was discontinued.

Attempts to purify the crude electrolysis product by solvent extraction or recrystallization were largely unsuccessful. The electrolysis product was insoluble in all but the most polar solvents (water and methanol) and heating of the product in these polar solvents caused decomposition (changes in color intensity and thin-layer chromatography). However, the best results were obtained when 40 mg of 9-methylxanthine in 25 ml of phosphate buffer were oxidized at 0.9 V. Lyophilization of this solution gave a bright orange-yellow residue. Dissolving this residue in 10 ml of distilled methanol removed the large excess of phosphate from the electrolysis solution and caused no appreciable loss in color intensity. The methanol was allowed to evaporate. To the resultant waxy residue, enough doubly distilled water was added to cause the residue to dissolve. This residue was

lyophilized leaving fluffy orange-yellow crystals. TLC and the phosphate test (vide supra) showed that purification had still not been completely achieved.

Even though the oxidation product could not be purified, u. v. vis., and mass spectrometry of the crude material yielded information regarding possible structures. The visible spectrum of the oxidation product showed no distinct peaks, but a general increase in absorbance beginning at 610 nm and continuing until 380 nm. The u. v. spectrum shown in Figure 44 had few distinquishing characteristics but showed some resemblance to spectrum 3 of Figure 28. The general rise in absorbance begun in the vis. region of the spectrum continues in the u. v. region until ca. 260 nm where a shoulder appears. From 260 nm to 202 nm there is a sharp increase in absorbance followed by a distinct decrease. The i. r. spectrum of the unknown oxidation product is reproduced in Figure 44.

Coupled gas chromatography mass spectroscopy and direct insertion mass spectroscopy of the oxidation product were unsuccessful. Field desorption mass spectroscopy was somewhat useful on this product. The field desorption spectrum (Figure 45a) was difficult to obtain for this molecule. The best result was at 20 mA, at which emitter current several groups of peaks were observed having m/e centered around 273 (most intense), 287, 299 and some isolated peaks with m/e of 317, 321, 322, 325, 328, and 344. The reason this sample behaved so poorly may be due to its stability or

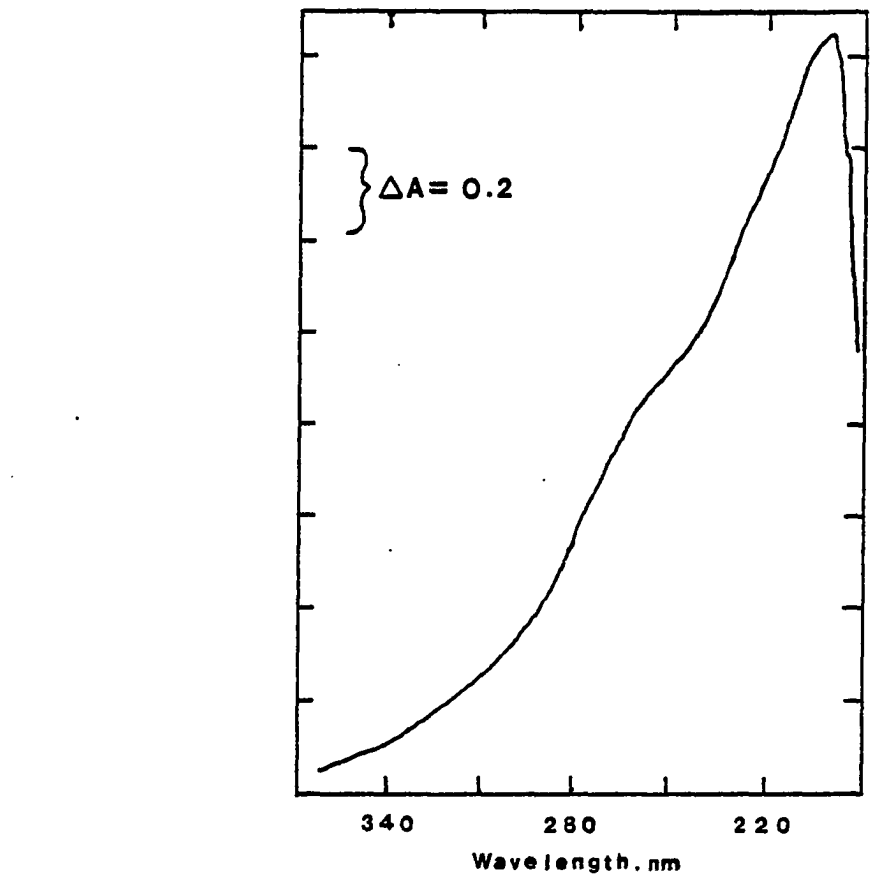

Figure 44. I. r. and u. v. spectra of oxidation peak IIa product. I. r. is of a KBr disc.

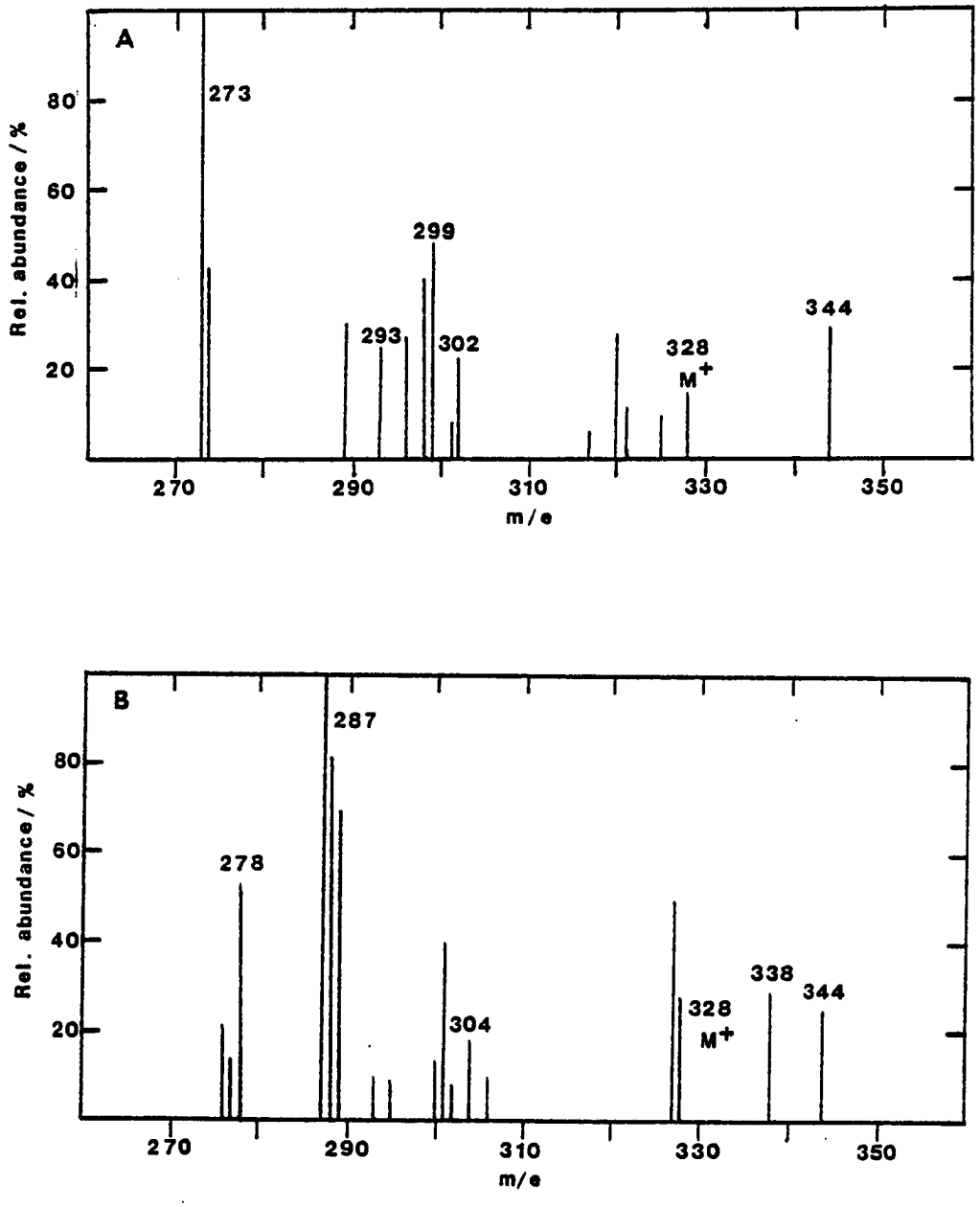

Figure 45. Field desorption mass spectra at (A) 20 mA and (B) 30 mA for oxidation peak IIa product.

the amount of inorganic salt present. A second FD spectrum (Figure 45b) obtained for this compound at 30 mA, yielded again several groups of peaks with m/e centers at 287 (most intense), 244, 261, 278, and 300. Though of poor quality, these mass spectra do provide information regarding a possible structure for the oxidation product. These spectra are similar to the spectra obtained from oxidation peak Ia in that as the emitter current is raised the spectral peak with m/e of 287 becomes more intense for both products. This may imply that both oxidation peak Ia product and oxidation peak IIa product thermally decompose to an identical molecule. Thus, the two initial oxidation products would have to be quite similar in structure. Coulometry and potentiostatic studies imply that oxidation peak IIa is a further 1 electron oxidation of each individual 9-methylxanthine molecule initially present. Since the molecules exist as dimeric structures after oxidation at peak Ia, the actual peak IIa oxidation mechanism is a 2 electron oxidation of the dimer formed in the oxidation peak Ia process. An oxidation of this type would require a molecular weight of 328 for the resultant product. A plausible structure for the oxidation peak IIa species is:

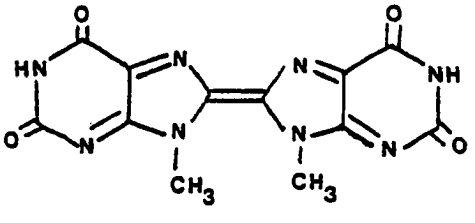

VIII

The i. r. spectrum of the peak IIa product (Figure 44) is poor in quality due to the inability of removing all of the phosphate from the electrolysis sample. Addition of a small excess of $BaCl_2$ to a solution of the peak IIa product to precipitate the phosphate ions as $Ba_3(PO_4)_2$ leaving NaCl and $BaCl_2$ in the solution did not lead to an improved i. r. spectrum. Thus the i. r. was of little use in structure determination.

The observed u. v.-vis. spectrum of the oxidation peak IIa product in phosphate buffer, pH 7, is in accord with structure VIII. The further increase in conjugation in structure IV compared to structure VIII should produce a bathochromic shift in absorbance similar to that which took place in the transition from monomer to the dimer. Therefore, it is probable to expect absorption in the visible spectrum for the $O{=}C_2{-}N_3{=}C_4{-}C_5{=}N_7{-}C_8{=}C_8{'}{-}N_7{'}{=}C_5{'}{-}C_4{'}{=}N_3{'}{-}C_2{'}{=}O$ grouping in VIII.

When the product of electrooxidation of 40 mg of 9-methylxanthine at peak IIa potentials was dissolved in 1 liter of doubly distilled water and allowed to stand for 48 hours, all the yellow color disappeared. This solution was lyophilized and the resultant cream colored residue was separated using a system identical to that used to separate oxidation peak Ia products. The chromatogram obtained was similar to that shown in Figure 46 (<u>vide infra</u>), with the peak having a retention volume of 360 ml being somewhat larger. The

first large peak with retention volume of 210 ml proved to be phosphate from the electrolysis cell. The large peak with retention volume of 311 ml proved to be 1-methylallantoin. The mass and i. r. spectra for this product are the same as those obtained from the product of oxidation peak IVa (vide infra). It would appear reasonable that the peak IIa oxidation product (structure VIII) could undergo hydration and air oxidation (vide infra) to form a similar observed product (1-methylallantoin) to that obtained at oxidation peak IVa.

Cyclic voltammetry of the peak IIa oxidation product (yellow dimer) showed several of the small voltammetric peaks observed during switching potential studies of 9-methylxanthine (Figure 21) in the vicinity of oxidation peaks Ia and IIa. The redox couple (reduction peak at -0.035V and oxidation peak at -0.020V) and the reduction peaks at -0.75 V. and -1.05 V. appeared during voltammetry of the oxidation peak IIa product (yellow dimer). No attempt was made to isolate or determine the products of these voltammetric peaks.

pH 7. Peak IIIa. Product analysis on oxidation peak IIIa produced similar results to that found with oxidation peak IVa. This coupled with coulometry, potentiostatic, and voltametric data implied that oxidation peak IIIa is an adsorption pre-peak where the product of peak IVa is strongly adsorbed.

pH 7. Peak IVa. After oxidation of a solution of 4 mg 9-methylxanthine (1 mM) in 25 ml of phosphate buffer, lyophilization gave a pale yellow residue. This residue was treated and separated in the same manner as the residue from oxidation peak Ia (vide supra). The resultant chromatogram is shown in Figure 46. There are two large chromatographic peaks (one having a retention volume of 210 ml and the other having a retention volume of 320 ml). The first chromatographic peak was shown to be phosphate from the electrolysis cell. The second was desalted[48] and through GC/MS, direct insertion mass, and i. r. spectroscopy shown to be 1-methylallantoin. The direct insertion mass, and i. r. spectra are shown in Figure 47. Several of the i. r. peaks in 1-methylallantoin are similar to those observed in allantoin (Part I, Figure 19).

Oxidation peak IVa product was sufficiently volatile for direct introduction into the mass spectrometer without chemical pretreatment, however chemical derivatization may offer certain distinct advantages. A trimethylsilyl (TMS) derivative, which is widely used in gas chromatography and mass spectrometry, was used to perform GC/MS experiments on the oxidation peak IVa product. Knowledge of the number of TMS groups added to the molecule may provide a degree of structural information independent of a detailed interpretation of the spectrum. Carboxyl and hydroxyl groups will each accept one TMS function, while amino groups will accept

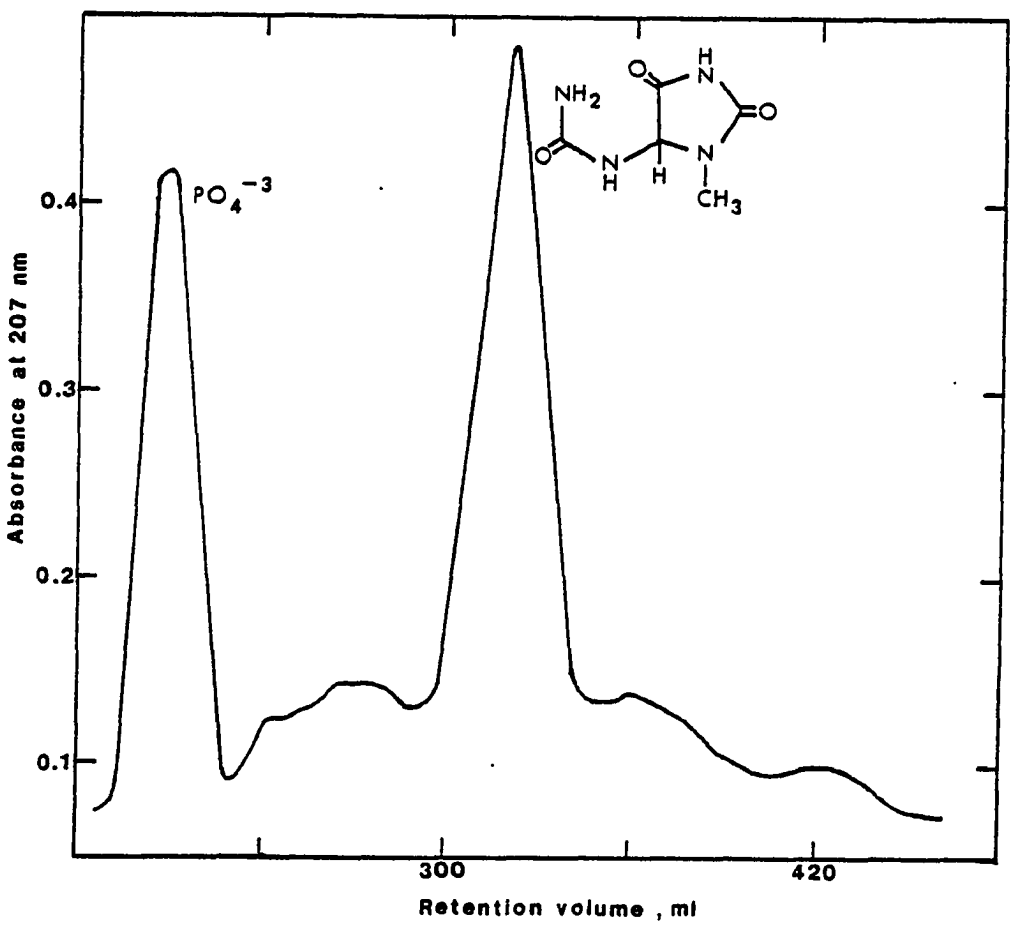

Figure 46. Chromatogram of oxidation peak IVa products using a gel-permeation resin (Sephadex G-10, 90 cm x 2.5 cm). The eluant was pH 7 phosphate buffer having an ionic strength of 0.1 M. Flow rate 30 $mlhr^{-1}$.

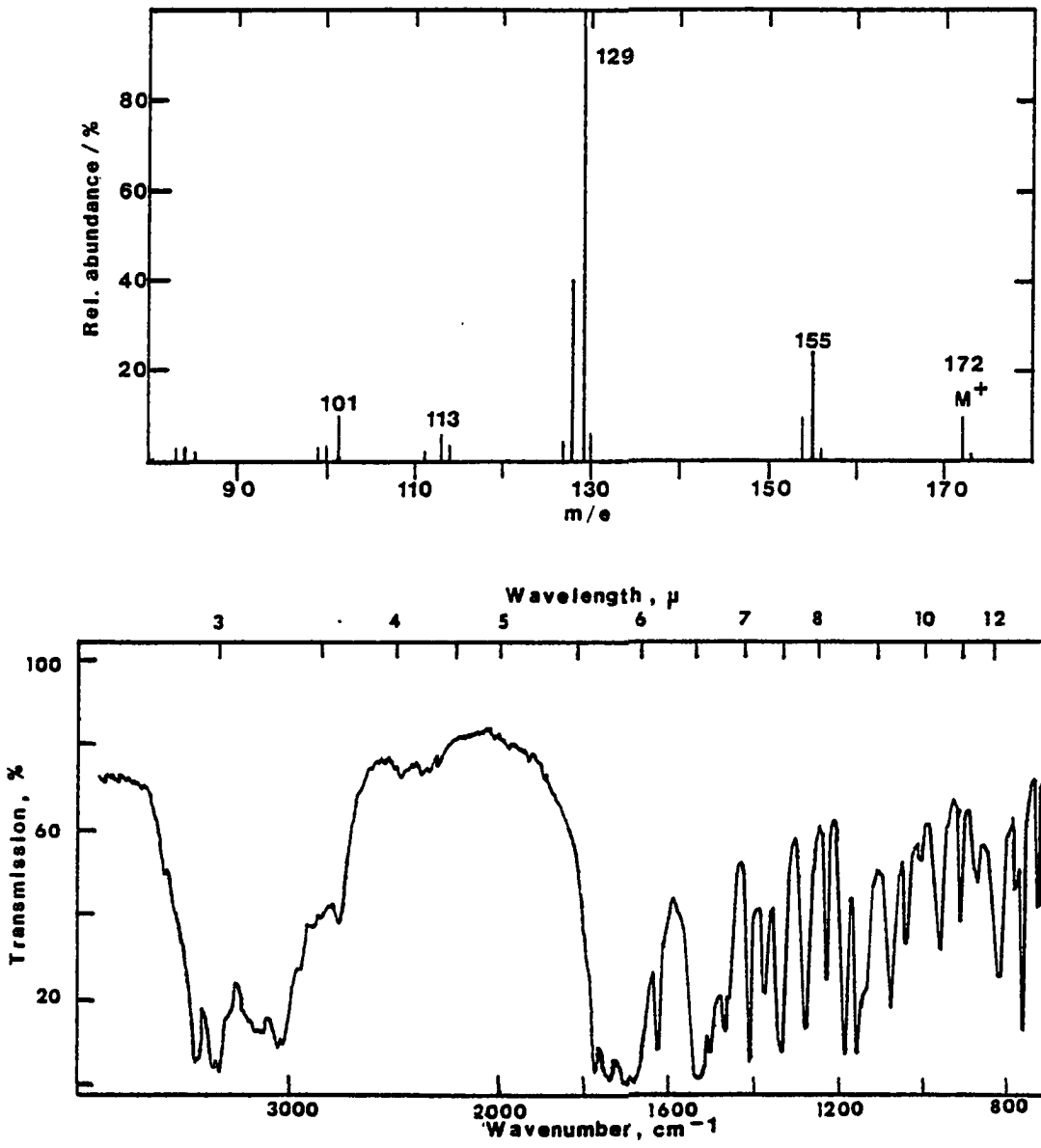

Figure 47. Mass and i. r. spectra of oxidation peak IVa product with retention volume of 320 ml. I. r. is of a KBr disc.

one or two TMS functions depending on the silylation technique. Loss of a TMS methyl radical generates a stable siliconium ion (M-15), whose mass may further by used to corroborate the molecular weight. If two methyl radicals are lost, a doubly charged ion equal in mass to (M-30)/2 will be formed. A number of minor fragmentation pathways lead to small but characteristic peaks, including elimination of CH_4 from the M-15 ion, giving a peak at M-31, and loss of an intact TMS radical to produce M-73. Other ubiquitous peaks are the trimethylsilyl cation (IX), m/e 73, and the rearranged species (X), m/e 147, which is characteristic and diagnostic for the presence of oxygen.

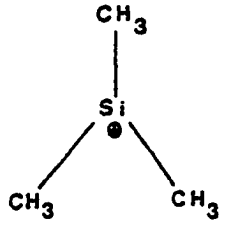

IX

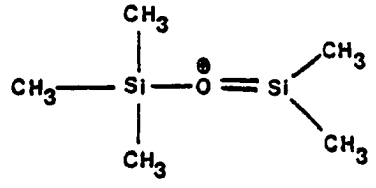

X

Approximately 0.1 mg of desalted oxidation peak IVa product was transferred to a 600 µl reaction vial. Then 100 µl of bis(trimethylsilyl)trifluoroacetamide (BSTFA) was added. The resultant solution was heated for 20 minutes at 125°C in an oil bath. Separation of the heated solution was performed by gas chromatography (Varian 2400 gas chromatograph)

on a SE-30 packing (3% on Chromosorb W (HP), 80/100 mesh) with flame-ionization detection. The column dimensions were 2 mm x 6 feet. A flow rate of 30 $ml\,hr^{-1}$ was established for the carrier gas. The temperature program maintained the temperature at 100°C for the first 12 minutes of the separation and then raised the temperature 6°C per minute until a temperature of 300°C was obtained. The chromatogram of this separation is shown in Figure 48. The first prominent peak with retention time of 8.5 min. was found to be due to thermal decomposition of BSTFA. This peak also appeared when BSTFA alone was heated at 125°C for 20 minutes. When BSTFA was heated for longer times at 125°C or at higher temperatures for 20 minutes the intensity of this peak increased. The chromatographic peak product with a retention time of 33.1 minutes showed a mass spectrum (Table 7) indicating a structure with a molecular weight of 460. 1-Methylallantoin with four TMS substituents (XI) would have a molecular weight of 460.

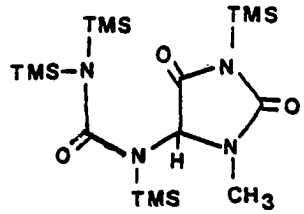

XI

The fragmentation pattern (Table 7) also supports structure XI as the TMS-substituted oxidation product from peak IVa. A base peak m/e = 73 is shown corresponding to structure IX. Another prominent ion appears at m/e = 147. This is characteristic of structure X. The ion with m/e = 388 would be correct

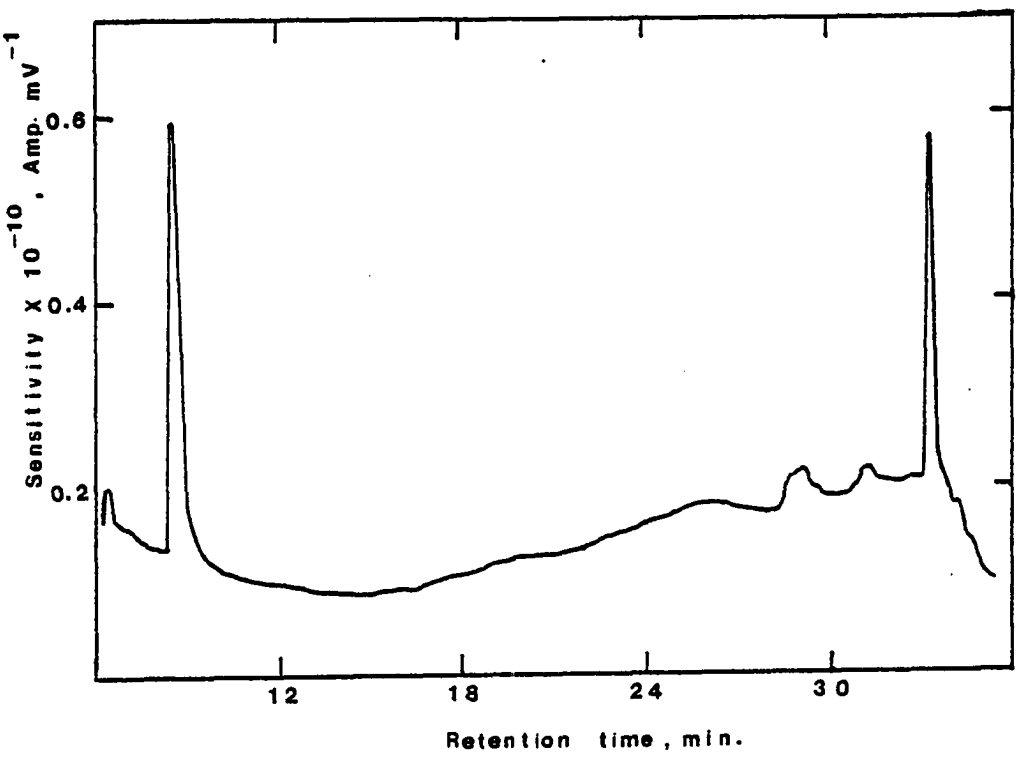

Figure 48. Gas chromatogram of oxidation peak IVa product with retention volume of 320 ml using SE-30 packing (column dimensions 2 mm x 6 ft). Flow rate 30 $mlhr^{-1}$. Temperature program: 100°C for 12 min., then raised 6°C per minute.

TABLE 7. GC mass spectrum of pH 7 oxidation peak IVa product with LC retention volume of 320 ml. and GC retention time of 33.1 sec.

MASS	%	MASS	%	MASS	%	MASS	%	MASS	%
54.0	.8	83.0	1.6	127.1	.4	172.0	1.1	272.1	.9
55.1	1.4	84.0	3.2	128.0	.4	173.1	1.0	273.0	.5
56.1	1.5	85.0	1.5	129.0	1.4	174.1	.7	274.1	.3
57.1	1.8	86.0	3.6	130.0	3.6	183.2	.3	283.1	.3
58.1	2.5	87.0	.7	131.0	2.0	184.0	3.6	284.1	.3
59.1	3.0	88.1	.9	132.0	.5	185.0	2.5	290.0	.7
60.1	.4	89.1	.3	132.9	1.3	186.0	.7	297.0	.3
61.0	.7	91.1	.5	134.0	.4	187.1	.7	298.2	1.5
63.0	.5	93.0	.9	135.0	.3	188.1	1.5	299.1	2.4
65.1	.5	94.1	.3	137.0	.3	189.1	.3	300.1	.9
65.9	.7	95.0	.5	138.1	.3	193.0	.3	301.2	.4
67.1	.4	98.0	.5	140.1	.6	198.1	.3	329.1	.3
68.0	.3	99.1	2.4	140.9	.5	199.2	.6	330.1	.7
69.0	2.3	100.1	11.2	142.0	.4	200.0	.3	344.0	1.3
70.0	5.3	101.0	1.9	145.1	.3	201.1	.3	345.1	7.0
71.0	1.3	102.0	.7	146.1	.9	205.2	.3	346.1	2.0
72.0	7.1	103.1	.6	147.1	4.3	207.0	.4	347.1	1.4
73.0	100.0	105.0	.5	148.0	.8	214.1	.5	370.2	.3
74.1	8.8	111.1	.4	149.0	.7	215.1	.3	372.2	.6
75.1	17.0	112.2	.3	155.1	.6	216.0	.3	445.1	2.2
76.1	1.6	113.1	2.8	156.1	.3	221.0	.4	446.2	.8
77.0	3.2	114.0	1.5	157.0	1.4	240.0	.3	446.9	.5
78.0	.5	115.1	1.9	158.0	.7	256.0	1.8	460.1	14.1
78.9	.4	116.1	1.5	159.0	.4	257.1	.5	461.1	5.0
80.8	.3	117.2	.9	170.1	.4	258.1	.4	462.1	2.6
81.8	.4	121.1	.4	171.1	1.1	271.1	1.0	463.0	.9

for 1-methylallantoin substituted in three locations with TMS. It is quite common for an amino group to substitute only one of its two hydrogens with TMS. The fact that there are two ions, one with m/e = 445 (M-15) and another with m/e = 215 ((m-30)/2) further proves the identity of the oxidation peak IVa TMS substituted product to be structure XI.

pH 4. Product isolation and characterization were different at pH 4 compared to pH 7, in that changes in potential caused no new products to be formed but only altered the relative amounts of the various products. In addition, varying the concentration of 9-methylxanthine oxidized, caused no alteration in the products observed.

Oxidation of 4 mg of 9-methylxanthine (1 mM) in 25 ml of phosphate buffer at 1.3 V vs SCE and subsequent lyophilization of the solution gave a cream colored residue. This residue was dissolved in two ml of doubly distilled water. Separation of the resultant solution was achieved by liquid chromatography on a dual gel-permeation and anion-exchange system similar to that reported in Part I using 0.025 M NaH_2PO_4 as the eluting solvent at a flow rate of 30 $ml\,hr^{-1}$. The column dimensions were somewhat different this time (Sephadex G-10, 90 cm x 2.5 cm and QAE-Sephadex A-25, 28 cm x 2.5 cm). In Figure 49, the chromatogram obtained is shown. Five prominent peaks (retention volumes 326 ml, 439 ml, 523 ml, 596 ml, and 652 ml) were observed (u. v. detector at

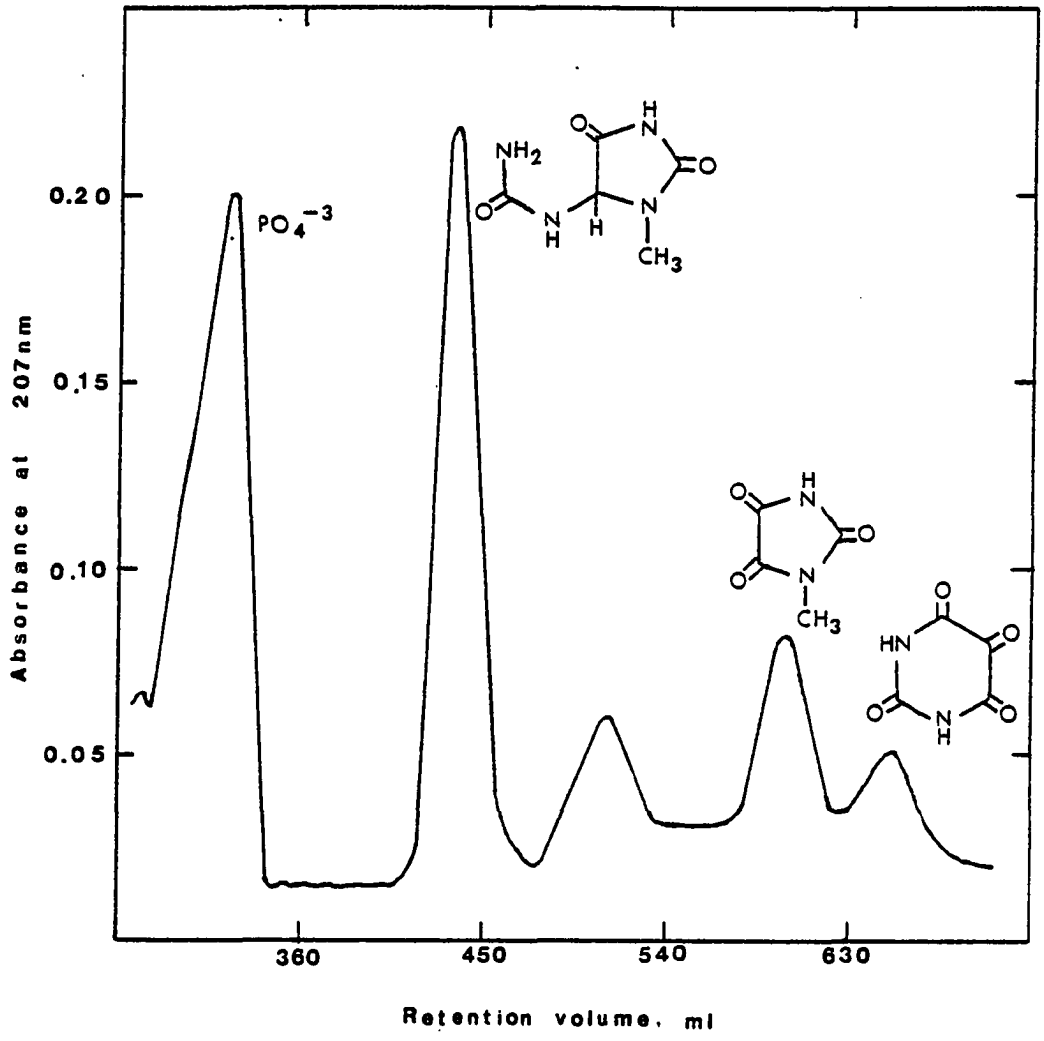

Figure 49. Liquid chromatogram of oxidation products at pH 4 at 1.3 V vs SCE using dual gel-permeation and anion-exchange system (Sephadex G-10, 90 cm x 2.5 cm and QAE-Sephadex A-25, 28 cm x 2.5 cm) The eluant was 0.025 M NaH_2PO_4. Flow rate 30 $mlhr^{-1}$.

207 nm). Chromatography of the product of electrooxidation of 4 mg of 9-methylxanthine in 25 ml phosphate buffer at 1.3 V. *vs* SCE gave a similar chromatogram to that shown in Figure 49. The difference in the chromatogram obtained from chromatography of the product of electrooxidation of a similar solution of 9-methylxanthine at 1.1 V was the chromatographic peak with retention volume 523 ml became more prominent and the height of chromatographic peak with retention volume 439 ml decreased. The relative peak heights of the two remaining chromatographic peaks (retention volumes 596 ml and 652 ml) did not change with variations in potential. When higher concentrations of 9-methylxanthine were oxidized, the chromatograms showed similar behavior to that discussed above. Concentration had no effect on the relative peak heights. The first chromatographic peak (retention volume 326 ml) again proved to be phosphate from the electrolysis cell.

The final four chromatographic peaks were desalted using Sephadex G-10 with 0.001 M HCl as an eluant as described by Owens, *et al.*[48].

Mass and i. r. spectra were obtained for the chromatographic peak product with retention volume 439 ml. These are shown in Figure 50. These were found to be identical to those obtained for 1-methylallantoin (*vide supra*), the major oxidation product of 9-methylxanthine in pH 7 buffer at low concentrations and high potentials. The mass and i. r. spectra

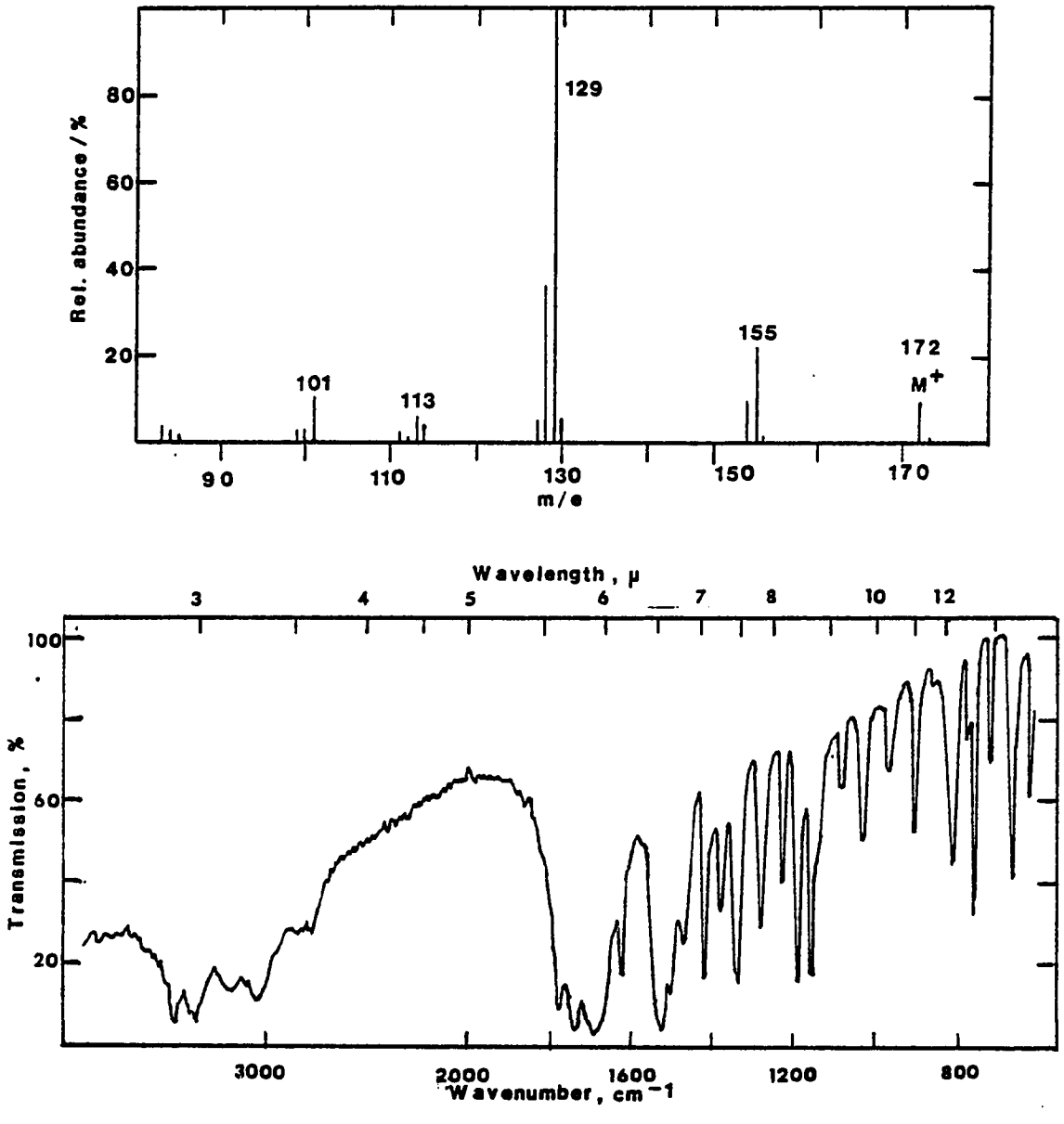

Figure 50. Mass and i. r. spectra for chromatographic peak product with retention volume 439 ml. I. r. is of a KBr disc.

obtained from the retention volume 596 ml chromatographic peak product (Figure 51) were compared to those for authentic methylparabanic acid and were observed to be the same. Authentic alloxan was found to display identical mass and i. r. spectra to those obtained for the product from chromatographic peak with retention volume 652 ml. Mass and i. r. spectra for this oxidation product are shown in Figure 52.

The direct insertion mass spectrum and i. r. spectrum for the product from the liquid chromatographic peak with retention volume 523 ml (LC Peak-523) are shown in Figure 53. Comparison of the direct insertion mass spectrum for this compound with the direct insertion mass spectrum of methylparabanic acid (Figure 51) showed both to be essentially the same. The i. r. spectrum (Figure 53) of the product from LC Peak-523, though of poor quality due to the small amount and hygroscopic nature of the sample, showed most of the same peaks that were observed in the i. r. of methylparabanic acid (Figure 51). The field desorption mass spectrum for this product shown in Figure 54 implied a molecular ion of mass 128. GCMS data were obtained on this product to provide additional structural information. Silation of this oxidation product was accomplished by mixing ca. 0.1 mg of sample with 70 µl BSTFA and 70 µl of acetonitrile and then heating the resultant solution at 125°C for 20 minutes. The chromatogram obtained of this solution is depicted in Figure 55. It shows five prominent peaks with retention times of

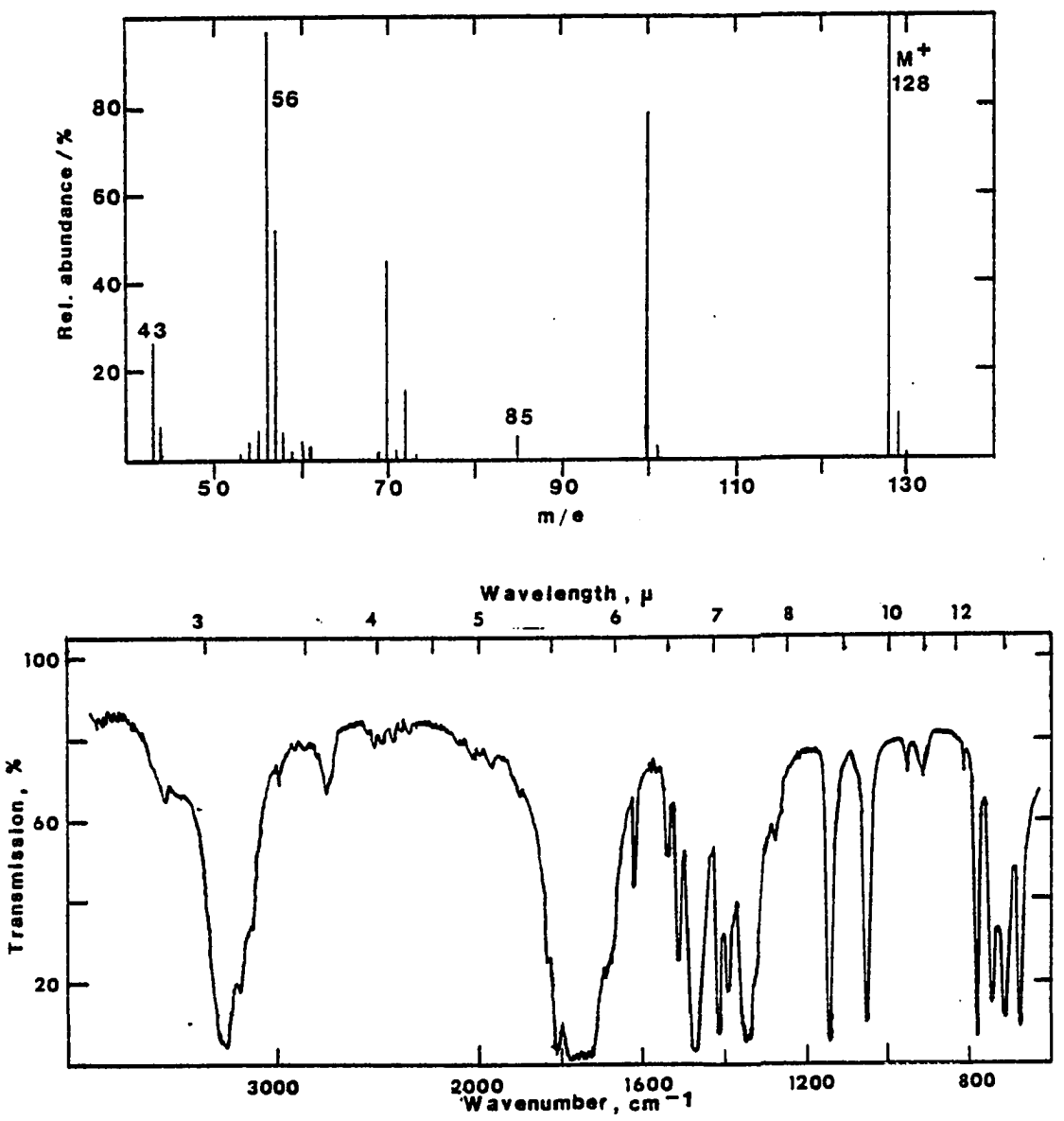

Figure 51. Mass and i. r. spectra for chromatographic peak product with retention volume 596 ml. I. r. is of a KBr disc.

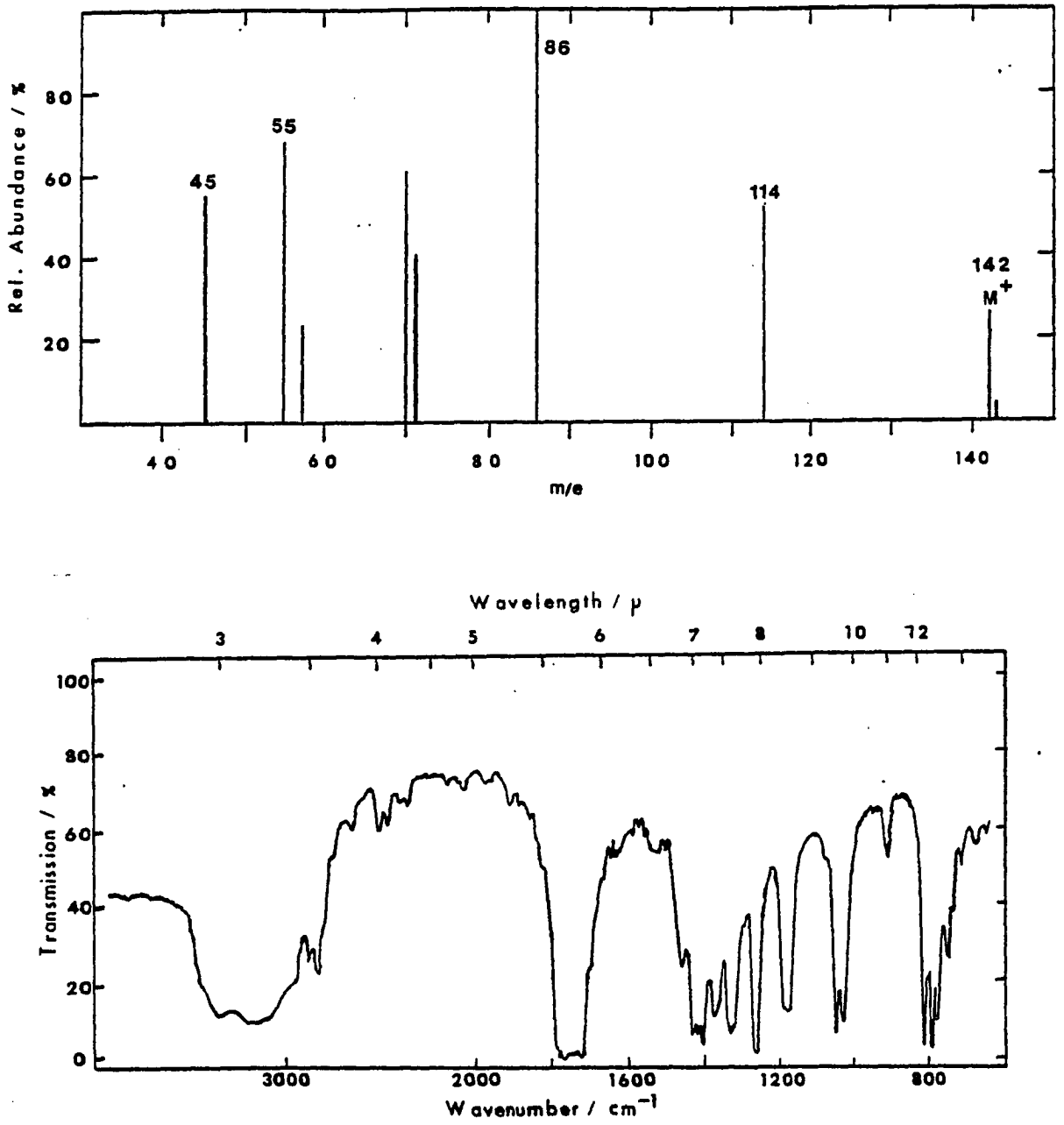

Figure 52. Mass and i. r. spectra for chromatographic peak product with retention volume 652 ml. I. r. is of a KBr disc.

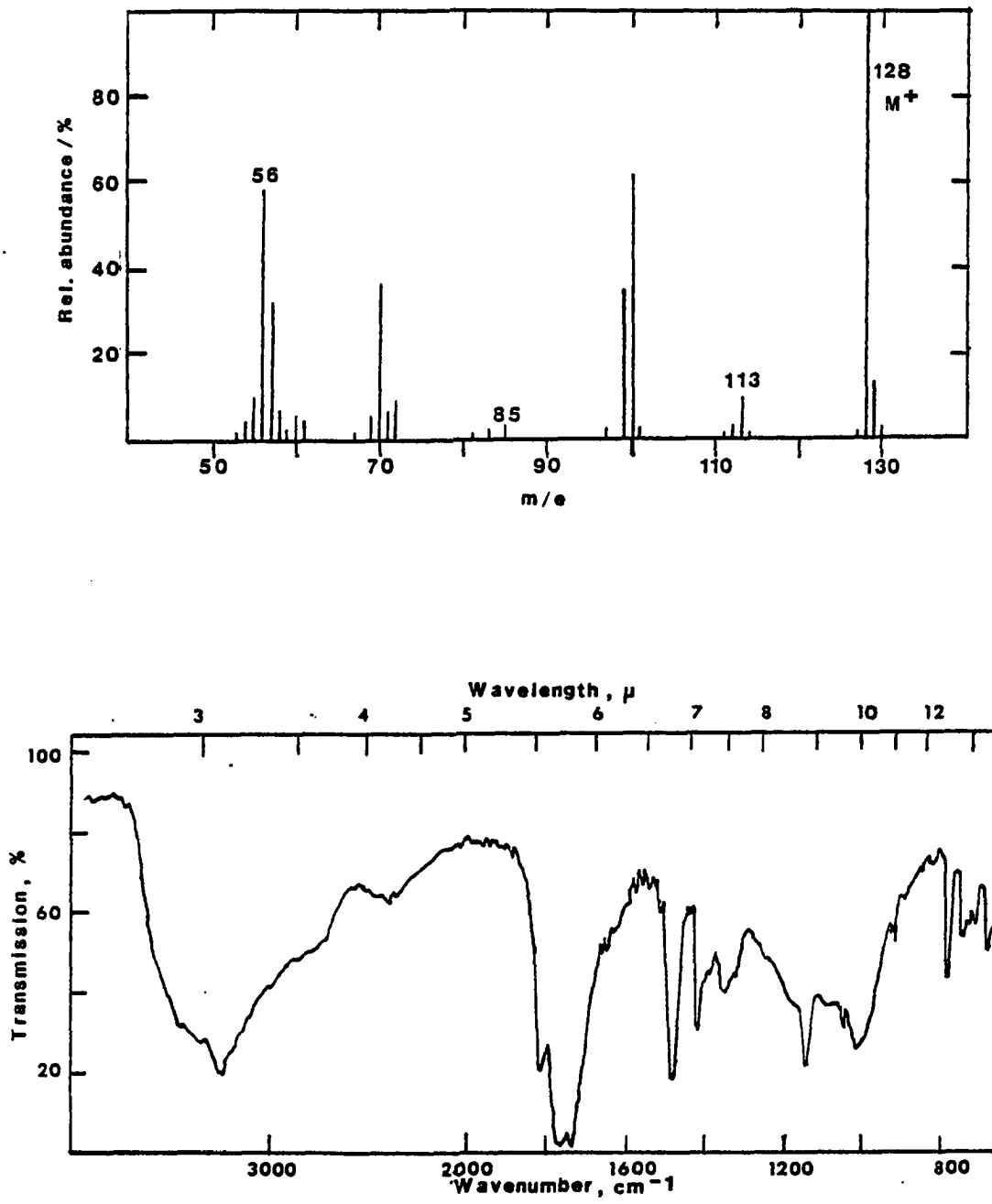

Figure 53. Mass and i. r. spectra for chromatographic peak product with retention volume 523 ml. I. r. is of a KBr disc.

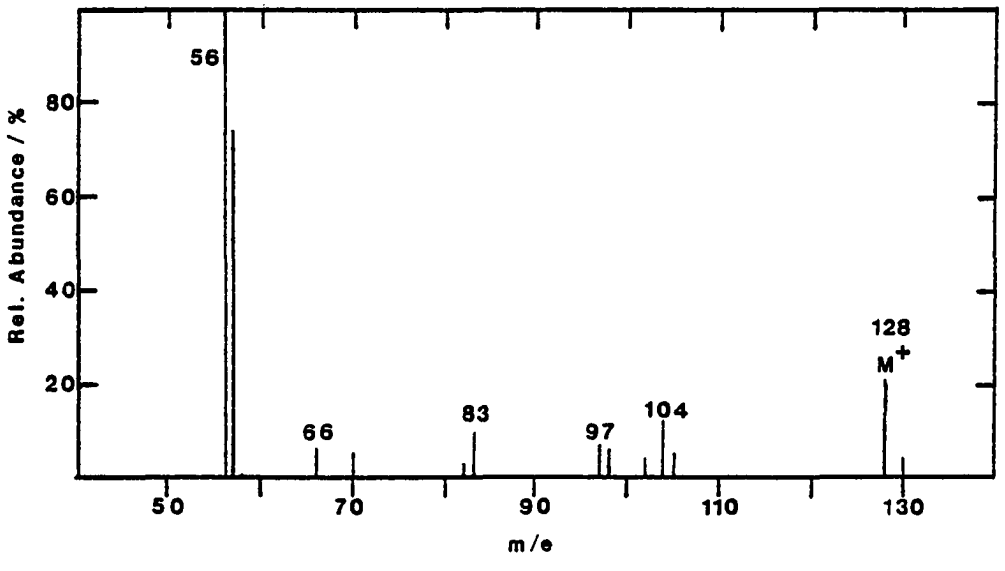

Figure 54. Field desorption mass spectrum for chromatographic peak product with retention volume 523 ml.

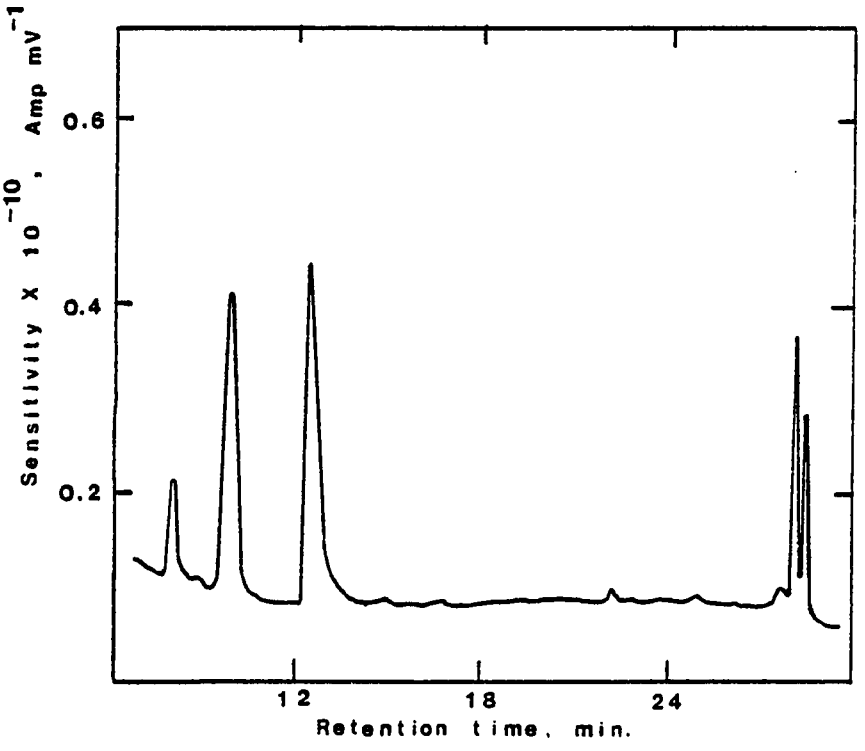

Figure 55. Gas chromatogram of product with LC retention volume 523 ml using SE-30 packing (column dimensions 2 mm x 6 ft). Flow rate 30 $mlhr^{-1}$. Temperature program: 100°C for 12 min. then raised 6°C per min.

7.8, 9.9, 12.5, 28.2, and 28.5 minutes. The first three peaks, GC Peaks-7.8, 9.9, and 12.5, are due to thermal decomposition of BSTFA or acetonitrile. When acetonitrile was heated by itself at 125°C for 20 minutes GC Peaks-7.8 and 12.5 were present. If higher temperatures or longer times were used a marked increase was observed in the peak heights of GC Peaks-7.8 and 12.5. Similar behavior was noticed for GC Peak-9.9 when BSTFA was treated in a like manner. A mass spectrum obtained for the product of GC Peak-28.2 is shown in Table 8. Other than mass 73 which is the base peak, the two most abundant masses occur at m/e = 274 (24.9% relative abundance) and m/e = 273 (19.6% relative abundance). A very similar mass spectrum was obtained for the product of GC Peak-28.5. It is shown in Table 9. Again, mass 73 is the base peak and the two next most abundant masses occur at m/e = 274 (14.0% relative abundance) and m/e = 273 (68.3% relative abundance). With such similar retention times and mass spectra, one would expect the products of each peak to also be very similar, possibly isomers. It is not uncommon for the M-1 ion to appear in the TMS spectrum[58], even at a greater abundance than the molecular ion. Assuming two silatable positions in the case of both GC peak products a possible molecular weight could be 130.

Data from the i. r., FDMS, and direct insertion mass spectrum indicate that the product of LC Peak-523 is primarily methylparabanic acid. However, GCMS gives small peaks perhaps

TABLE 8. GC mass spectrum of pH 4 oxidation product from LC Peak-523 and GC Peak-28.2.

MASS	%	MASS	%	MASS	%	MASS	%	MASS	%	MASS	%	MASS	%
49.1	.2	76.1	1.2	104.1	.1	135.0	.5	173.1	1.1	207.1	.3	260.1	.7
50.1	.2	77.0	1.7	105.1	.3	137.1	.1	174.1	1.9	208.1	.1	261.0	.1
51.1	.3	78.1	.3	107.2	.1	140.1	.1	175.1	.5	209.0	.1	269.0	.1
52.1	.2	79.1	.3	108.7	.2	141.1	.3	176.1	.2	211.2	.2	270.1	.1
52.9	.2	80.0	.1	110.1	.1	142.0	.3	179.2	.1	212.0	.2	273.1	19.6
54.0	.3	81.1	.2	111.1	.2	143.0	.2	181.0	.1	213.1	.1	274.2	24.9
55.1	1.1	82.0	.2	112.1	.1	144.1	.5	183.1	.3	214.1	.1	275.2	6.1
56.1	1.2	83.1	.4	113.1	.5	145.0	.2	184.0	.1	215.1	7.4	276.2	2.5
57.1	1.3	84.0	1.9	114.1	.6	146.1	.4	185.1	.7	216.1	1.7	277.2	.4
58.0	2.8	85.0	.7	115.1	1.8	147.1	8.6	186.1	.1	217.1	.6	278.2	.1
59.1	3.2	86.1	2.0	116.1	1.9	148.1	1.2	187.1	.6	218.1	.1	283.2	.1
60.1	.5	87.1	2.7	117.1	1.3	149.1	1.1	188.1	.7	221.1	.2	284.1	1.4
61.1	1.0	88.1	1.1	118.1	.3	150.1	.1	189.1	.7	227.2	.1	285.1	.3
62.2	.1	89.0	.5	119.1	.2	151.0	.1	190.1	.2	229.1	.1	286.2	.2
63.0	.2	90.0	.1	120.1	.2	155.0	.1	191.2	.2	230.1	.7	287.1	.1
65.2	.1	91.2	.1	121.1	.1	156.1	.2	191.9	.1	231.2	.3	299.2	.7
66.1	.4	92.0	.1	125.1	.1	157.0	.2	193.0	.2	232.1	.1	300.2	.2
67.1	.4	93.0	.2	126.1	.1	158.0	3.5	195.1	.1	242.1	.1	301.1	.1
68.1	.4	95.1	.2	127.2	.3	159.1	.6	197.0	.1	243.1	.3	314.1	.1
69.1	.7	97.0	.1	128.0	.2	160.0	.6	199.1	.3	244.1	.2	315.2	.1
70.0	3.1	98.1	.5	129.1	.5	161.1	.2	200.0	.1	245.1	.1	347.2	.5
71.1	.9	99.1	.5	130.1	2.6	162.2	.1	201.1	.2	246.2	.1	348.2	.1
72.1	6.2	100.1	9.0	131.1	3.0	169.1	1.2	202.1	.4	256.1	.1	349.3	.1
73.1	100.0	101.0	1.7	132.0	.9	170.1	.3	203.2	.2	257.1	.2	374.2	2.6
74.1	9.0	102.1	.9	133.0	2.3	171.1	.2	204.0	.1	258.1	5.2	375.3	.8
75.1	16.8	103.1	.5	134.0	.3	172.1	.4	205.1	.1	259.2	1.4	376.2	.4

TABLE 9. GC mass spectrum of pH 4 oxidation product from LC Peak-523 and GC Peak-28.5.

MASS	%	MASS	%	MASS	%	MASS	%	MASS	%	MASS	%	MASS	%
49.1	.3	76.1	1.2	103.1	.5	134.0	.5	166.1	.2	198.2	.6	245.3	.1
50.1	.2	77.0	2.4	104.0	.1	135.1	.6	168.1	.3	199.1	.3	253.1	.2
51.1	.3	78.1	.3	105.1	.5	136.0	.1	169.3	.2	200.1	.1	255.0	.1
52.1	.3	79.1	.4	108.2	.1	139.0	.2	170.1	.7	201.0	.5	256.1	.2
53.1	.4	80.1	.5	109.1	.4	140.1	.3	171.1	.3	202.1	.1	257.1	.5
54.2	.3	81.1	.3	110.2	.1	141.0	.4	172.1	.4	204.1	.1	258.1	.5
55.1	1.2	82.0	.2	111.2	.3	142.0	.3	173.1	.6	207.1	.4	259.2	.2
56.1	.7	83.0	.6	112.1	.3	143.0	.3	174.1	1.1	208.0	.1	269.1	.3
57.1	1.0	84.0	.6	113.0	.7	144.1	.2	175.1	.2	211.1	.1	270.1	.2
58.0	1.5	85.0	.9	114.1	1.0	145.0	.2	179.1	.1	214.1	.2	271.2	.3
59.1	2.8	86.0	1.4	115.1	.9	146.0	.2	181.1	.1	215.1	.3	272.1	3.2
60.2	.4	87.1	.9	116.1	.4	147.1	8.0	182.1	.5	216.1	.2	273.2	68.3
61.0	.9	88.1	.5	117.1	.9	148.1	1.4	183.2	.9	221.2	.2	274.2	14.0
62.1	.1	89.0	.3	118.1	.1	149.1	1.0	184.1	.3	223.2	.3	275.2	5.4
63.1	.2	91.2	.2	119.1	.4	150.1	.2	185.1	.4	223.9	.1	276.1	1.1
65.0	.2	92.2	.1	120.1	.1	151.0	.1	186.1	.2	225.1	.3	277.2	.2
66.1	.5	93.0	.3	121.1	.2	152.9	.1	187.1	.2	226.1	.1	285.2	.2
67.0	.7	94.1	.2	125.2	.1	154.1	.3	188.1	.4	228.2	.2	286.2	.1
68.0	.4	95.1	.3	126.1	.2	155.1	.2	189.1	.3	229.1	.2	297.2	1.3
69.0	1.0	96.1	.3	127.1	.2	156.0	.8	190.2	.1	231.2	.4	298.2	.3
70.0	2.0	97.1	.4	128.1	.2	157.0	1.0	191.0	.1	232.2	.1	299.2	.6
71.1	.8	98.1	1.1	129.0	1.1	158.1	1.3	192.0	.1	235.1	.1	300.1	.2
72.1	4.8	99.1	1.4	130.1	3.0	159.1	.3	193.0	.1	240.2	.2	314.1	.2
73.1	100.0	100.1	4.1	131.1	2.4	160.0	.2	195.1	.1	241.1	.1	387.1	1.8
74.1	8.9	101.1	1.2	132.0	.6	161.1	.1	196.0	.2	242.1	.2	388.2	.6
75.1	16.7	102.1	.7	133.0	2.7	165.2	.1	197.1	.5	244.2	.3	389.1	.3

having a molecular weight of 130, i.e. the methylparabanic acid is contaminated with a small amount of a hygroscopic material with molecular weight equal to 130. This could suggest that a precursor of methylparabanic acid decomposes to give a product of molecular weight 130 and methylparabanic acid. The fact that GCMS data did not show the presence of methylparabanic acid was anticipated. Dryhurst[59] was unable to obtain GCMS data of parabanic acid.

Possible identities for a molecule with molecular weight 130 could be structures XII, XIII, and XIV. It has been proposed that in the electrochemical oxidation of uric

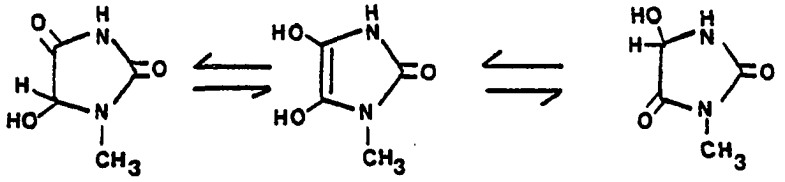

XII XIII XIV

acid[28], 2-oxy-4,5-dihydroxyimidazole (structure XV) is an

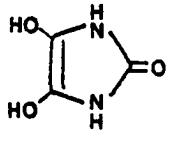

XV

intermediate. 2-Oxy-4,5-dihydroxyimidazole (XV) is an enediol. Enediols are normally very readily oxidizable to ∝-di-ketones even by such weak oxidizing agents as cupric ion and oxygen[60]. Accordingly it was proposed[28] that the parabanic acid which appeared during the electrooxidation of uric acid is formed as a result of oxidation of the enediol (XV) in a $2e^{\ominus}$, $2H^{\oplus}$

process. In an analogous manner it can be proposed that in the electrochemical oxidation of 9-methylxanthine (vide infra), 1-methyl-2-oxy-4,5-dihydroxyimidazole (structure XIII) is an intermediate. This molecule could undergo keto-enol tautomerization to form 1-methyl-2,4-oxy-5-hydroxyimidazole (XII) and 1-methyl-2,5-oxy-4-hydroxyimidazole (XIV). Either of these compounds could give a GCMS spectrum with a m/e = 274 molecular ion.

It is thought that 9-methyluric acid-4,5-diol (structure XVI), a precursor to 1-methyl-2-oxy-4,5-dihydroxyimidazole

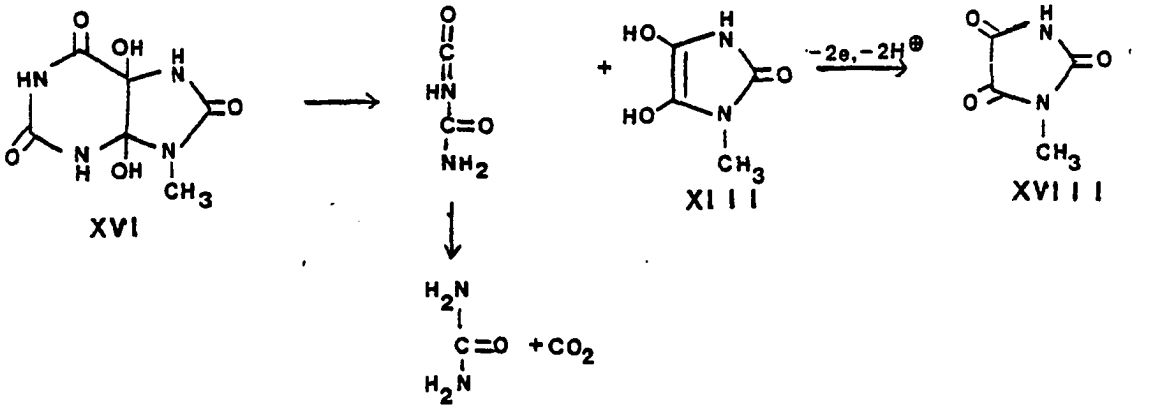

(XIII), is sufficiently long lived that some is present at the start of liquid chromatography. This allows a small amount of compound XIII (or tautomers XII and XIV) to separate (GC Peaks-28.2 and 28.5). However, air oxidation in a $2e^{\ominus}$, $2H^{\oplus}$ process converts most of compound XIII produced during separation to methylparabanic acid (XVIII). This could explain the observation of methylparabanic acid as a product in two different liquid chromatography peaks (LC Peaks-523 and 596). If methylparabanic acid is formed during chromatography from

decomposition of 9-methyluric acid-4,5-diol, urea (structure XVII) might also be present in LC Peak-523. Comparison of the i. r. spectra for methylparabanic acid (LC Peak-596, Figure 51) and the LC Peak-523 product (Figure 53) shows the major difference between them to be in the 1000-1200 cm^{-1} region. Methylparabanic acid has two distinct, prominent peaks (1050 and 1140 cm^{-1}) in this range. LC Peak-523 product shows both these peaks, however they are part of a broad rise in absorbance over the whole 900-1300 cm^{-1} region. The i. r. spectrum of urea (Part I, Figure 18) has an almost identical broad absorbance rise in the 900-1300 cm^{-1} range as that observed for the LC Peak-523 product. This could indicate the presence of some urea in the LC Peak-523 product.

The identification of alloxan as a product implies that methylurea should also be a product due to the proposed mechanism (vide infra). However, using the liquid chromatographic conditions reported (vide supra) methylurea eluted with the same retention volume as the large phosphate peak from the high ionic strength electrolysis solution. This conclusion was based upon essentially identical behavior of authentic methylurea. It was therefore impossible to desalt and positively identify methylurea using liquid column chromatography. Methylurea was detected using thin-layer chromatography (Cellulose, Polygram CEL 300 U. $V._{254}$). Butanol-acetic acid-water (120:30:50) was employed as the developing solvent. Upon completion of the liquid column separation, the chromato-

graphic peak with retention volume of 326 ml (Figure 49) was lyophilized. The freeze-dried solid was dissolved in a solution of the developing solvent. The resultant solution was spotted on the thin-layer sheet along with authentic methylurea. Identification was based upon essentially parallel behavior of the test sample (r_f = 0.79) and authentic compound (r_f = 0.72).

The methylparabanic acid found in LC Peak-596 is thought to be due to oxidation of 1-methyl-2-oxy-4,5-dihydroxyimidazole (XIII) in the electrolysis solution before chromatography. Thus, urea should also be produced in the electrolysis solution due to the proposed decomposition mechanism of the diol (XVI) (vide supra). Authentic urea was shown to have a similar retention volume to that observed for 1-methylallantoin using the employed chromatographic conditions (vide supra). Thus, thin-layer chromatography (Cellulose, Polygram CEL 300 U. $V._{254}$) was used to detect the small amount of urea expected in LC Peak-439 (Figure 49). Butanol-acetic acid-water (120:30:50) was employed as the developing solvent. The thin-layer chromatogram of the LC Peak-439 product showed one dark spot (r_f = 0.80) and a faint spot (r_f = 0.91). Authentic urea displayed similar behavior to the faint spot. It is thought the dark spot is due to 1-methylallantoin.

It should perhaps be stressed that the structures of the dimers, 1-methylallantoin, and the molecular weight 130 product have not been absolutely confirmed. In order to prove

the absolute structures independent chemical syntheses or x-ray studies are required. In addition, the presence of urea and methylurea have not been absolutely varified. Different methods to separate and isolate them are required to confirm the presence of urea and methylurea as products.

Reaction Mechanism

Peaks IIIa/IVa. Peak IIIa has been shown to be an adsorption prepeak of peak IVa by voltammetry (Figures 15 and 16) and product analysis. Mass electrolysis at potentials corresponding to either oxidation peak produced the same products (vide supra).

The mechanism of the electrochemical oxidation of 9-methylxanthine (I, Figure 56) at peaks IIIa/IVa (Figure 20) proceeds by an initial $2e^{\ominus},2H^{\oplus}$ oxidation of the $N_7=C_8$ bond to give 9-methyluric acid (II, Figure 56). Inclusion of $2H^{\oplus}$ in the electrochemical process is due to the pH dependency of peak potential shown by peaks IIIa and IVa in Figures 7-10. Since 9-methyluric acid is more readily oxidized[19] than 9-methylxanthine, it is immediately oxidized in a further $2e^{\ominus},2H^{\oplus}$ process (pH 4) or $2e^{\ominus},1H^{\oplus}$ process (pH 7) to 9-methyluric acid diimine (III, Figure 56). Thus, voltammetric peaks IIIa/IVa (Figure 20) of 9-methylxanthine correspond to the $4e^{\ominus},4H^{\oplus}$ (pH 4) or $4e^{\ominus},3H^{\oplus}$ (pH 7) oxidation to the diimine (III, Figure 56). The system of conjugated double bonds, proposed in the diimine, would be expected to be very readily electrochemically reducible, indeed molecules having somewhat similar diimine structures such as riboflavin[61]

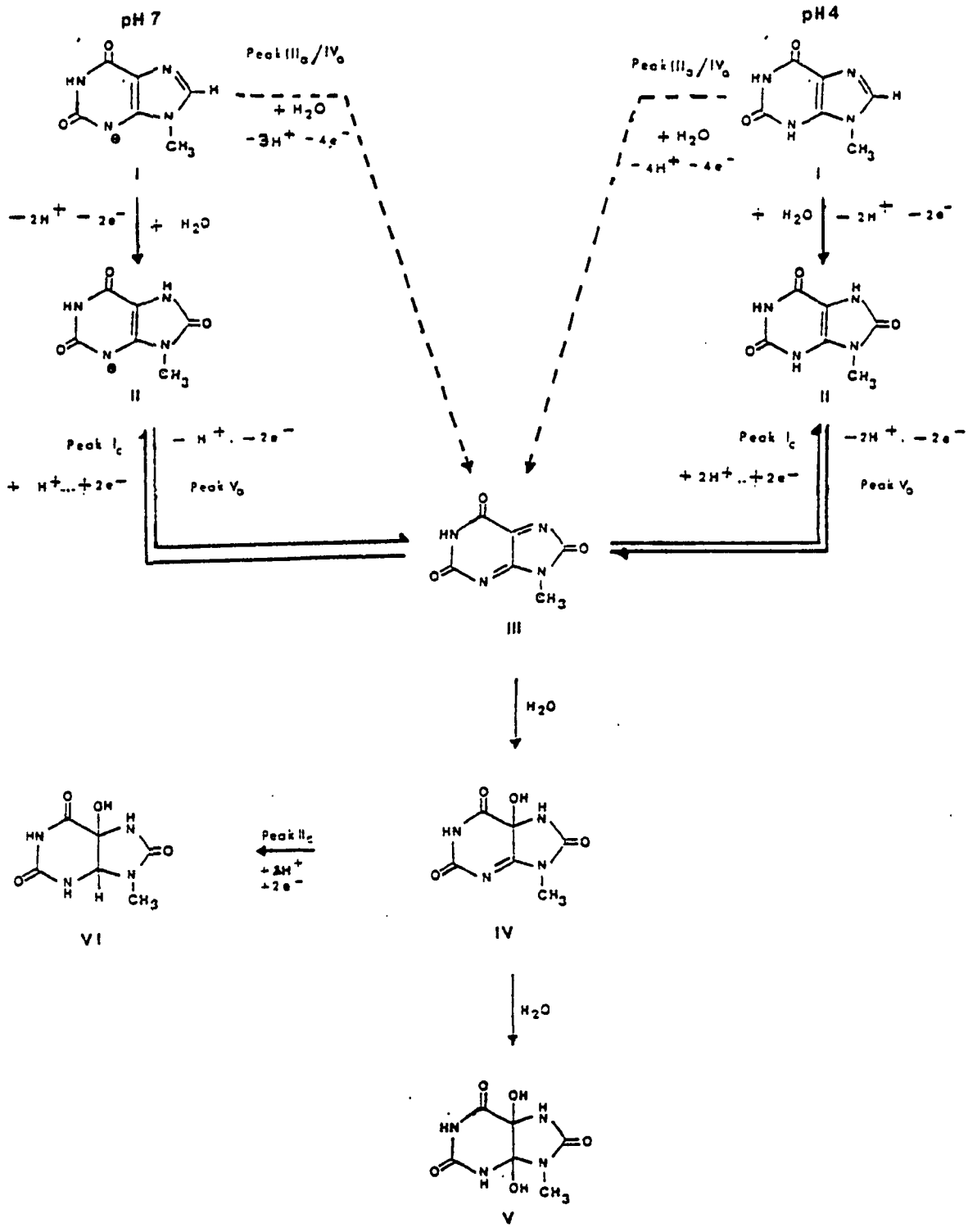

Figure 56. Products and mechanism of the electrochemical oxidation of 9-methylxanthine at peaks IIIa/IVa at PGE.

(structure XIX), quinoxalines[62] (structure XX), and bis-quinazolines[63] (structure XXI). The expected ease of reduct-

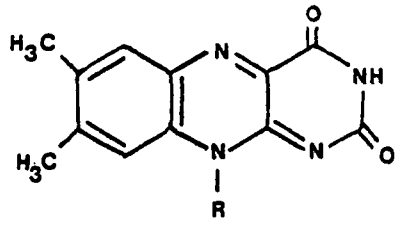

XIX

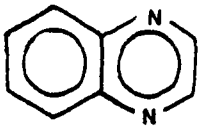

XX

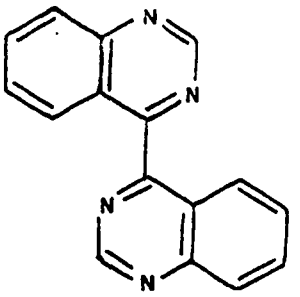

XXI

ion of structure III along with its expected facile hydration across the imine -N=C- double bonds to give a 4,5-diol accounts nicely for part of the observed cyclic voltammetry of 9-methylxanthine. Thus, provided the sweep rate is sufficiently fast, the diimine (III, Figure 56) formed from oxidation of 9-methylxanthine can be detected as a reducible species (peak Ic, Figure 20). This cathodic process is due to reduction of the diimine back to 9-methyluric acid (III → II, Figure 56). The anodic peak (peak Va) observed on the second positive-going sweep of 9-methylxanthine is either reoxidation of 9-methyluric acid (III), formed in the peak Ic process, back to the diimine or oxidation of 9-methyluric acid formed during the peak IIIa/IVa process under voltammetric conditions. At slow scan rates the diimine cannot be detected because it is hydrated too rapidly to 9-methyluric acid-4,5-diol (Figure 56) or other species (vide infra). It is proposed that the diimine formed on oxidation of 9-methylxanthine hydrates in two stages, the first fast, the second slower ($k = 0.015\ s^{-1}$, pH 7 or

$k = 0.0014\ s^{-1}$, pH 4). Addition of the elements of one molecule of water gives rise to an imine-alcohol (IV, Figure 56). It is believed that this imine-alcohol gives rise to peak IIc of 9-methylxanthine being due to reduction to compound VI (Figure 56). That the imine-alcohol intermediate is responsible for reduction peak IIc was demonstrated by thin-layer spectroelectrochemical experiments (vide supra). Addition of a second molecule of water to the imine-alcohol would give rise to the formation of 9-methyluric acid-4,5-diol (V, Figure 56). This diol is a typical intermediate of an imine-like hydrolysis and would be expected to readily fragment to the observed products. A plausible mechanism for formation of 1-methylallantoin from 9-methyluric acid-4,5-diol involves cleavage of the C_5-C_6 bond of the diol (I, Figure 57) giving an imidazole isocyanate (II, Figure 57). A hydrogen shift reaction must occur in compound II to give III which on hydrolysis would readily form CO_2 and allantoin (V, Figure 57). A simple fragmentation of the 4,5-diol to alloxan (VI, Figure 57) and methylurea (VII, Figure 5) can also be written. Formation of methylparabanic acid necessarily involves some secondary oxidation. A mechanism is proposed in Figure 57 where 9-methyluric acid-4,5-diol undergoes a ring opening reaction tc give structure VIII. In acid solution VIII should readily cleave across the original C_5-C_6 bond to give an isocyanate (IX) and 1-methyl-2-oxy-4,5-dihydroxyimidazole (X). Simple hydrolysis of the isocyanate IX would give urea (XII) and CO_2.

SECONDARY REARRANGEMENT and HYDROLYSIS to METHYLALLANTOIN

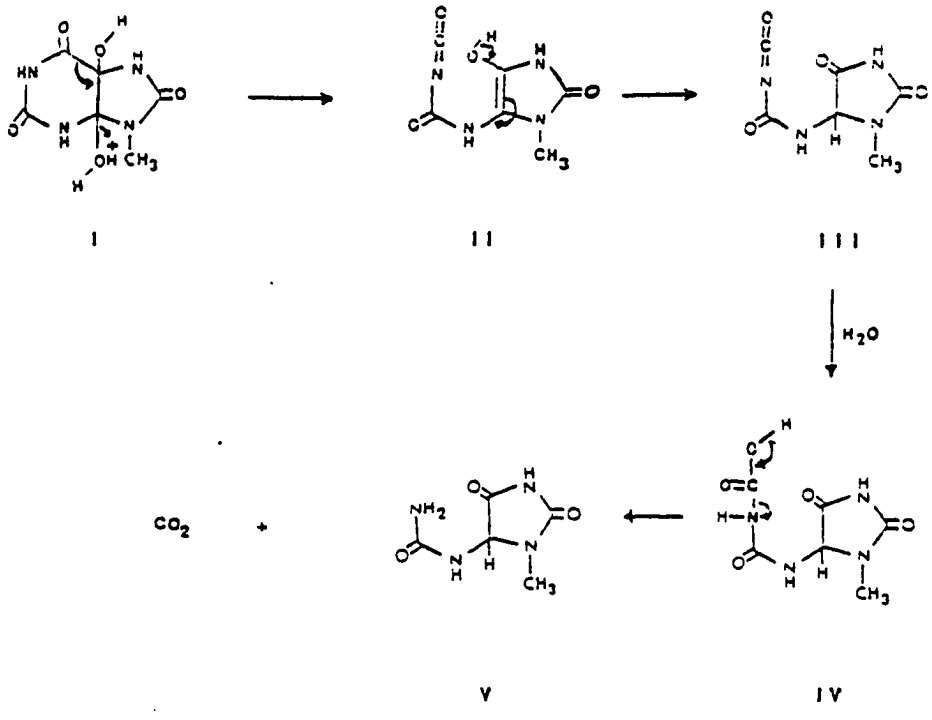

I II III IV V

SECONDARY REARRANGEMENT to ALLOXAN

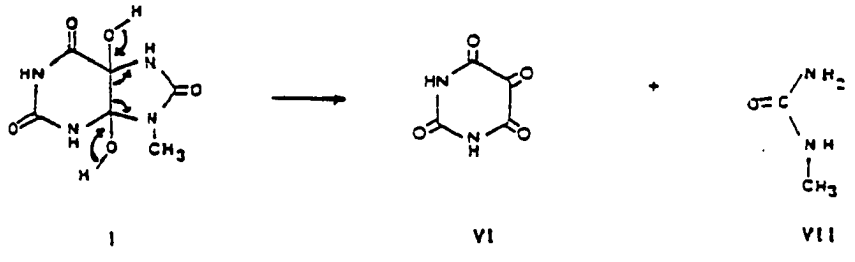

I VI VII

(continued on p. 206)

Figure 57. Proposed mechanisms for decomposition of 9-methyluric acid-4,5-diol to 1-methylallantoin (V), alloxan (VI), methylurea (VII), methylparabanic acid (XIV), urea (XIII), 1-methyl-2-oxy-4,5-dihydroxyimidazole (X), and CO_2.

Figure 57. (continued)

SECONDARY REARRANGEMENT and OXIDATION to METHYLPARABANIC ACID

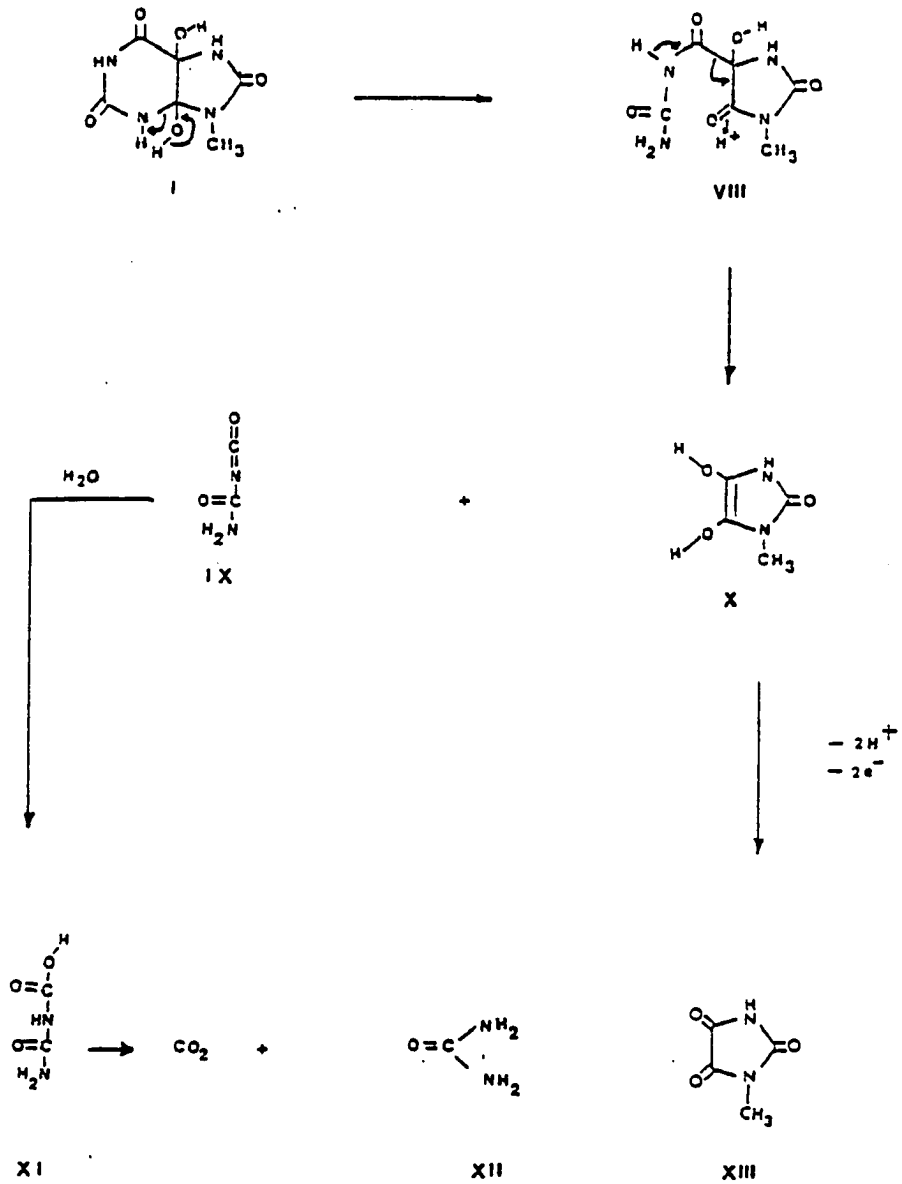

1-Methyl-2-oxy-4,5-dihydroxyimidazole (X, Figure 57) is very readily oxidizable to ∝-di-ketones (vide supra). Accordingly it is proposed that the methylparabanic acid (XIII, Figure 57) which appears during the electrooxidation of 9-methylxanthine is formed as a result of oxidation of the enediol (X) in a $2e^{\ominus}$, $2H^{\oplus}$ process.

Peak Ia. Switching potential studies (Figures 21 and 24) of 9-methylxanthine in the vicinity of peak Ia indicated, by the presence of voltammetric peak Va in the second positive potential sweep that oxidation at peak Ia produced some 9-methyluric acid and 9-methyluric acid-4,5-diol. This would be indicative of a 4-electron transfer. Such behavior was more prominent at pH 4 where the peak potential was dependent on pH (Figures 7-10). Under voltammetric conditions, determined from i_p and $\propto n_a$ values, the peak Ia process involves between 1-2 electrons per molecule of 9-methylxanthine (vide supra). Potentiostatic n-value determinations were concentration dependent (Table 5). At pH 7 the n-value for the peak Ia process 9-methylxanthine varied from 1 at a concentration of 3.0 mM to 2 at a concentration of 0.5 mM. A potentiostatic n-value of 1.5 was obtained for a 3.0 mM concentration of 9-methylxanthine at pH 4. Spectroelectrochemistry of solutions of 9-methylxanthine at concentrations greater that 1 mM at pH 7 (Figure 28) showed an absorbance peak at 340 nm. This peak was not observed at pH 4 (Figure 33) or pH 7 at concentrations below 1 mM (Figure 30). To account for the varying

electron number, the observed spectroelectrochemistry, and the obtained products (8, 8´-Bi-9-methyl-9H-purine-2,6-(1H, 3H)-dione, 1-methylallantoin, methylparabanic acid, alloxan, urea, methylurea, and 1-methyl-2-oxy-4,5-dihydroxy-imidazole) two oxidative routes must be involved. The proposed mechanism of electrochemical oxidation of 9-methylxanthine at oxidation peak Ia is dependent on the pH of the electrolysis solution. At pH 7, the monoanion of 9-methylxanthine (I, Figure 58) is initially electrochemically oxidized in a $1e^{\ominus}$ process to give a radical cation (II, Figure 58). This reaction would explain the independence of Ep vs pH shown by 9-methylxanthine above the pK_a = 6.3 (Figures 7-10). Structure II subsequently loses a hydrogen at the C-8 position to form a free radical (III, Figure 58). This can either dimerize to give 8, 8´-Bi-9-methyl-9H-purine-2,6-(1H, 3H)-dione (IV, Figure 58) or be further oxidized to 9-methyluric acid (V, Figure 58) in a further $1e^{\ominus}$, $1H^{\oplus}$ oxidation. Potentiostaic n-values (Table 5) and product analysis (Figure 41) indicated that dimerization is the preferred pathway at $\geq$ 1 mM concentrations of 9-methylxanthine. Any 9-methyluric acid (V) formed is very rapidly oxidized in a $2e^{\ominus}$, $1H^{\oplus}$ process to 9-methyluric acid diimine (VI, Figure 58). This diimine hydrates in two stages, as in Figure 56, to give 9-methyluric acid-4,5-diol (VII, Figure 58). 1-Methylallantoin would be formed from the diol in the same manner proposed in Figure 57. The neutral species of 9-methylxanthine (I, Figure 59) at pH 4

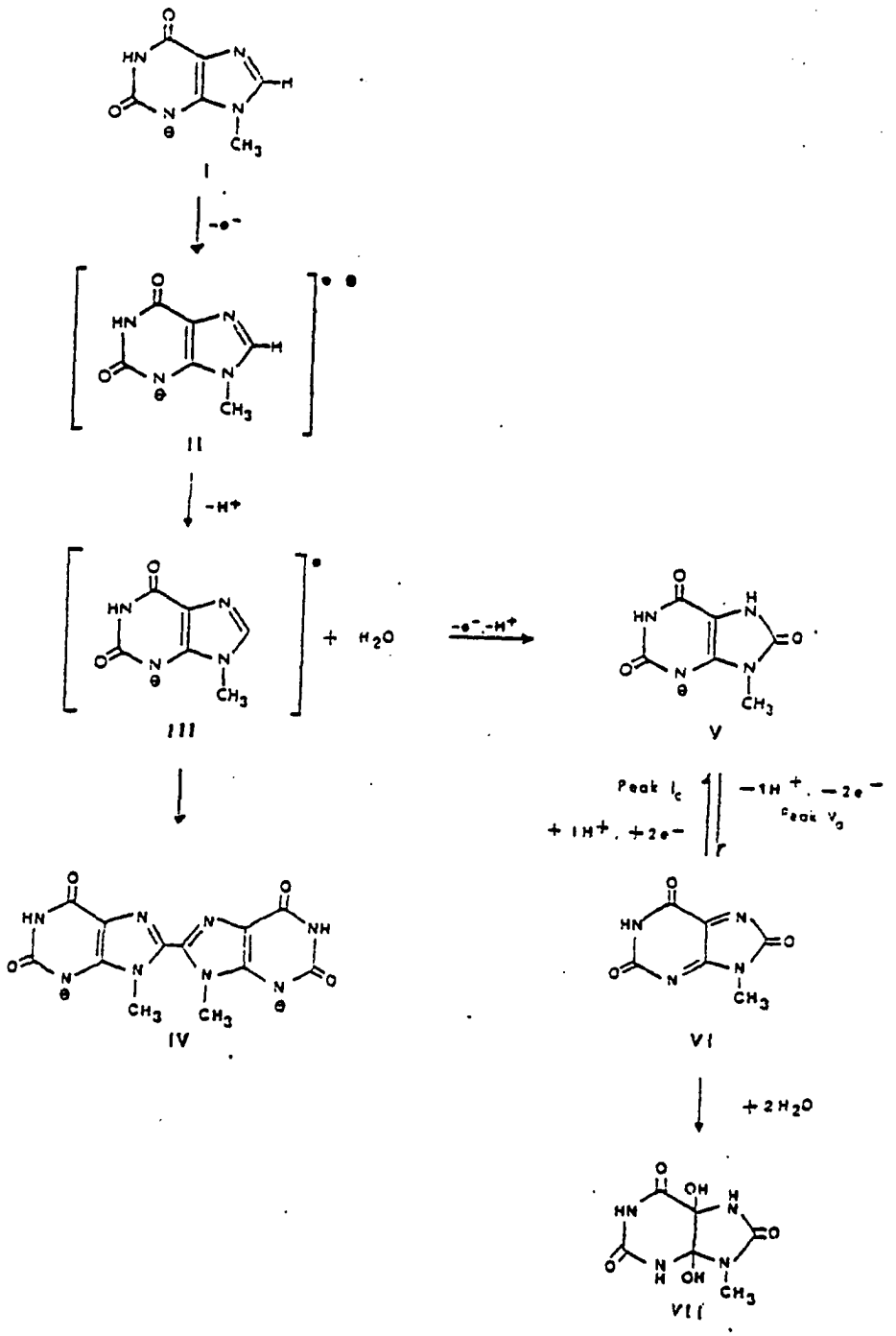

Figure 58. Products and mechanism of the electrochemical oxidation of 9-methylxanthine at peak Ia in pH 7 phosphate buffer.

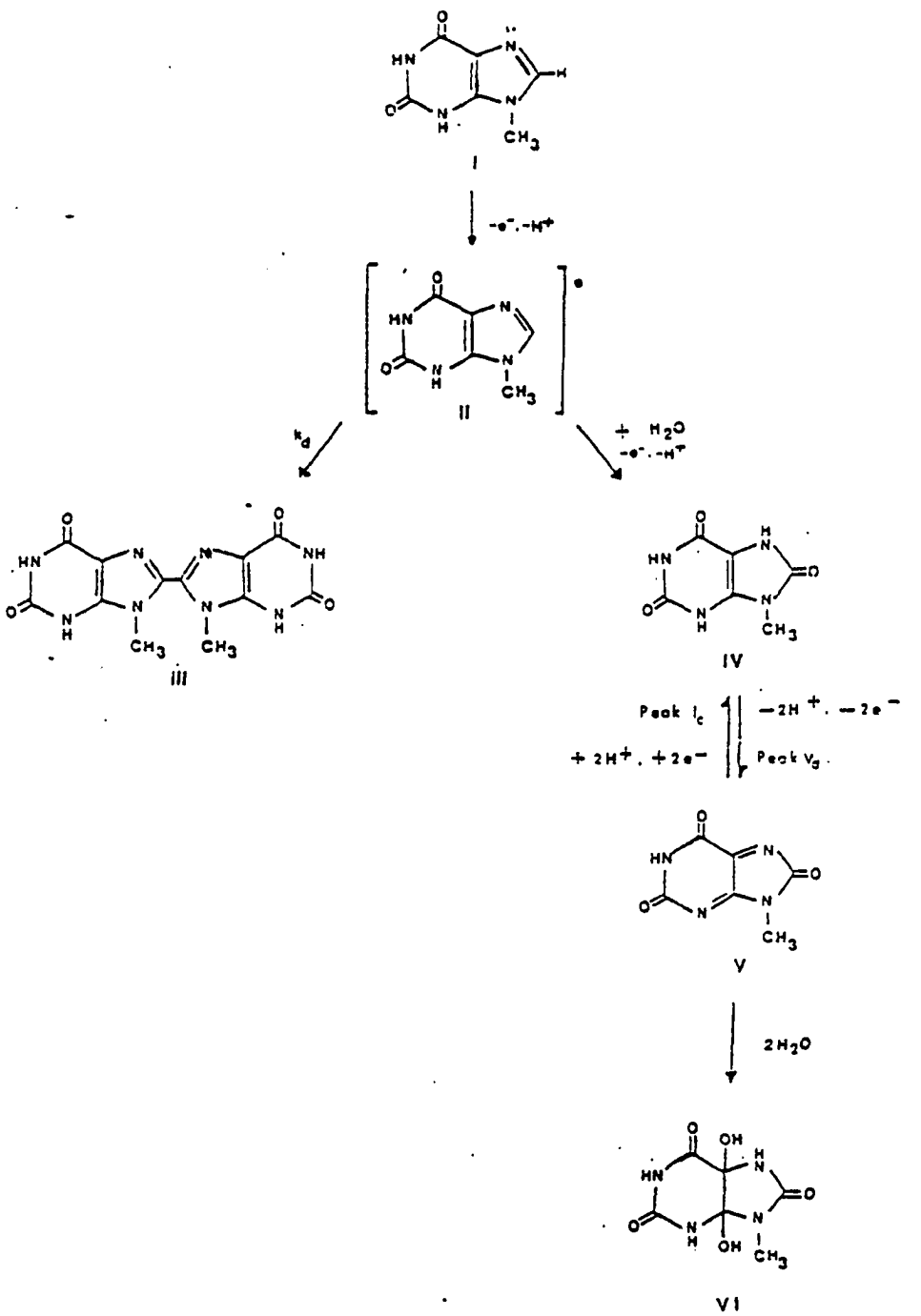

Figure 59. Products and mechanism of the electrochemical oxidation of 9-methylxanthine at peak Ia in pH 4 phosphate buffer.

is electrochemically oxidized in a primary $1e^{\ominus}$, $1H^{\oplus}$ process to give a free radical (II, Figure 59). This reaction scheme explains the dependency of Ep *vs* pH displayed by 9-methylxanthine below the $pK_a = 6.3$ (Figures 7-10). This free radical can either dimerize to give 8,8´-Bi- 9-methyl-9H-purine-2,6-(1H, 3H)-dione (III, Figure 59) or be further oxidized to 9-methyluric acid (IV, Figure 59) in a further $1e^{\ominus}$, $1H^{\oplus}$ oxidation. Product analysis (similar to Figure 49) and thin-layer spectroelectrochemistry (no 340 nm absorbance peak, Figure 33) implies no dimerization occurs. However, voltammetric and potentiostatic (Table 5) n-values indicate some dimerization takes place. This discrepancy can be explained by considering the small potential difference between oxidation peaks Ia and IIa at pH 4 (B, Figure 23). Any dimer formed is immediately oxidized in the peak IIa process and subsequently decomposes to products similar to those observed for peaks IIIa/IVa (*vide infra*). The 9-methyluric acid (IV) formed is very rapidly oxidized in a $2e^{\ominus}$, $2H^{\oplus}$ process to 9-methyluric acid diimine (V, Figure 59). This diimine, identical to those in Figures 56 and 58, hydrates in two stages to give 9-methyluric acid-4,5-diol (VI, Figure 59). The diol would be expected to readily fragment to the observed products, 1-methylallantoin (V, Figure 57), alloxan (VI, Figure 57), methylparabanic acid (XIII, Figure 57), 1-methyl-2-oxy-4,5-dihydroxyimidazole (X, Figure 57), methylurea (VII, Figure 57), and urea (XIII, Figure 57).

It is thought that dimerization occurs to a greater extent as the concentration increases. This would account for the higher potentiostatic n-value observed at low concentration (Table 5). In addition the absence of peak IIa, which is a further oxidation of the dimer formed at peak Ia (vide infra), in the voltammetry of 0.1 mM 9-methylxanthine (Figures 17 and 18) implies no dimerization occurs at these low concentrations. By analogy, the increased prominence of oxidation peak IIa in the voltammetry of 0.5 mM and higher concentrations of 9-methylxanthine (Figures 17 and 18) indicates dimerization increases with concentration.

Peak IIa. Voltammetry showed the presence of oxidation peak IIa to be concentration dependent (Figures 17 and 18). In addition, voltammetry performed during coulometry at potentials corresponding to peak Ia (Figure 25) showed the peak height of IIa increased during the initial phase of the electrolysis. These results imply the peak IIa process is a further oxidation of a high concentration product formed at peak Ia. Coulometric n-values were concentration dependent (Table 4). At pH 7, the n-value at peak Ia/IIa potentials of 9-methylxanthine varied from 2.8 at a concentration of 3.0 mM to 3.5 at a concentration of 0.1 mM. The coulometric n-values at pH 4 varied from 3.6 at a concentration of 3.0 mM to 3.9 at 0.1 mM. It was noticed during the course of the coulometric experiments a yellow color developed. This color remained after completion of the electrolysis at higher

concentrations (Table 4). While at low concentration the yellow color fades and completely disappears. Potentiostatic n-values also showed a concentration dependency (Table 5). These varied at pH 7 at peak potentials Ia/IIa of 9-methylxanthine from 1.8 at 10.0 mM to 2.2 at 0.5 mM. To account for the varying electron number and the observed products (8,8´-Bi-9-methyl-9H-purine-2,6-(1H)-dione-3,5-(3H)-diiminylidene (yellow dimer), 1-methylallantoin, methylparabanic acid, alloxan, urea, methylurea, and 1-methyl-2-oxy-4,5-dihydroxy-imidazole) secondary chemical reactions and oxidations are proposed to be involved. It was assumed the peak Ia process must precede the peak IIa oxidation (vide supra). Thus under these conditions the peak IIa process involves a further 1 electron per molecule of 9-methylxanthine oxidation of a high concentration product from peak Ia. In view of these facts, a mechanism is proposed where 8,8´-Bi-9-methyl-9H-purine-2,6-(1H,3H)-dione (Ia and Ib, Figure 60) is initially electrochemically oxidized in a $2e^{\ominus}$ process at pH 7 or a $2e^{\ominus}$, $2H^{\oplus}$ process at pH 4 to give 8,8 -Bi-9-methyl-9H-purine-2,6-(1H)-dione-3,5-(3H)-diiminylidene (II, yellow dimer, Figure 60). This mechanism would explain the independence of Ep vs pH above the pK_a = 6.3 and the dependency of Ep vs pH below this pK_a shown by 9-methylxanthine (Figures 7-10). This yellow dimer (II) with such a system of conjugated double bonds would be expected to be very readily electrochemically reducible[61-63]. In fact the small reduction peaks observed

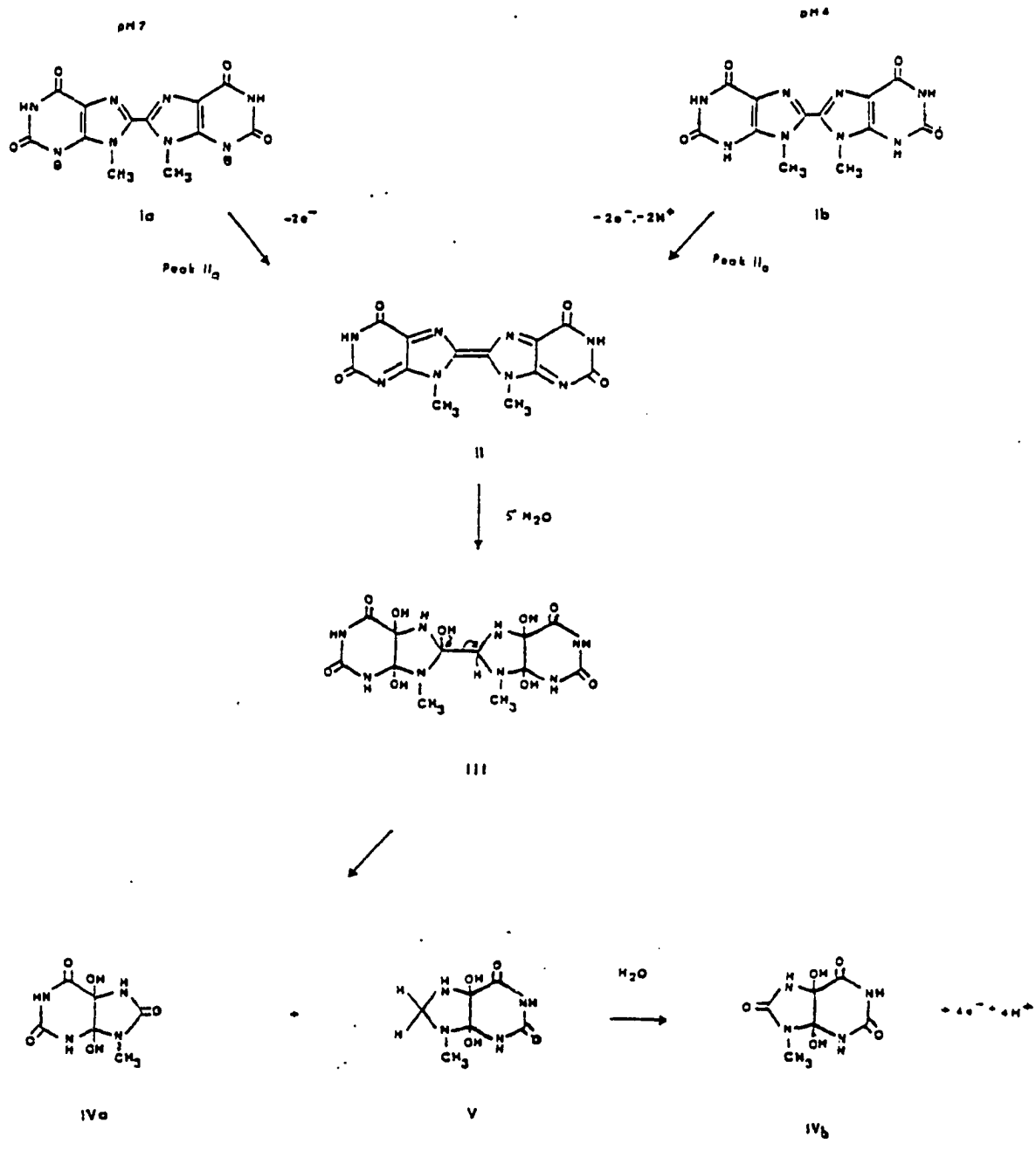

Figure 60. Products and mechanism of electrochemical oxidation at peak IIa of 9-methylxanthine.

in cyclic voltammetry of 9-methylxanthine (Figures 21 and 24) were shown to be due to the yellow dimer (II). The yellow dimer was sufficiently stable at pH 7 to permit voltammetric experiments. However, II hydrates slowly at pH 7 and more quickly at pH 4 to give structure III (Figure 60). A simple fragmentation of structure III to 9-methyluric acid-4,5-diol (IVa, Figure 60) and 8,8-dihydro-9-methyluric acid-4,5-diol (V, Figure 60) can be written. 9-Methyluric acid-4,5-diol (IVb, Figure 60) may be formed as a result of electrochemical or air oxidation of compound V in a $4e^{\ominus}$, $4H^{\oplus}$ process. This diol would be expected to readily fragment in the Figure 57 mechanisms to the observed products. The proposed peak IIa mechanism can be used to explain the difference in the potentiostatically and coulometrically determined n-values. Only a few seconds are required to complete the potentiostatic experiments. This is insufficient time for compound II (Figure 60) to hydrate to compound V. Therefore, the oxidation of V does not take place. The result is an n-value (Table 6) due to the oxidation of only compound I to the yellow dimer (II, Figure 60). In the case of coulometry, several hours are required to complete these experiments. This is sufficient time to produce and oxidize compound V. As a result coulometric n-values (Table 4) imply some or all of compound I (Figure 60) has decomposed to the fragmentation products of 9-methyluric acid-4,5-diol. The low coulometric n-values for 0.5 mM and 3.0 mM concentrations of 9-methyl-

xanthine at pH 7 (Table 4) are due to slower hydration at this pH. This was confirmed by allowing 40 mg of the yellow dimer to stand in one liter of water for 48 hours. After this length of time lyophilization revealed no yellow color and 1-methylallantoin was present (vide supra). This suggests given sufficient time II may hydrate to 9-methyluric acid-4,5-diol (IVa) and compound V. Subsequently, compound V might air oxidize to 9-methyluric acid-4,5-diol (IVb), which would then fragment to 1-methylallantoin.

It should perhaps be noted there is insufficient evidence at this time to definitively explain the effect of pH on the yield of products. It is likely however that the various decomposition reactions of 9-methyluric acid-4,5-diol are acid or base catalyzed hence changing the yields and nature of products with pH. The mechanisms actually proposed for the decomposition of the 9-methyluric acid-4,5-diol (Figure 57) should accordingly be regarded as tentative since actually several equally plausible mechanism could be written. However, the basic mechanisms presented here can be used to satisfactorily account for the electrochemistry and products formed on electrooxidation of other purines[17].

Experimental

Chemicals

Methylparabanic acid was prepared according to the method of Biltz and Topp[64]. It was obtained by heating a

mixture of 4.45 g methylurea, 7.5 g oxalyl chloride, and 100 g anhydrous ether. The ether portion was separated from a yellow substance formed by the reaction and evaporated. The product was recrystallized from water (mp 151-154°C).

Other chemicals were obtained from the sources listed: 9-methylxanthine and 9-methyluric acid (Adams Chemical Co., Round Lake, IL.); xanthine, uric acid, and alloxan monohydrate (Nutritional Biochemicals Corp., Cleveland, OH.); potassium ferricyanide (Mallinckrodt, St. Louis, MO.); bacto-agar (Difco Labs, Detroit, MI.); reticulated vitreous carbon (Fluorocarbon, Anaheim, CA.); bis(Trimethylsilyl)trifluoroacetamide and acetonitrile (Supelco, Bellefonte, PA.); Liquid Organic Silver No. 9167 (Englehard Industries, East Newark, N. J.). Column chromatography utilized Sephadex G-10 and QAE-Sephadex A-25 (Pharmacia Fine Chemicals, Piscataway, N. J.). 3% SE-30 on Chromosorb W (HP) 80/100 mesh (Supelco, Bellefonte, PA.) was used for gas chromatography. Compressed air and hydrogen used as the oxidant and the fuel, respectively, for the flame ionization detector were employed without purification. The nitrogen carrier gas was dried with Drierite (W. A. Hammond Drierite Co., Xenia, OH.) and Davison^{R} Molecular Sieves (Fisher Scientific Co., Fair Lawn, N. J.). Any other chemicals and reagents used were of analytical reagent grade.

Buffer solutions were prepared with an ionic strength of 1.0 M, giving a 0.5 M ionic strength upon 1:1 dilution.

Nitrogen was used for deoxygenation of working cells without purification.

Apparatus

The gold optically transparent thin-layer electrochemical cells were designed and constructed after those described by Murray et al.[65] and Heineman et al.[66]. Gold minigrids, used for the optically transparent electrodes were purchased from Buckbee Mears Co., St. Paul, MN. The gold minigrid employed had 1000 wires per inch and had a transmittance of approximately 50 % relative to air. A strip of minigrid was cut to about 1 x 4 cm. and placed between two 25 x 50 x 1 mm quartz plates (Esco Optics Products, Oak Ridge, N. J.). Four layers, one-inch wide 3/4-mil of Fluro-film Type C Teflon tape (Dilectix Corp., Farmingdale, NY.), were used for spacing the two slides. This tape was placed on the quartz slides and a section of the tape was cut away, leaving strips of about 3 mm on the two vertical edges and all but 5 mm on the top edge. The gold minigrid was positioned such that about 1.5 cm extended past the vertical edge of the slides; this extention was for electrical contact. The lower edge was positioned about 5 mm from the bottom of the quartz slide. Once the gold minigrid was firmly sandwiched between the quartz plates and Teflon spacers, the edges were painted with Tygon paint (Carboline K-63 White, Carboline Co., St. Louis, MO.) in order to seal the cell and hold it firmly together. The bottom edge and the 5 mm space on the top

edge were left unpainted. This open bottom allowed contact with the test solution and the opening at the top was used to draw solutions into the cell. The thickness of the cell was determined spectrophotometrically at 283 nm using a solution of O-tolidine in ethanol (ε = 2.39 x 10^4 $\underline{M}^{-1}$ cm^{-1})[67]. The thickness of the cells was found to range from 101 to 104 μm.

The reticulated vitreous carbon (RVC) optically transparent thin-layer electrochemical cells were constructed and designed after those described by Norvell and Mamantov[68]. The reticulated vitreous carbon had a porosity of 60 pores per inch. This material was cut into slices of approximate dimensions 2 cm x 4.5 cm with a thickness of 1.5 mm and used as the working electrode. Electrical contact to the RVC was made by threading a fine Cu wire through a corner of the electrode and folded over to secure it. Liquid organic silver No. 9167 was then applied to the surrounding area and the organic portion burned away leaving a silver coating. This was repeated several times until a sturdy contact was achieved. The optically transparent electrode was assembled by sealing the RVC electrode between two quartz plates with epoxy in a configuration similar to that used for the gold minigrid cell.

The solutions to be studied were placed in a 6 ml glass cap and the open end of the thin-layer cell was dipped into these solutions. A saturated calomel reference electrode (SCE) fitted with a Luggin capillary was positioned in the

test solution beneath the open base of the thin-layer cell. A piece of platinum foil, shaped to line the inside of the glass cup, was utilized for the counter electrode.

Potentials were applied and maintained with a Wenking Model LT 73 potentiostat (Brinkmann Instruments Inc., Westbury, NY.). Spectra and absorbance-time data were recorded on a Hewlett-Packard Model 7001A X-Y Recorder (Hewlett-Packard, Oklahoma City, OK.).

Optical measurements employed a Harrick Rapid Scan Spectrometer (RSS) with a Signal Processing Module (Harrick Scientific Co., Ossining, NY.). Kuwana[69] originally developed this type of oscillating mirror spectrometer. The optical layout and description for this instrument is described elsewhere[70]. Spectral scanning is possible from several minutes per spectrum to less than a millisecond per spectrum with an RSS. This instrument offers a high degree of flexibility because the frequency of scan, scan width, and wavelength region can all be varied simultaneously. The RSS incorporates double beam signal processing for absorbance readout. A second, essentially identical thin-layer cell arrangement containing the appropriate background buffer solution only was placed in the reference beam of the RSS.

The apparatus employed for voltammetry and coulometry was the same as that described in Part I, Chapter 6.

An Isco Model 328 fraction collector (Instrumentation Specialties Co., Lincoln, NE.) was utilized in the separation

of the oxidation products. U. v. absorption was measured in a Gilson Model HM Uv-vis Holochrome flow-through detector (Gilson Medical Electronics Inc., Middleton, WI.) employing a 32 µl cell having a path length of 2.5 mm. Desalted samples were collected using an Isco Model 1200 fraction collector. Product separation and desalting were performed in columns that have been described in Part I. Gas chromatography utilized a Varian Model 2400 gas chromatograph (Varian, Palo Alto, CA.).

Field desorption mass spectra were obtained at MIT by Dr. Catherine E. Costello. Direct insertion and coupled gas chromatography mass spectra were obtained using a Hewlett-Packard Model 5985 GCMS.

pH measurements, i. r. spectra, u. v. absorption, and lyophilization were accomplished using equipment previously described.

Procedures

Thin-layer spectroelectrochemistry. The solution of interest was placed in the glass cap and the thin-layer cell was lowered into this solution until its open end was immersed to a depth of 3-5 mm. The solution was drawn up into the cell using vacuum and held by capillary action. The light beam was positioned approximately in the center of the working electrode for both the sample and reference cells. Usually, a slow sweep rate voltammogram (2 $mVsec^{-1}$) was run in the thin-layer cell to determine the potential for controlled

potential electrolysis. Once the latter potential was decided, controlled potential electrolysis experiments were carried out during which the u. v. spectrum was continuously scanned. The wavelength range scanned normally extended from 200-400 nm. It was necessary to remove the electrolyzed solution after each experimental run and replenish the cell with fresh solution. After 8-10 oxidation experiments in the RVC cell, the time required to complete an electrolysis increased noticably. Deterioration of the RVC electrode also occurred after every reduction experiment. Adsorption of electrolysis products to the electrode surface was the probable cause of this behavior. In order to rejuvanate the electrode 250-500 milliliters of doubly distilled water were drawn through the cell.

Gas chromatography. 3% SE-30 on Chromosorb W (HP) 80/100 mesh was introduced into the glass columns by use of vacuum. To one end of the column, which had been plugged with glass wool, a rubber hose was attached connecting the column to the house vacuum. Small amounts of the packing material were added to the other end of the column. Through a combination of the vacuum and vibration from an electronic vibrator the packing material was made to migrate through the column and pack tightly against the glass wool. When the column was filled, glass wool was added to secure both ends of the column. The general procedure for obtaining a gas chromatogram began with the heating of ca. 0.1 mg of

sample in a 100-140 µl solution containing a silylating reagent, BSTFA, for approximately 20 minutes at 120°C. 5 µl of the resulting solution was introduced into the gas chromatograph. Here the temperature was held at 100°C for 12 minutes. After this period the temperature was raised 6°C per minute until a temperature of 300°C was achieved.

The liquid chromatographic, voltammetric, and coulometric procedures are the same as those previously described.

Summary

Between pH 2-9, 9-methylxanthine exhibits upto four voltammetric oxidation peaks at the pyrolytic graphite electrode. Peak Ia is an irreversible $1e^{\ominus}$ oxidation at a pH value above the pK_a (6.3) of the C_8 position to give a radical cation. A $H^{\oplus}$ is then lost from the C_8 position. Below the pK_a, peak Ia is an irreversible $1e^{\ominus}$, $1H^{\oplus}$ oxidation to give a similar free radical. These radicals can subsequently follow two mechanistic routes. At concentrations greater than ca. 1 mM they dimerize to form 8,8´-Bi-9-methyl-9H-purine-2,6-(1H,3H)-dione. At concentrations below ca. 1 mM the radicals are both further oxidized in $1e^{\ominus}$, $1H^{\oplus}$ processes to 9-methyluric acid. Since 9-methyluric acid[19] is more readily oxidized than is 9-methylxanthine the former compound is immediately oxidized in a $2e^{\ominus}$, $2H^{\oplus}$ (pH 4) or $2e^{\ominus}$, $1H^{\oplus}$ (pH 7) process to 9-methyluric acid diimine. The diimine hydrates to give 9-methyluric acid-4,5-diol. 9-Methyluric acid-4,5-diol is a

typical intermediate of an imine-like hydrolysis and would be expected to readily fragment to the observed products, 1-methylallantoin, alloxan, methylurea, methylparabanic acid, urea, and 1-methyl-2-oxy-4,5-dihydroxyimidazole. Oxidation peak IIa is due to further irreversible electrochemical oxidation of 8,8´-Bi-9-methyl-9H-purine-2,6-(1H,3H)-dione in a $2e^{\ominus}$ process above the pK_a (6.3) or a $2e^{\ominus}$, $2H^{\oplus}$ process below the pK_a to form 8,8´-Bi-9-methyl-9H-purine-2,6-(1H)-dione-3,5-(3H)-diiminylidene. This compound is only moderately stable. It hydrates (slowly at pH 7, more readily at pH 4) and fragments to give 9-methyluric acid-4,5-diol and 8,8-dihydro-9-methyluric acid-4,5-diol. The later compound is oxidized in a $4e^{\ominus}$, $4H^{\oplus}$ process to 9-methyluric acid-4,5-diol. This diol fragments to the same products as were formed in the peak Ia mechanism. Oxidation peak IIIa was shown to be an adsorption pre-peak of IVa. Peak IVa is due to irreversible electrochemical oxidation of 9-methylxanthine in an overall $4e^{\ominus}$, $3H^{\oplus}$ process above the pK_a (6.3) or a $4e^{\ominus}$, $4H^{\oplus}$ process below the pK_a to give 9-methyluric acid diimine. Initially, 9-methylxanthine undergoes an irreversible $2e^{\ominus}$, $2H^{\oplus}$ electro-oxidation to form 9-methyluric acid. This latter compound is rapidly oxidized in a $2e^{\ominus}$, $1H^{\oplus}$ process above the pK_a or a $2e^{\ominus}$, $2H^{\oplus}$ process below the pK_a to give 9-methyluric acid diimine. The diimine hydrates to form 9-methyluric acid-4,5-diol. Again, this diol fragments to the products observed in the peaks Ia and IIa processes. The electrochemical

products of all four peak processes were examined by u. v., i. r., and mass spectrometry plus voltammetry at the PGE. Chemical and electrochemical mechanism were studied using thin-layer spectroelectrochemistry.

CHAPTER III

ELECTROCHEMICAL OXIDATION OF XANTHOSINE

(9-RIBOSYLXANTHINE)

Introduction

Xanthosine (I) is a purine nucleoside. Since the

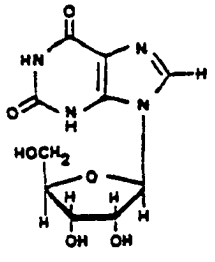

I

electrochemical oxidation of xanthine[28,34] and 9-methylxanthine (Part II, Chapter 2) has been investigated in some detail, xanthosine was a likely purine nucleoside to be studied.

Owens[34] has shown that xanthosine is electrochemically oxidizable at the PGE. This work was limited to a study of voltammetry and some spectroelectrochemistry of xanthosine. No attempt was made to determine mechanisms or to separate products.

Therefore, the present study was directed toward a detailed examination of the electrochemical oxidation of xanthosine, including a determination of rate constants,

isolation and identification of reaction products, and elucidation of reaction mechanisms. Experiments revealed that xanthosine is not electrochemically reducible at the pyrolytic graphite electrode over the pH range 2-8.

Results and Discussion

Physical properties of xanthosine

Xanthosine solutions at a concentration of 1 mM are stable in pH 4 and pH 7 phosphate buffer for 72 hours as determined by voltammetry. A plot of λ_{max} vs. pH of the two u. v.-absorbing peaks of xanthosine is shown in Figure 61. Both peaks show a large shift in λ_{max} between pH 5 and 6. Indeed, xanthosine has a reported pK_a of 5.7[71].

Linear and cyclic sweep voltammetry

Over the pH range 2-8, xanthosine exhibits up to four well-defined oxidation peaks (peaks Ia, IIa, IIIa, and IVa) at the PGE. Under voltammetric conditions, peak IIa only appears at concentrations ≥ 1 mM in xanthosine. At these high concentrations reliable peak potentials for the other three peaks could not be obtained. Variation of Ep with pH for solutions 0.5 mM in xanthosine are illustrated in Figures 62-65. The oxidation occurring most readily (Ia) is observed throughout the pH range 2-8. The variation in peak potential with pH for this peak is as follows:

500 $mVsec^{-1}$; pH 2-6, Ep = (1.31 - 0.070 pH) V.

pH 6-8, Ep = 0.88 V.

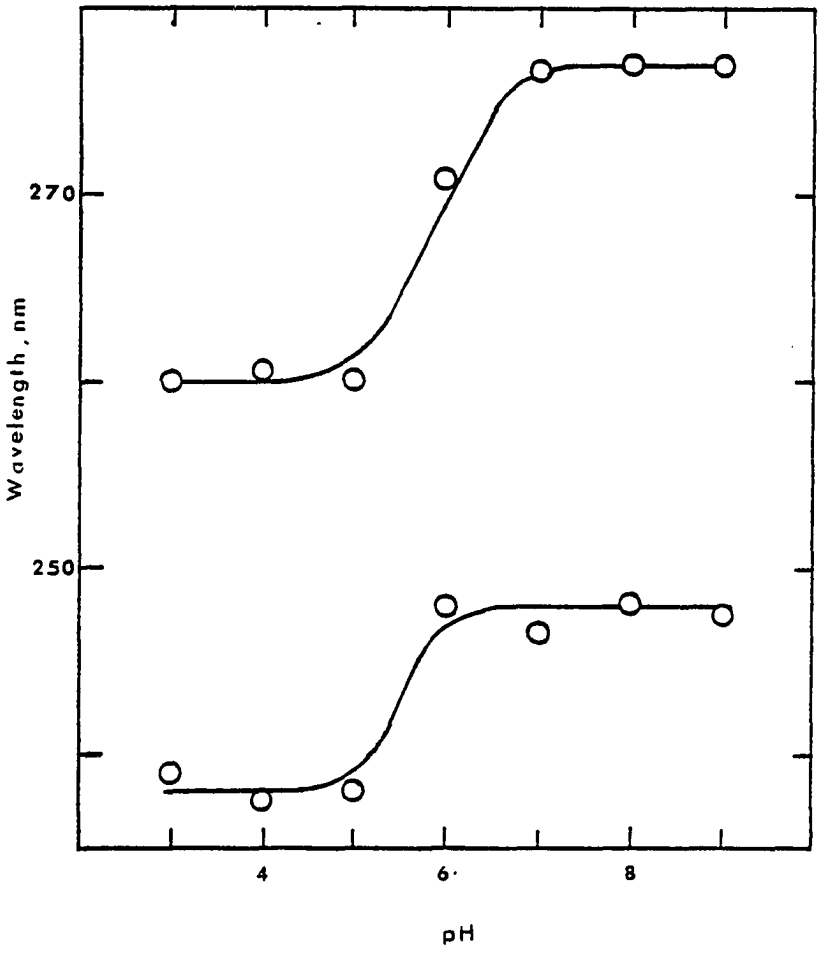

Figure 61. Wavelength versus pH for the two u. v.-absorbing peaks of 1 mM xanthosine.

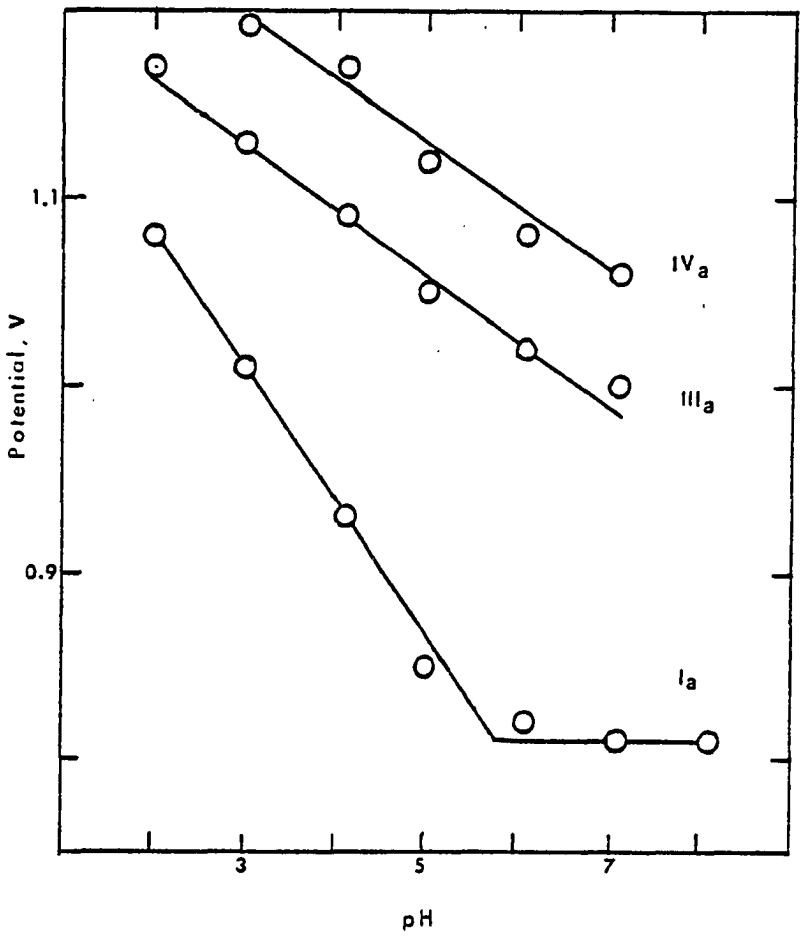

Figure 62. Dependence of Ep on pH for xanthosine peaks Ia, IIIa, and IVa. Solutions ca. 0.5 mM. Scan rate 5 $mVsec^{-1}$.

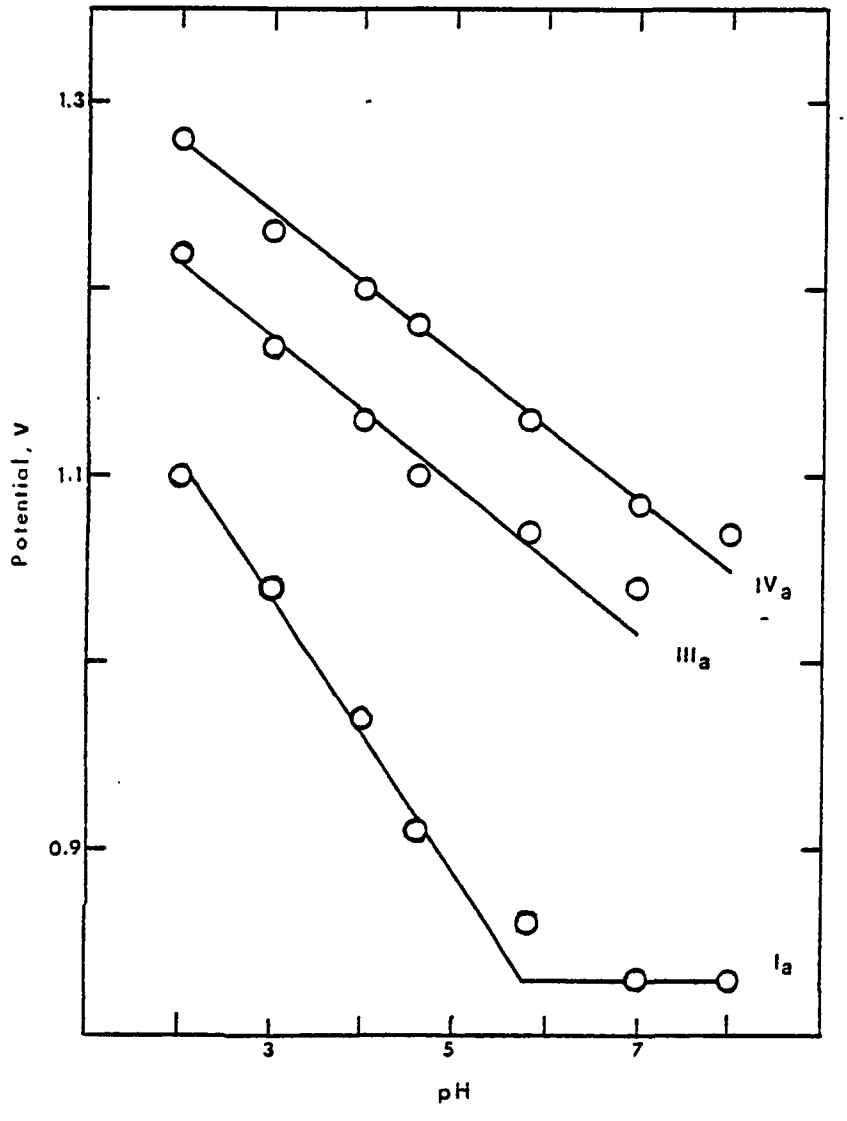

Figure 63. Dependence of Ep on pH for xanthosine peaks Ia, IIIa, and IVa. Solutions ca. 0.5 mM. Scan rate 20 $mVsec^{-1}$.

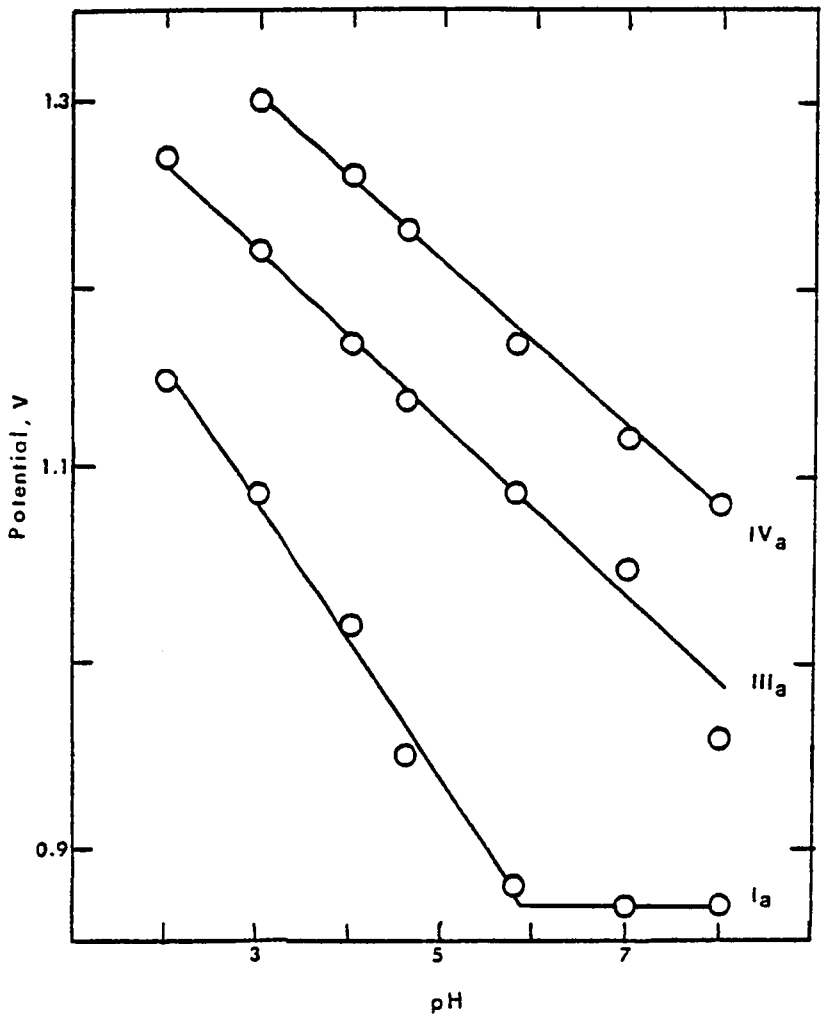

Figure 64. Dependence of Ep on pH for xanthosine peaks Ia, IIIa, and IVa. Solutions ca. 0.5 mM. Scan rate 200 $mVsec^{-1}$.

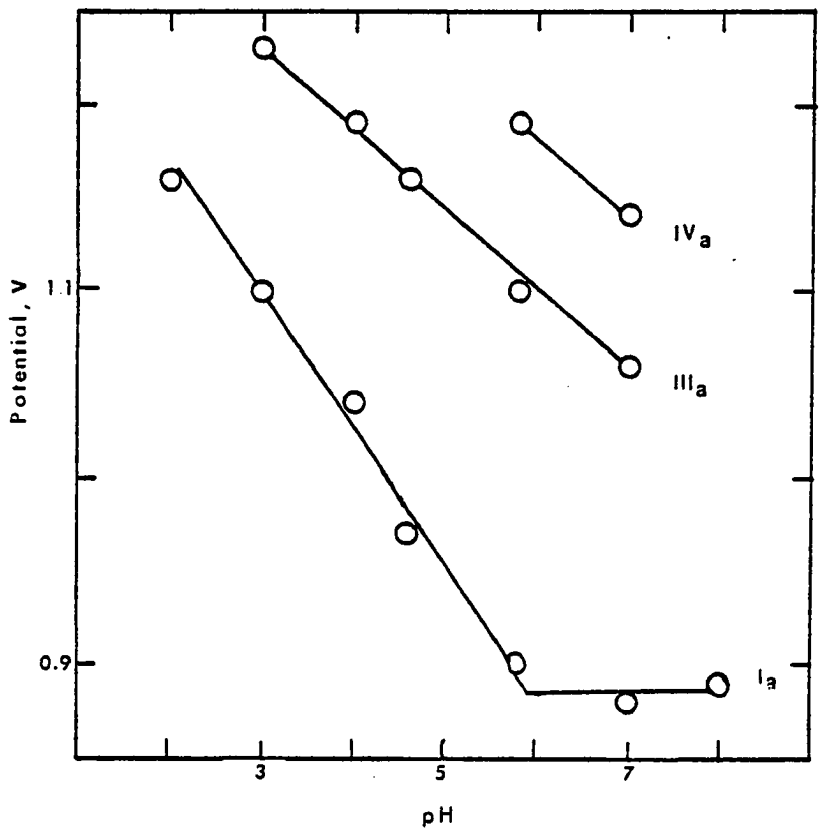

Figure 65. Dependence of Ep on pH for xanthosine peaks Ia, IIIa, and IVa. Solutions ca. 0.5 mM. Scan rate 500 $mVsec^{-1}$.

200 $mVsec^{-1}$; pH 2-6, Ep = (1.30 - 0.073 pH) V.

pH 6-8, Ep = 0.87 V.

20 $mVsec^{-1}$; pH 2-6, Ep = (1.25 - 0.072 pH) V.

pH 6-8, Ep = 0.83 V.

5 $mVsec^{-1}$; pH 2-6, Ep = (1.23 - 0.075 pH) V.

pH 6-8, Ep = 0.82 V.

The second process observed at the 0.5 mM concentration level (peak IIIa) is dependent on pH. Equations for variation of peak potential with pH are as follows:

500 $mVsec^{-1}$; pH 3-7, Ep = (1.36 - 0.044 pH) V.

200 $mVsec^{-1}$; pH 2-8, Ep = (1.37 - 0.042 pH) V.

20 $mVsec^{-1}$; pH 2-7, Ep = (1.28 - 0.036 pH) V.

5 $mVsec^{-1}$; pH 3-7, Ep = (1.22 - 0.032 pH) V.

A third, completely pH dependent electrode process (peak IVa) occurs. At a scan rate of 500 $mVsec^{-1}$, this process is detected only in the pH range 6-7. Its variation in peak potential with pH is as given below:

500 $mVsec^{-1}$; pH 6-7, Ep = (1.43 - 0.042 pH) V.

200 $mVsec^{-1}$; pH 3-8, Ep = (1.43 - 0.043 pH) V.

20 $mVsec^{-1}$; pH 2-8, Ep = (1.34 - 0.036 pH) V.

5 $mVsec^{-1}$; pH 3-7, Ep = (1.31 - 0.036 pH) V.

It is noted that the Ep vs pH equations are very similar for each individual oxidation process at the different scan rates.

Voltammograms of 0.5 mM xanthosine in solutions of phosphate buffer having an ionic strength of 0.5 mM (pH 2, 4, and 7) are reproduced in Figure 66 (scan rate 5 $mVsec^{-1}$) and

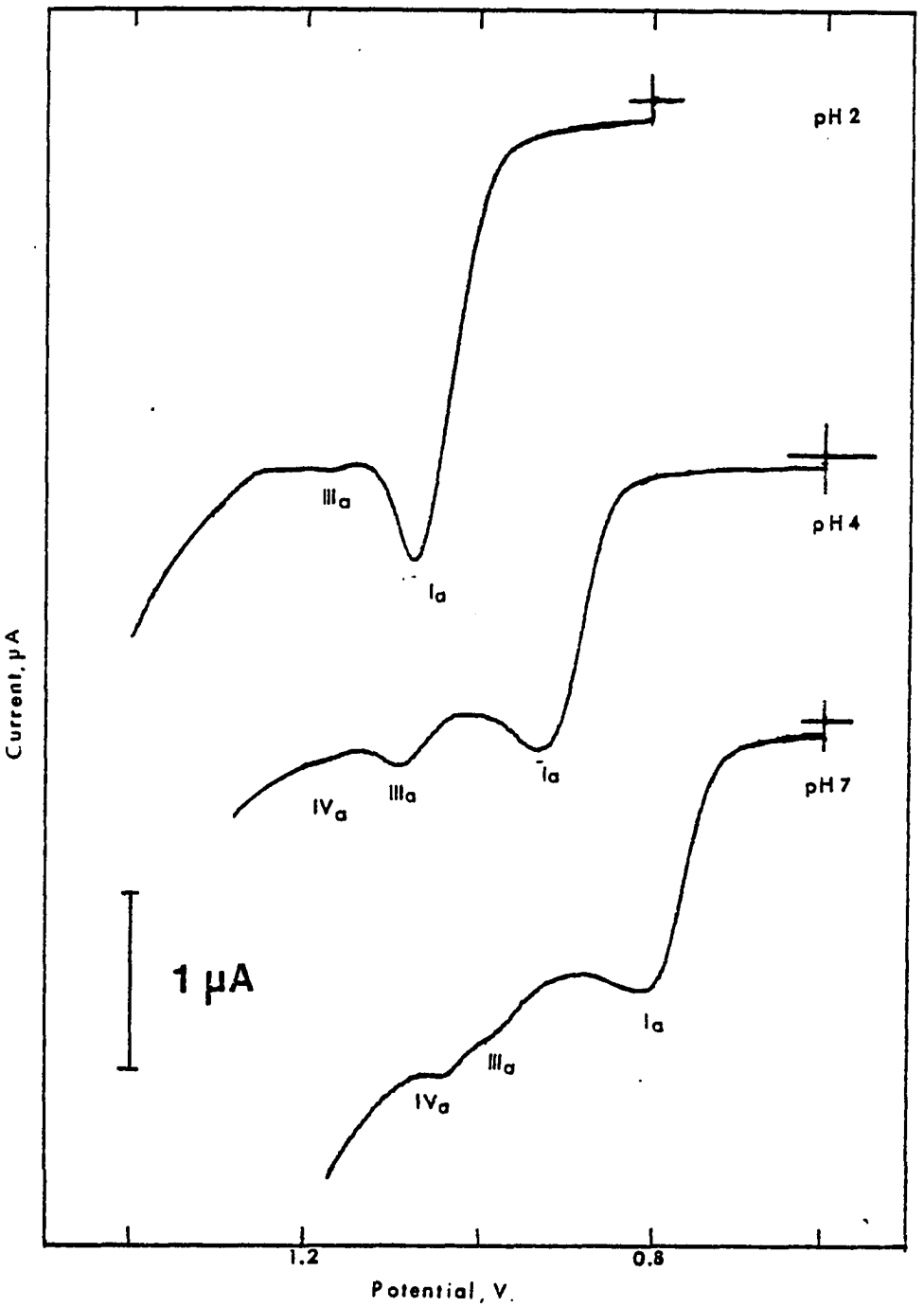

Figure 66. Voltammograms of 0.5 mM xanthosine in various pH solutions at a scan rate of 5 $mVsec^{-1}$.

Figure 67 (scan rate 200 $mVsec^{-1}$). As the scan rate is increased it is observed that the oxidation peaks shift toward more positive potentials at pH values less than 6 (at pH 4 and 5 $mVsec^{-1}$, Ep^{Ia} = 0.93 V., Ep^{IIIa} = 1.09 V., Ep^{IVa} = 1.18 V.; at 200 $mVsec^{-1}$, Ep^{Ia} = 1.03 V., Ep^{IIIa} = 1.18 V., Ep^{IVa} = 1.27 V. Dryhurst[37] noted similar effects in the oxidation of 6-thiopurine at the PGE. Such effects are characteristic of an adsorption peak where the product of the electrochemical reaction is adsorbed[38]. Remembering equation 1 (the theoretical peak voltammogram equation), the peak current function, $i_p/AC\ v^{1/2}$, should remain constant with variation in scan rate and a plot of i_p/C vs C should be linear and parallel to the concentration axis. Experimental peak Ia peak current function values are presented in Table 10.

Studies of the dependence of peak current function for peak Ia upon potential scan rate (Figure 68) showed that at pH 2, 4, and 7 the peak current function was essentially constant at slow sweep rates (5 and 20 $mVsec^{-1}$). However at all three pH values a scan rate of 200 $mVsec^{-1}$ produced an increase in peak current function. The values of peak current function at a scan rate of 500 $mVsec^{-1}$ are slightly higher than those at 200 $mVsec^{-1}$ for all pH values. Such behavior can be indicative of reactant adsorption at the electrode surface[38]. Thus it would appear that both the product (vide supra) and xanthosine adsorb to the electrode

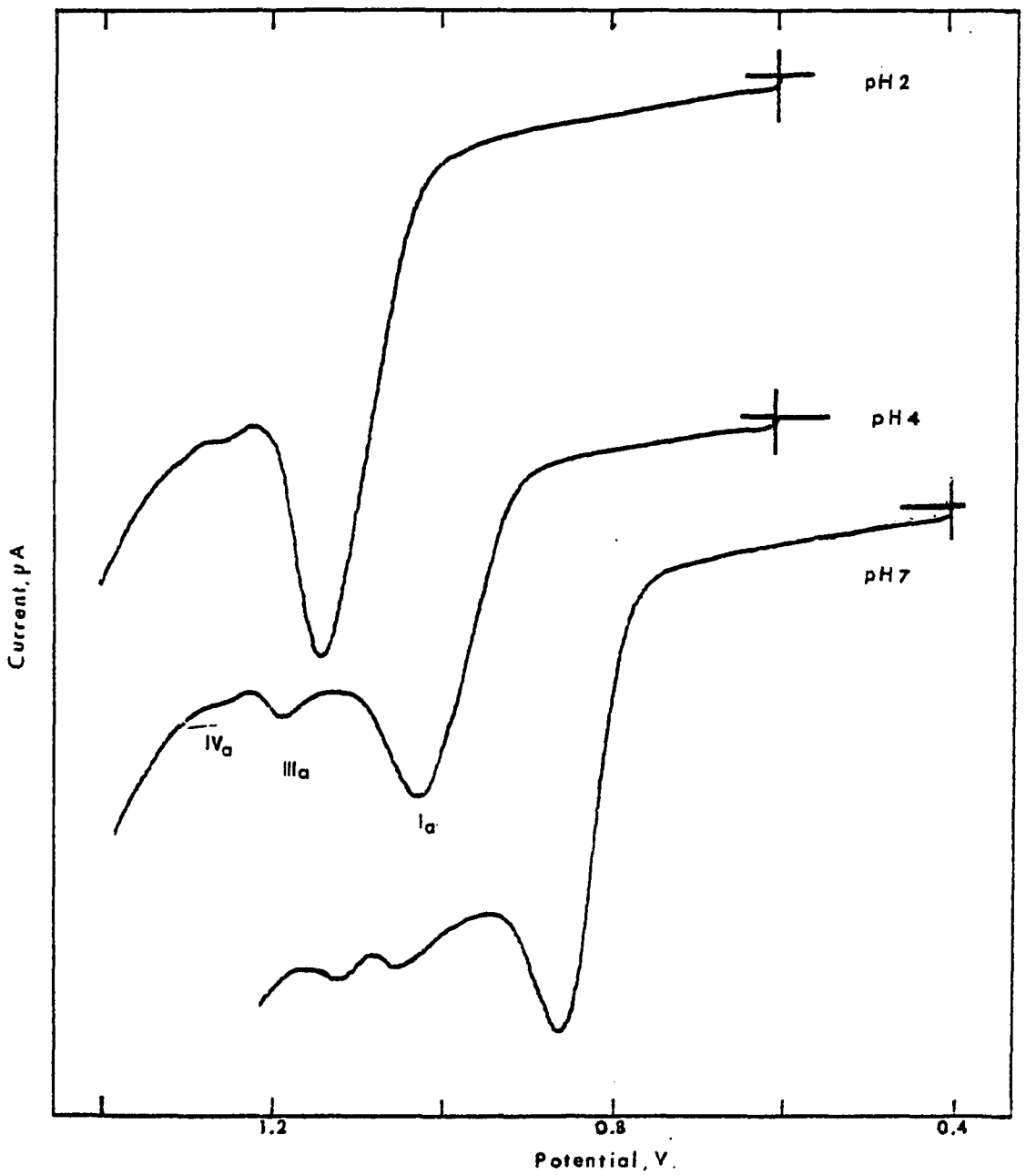

Figure 67. Voltammograms of 0.5 mM xanthosine in various pH solutions at a scan rate of 200 $mVsec^{-1}$.

TABLE 10

Peak current function values for the oxidation of xanthosine at the PGE at peak Ia.

pH	i_p [a]	V	$i_p/AC_v^{1/2}$
2	2.2	0.005	1763
4	1.5	0.005	1202
7	1.4	0.005	1122
2	4.6	0.020	1843
4	3.6	0.020	1442
7	2.8	0.020	1122
2	29	0.200	3674
4	16	0.200	2027
7	13	0.200	1647
2	46	0.500	3686
4	35	0.500	2804
7	24	0.500	1923

a i_p = voltammetric peak current

A = electrode area, cm^2 = 0.0353 cm^2

C = concentration of electroactive species, mM = 0.5 mM

v = voltage sweep rate, $Vsec^{-1}$

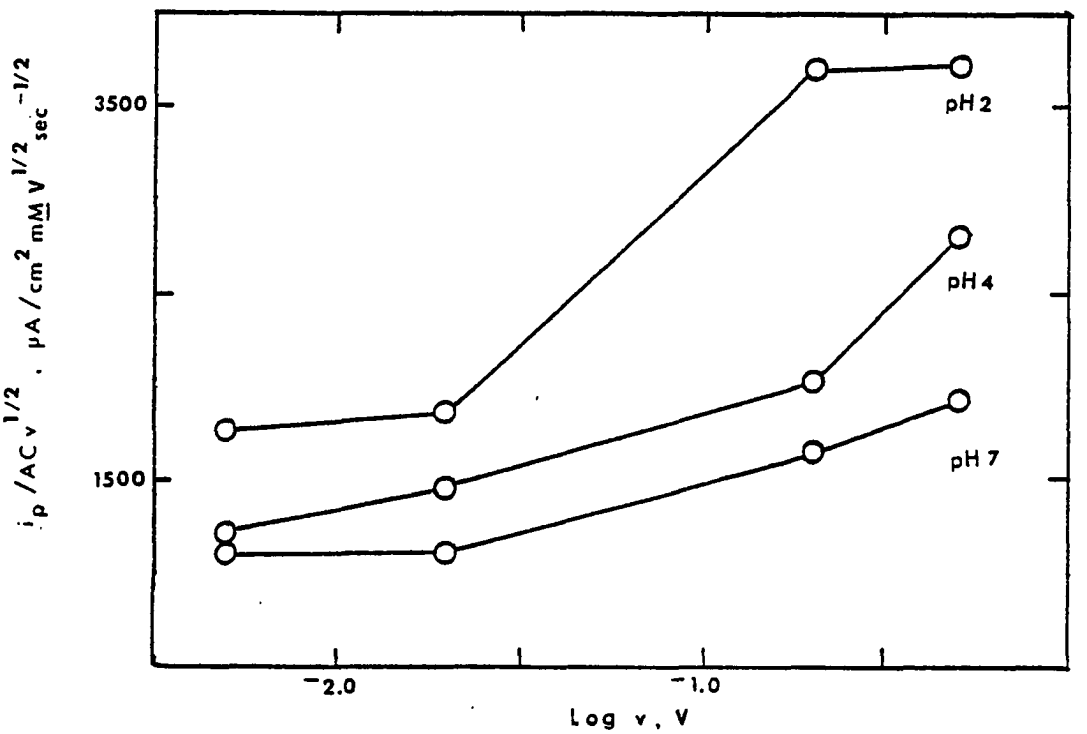

Figure 68. Variation of peak current function for peak Ia with voltage sweep rate at several pH values for 0.5 mM solutions of xanthosine at the PGE.

surface. At pH below 5, peaks IIIa and IVa begin to merge with background discharge making studies of these latter peaks at low pH as a function of voltage sweep rate impossible. However, voltage sweep studies were possible at pH 7. The values of peak current as a function of potential scan rate for peak IIIa and IVa are shown in Table 11.

Studies of the dependence of peak current upon potential sweep rate for peak IIIa of xanthosine showed that at pH 7 $i_p/v^{1/2}$ increased with increasing scan rate. Whereas, for peak IVa the value of $i_p/v^{1/2}$ remained essentially constant. The latter is the behavior expected for a diffusion controlled process. In Figure 69, graphs of $i_p/v^{1/2}$ vs Log v for peaks IIIa and IVa are shown.

At low scan rates (5 and 20 $mVsec^{-1}$) oxidation peak IVa of xanthosine is much more prominent than peak IIIa. However as the scan rate is increased to 200 or 500 $mVsec^{-1}$, peak IIIa becomes larger that peak IVa. Examples of these results are shown in Figure 70. Such behavior, as was explained in chapter 2, Part II, could imply that peak IIIa is an adsorption pre-peak for peak IVa. Another explanation could be that oxidation peak IIIa could be due to further oxidation of an unstable peak Ia product such that it is very small at slow sweep rates and much larger at faster sweep rates.

Using equation 2 (from Part II, chapter 2) the experimental value of αn_a for peak Ia was determined between pH 2

TABLE 11

Peak current values for the oxidation of xanthosine at the PGE for the peaks IIIa and IVa at pH 7.

v	i_p	$i_p/v^{1/2}$
Peak IIIa		
0.005	0.6	9.1
0.020	1.4	9.9
0.200	6.4	14.3
0.500	12	17.0
Peak IVa		
0.005	0.9	12.7
0.020	1.7	12.0
0.200	6.1	13.6
0.500	9.2	13.0

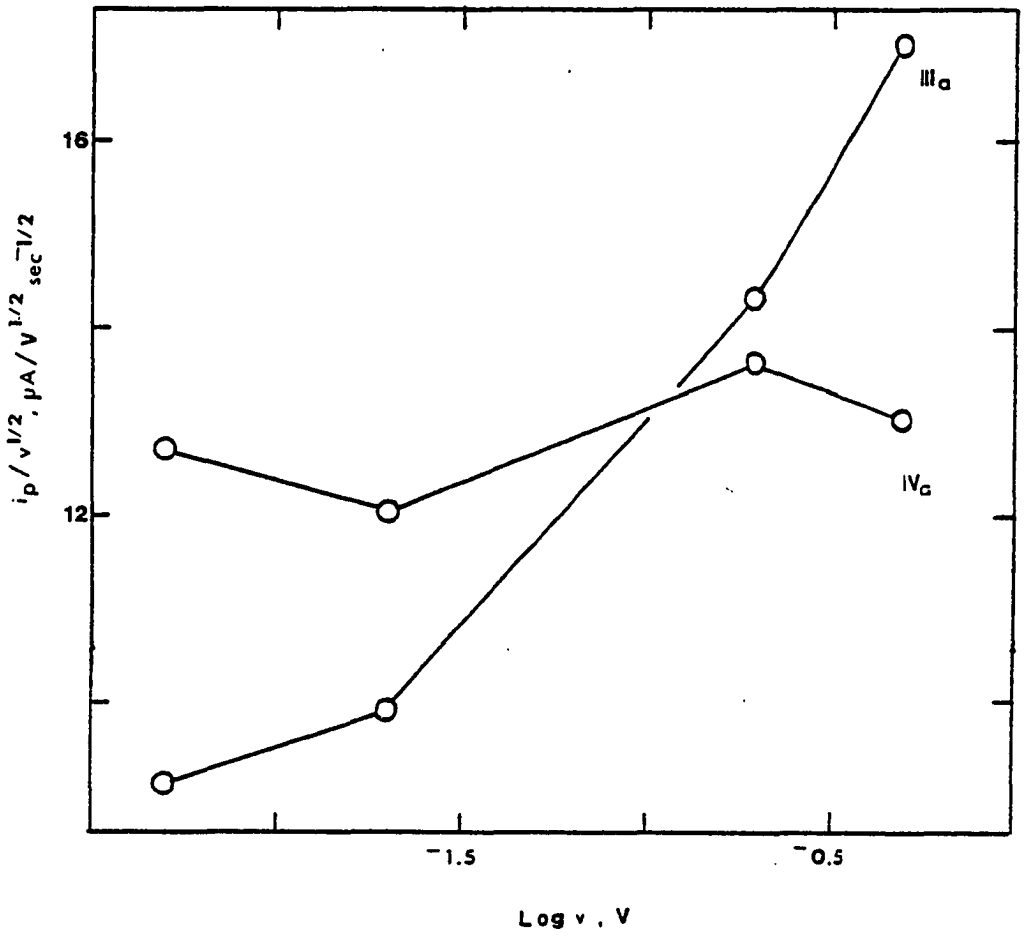

Figure 69. Variation of peak current for peaks IIIa and IVa with voltage sweep rate at pH 7 for 0.5 mM solutions of xanthosine at the PGE.

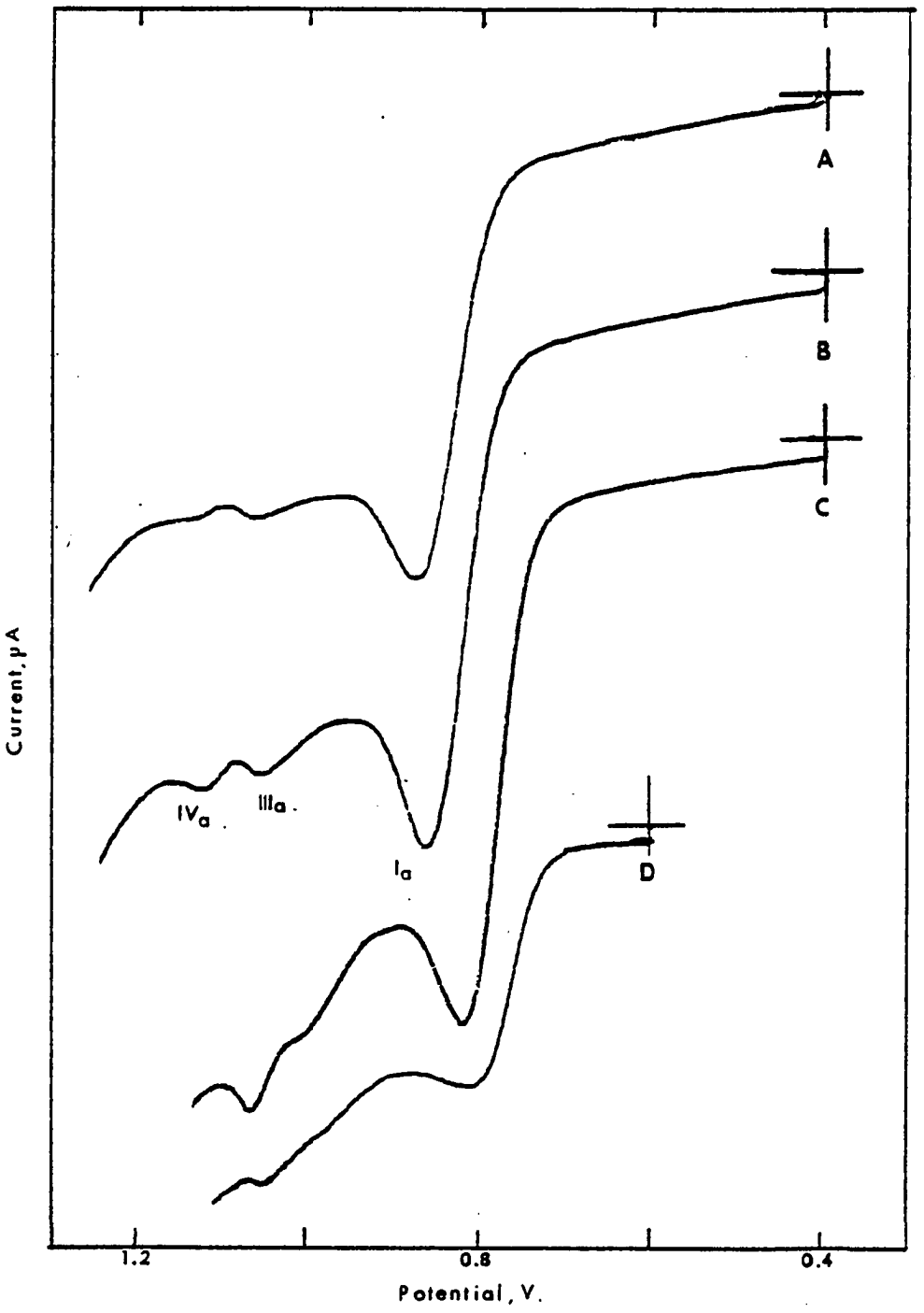

Figure 70. Voltammograms of 0.5 mM xanthosine in pH 7 phosphate buffer at (A) 500 $mVsec^{-1}$, 10 μAin^{-1}; (B) 200 $mVsec^{-1}$, 5 μAin^{-1}; (C) 20 $mVsec^{-1}$, 1 μAin^{-1}; (D) 5 $mVsec^{-1}$, 1 μAin^{-1}.

and 8 at 0.02 $Vsec^{-1}$ (Table 12). Using the appropriate value of αn_a and a diffusion coefficient for xanthosine of 9.5 x 10^{-6} cm^2s^{-1} (a value obtained from the experimental diffusion coefficient of adenosine[72], a molecule of similar size), application of equation 1 (Chapter 2) for a totally irreversible uncomplicated process will allow the determination of n (the total number of electrons involved in the voltammetric reaction). The peak Ia process is clearly not an uncomplicated one due to adsorption phenomena (vide supra) and several follow-up reactions (vide infra). At a sweep rate of 0.02 $Vsec^{-1}$ and a concentration of 0.5 mM the experimental n-value is 2.1, 1.6, and 1.3 at pH 2, 4, and 7 respectively. Although still noticable, enhancement of the peak current by adsorption is less at higher values of pH (Figure 68). Thus it was concluded the peak Ia process involves between 1-2 electrons per molecule of xanthosine under voltammetric conditions.

Figure 71 shows the dependency of peak current on concentration at pH 7 for oxidation peaks Ia, IIa, IIIa, and IVa of xanthosine. At a concentration of 0.1 mM and a scan rate of 5 $mVsec^{-1}$ only peaks Ia and IVa are present. At 1.0 mM peak IIa appears and peak Ia becomes less prominent. At a concentration of 5 mM, peak IIa is the most prominent with IVa still visible and Ia almost undetectable. Peak IIIa is no longer present. The peak current of all four oxidation peaks at pH 4 is also dependent on concentration (Figure 72). Only peaks Ia and IVa are visible at a concentration of 0.1 mM.

TABLE 12

Experimental values of αn_a for peak Ia of xanthosine.

pH	$Ep - Ep_{/2}$	αn_a
2	0.053	0.906
3	0.056	0.857
4	0.051	0.941
5	0.050	0.960
6	0.051	0.941
7	0.045	1.07
8	0.046	1.04

Scan rate = 0.02 $Vsec^{-1}$

Concentration = 0.5 mM

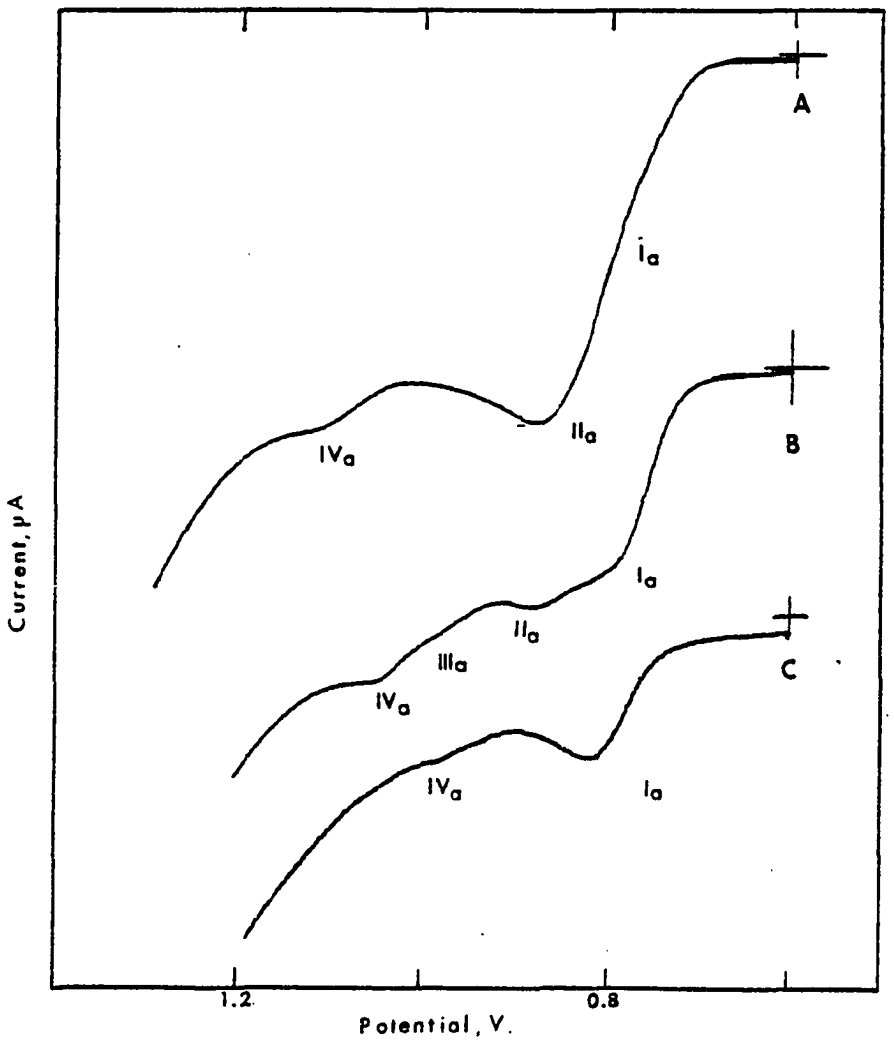

Figure 71. Voltammograms of xanthosine in pH 7 phosphate buffer at (A) 5 m<u>M</u>, 5 $\mu A in^{-1}$; (B) 1.0 m<u>M</u>, 2 $\mu A in^{-1}$; (C) 0.1 m<u>M</u>, 1 $\mu A in^{-1}$. Scan rate 5 $mV sec^{-1}$.

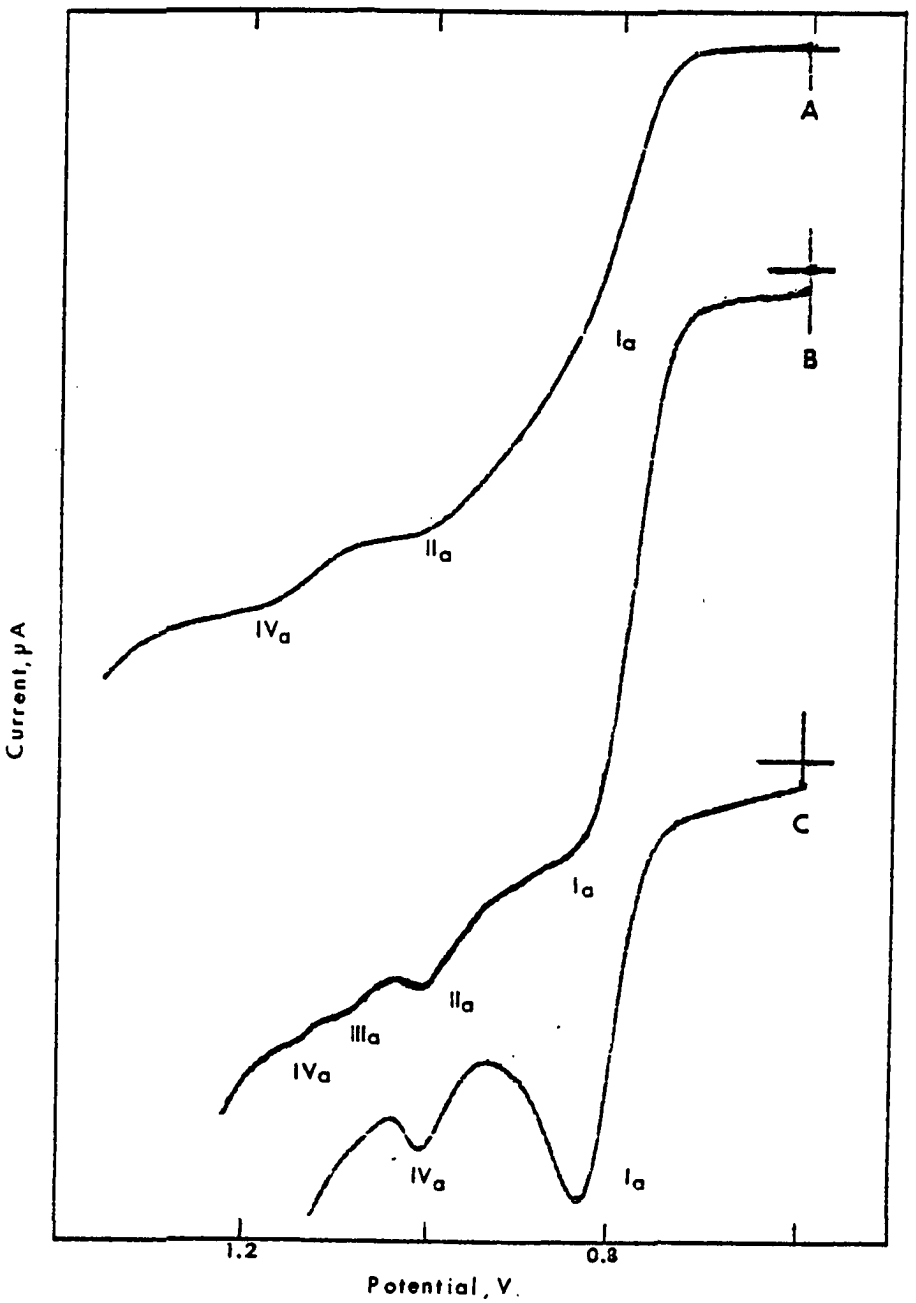

Figure 72. Voltammograms of xanthosine in pH 4 phosphate buffer at (A) 5 m<u>M</u>, 5 $\mu A in^{-1}$; (B) 1.0 m<u>M</u>, 1 $\mu A in^{-1}$; (C) 0.1 m<u>M</u>, 0.5 $\mu A in^{-1}$. Scan rate 5 $mV sec^{-1}$.

At 1.0 mM peak IIa appears and the three other peaks are visible. Peak IIa is the most prominent at a concentration of 5.0 mM and IVa is still visible. However, peak IIIa is no longer present and Ia is almost undetectable. The behavior at pH 7 parallels that at pH 4 quite well. The involvement of adsorption was confirmed by studies of the dependence of peak current upon concentration. It can be seen from Figure 73 that peak Ia of xanthosine exhibits behavior characteristic of adsorption processes. Adsorption at peaks IIa and IVa is apparently less extensive. The plots of i_p/C vs C for these two peaks are essentially parallel to the concentration axis over the range 2.5-10.0 mM. Also, for peak IVa the peak current changes only slightly with scan rate (Figure 69).

Cyclic voltammetry of 0.5 mM xanthosine at pH 7, shown in Figure 74, is similar to that observed for 9-methylxanthine (Figure 20). Xanthosine shows a much more prominent peak Ic. However, xanthosine shows no peak IIa and a barely detectable peak IIc. This behavior might imply that the diimine formed upon electrooxidation of xanthosine is more stable than its 9-methylxanthine counterpart. Switching potential studies of xanthosine (Figure 75) reveal that the Ic-Va couple is more distinct after sweeping into the peak IIIa or IVa region. When the potential is reversed in the vicinity of peak Ia several small peaks become noticable. These small peaks have been shown to be the reduction or oxidation of decomposition products from the peak IIa process

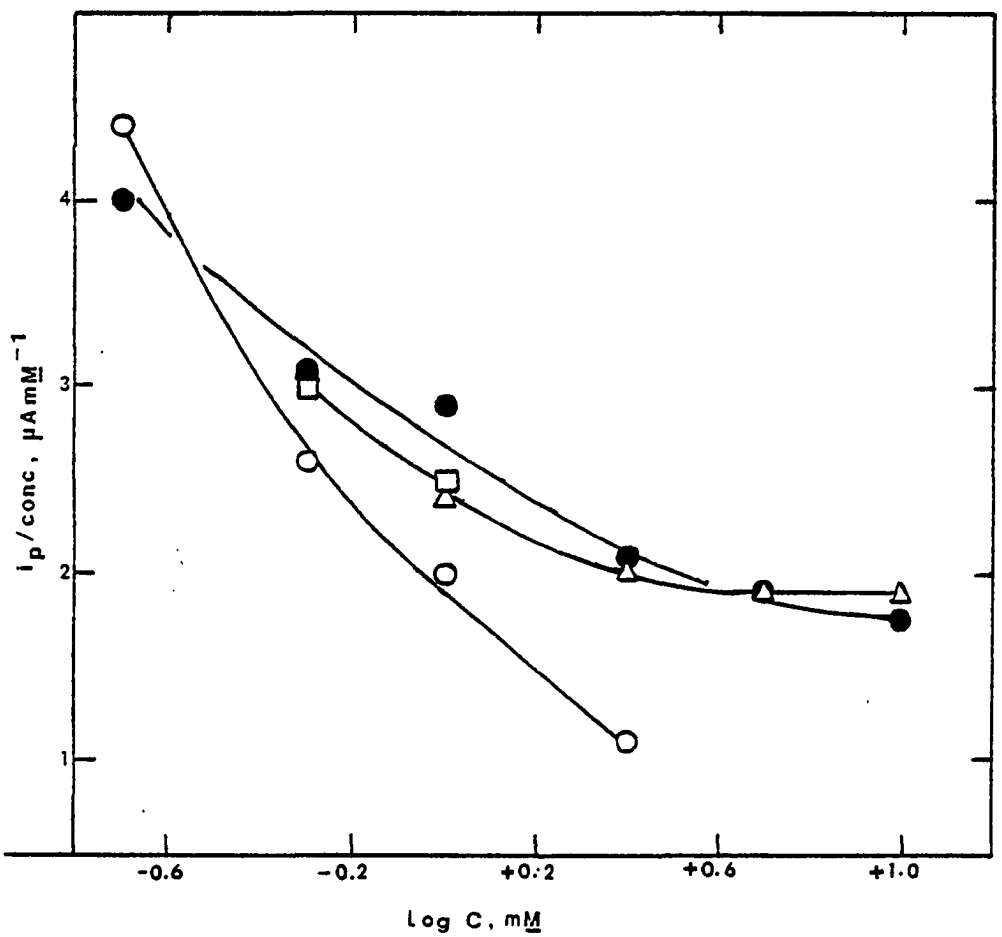

Figure 73. Variation of i_p/C with concentration for xanthosine. Peak Ia (O—O), peak IIa (Δ—Δ), peak IIIa (□—□), and peak IVa (●—●). Scan rate 5 mVsec^{-1}.

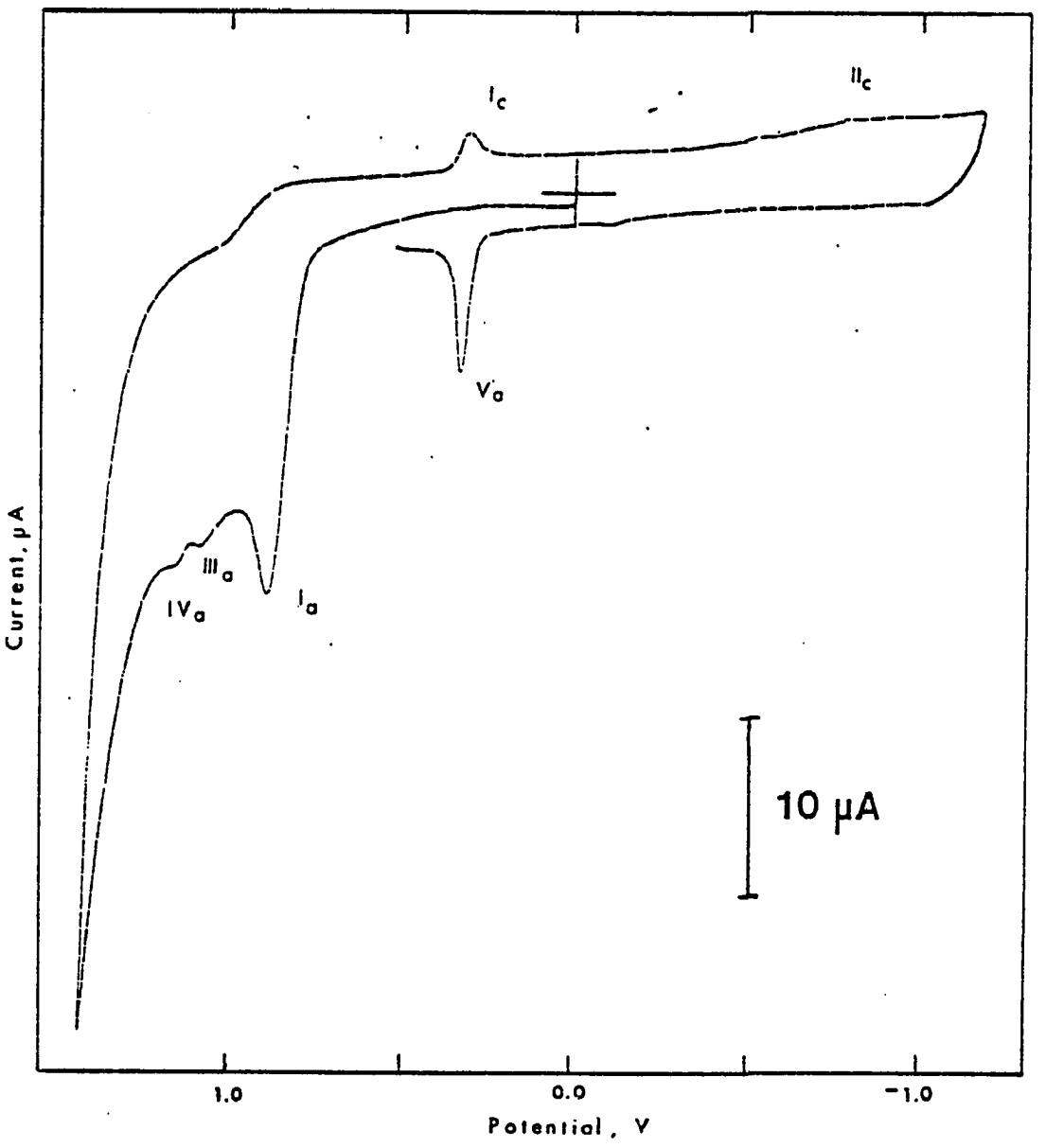

Figure 74. Cyclic voltammogram of 0.5 m<u>M</u> xanthosine at pH 7 in phosphate buffer. Scan rate 200 $mVsec^{-1}$.

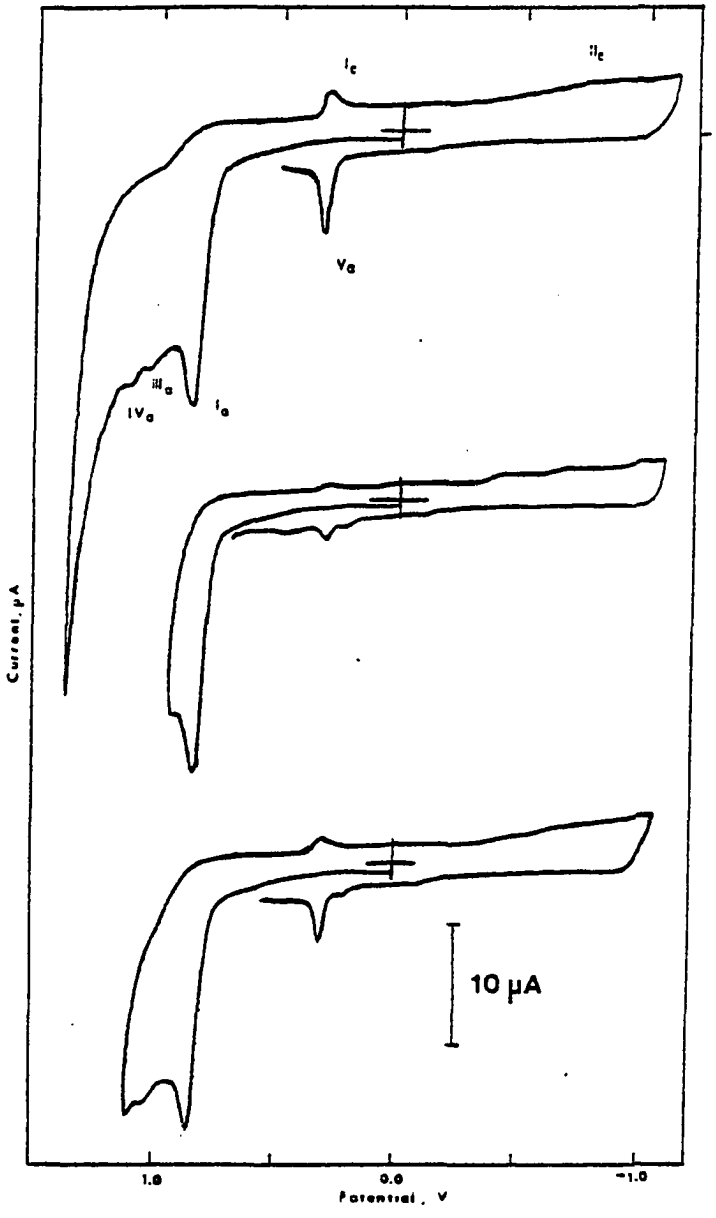

Figure 75. Switching potential study on the cyclic voltammetry of 0.5 mM xanthosine at pH 7 in phosphate buffer. Scan rate 200 $mVsec^{-1}$.

(vide infra). The peak potentials of peak IIc and the Ic-Va system obtained in the voltammetry of xanthosine are similar to those observed in the voltammetry of uric acid, xanthine, 9-methyluric acid, and 9-methylxanthine. The nature of those voltammetric peaks will be discussed later.

Cyclic voltammetry of xanthosine at varying concentrations (0.1 mM - 20 mM) was performed in pH 7 buffer. As the concentration was raised above 2 mM peak IIa became the most prominent peak (example, 3 mM, Figure 76).

Cyclic voltammetry of xanthosine below its pK_a of approximately 5.7 was very similar to that observed at pH 7. This is shown in Figure 77. The major differences between the 0.5 mM voltammograms are the near absence of peaks Ic and IIc and the enhanced peak height of oxidation peak IIIa at pH 4. Switching potential studies at pH 4 revealed other similarities with behavior observed at pH 7 (Figure 78). When sweeping into the peak IIIa, IVa region, the peaks Va and IIc are more significant. Also the small peaks due to decomposition product electrochemistry are noticed when the potential is reversed in the vicinity of peak Ia (vide infra).

Again at pH 4, the peak potential observed for peak Va in the voltammetry of xanthosine agrees well with those observed in the voltammetry of uric acid, xanthine, 9-methyluric acid, and 9-methylxanthine at similar pH.

Controlled potential coulometry

Controlled potential coulometry of xanthosine varied

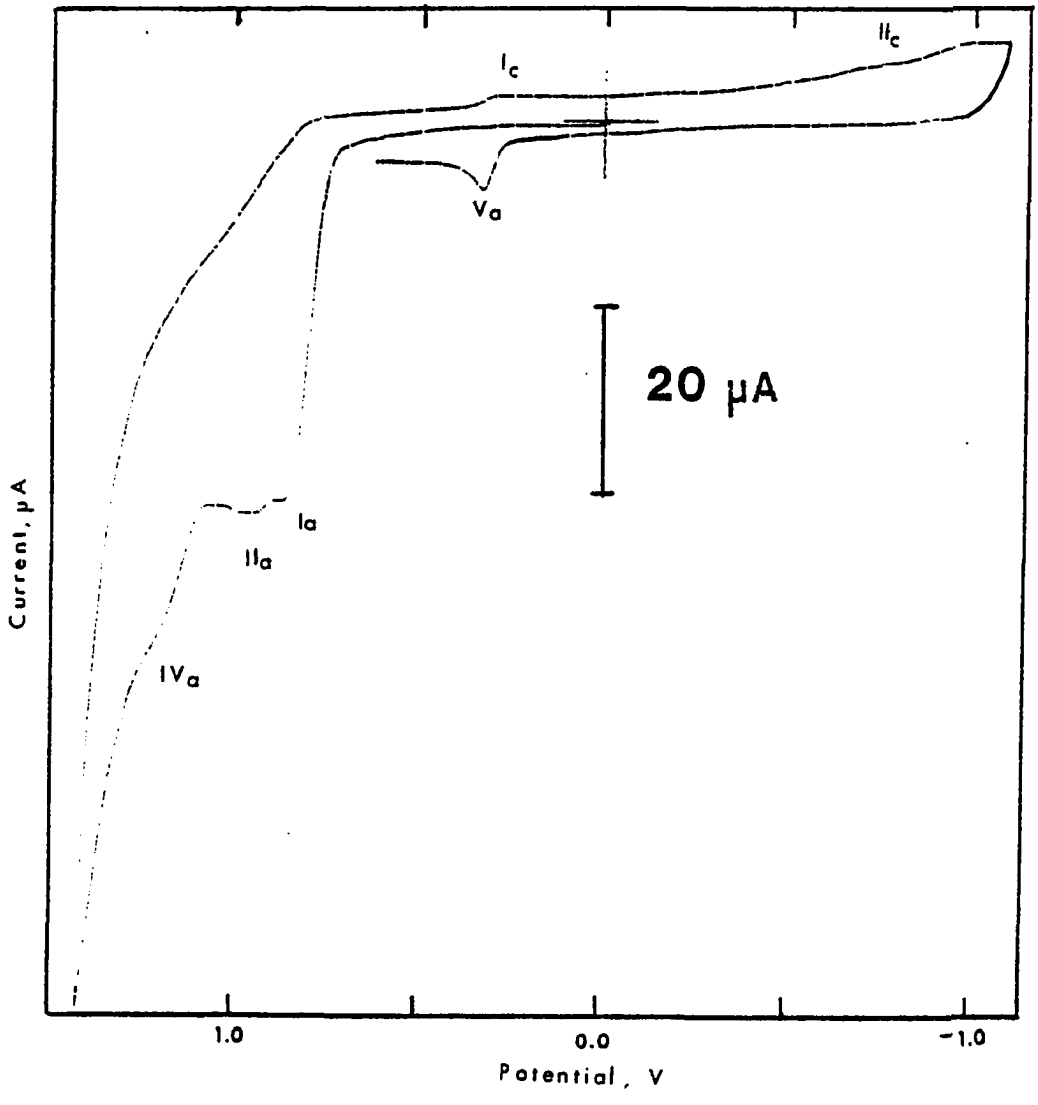

Figure 76. Cyclic voltammogram of 3 mM xanthosine at pH 7 in phosphate buffer. Scan rate 200 $mVsec^{-1}$.

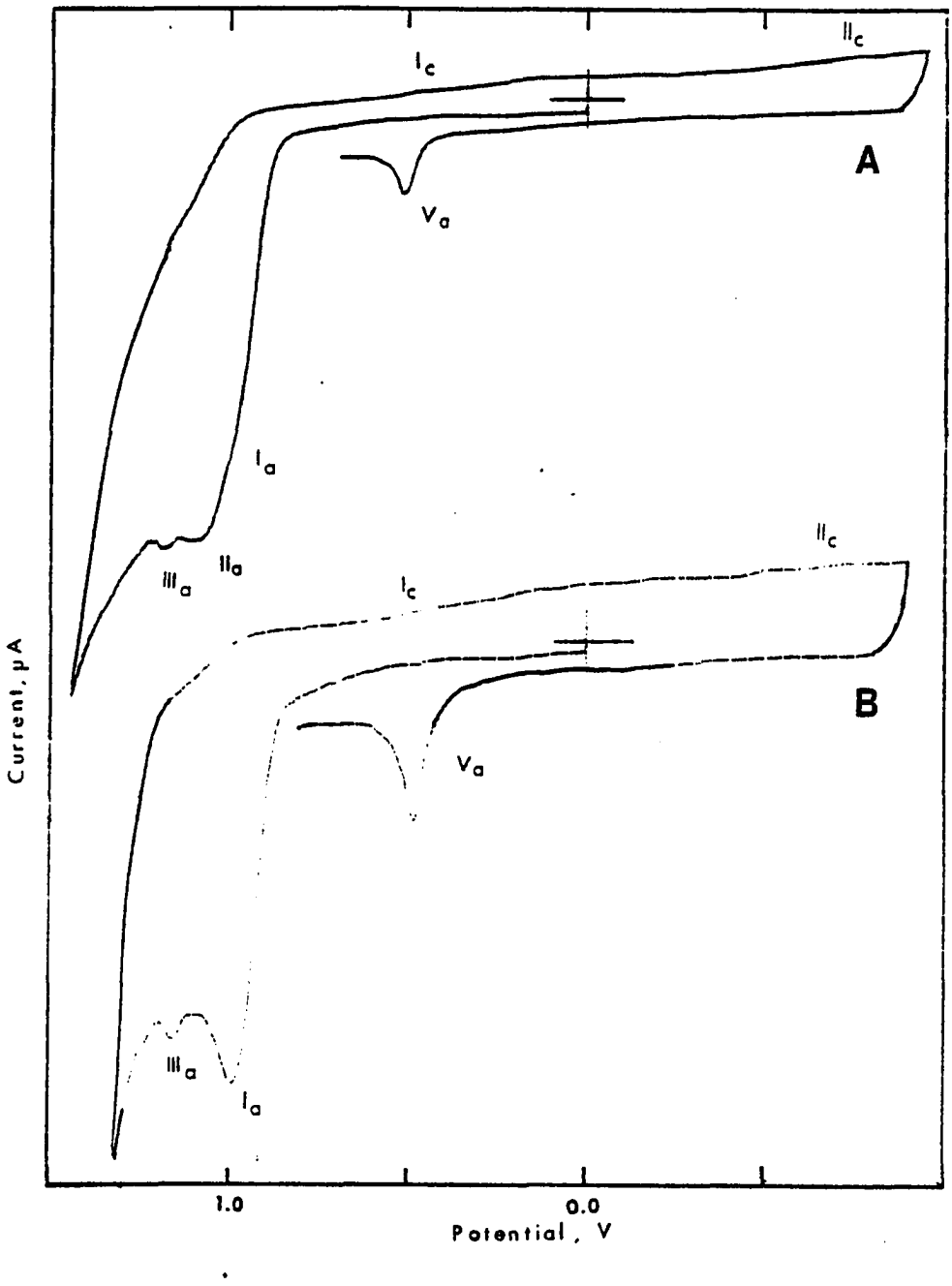

Figure 77. Cyclic voltammograms of xanthosine at pH 4 in phosphate buffer at (A) 3 m<u>M</u>, 20 $\mu A in^{-1}$; (B) 0.5 m<u>M</u>, 10 $\mu A in^{-1}$. Scan rate 200 $mV sec^{-1}$.

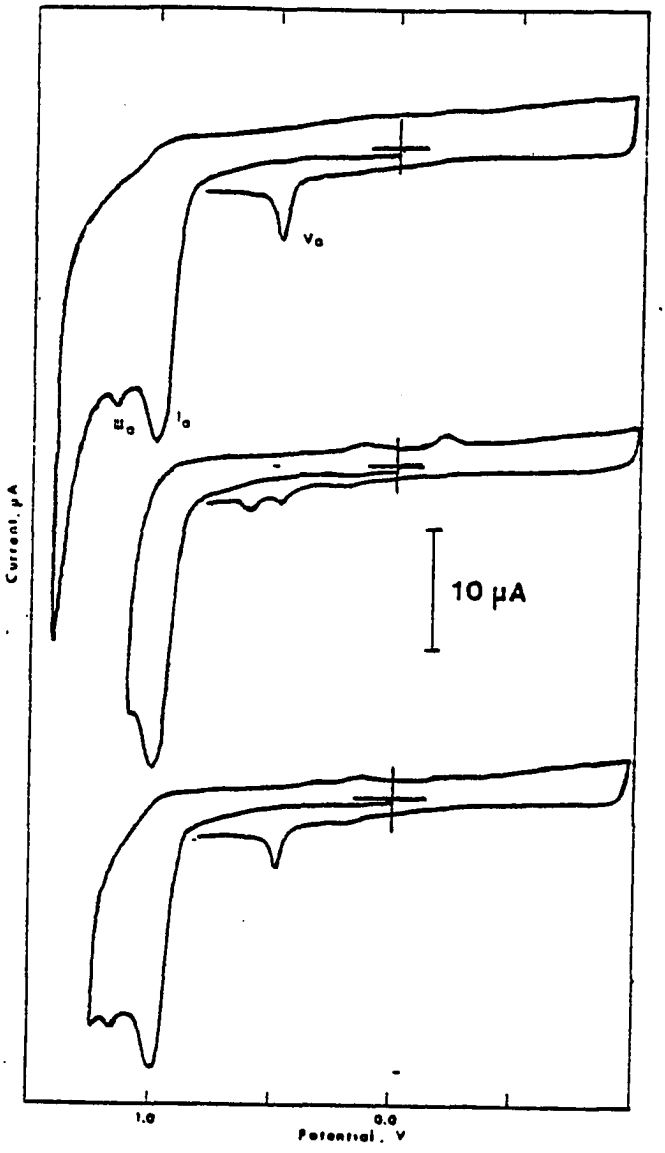

Figure 78. Switching potential study on the cyclic voltammetry of 0.5 m<u>M</u> xanthosine at pH 4 in phosphate buffer. Scan rate 200 $mVsec^{-1}$.

with pH, potential, and concentration (Table 13). At potentials corresponding to peaks IIIa and IVa, coulometry of xanthosine yielded a faradaic n-value approaching about four at concentrations less than about 1 mM and at pH values greater than the pK_a of 5.7. The n-value fell to as low as 3.0 in higher concentration solutions of similar pH. With the applied potential in the vicinity of peaks Ia and IIa for xanthosine, the observed faradaic n-value range from ca. 2.8-3.1 at low concentration to approximately 2.4-2.7 at high concentration. At pH values below the pK_a of 5.7, the variation in the faradaic n-value is not as pronounced with changes in potential and concentration, ranging from 3.2-3.7. Throughout this study it was found that the experimental n-values were quite variable from run to run.

The phenomenon observed during controlled potential electrolysis of 9-methylxanthine at pH 7, the formation of a yellow species, was also observed in the case of xanthosine. At potentials of 1.0 V (peak IIa) and higher and at concentrations below approximately 0.5 mM the yellow color appeared within 25 minutes. The intensity of this color reached its maximum in about one hour, gradually faded, and disappeared completely within four hours. With xanthosine concentrations greater than 0.5 mM, the intensity of the yellow color was greater when it reached its maximum and did not fade completely when voltammetry indicated that all the xanthosine had been oxidized.

TABLE 13

Coulometric[a] n-values for the electrochemical oxidation of xanthosine at the PGE.

pH[b]	Initial Concentration, mM	Controlled Potential V vs SCE	n-value[c]
4	3.0	1.0 (peaks Ia/IIa)	3.2
4	3.0	1.4 (peak IVa)	3.4
4	0.5	1.0	3.7
4	0.5	1.4	3.7
4	0.1	1.0	3.6
4	0.1	1.4	3.7
7	3.0	0.9 (peaks Ia/IIa)	2.7*
7	3.0	1.3 (peak IVa)	3.3**
7	0.5	0.9	2.9**
7	0.5	1.3	3.7
7	0.1	0.9	3.1
7	0.1	1.3	3.9
9	3.0	0.9 (peaks Ia/IIa)	2.4*
9	3.0	1.3 (peak IVa)	3.0**
9	0.5	0.9	2.7**
9	0.5	1.3	3.5
9	0.1	0.9	2.8
9	0.1	1.3	3.7

a Electrolyses continued until voltammetry and u. v. spectrum of initial xanthosine gone

b All buffers made using mixed NaH_2PO_4 and Na_2HPO_4 .

c Each n-value is the average of at least three experiments

** slight yellow solution after electrolysis

* yellow solution after electrolysis

When the applied potential corresponded to values negative of the peak potential for peak Ia (0.82 V) at pH 7 of xanthosine the appearance of the yellow color was also observed. At these potentials and with a concentration of 3 mM a coincidence of the maximum in intensity of the yellow solution and the disappearance of peak IIa was observed.

During the course of these experiments, cyclic voltammetry was periodically run on the electrolysis solutions. Oxidation of xanthosine most notably at potentials in the vicinity of peaks Ia and IIa (ca. 0.8-1.0 V) revealed that peak IIa grew significantly (Figure 79) during the initial phase of the electrolysis. Peak IIa continued to grow while the peaks IIIa, IVa, Va, and Ic diminished as the electrolysis progressed. This behavior would imply that the peak IIa process was a further oxidation of a peak Ia product. Also it would appear from these data that peaks IIIa and IVa represent oxidation of the initially present xanthosine and not of a peak Ia product.

Similar behavior was not observed at low pH. All oxidation peaks disappeared uniformly as the electrolysis proceeded at pH values below the pK_a (5.7).

A similar mechanism to that proposed for 9-methylxanthine can be used to explain the observed concentration dependency of the coulometric data for xanthosine. That is, following the initial electrode oxidation at peak Ia two different mechanistic pathways are possible depending on the concentra-

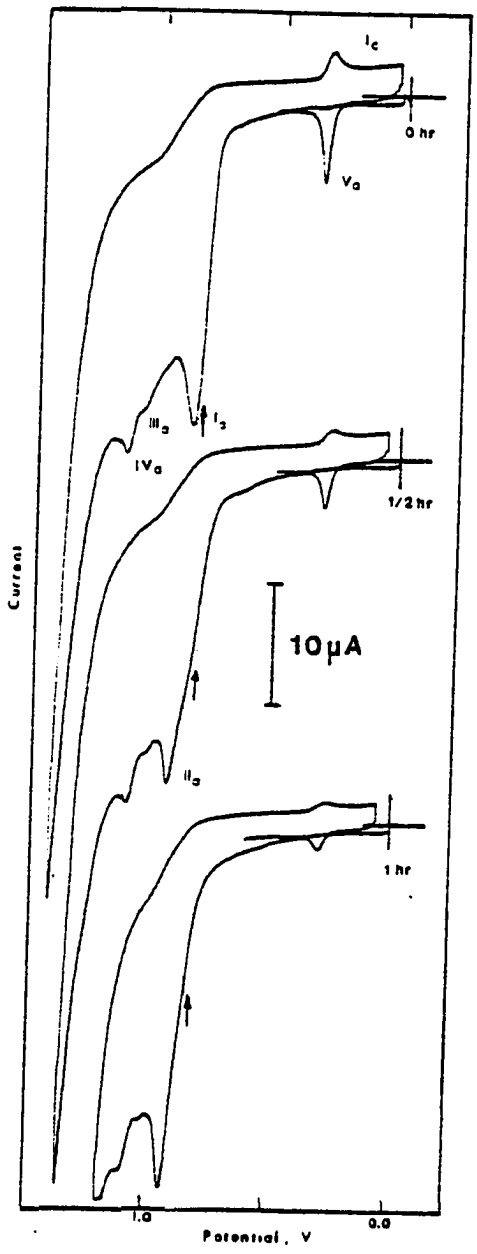

Figure 79. Cyclic voltammograms at various stages during electrolysis of 1 mM xanthosine at pH 7. Arrow at applied potential (0.83 V.). Scan rate 200 $mVsec^{-1}$.

tion of xanthosine. At high concentrations of xanthosine the primary electrochemical oxidation product dimerizes to form an electrochemically inactive species (inactive at peak Ia potentials). Whereas at low concentrations, the primary oxidation product undergoes a second electrochemical oxidation at peak Ia potentials. There would be a combination of these two mechanisms at intermediate concentrations. Such mechanisms could explain the fact that lower n-values are obtained with higher initial concentrations of xanthosine. It would appear the dimerization pathway is apparently negligible at pH 4.

Potentiostatic Studies

Potentiostatic current-time curves were obtained at pH 4 and 7 to clarify the nature of the peaks Ia, IIa, and IVa processes. At the high concentrations required to obtain good cuurent-time curves, oxidation peak IIIa was not present. The values of n determined by potentiostatic methods were found to be concentration dependent. Typical curves used for obtaining n-values via potentiostatic studies are shown in Figure 80 (pH 4, 3 mM) and Figure 81 (pH 7, 3 mM).

Potentiostatically determined n-values (Table 14) parallel those obtained by coulometry (Table 13) in that there is a general increase in the n-value as the potential is also increased. However, all potentiostatic n-values are lower than their coulometric counterparts at similar potentials and concentrations. The reason for this behavior may be due to the time difference required to complete each experiment.

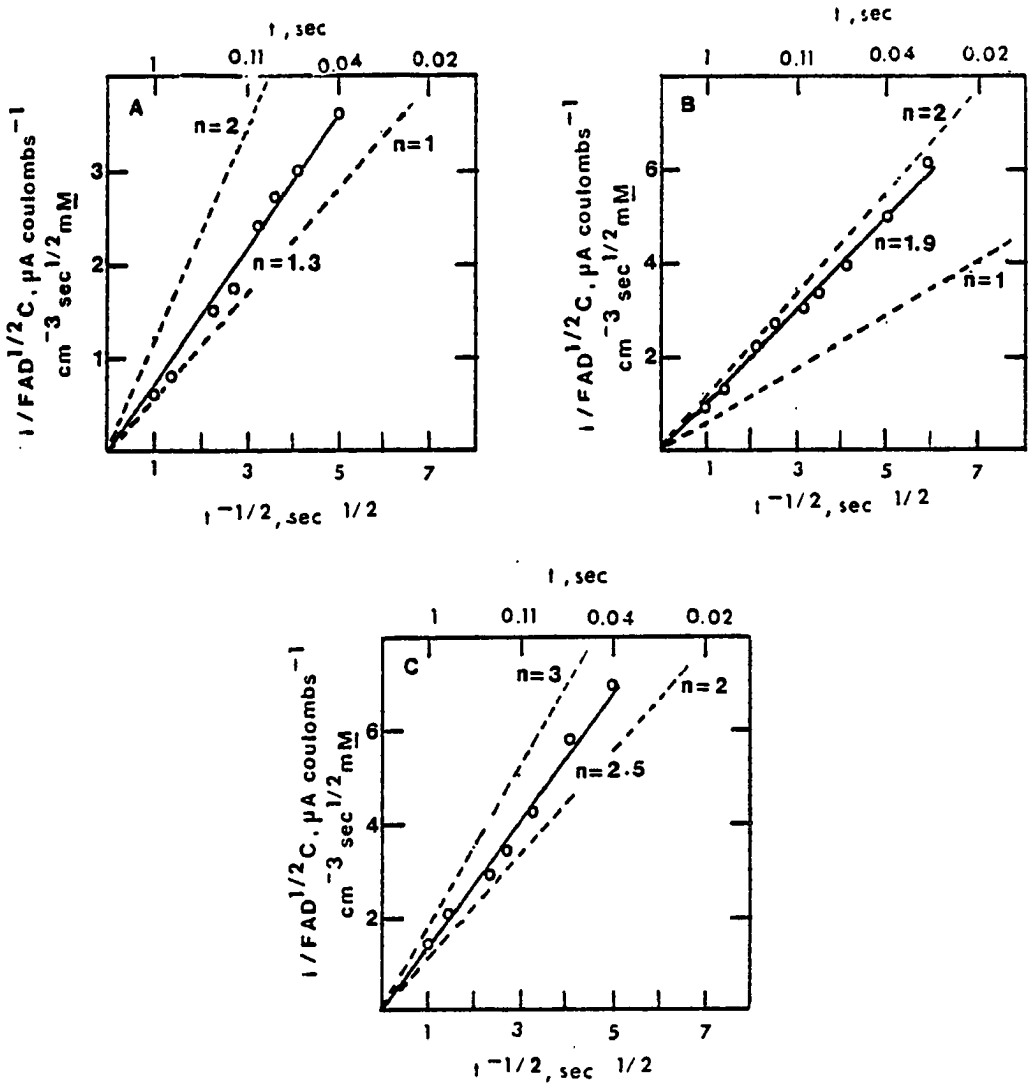

Figure 80. Comparison of experimental with the theoretical normalized current-time curves for the electrochemical oxidation of xanthosine at pH 4; (A) at 1.05 V , peak Ia, (B) at 1.25 V , peak IIa and (C) at 1.50 V , peak IVa. Circles represent experimental values. Dotted lines represent theoretical curves calculated from the Cottrell equation.

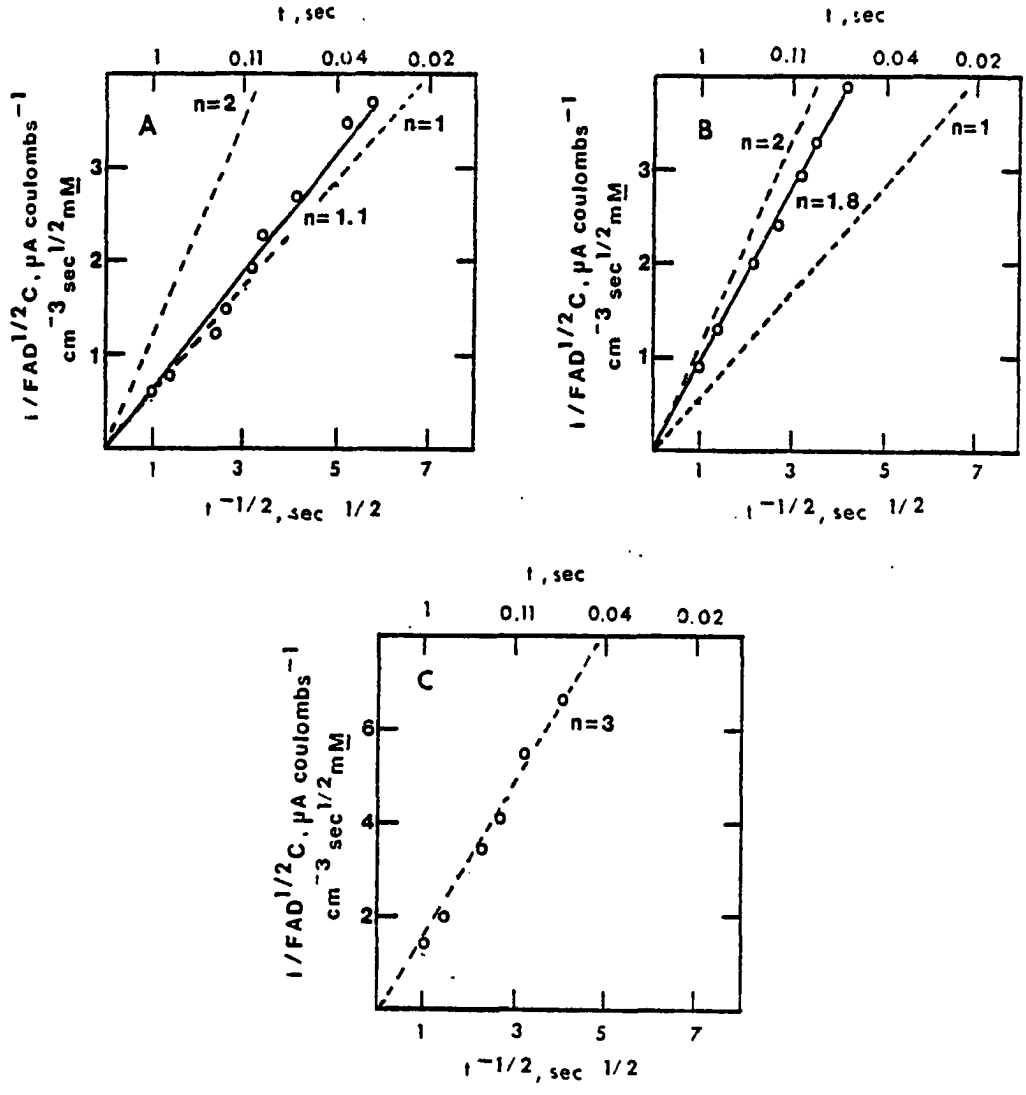

Figure 81. Comparison of experimental with the theoretical normalized current-time curves for the electrochemical oxidation of xanthosine at pH 7; (A) at 0.85 V , peak Ia, (B) at 1.00 V , peak IIa, (C) at 1.30 V , peak IVa. Circles represent experimental values. Dotted lines represent theoretical curves calculated from the Cottrell equation.

TABLE 14

Potentiostatic n-values for the electrochemical oxidation of xanthosine

pH	Initial Concentration, mM	Applied Potential, V vs SCE	n-value
4	3.0	1.00 (Peak Ia)	1.3
4	3.0	1.15 (Peak IIa)	1.9
4	3.0	1.50 (Peak IVa)	2.5
4	10.0	1.00	0.8
4	10.0	1.15	1.4
4	10.0	1.50	1.8
7	3.0	0.85 (Peak Ia)	1.1
7	3.0	1.00 (Peak IIa)	1.8
7	3.0	1.30 (Peak IVa)	3.0
7	10.0	0.85	0.7
7	10.0	1.00	1.4
7	10.0	1.30	2.3

Potentiostatic experiments would not take into account any electrochemical process which was preceded by a slow chemical step. There is clearly no evidence for an ece or similar mechanism over the time scale of these experiments since there is no tendency for n to veer from, e.g., 1 to 2, 2 to 4, etc. From potentiostatic data the implication is that all peak processes for both pH 4 and 7 are the same owing to their similar n-values. This was not obvious from controlled potential coulometry experiments.

Spectroelectrochemistry

It was found that xanthosine exhibits different spectroelectrochemistry at pH 8 with change in concentration but pH 4 does not show such an effect. A typical u. v. spectrum of xanthosine obtained prior to electrolysis in pH 8 buffer at a concentration of 5 mM at a gold minigrid electrode is shown in curve 1 of Figure 82. It was observed that xanthosine exhibits two absorption bands with λ_{max} values of 282 nm and 252 nm. Upon application of a potential of 1.2 V (which using a gold minigrid electrode corresponds to peak IIa) both u. v. bands begin to decrease with time. This effect is more pronounced for the band at longer wavelengths. Simultaneously, two new absorption bands, λ_{max} = 340 and 225 nm, respectively, appear and grow. These bands reach maximal values and then they also decrease. Curve 2 in Figure 82 is the spectrum obtained when essentially all xanthosine has been oxidized and the bands having λ_{max} = 340 and 225 nm

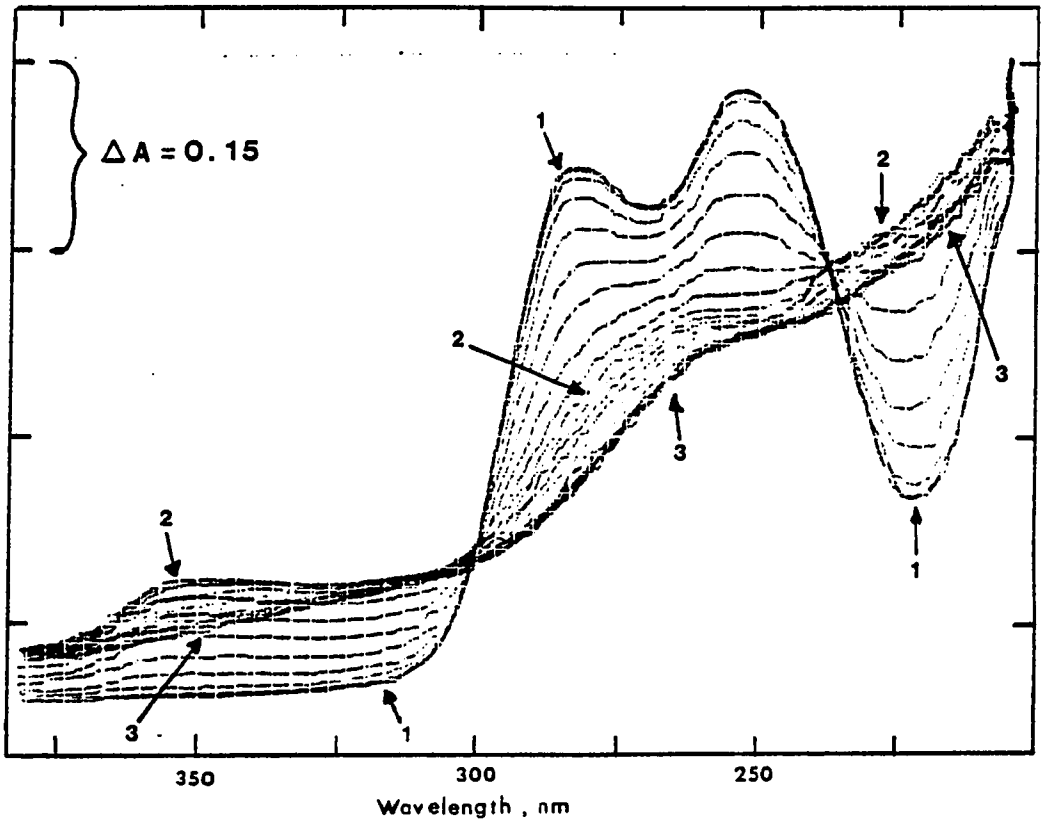

Figure 82. Spectra of 5 mM xanthosine electrolyzed at 1.2 V (peak IIa) at pH 8 at a gold minigrid electrode in a thin-layer cell. Curve (1) is spectrum before electrolysis. Electrolysis when absorption peak with λ_{max} = 340 nm has reached its maximum, curve (2). Curve (3) is spectrum after exhaustive electrolysis. Repetitive scans are 23.5 sec.

have reached their maximal values. Curve 3 (Figure 82) is the spectrum of an exhaustively electrolyzed solution of xanthosine. Both u. v. spectra (curves 2 and 3) are similar to some obtained for isolated products of mass electrolyses (vide infra). For xanthosine, thin-layer spectroelectrochemical studies between pH 7 and 9 at potentials ranging from 0.9 to 1.2 V (peak Ia-IIa) over a concentration range of 2-20 mM gave results similar to those shown in Figure 82. One important difference was observed. As the concentration of xanthosine was increased, the maximum absorbance at 340 nm became a greater percentage of the initial absorbance of xanthosine at 282 nm. This concentration dependence suggests that xanthosine forms a primary electrochemical product which may undergo a second-order reaction such as dimerization. If the electrolysis is discontinued when the peaks at 340 and 225 nm reach their maximum absorbance (curve 2, Figure 82) an absorbance decay is observed in the region 330-360 nm which is different from the decay in that region when the electrolysis is continued. The decay in the 225 nm region is very similar to its decay in the same region when the electrolysis in continued. The effect on these absorption peaks of terminating the electrolysis at their maximum absorbance is shown in Figure 83. It should be noted that there is no change in the shape of the absorption peak at 340 nm, just a general decay over the whole 330-360 nm region.

Xanthosine was also studied at a concentration of

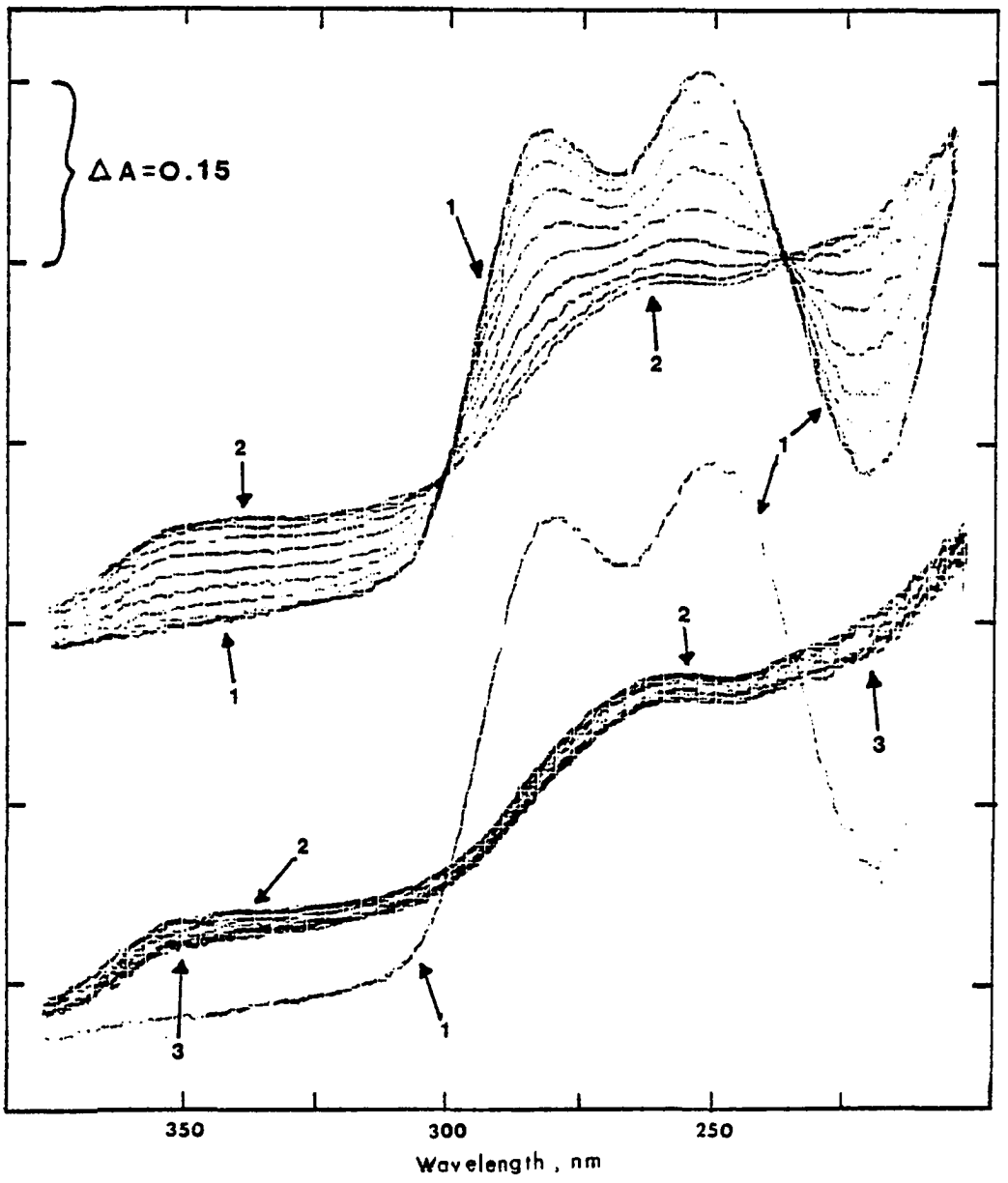

Figure 83. Spectra of 5 mM xanthosine electrolyzed at 1.2 V (peak IIa) at pH 8 at a gold minigrid electrode in a thin-layer cell. Curve (1) is spectrum before electrolysis. Electrolysis stopped at curve (2). Curve (3) is spectrum after decay of intermediate. Repetitive scans are 23.5 sec.

0.2 m$\underline{M}$ in the pH 8-9 range. At potentials corresponding to all four oxidation peaks no absorption band with a λ_{max} at 340 nm appears similar to that depicted in curve 2 of Figure 83. Due to equipment limitations the spectra obtained at 0.2 m$\underline{M}$ concentrations were of poor quality. However it is possible to observe an absorbance band at approximately 225 nm appear and grow upon application of a potential of 1.10 V (Peak Ia). This behavior is shown in Figure 84. When the electrolysis (at potentials 0.8-1.2 V, peaks Ia-IVa) is terminated before total decay of the initial absorption peaks takes place a similar rise in absorbance at $\underline{ca}$. 225 nm is observed (Figure 85). A comparable result was obtained for 0.2 m$\underline{M}$ uric acid-9-riboside (Figure 86). This may imply that at low concentration in the pH range 7-9, xanthosine and uric acid-9-riboside give rise to an identical intermediate. No meaningful spectrochemical data could be obtained in the 0.5-1.0 m$\underline{M}$ concentration range at pH 8. There was neither a rise nor a decay in the absorbance at any wavelength when the electrolysis was terminated. Competition between the high concentration process (2-20 m$\underline{M}$, Figure 83) and the low concentration process (0.2 m$\underline{M}$, Figure 85) could be the cause of this observed behavior at intermediate concentrations (0.5-1.0 m$\underline{M}$).

Thin-layer spectroelectrochemical studies of xanthosine were also conducted at low pH (2-5). Over a concentration range of 0.2-2.0 m$\underline{M}$ and a potential span between 1.0-1.4 V

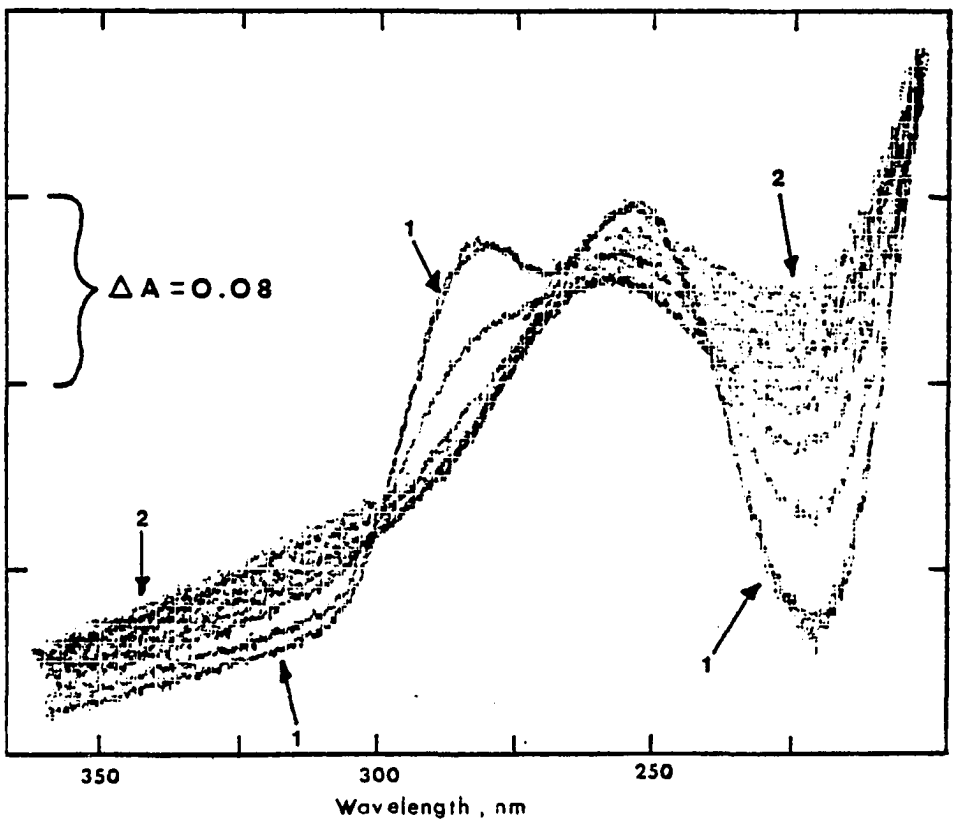

Figure 84. Spectra of 0.2 mM xanthosine electrolyzed at 1.1 V. (peak IVa) at pH 8 at a reticulated vitreous carbon electrode in a thin-layer cell. Curve (1) is spectrum before electrolysis. Curve (2) is spectrum after electrolysis. Repetitive scans are 47 sec.

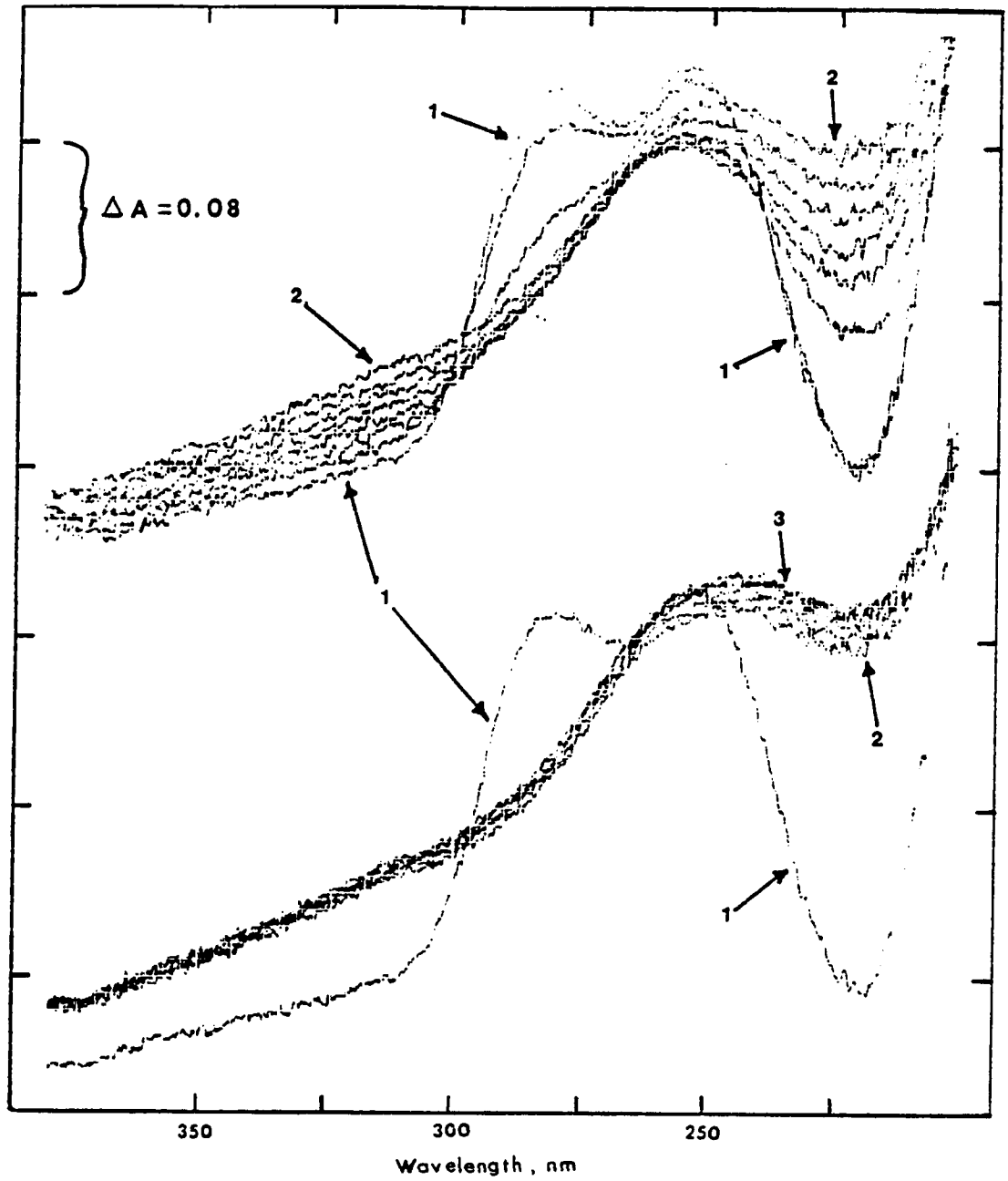

Figure 85. Spectra of 0.2 mM xanthosine electrolyzed at 1.3 V. (peak IVa) at pH 8 at a RVC electrode in a thin-layer cell. Curve (1) is spectrum before electrolysis. Electrolysis stopped at curve (2). Curve (3) is spectrum after decay of intermediate. Repetitive scans are 23.5 sec.

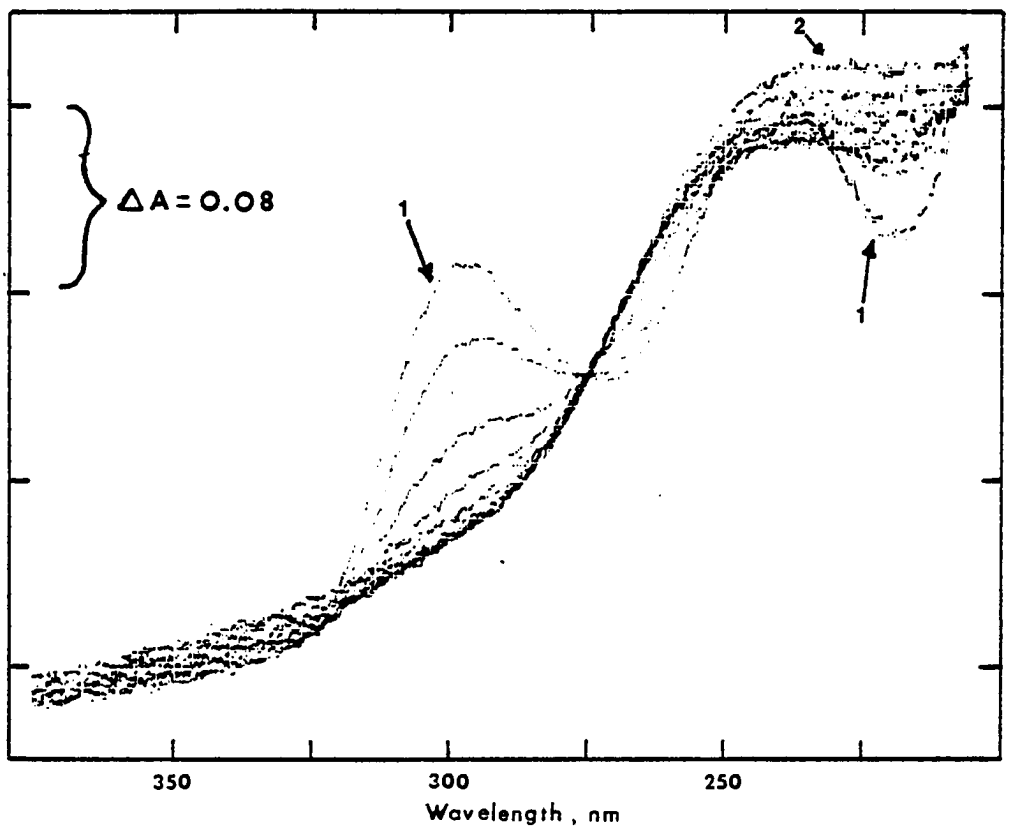

Figure 86. Spectra of 0.2 mM uric acid-9-riboside electrolyzed at 1.30 V (positive of the major oxidation peak) at pH 8 at a RVC electrode in a thin-layer cell. Curve (1) is spectrum before electrolysis. Curve (2) is spectrum after electrolysis. Repetitive scans are 18.9 sec.

(Peaks Ia-IVa), similar results to those shown in Figure 87 were obtained. A typical u. v. spectrum of 1 mM xanthosine prior to electrolysis at pH 4 is depicted in curve 1 of Figure 87. Two absorption bands with λ_{max} values of 267 and 236 nm are observed for xanthosine. Upon application of a potential of 1.30 V (peak IVa) both u. v. bands begin to decrease with time. Simultaneously, a new absorption band ($\lambda_{max} \simeq 220$ nm) appears and grows. This band reaches a maximal value and then it also decreases and disappears. Curve 2 in Figure 87 is the spectrum observed when essentially all xanthosine has been oxidized and the band having a λ_{max} = 220 has reached its maximal value. The obtained data supports the view that upon electrochemical oxidation of xanthosine an unstable intermediate is formed which has an absorption peak at a different wavelength than the absorption peaks for xanthosine. Curve 3 (Figure 87) is the spectrum of an exhaustively electrolyzed solution of xanthosine at a time when all of the absorbing intermediate species has disappeared. The decrease in absorbance at 220 nm occurred regardless of whether the initial potential applied to the electrode was maintained or turned off as shown in Figure 88. At no potential or concentration did an absorption band with a λ_{max} = 340 nm appear, as is the case for xanthosine at pH 7-9 and concentrations of 1.0 mM and above.

Similar thin-layer spectroelectrochemical behavior was observed for the oxidation of uric-acid-9-riboside (Figure 89)

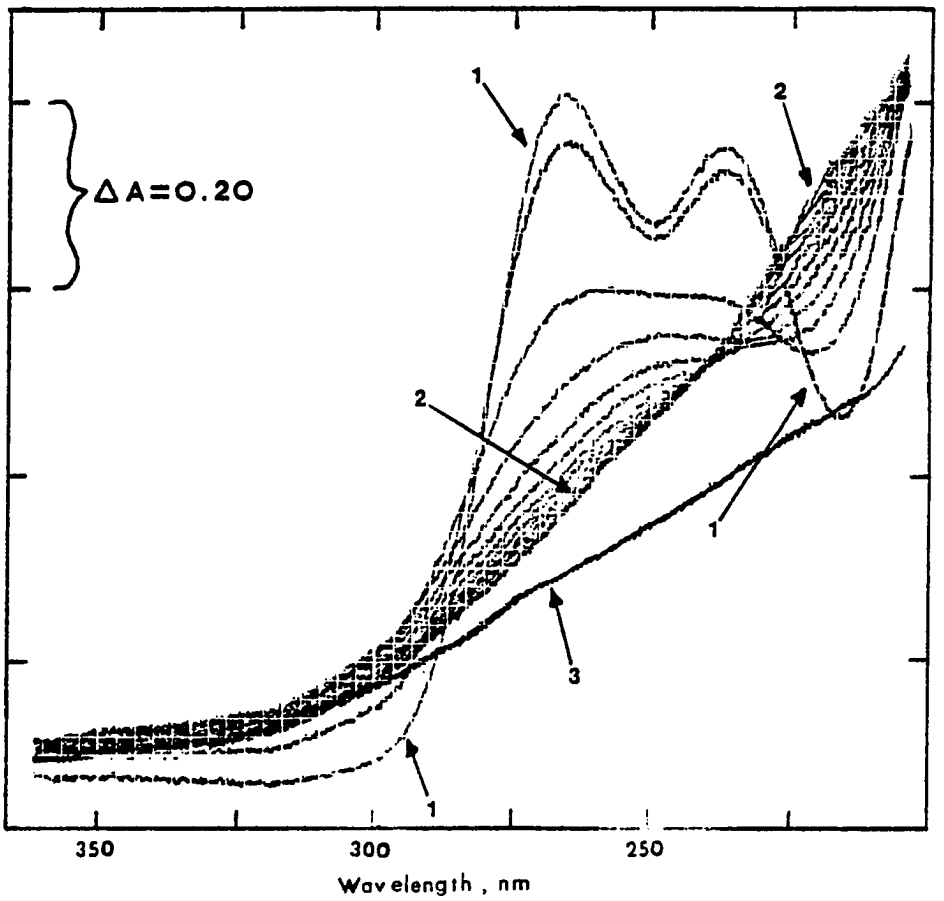

Figure 87. Spectra of 1 mM xanthosine electrolyzed at 1.30 V. (peak IVa) at pH 4 at a RVC electrode in a thin-layer cell. Curve (1) is spectrum before electrolysis. Electrolysis when absorption peak with λ_{max} = 220 nm has reached its maximum, curve (2). Curve (3) is spectrum after exhaustive electrolysis. Repetitive scans 47 sec.

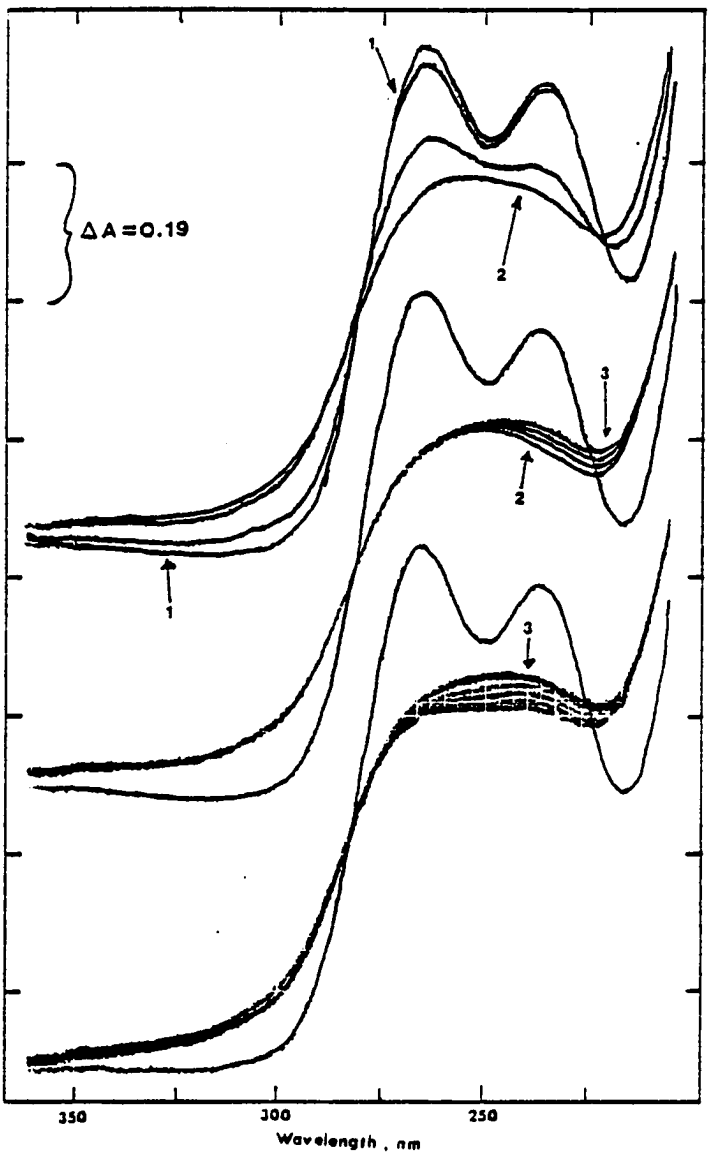

Figure 88. Spectra of 1 mM xanthosine electrolyzed at 1.3 V (peak IVa) at pH 4 at a RVC electrode in a thin-layer cell. Curve (1) is spectrum before electrolysis. Electrolysis stopped at curve (2). Curve (3) is spectrum when absorption peak with λ_{max} = 220 nm has reached its maximum. This peak subsequently decays. Repetitive scans are 47 sec. for upper spectra and middle spectra, and 94 sec. lower spectra.

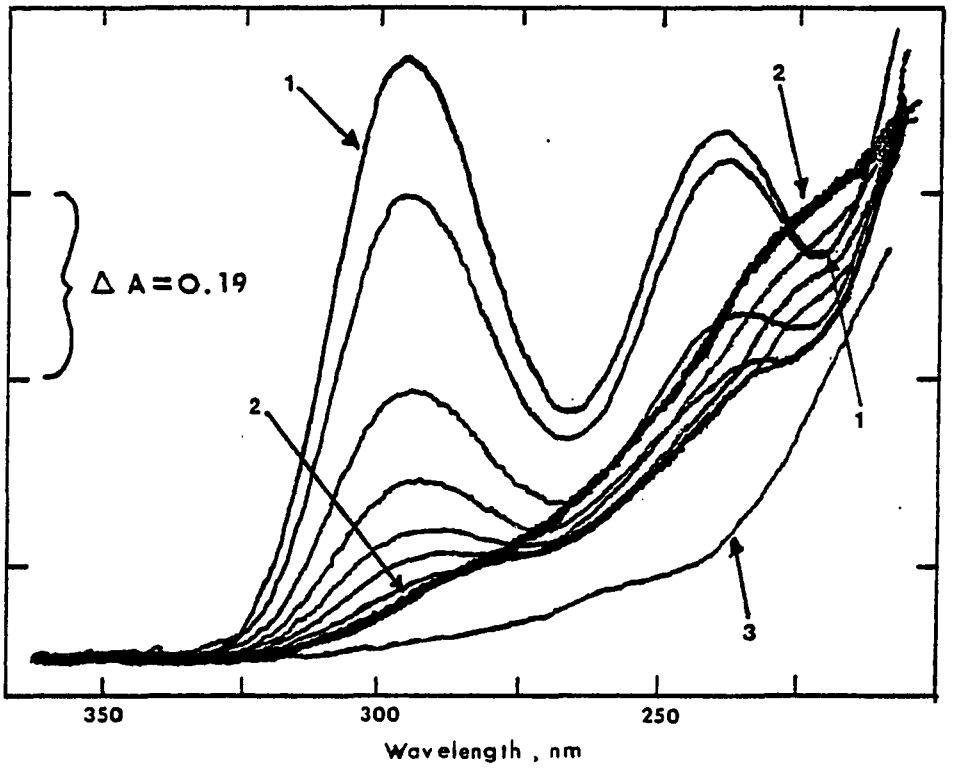

Figure 89. Spectra of 1 mM uric acid-9-riboside electrolyzed at 0.9 V. (positive of the major oxidation peak) at pH 4 at a RVC electrode in a thin-layer cell. Curve (1) is spectrum before electrolysis. Electrolysis when absorption peak with λ_{max} = 220 nm has reached its maximum, curve (2). Curve (3) is spectrum after exhaustive electrolysis. Repetitive scans 18.9 sec.

at pH 4 as was observed for xanthosine.

It is believed, for the same reasons detailed in Chapter 2 for 9-methylxanthine, that an u. v.-absorbing imine-alcohol intermediate similar to structure III of Figure 1 formed by partial hydration of the diimine primary electrooxidation product of uric acid is also the u. v.-absorbing intermediate species detected by thin-layer spectroelectrochemistry for xanthosine below the pK_a (5.7) at 220 nm and above it at a concentration of 0.2 mM at 225 nm.

Switching potential experiments were performed to show that reduction peak IIc observed during cyclic voltammetry of xanthosine was caused by the u. v.-absorbing imine-alcohol intermediate. As with 9-methylxanthine (vide supra), xanthosine was oxidized at a potential (at both pH 8 and 4) where the imine-alcohol was formed and could be observed via its u. v. spectrum (225 nm, pH 8 and 220 nm, pH 4). After approximately 50 seconds the potential was switched to a potential negative of reduction peak IIc. Under these conditions the imine-alcohol spectrum disappeared more quickly than when no potential was applied. Thus at reduction peak IIc the intermediate absorbing at 220-225 nm is electrochemically reduced.

From similar behavior shown in 9-methylxanthine studies and voltammetric, coulometric,and spectroscopic data (vide infra) it is thought an u. v. and vis. (yellow) absorbing dimer is a decaying species detected by spectroelectrochemistry above the pK_a (5.7) at concentrations greater than 1 mM in

xanthosine. The yellow dimer is formed as a result of further oxidation of the dimer produced in the peak Ia process (vide infra). The peak Ia dimer causes the absorbance peak at 340 nm. The yellow dimer also shows u. v. absorption in the wavelength range 330-360 nm. However, this yellow dimer displays only a gradual rise in absorbance (no peaks) from longer to shorter wavelength over this range. Unlike the peak Ia dimer, the yellow dimer is only moderately stable in water ultimately decomposing to allantoin-riboside (vide infra). The fact that the peak Ia dimer is stable (vide infra) and that the relative shape of the absorption peak at 330-360 nm in Figure 83 did not change, but the whole peak decreased, during the absorbance decay indicates it was not the peak Ia dimer that decayed. A species having similar absorption over the entire 330-360 nm range, i.e. the yellow dimer, must have decayed.

Kinetic measurements

The kinetics of several decomposition reactions of u. v.-absorbing intermediate species formed by electrochemical oxidation of xanthosine were studied by thin-layer spectro-electrochemical techniques. A typical absorbance at 340 nm. vs time graph for 2-20 mM xanthosine in pH 7-9 buffer at potentials from 1.0-1.4 V (peaks Ia-IVa) is shown in Figure 90. A plot of log $|A - A_\infty|$ vs time (Figure 90) was linear implying the decomposition reaction followed first order kinetics. Values of the observed first order solution rate

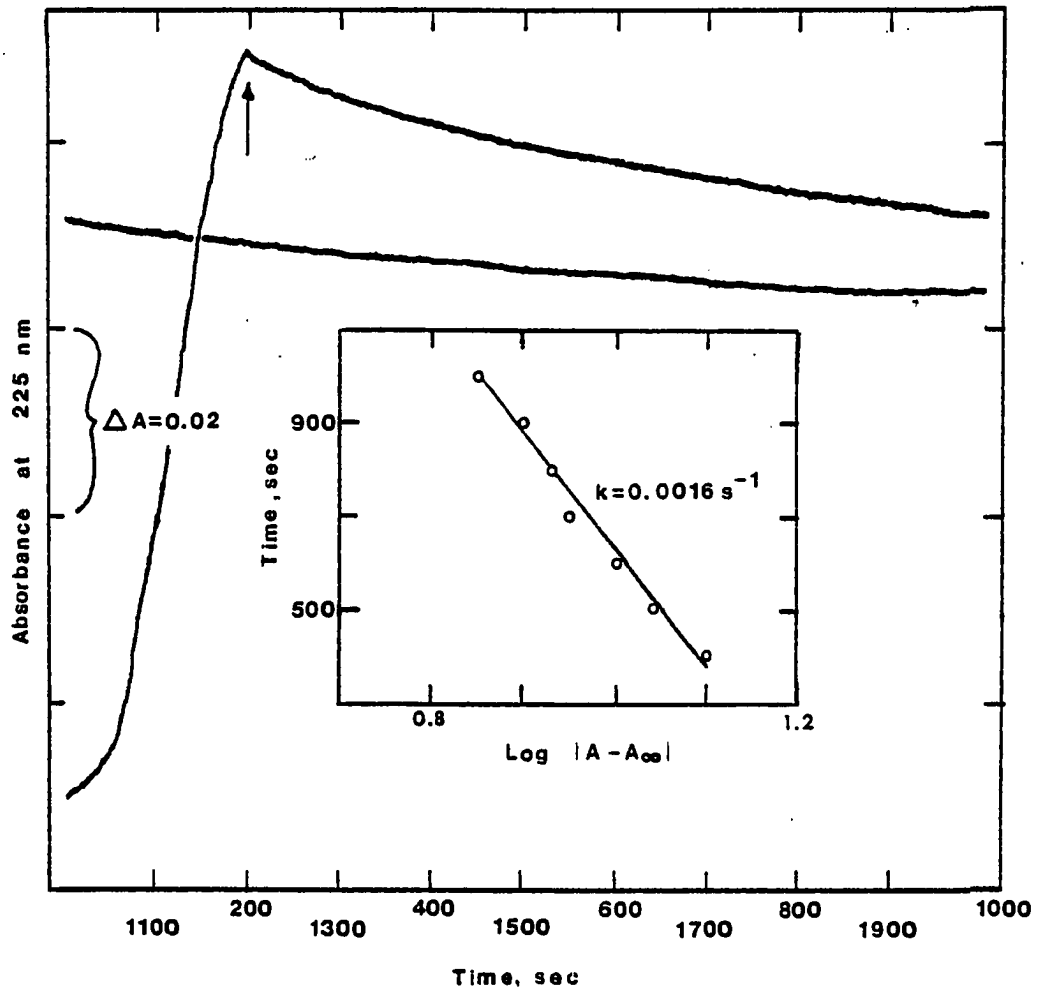

Figure 90.a.Absorbance vs. time for electrooxidation of 5 mM xanthosine at pH 8 at 340 nm. Electrolysis at 1.2 V (peak IIa) stopped at arrow.

b.Time vs. log $|A - A_\infty|$ at 340 nm of the intermediate species formed on electrooxidation of 5 mM xanthosine at pH 8.

constant at concentrations 2.0 mM and higher above the pK_a (5.7) are shown in Table 15. Note that somewhat higher rate constants are observed when the monitored wavelength was 272 or 225 nm.

The absorbance at 225 nm vs time graph shown in Figure 91 is representative of 0.2 mM xanthosine solutions in pH 8-9 buffer at potentials 0.8-1.3 V (peaks Ia-IVa). Figure 91 also contains the plot of $\log |A - A_\infty|$ vs time for the 0.2 mM xanthosine solution. It was linear implying the decomposition mechanism followed first order kinetics. The value of the observed rate constant is shown in Table 15. No meaningful kinetic data could be obtained in the 0.5-1.0 mM concentration range at pH 8 for the same reasons discussed in the spectroelectrochemistry section (vide supra).

Solutions of xanthosine (0.2-2.0 mM) in pH 3-4 buffer at potentials 1.0-1.5 V (peaks Ia-IVa) gave absorbance at 220 nm vs time graphs similar to that shown in Figure 92. The plot of $\log |A - A_\infty|$ vs time (Figure 92) was linear. This implies that the decay reaction followed first order kinetics at pH 3-4.

Under pH 4 conditions, uric acid-9-riboside (Figure 93) displayed similar rate constants and absorbance vs time graphs as were obtained for xanthosine.

The shapes of the absorbance vs time graphs for xanthosine and uric acid-9-riboside above the pK_a (5.7) and at a concentration of 0.2 mM are quite similar (Figures 91 and

TABLE 15

Observed first order rate constants for reaction of the u. v.-absorbing intermediates formed on electrochemical oxidation of xanthosine and uric acid-9-riboside

Compound oxidized	λ_{max} for absorption of intermediate, nm	pH	Initial Concentration, mM	k_{obs}, s^{-1}
Xanthosine	220	3	1.0	0.0017
Xanthosine	220	4	0.2	0.0016
Xanthosine	220	4	0.5	0.0015
Xanthosine	220	4	1.0	0.0016
Xanthosine	220	4	2.0	0.0018
Xanthosine	340	7	2.0	0.0017
Xanthosine	225	8	0.2	0.0051
Xanthosine	340	8	2.0	0.0018
Xanthosine	225	8	5.0	0.0022
Xanthosine	272	8	5.0	0.0018
Xanthosine	340	8	5.0	0.0016
Xanthosine	340	8	10.0	0.0015
Xanthosine	225	9	0.2	0.0041
Xanthosine	340	9	2.0	0.0020
Uric Acid-9-Riboside	220	4	1.0	0.0015
Uric Acid-9-Riboside	225	8	0.2	0.0065

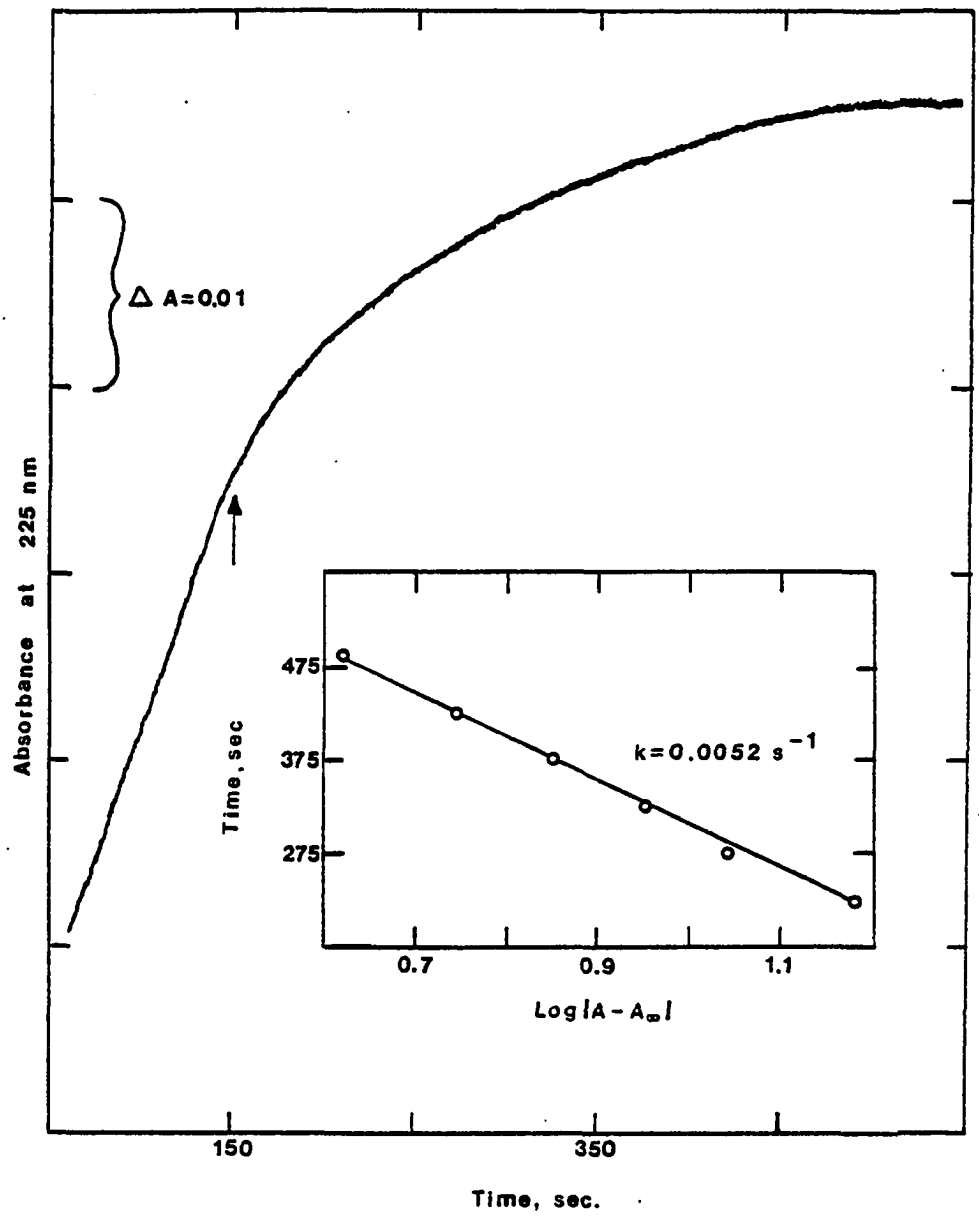

Figure 91. a. Absorbance vs. time for electrooxidation of 0.2 mM xanthosine at pH 8 at 225 nm. Electrolysis at 1.3 V. (peak IVa) stopped at arrow.

b. Time vs. Log $|A - A_{\infty}|$ at 225 nm of the intermediate species formed on electrooxidation of 0.2 mM xanthosine at pH 8.

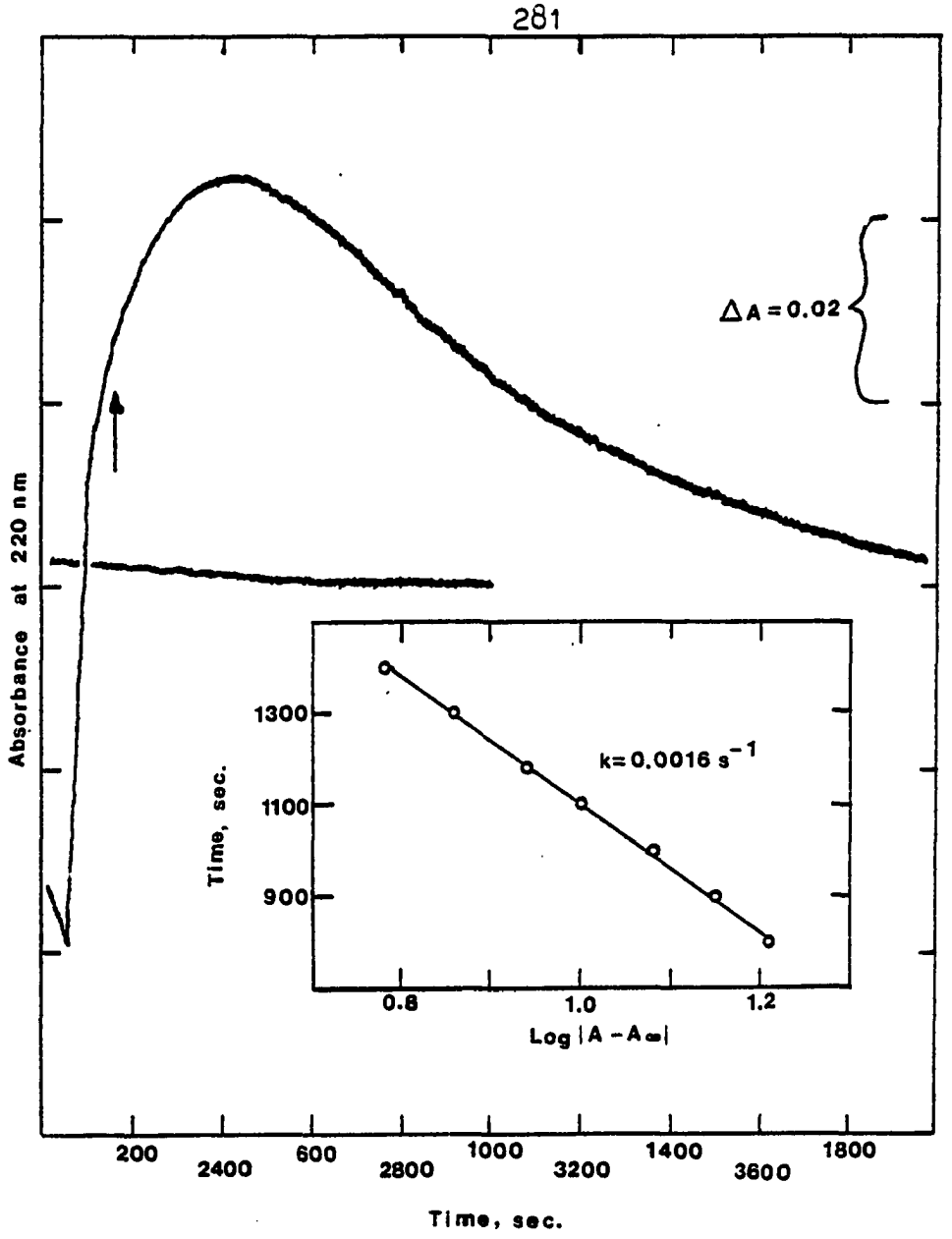

Figure 92. a. Absorbance vs. time for electrooxidation of 1 mM xanthosine at pH 4 at 220 nm. Electrolysis at 1.4 V. (peak IVa) stopped at arrow.

b. Time vs. Log $|A - A_\infty|$ at 220 nm of the intermediate species formed on electrooxidation of 1 mM xanthosine at pH 4.

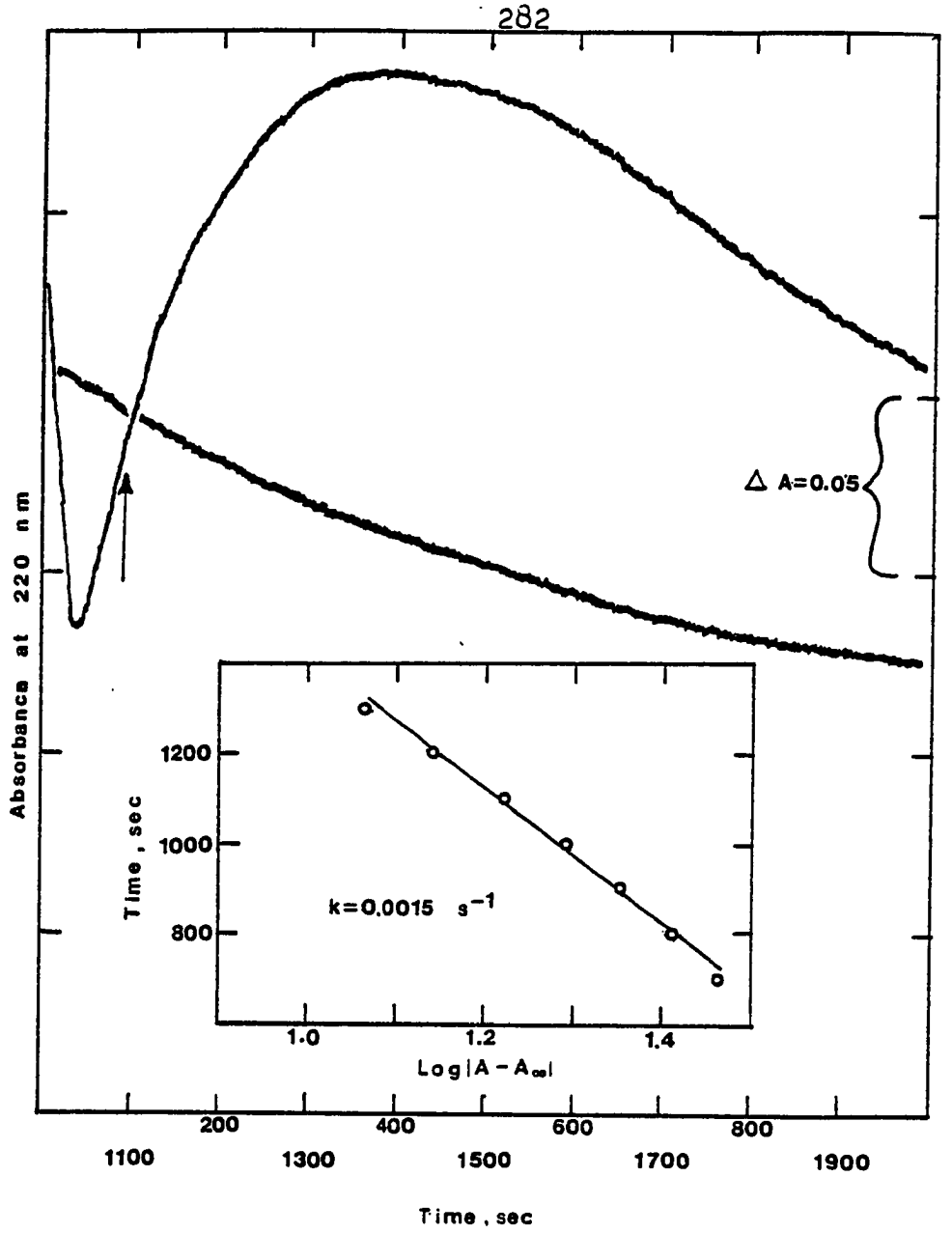

Figure 93. a. Absorbance vs. time for electrooxidation of 1 mM uric acid-9-riboside at pH 4 at 220 nm. Electrolysis at 1.2 V (positive of major oxidation peak) stopped at arrow.

b. Time vs. Log $|A - A_\infty|$ at 220 nm of the intermediate species formed on electrooxidation of 1 mM uric acid-9-riboside at pH 4.

94). However, their rate constants are not in good agreement. This may be due to influence from the "high concentration" process in the case of xanthosine.

For xanthosine and uric acid-9-riboside at pH 4, the rise in absorbance of the kinetic curves can be hypothesized to be the partial hydration of a diimine (similar to the one hypothesized for 9-methylxanthine) to a corresponding imine-alcohol. Since the intermediates continue to grow after the potential is turned off, it is thought that the observed rise is absorbance is due to the formation of a species in homogeneous solution. Further hydration of the imine-alcohol to a 4,5-diol is the hypothesized mechanism for the decreasing portion of the pH 4 kinetic curves. It is also believed that the decay of a diimine to a 4,5-diol is the phenomena monitored kinetically at pH 8 in 0.2 m$\underline{M}$ xanthosine and uric acid-9-riboside solutions. The initial steep rise in absorbance observed before the electrolysis is terminated may be due to the partial hydration of a diimine to a corresponding imine-alcohol. Further hydration of the imine-alcohol to the 4,5-diol is the hypothesized mechanism for the second, more gradual rising portion of the pH 8 low concentration (0.2 m$\underline{M}$) kinetic curves.

It is thought that the rise in absorbance at 340 nm of the kinetic curve for 2.0-20 m$\underline{M}$ xanthosine at pH 8 is due to the electrochemical formation of two dimers, one stable and the other only moderately stable (vide infra). The fact

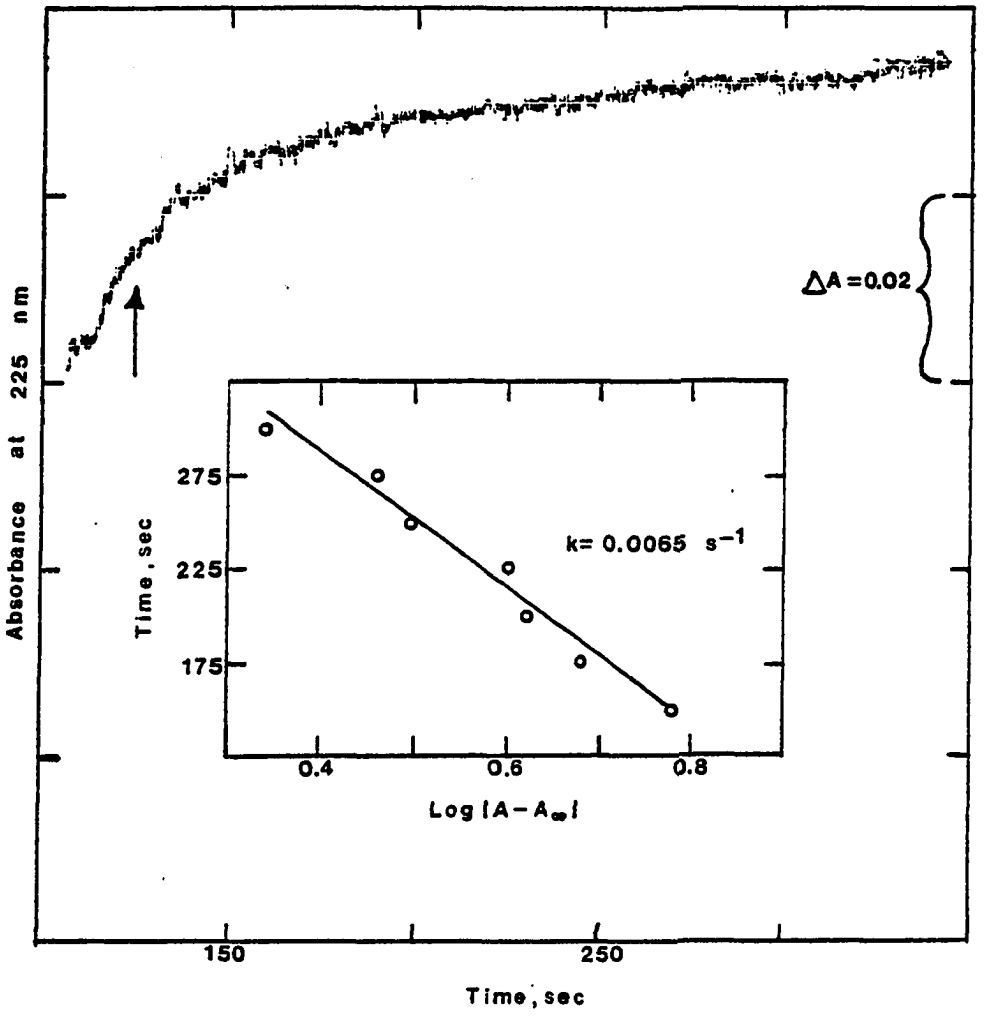

Figure 94. a. Absorbance vs. time for electrooxidation of 0.2 mM uric acid-9-riboside at pH 8 at 225 nm. Electrolysis at 1.2 V. (positive of major oxidation peak) stopped at arrow.

b. Time vs. Log $|A - A_\infty|$ at 225 nm of the intermediate species formed on electrooxidation of 0.2 mM uric acid-9-riboside at pH 8.

that the rise in absorbance stops and an immediate decay is observed when the potential is turned off supports the hypothesis that the decaying species was electrochemical generated. The subsequent decreasing portion of the kinetic curve is thought to be the hydration of the moderately stable dimer to allantoin-riboside (vide infra).

Product Isolation and Characterization

The electrochemical behavior of xanthosine at pH 4 and 7 was judged to be representative of the electrochemical tendencies of xanthosine below and above the pK_a (5.7). Therefore, product analyses were conducted exclusively in these media. The definite structures of all the products could not be established. However, the evidence obtained from mass, i. r., and u. v.-vis. spectroscopy plus chromatography and voltammetry allowed conclusions to be drawn regarding the nature of the electrochemical products.

pH 7. Peak Ia. Oxidation at 0.84 V of 1 mM xanthosine (8 mg) and subsequent lyophilization gave a pale yellow residue. This residue was dissolved in approximately 2 ml of doubly distilled water. Separation of the resultant solution was accomplished by liquid chromatography using Sephadex G-10 (90 cm x 2.5 cm). The solvent, 0.1 M pH 7 phosphate buffer, was eluted at a flow rate of 30 $mlhr^{-1}$. A typical chromatogram is shown in Figure 95. Two very large peaks (retention volumes 198 ml and 441 ml) were observed. Four additional small peaks (retention volumes 225 ml, 258 ml, 306 ml,

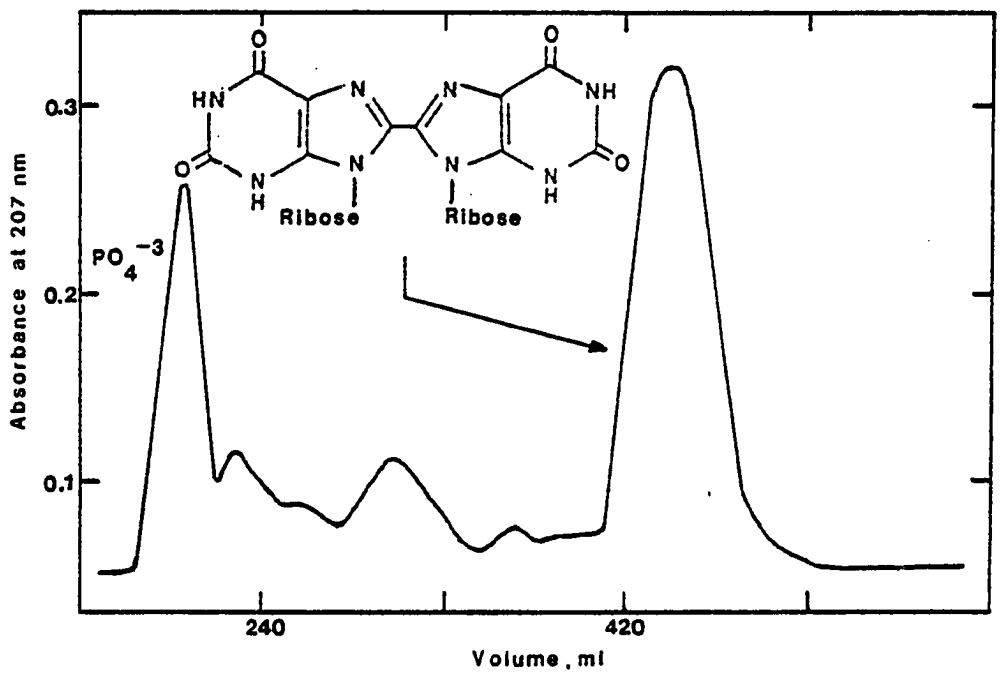

Figure 95. Chromatogram of oxidation peak Ia products at pH 7 using a gel-permeation resin (Sephadex G-10, 90 cm x 2.5 cm). The eluant was pH 7 phosphate buffer, having an ionic strength of 0.1. Flow rate 30 $mlhr^{-1}$.

and 363 ml) were also obtained. These small chromatographic peaks were shown to be peak IIa decomposition products (vide infra). There is only a small potential difference between oxidation peak Ia and IIa. Therefore it is impossible when running an electrolysis to completely separate these processes. The liquid chromatographic peak with a retention volume of 211 ml (LC Peak-211) was shown to be due to phosphate from the electrolysis solution. The final large peak (LC Peak-441) could not be completely desalted. However, u. v. and i. r. spectroscopy plus comparison with the electrochemistry of 9-methylxanthine of the crude material yielded information leading to the probable structure. Attempts were made to purify the crude material by solvent extraction and recrystallization due to the failure of chromatography. These were also unsuccessful. This electrolysis product was only soluble in water. Thus, there was too much phosphate present to obtain a mass spectrum of any kind for this oxidation product.

The u. v. spectrum of the LC Peak-441 product is reproduced in Figure 96. This u. v. spectrum is very similar to the one reported by Hansen and Dryhurst[31] for the dimer of theophylline. In addition it is nearly identical to the u. v. spectrum of the proposed dimer for 9-methylxanthine (Figure 43). Due to the large excess of phosphate in this sample, an i. r. spectrum could not be obtained. The observed n-values, potentiostatically determined (Table 5 and 14), for

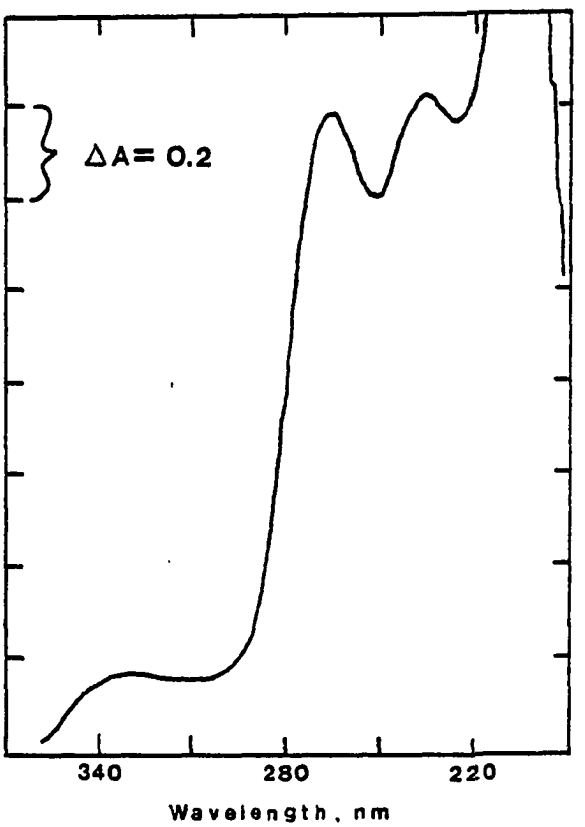

Figure 96. U. v. spectrum of oxidation peak Ia product with retention volume of 441 ml.

both xanthosine and 9-methylxanthine resemble each other at their respective peak Ia. In addition, voltammetry run during coulometry for both of these molecules (Figures 25 and 79) show identical behavior. It would therefore appear that similar dimerization (C-C dimerization at the C_8 position) as was observed for theophylline and 9-methylxanthine has occurred with xanthosine. Thus the probable structure (II) is the following:

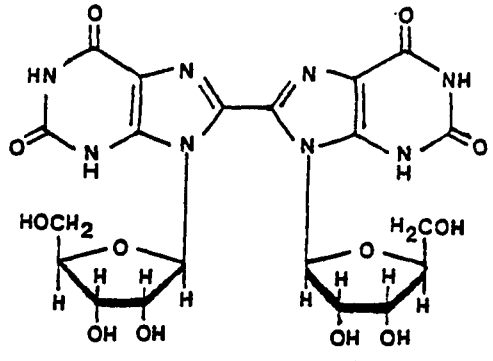

II

The same u. v. comparisons made with analogous structures (Chapter 2, VI and VII) of the 9-methylxanthine dimer to support its actual structure can be used in a similar manner to support the proposed structure of the xanthosine dimer (Chapter 2, page 168).

pH 7. Peak IIa. Upon completion of an oxidation at 1.00 V (until no voltammetric peaks remain) of 1 mM xanthosine (8 mg) lyophilization gave a yellow residue. Attempts to separate this residue using previously described liquid chromatographic techniques were for the most part unsuccessful. None of these procedures provided a yellow

separated product. One could observe the loss in intensity of the yellow material as it was eluting through the column. The major product obtained via this separation was allantoin-riboside (vide infra). Thus, it is quite apparent that in the time frame required for separation (12 hours) the yellow product underwent decomposition. This decomposition takes place more readily upon dilution.

Chromatography failing, attempts were made to purify the crude yellow product by solvent extraction or recrystallization. These were also largely unsuccessful. This electrolysis product was insoluble in all but the most polar solvents (methanol and water) and heating the product in these polar solvents caused decomposition (changes in color intensity). The best results were obtained when 8 mM xanthosine (64 mg) was oxidized at 1.00 V. Upon lyophilization this solution gave a bright yellow residue. The large excess of phosphate from the electrolysis solution was removed by dissolving the yellow residue in approximately 75 ml of distilled methanol. The methanol was allowed to evaporate. This procedure causes no appreciable loss in color intensity. Evaporation of methanol left a waxy residue. Enough doubly distilled water was added to the residue to cause it to dissolve. The residue was lyophilized leaving fluffy yellow crystals. Purification was not complete as determined by the phosphate test (vide supra).

Although not pure, u. v., vis. and mass spectrometry

of the crude yellow product yielded information regarding possible structures. There were no distinct peaks in the visible spectrum of this oxidation product just a general rise in absorbance beginning at 610 nm and continuing until 380 nm. The u. v. spectrum shown in Figure 97 had few distinquishing characteristics but showed some resemblance to spectrum 3 of Figure 82. The general rise in absorbance which began in the visible region of the spectrum continued in the u. v. region until ca. 260 nm where a shoulder appeared. Below 260 nm there was a sharp increase in absorbance followed by a distinct drop at 200 nm. In Figure 97 the i. r. spectrum of the yellow oxidation product is reproduced.

GCMS and direct insertion mass spectra could not be obtained for this oxidation product. A field desorption mass spectrum (Figure 98), though very weak, was somewhat more useful for this product. The best result was at 25 mA, at which emitter current several peaks were observed having m/e values of 58, 115, 151, 412, and 457. This sample could have behaved poorly due to its instability or the amount of inorganic salt present. Though of poor quality the FD mass spectrum does provide useful information. The appearance of a peak with an m/e value of 457, though this does not correspond to a likely molecular weight of a product of xanthosine, does imply by its large value that some form of dimerization has occurred. Potentiostatic studies imply oxidation peak IIa is further 1 electron (per molecule of

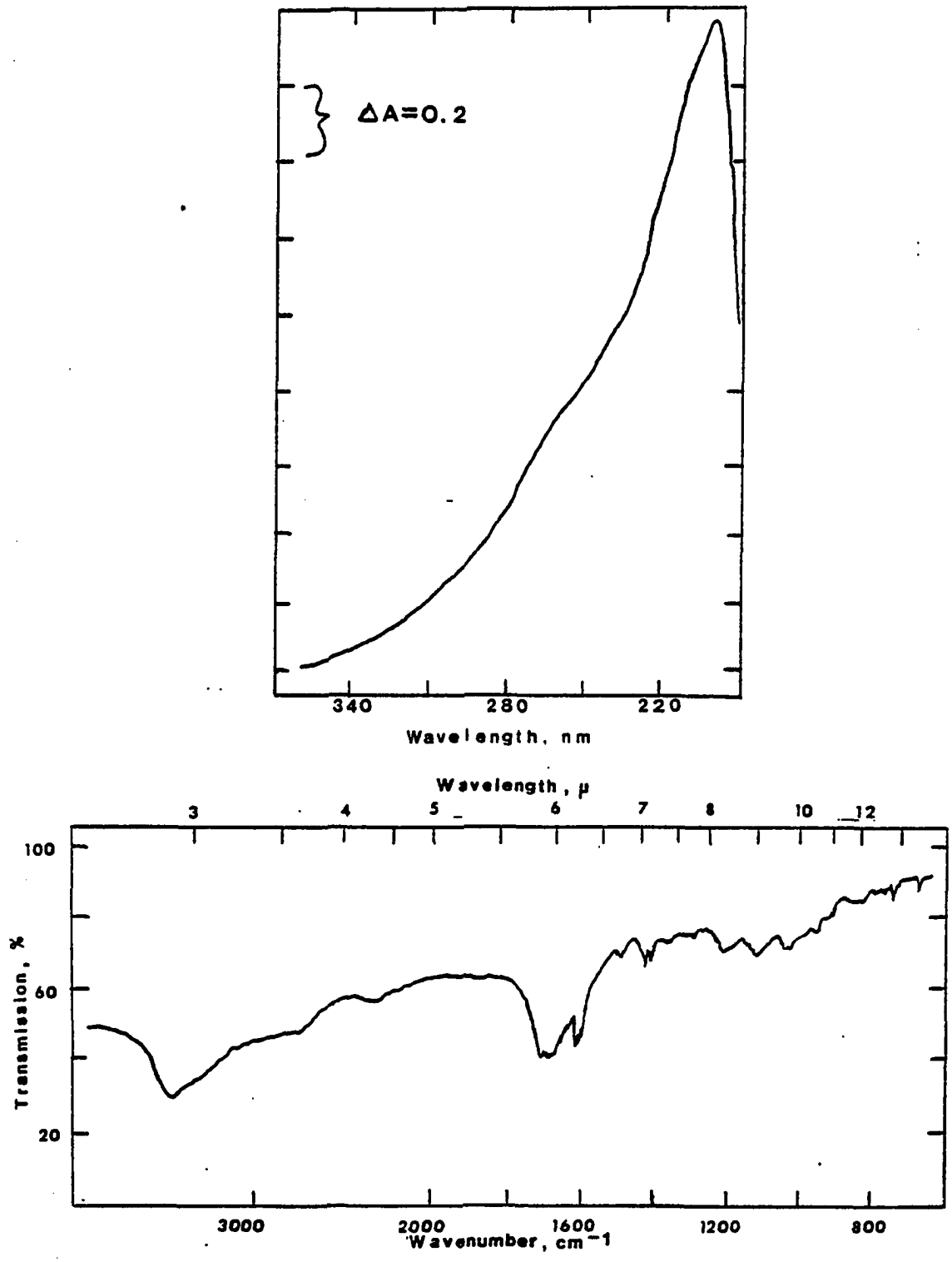

Figure 97. I. r. and u. v. spectra of oxidation peak IIa product. I. r. is of a KBr disc.

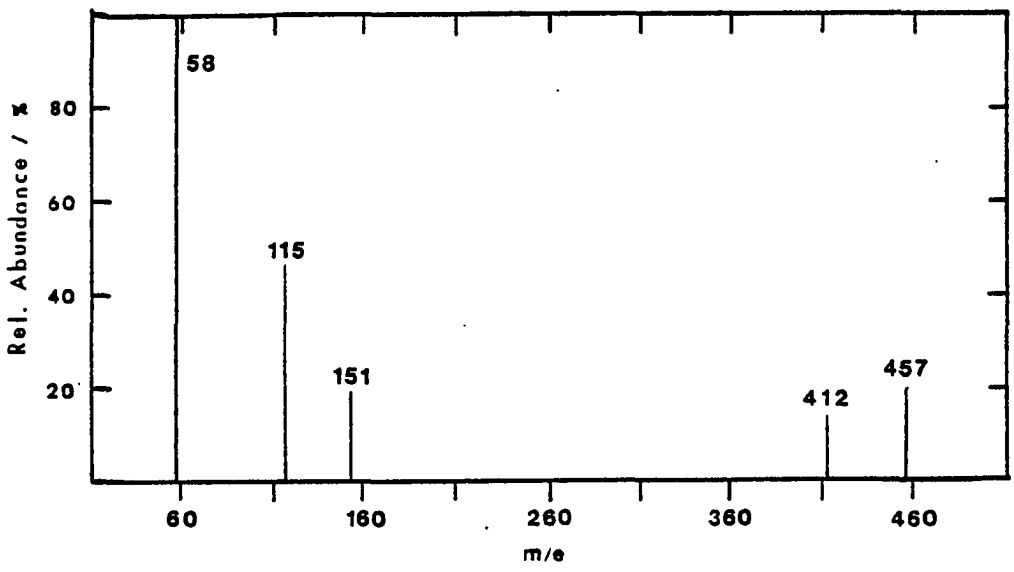

Figure 98. Field desorption mass spectrum at 25 mA for oxidation peak IIa product.

initial xanthosine) oxidation. Since the molecules exist in dimeric form after oxidation at peak Ia, the actual peak IIa oxidation mechamism is a 2 electron oxidation of the dimer formed in the oxidation peak Ia process. The product of such an oxidation would have a molecular weight of 566. A possible structure (III) for such an oxidation is:

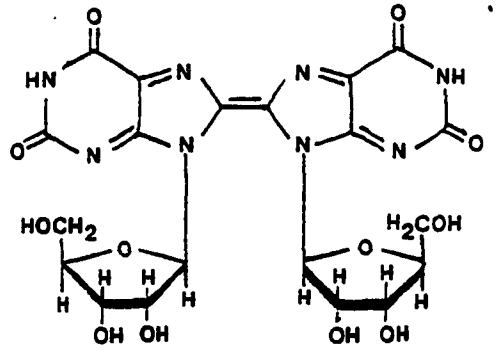

III

Due to the inability of removing all of the phosphate from the electrolysis sample, the i. r. spectrum (Figure 97) is poor in quality. Thus it was of little use in structure determination.

One would expect a compound with a structure like III to show an u. v.-vis. spectrum similar to that obtained for the oxidation peak IIa product. The further increase in conjugation in structure II compared to structure III should produce a bathochromic shift in absorbance. Thus, absorption is expected in the visible spectrum for the $O{=}C_2{-}N_3{=}C_4{-}C_5{=}N_7{-}C_8{=}C_8'{-}N_7'{=}C_5'{-}C_4'{=}N_3'{-}C_2'{=}O$ grouping in III, using an

analogous argument to that in Chapter 2.

All the yellow color disappeared after the product of electrooxidation of 70 mg of xanthosine was allowed to stand in 1 liter of doubly distilled water for 48 hours. Upon lyophilizing a cream colored residue was obtained. This material was separated using an identical chromatographic system as was employed for the peak Ia experiments. A similar chromatogram to that from peak IIIa/IVa products (vide infra, Figure 99) was obtained. As usual the first large peak product proved to be phosphate from the electrolysis cell. The second large peak product proved to be allantoin-riboside. The products from the small chromatographic peaks could not be identified (vide infra). Thus it is proposed that the peak IIa oxidation product (structure III) might undergo hydration and air oxidation (vide infra) to form allantoin-riboside.

When cyclic voltammetry was performed on the peak IIa product (yellow dimer) it showed several of the small voltammetric peaks observed during switching studies of xanthosine (Figure 75) in the vicinity of the first two oxidation peaks. The redox couple (reduction peak at -0.02 V and oxidation peak at 0.04 V) and the reduction peaks at -0.4 V, -0.68 V and -1.00 V were those that appeared during this voltammetry. Thus it would appear the yellow dimer is readily reducible. It would be expected that the system of conjugated double bonds proposed in the yellow dimer should be very readily electrochemically reducible[61-63]. This voltammetry lends

additional support to the proposed structure of the yellow oxidation peak IIa product.

pH 7. Peak IIIa. The results of product analysis at oxidation peak IIIa closely resembled those at peak IVa. This coupled with coulometry, potentiostatic, and voltammetric data implied that oxidation peak IIIa is an adsorption pre-peak of peak IVa.

pH 7. Peak IVa. Oxidation at 1.30 V of 0.2 mM xanthosine (4 mg) gave a pale yellow residue. Similar chromatography to that used for xanthosine oxidation peak Ia was employed to separate this pale yellow residue. The resultant chromatogram is shown in Figure 99. There are two large chromatographic peaks (LC Peak-186 and LC Peak-252). In addition there are three small peaks (LC Peak-222, 282, and 354). As in previous cases the first chromatographic peak (LC Peak-195) was shown to be phosphate from the electrolysis cell. The second was shown to be allantoin-riboside via GC/MS and i. r. spectroscopy. The i. r. spectrum of the LC Peak-252 product is shown in Figure 100. Many of the i. r. peaks in allantoin-riboside are similar to those observed in 1-methylallantoin (Figure 47) and allantoin (Part I, Figure 19). The GC/mass spectrum was obtained by adding ca. 0.1 mg of LC Peak-252 product to a reactor vial. Seventy µl of BSTFA and acetonitrile were added to the vial and heated at 135°C for 20 minutes. This solution was subjected to gas chromatography using the same column and conditions reported

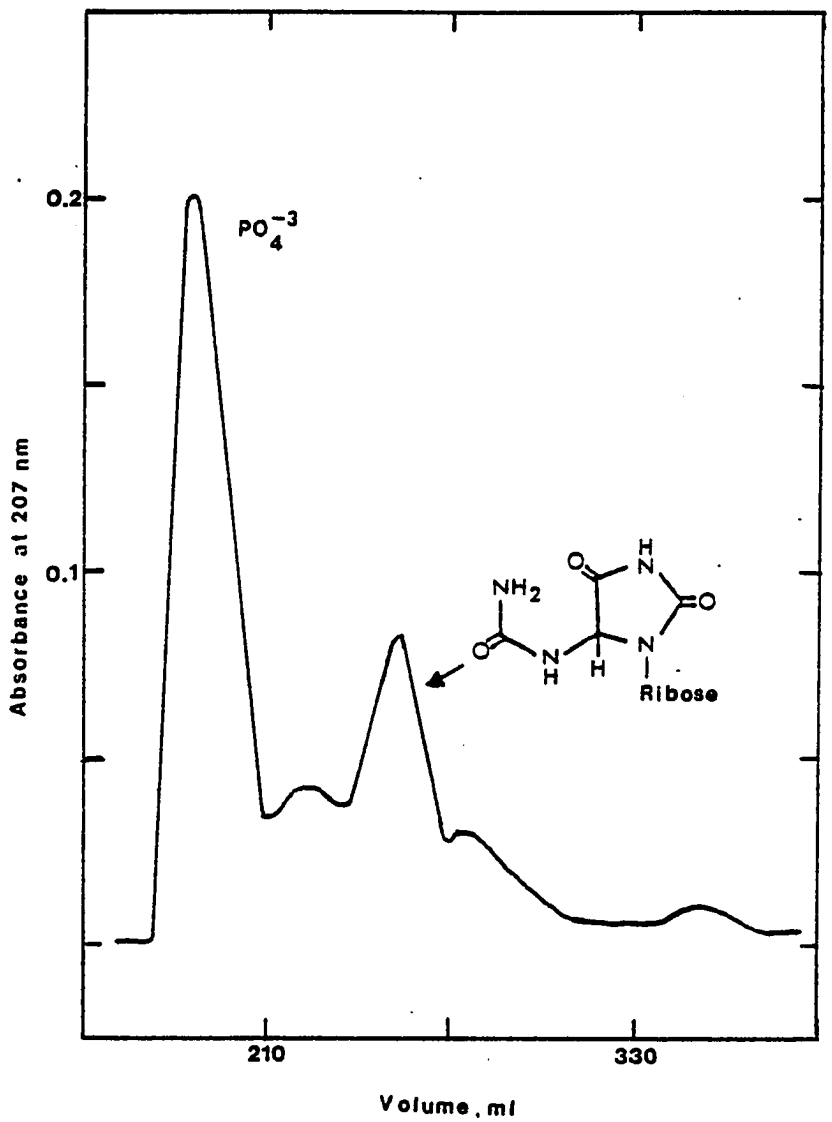

Figure 99. Chromatogram of oxidation peak IVa products at pH 7 using a gel-permeation resin (Sephadex G-10, 90 cm x 2.5 cm). The eluant was doubly distilled water. Flow rate 30 $mlhr^{-1}$.

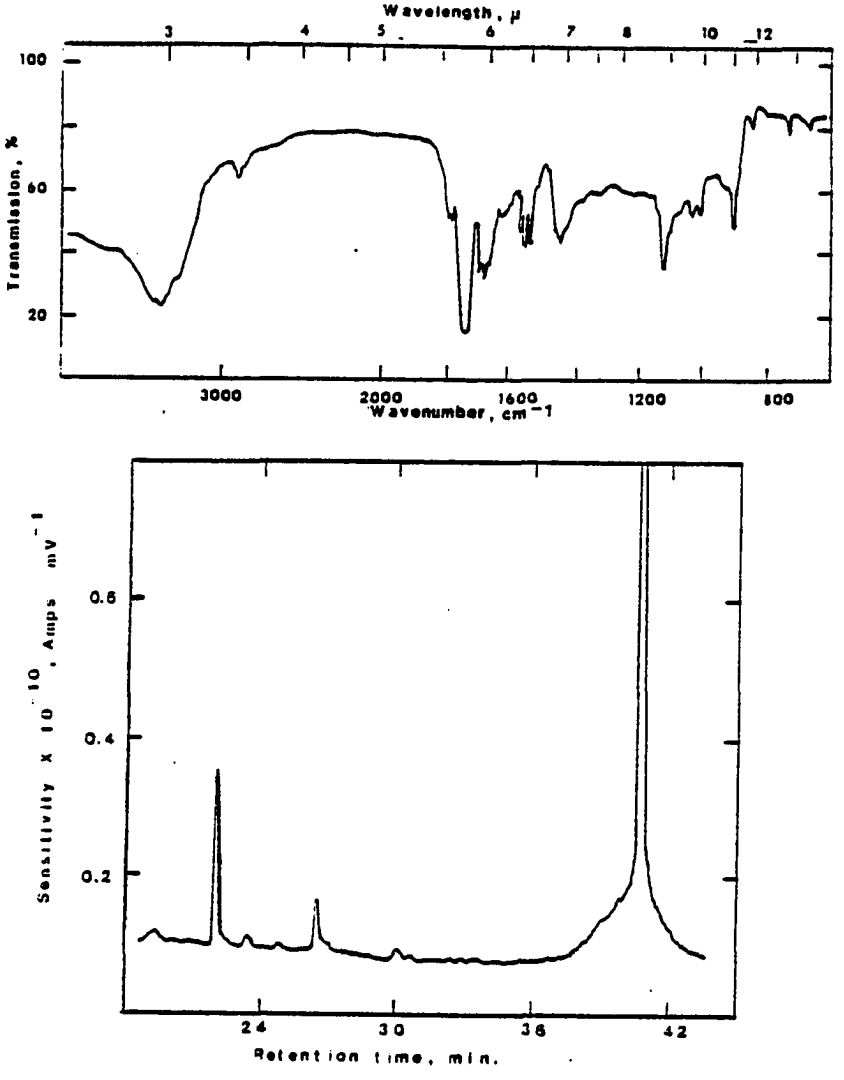

Figure 100. a. I. r. spectrum of oxidation peak IVa product with retention volume of 252 ml.

b. Gas chromatogram of oxidation peak IVa product with retention volume of 252 ml using SE-30 packing (column dimensions, 2 mm.x 6 ft.). Flow rate 30 $mlhr^{-1}$. Temperature program: 100°C for 12 min., then raised 6° per min. I. r. is of a KBr disc.

in Chapter 2. The resultant gas chromatogram is shown in Figure 100. GC Peak-40.88 showed a mass spectrum (Table 16) indicating a structure with a molecular weight of 794. Allantoin-riboside with 7 TMS substituents (IV) would have a molecular weight of 794.

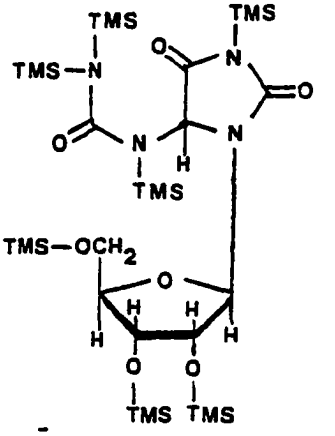

IV

The fact that an ion with m/e = 779 (m-15) appears in the fragmentation pattern further proves the identity of the GC Peak-40.88 product to be the seven TMS substituted derivative of allantoin-riboside. GC Peak-26.63 showed a mass spectrum (Table 17) implying a molecular ion of 391. However there are no ions in the fragmentation pattern to support 391 as the molecular ion. Assuming 3 TMS substituents, a molecular ion of 391 would give a species of molecular weight 175. At this time there is no mechanism to account for a molecule with such a low molecular weight. Thus it is thought that GC Peak-26.63 is due to decomposition of allantoin-riboside. The mass spectrum of GC Peak-22.13 product is shown in Table 18. An ion with m/e of 385 is the possible molecular ion. There is no supporting evidence in the

TABLE 16. Mass spectrum of pH 7 LC Peak-252 and GC Peak-40.88 product

MASS	%	MASS	%	MASS	%	MASS	%	MASS	%	MASS	%	MASS	%
53.1	.5	93.0	1.4	142.0	1.1	205.1	.8	258.1	3.6	329.0	1.1	385.1	.4
54.1	.5	95.1	.8	143.0	1.6	207.0	5.3	259.1	3.6	330.1	10.1	386.9	.4
55.1	1.0	96.2	.4	144.1	.6	208.0	1.0	260.0	1.0	331.1	3.9	388.1	.6
56.2	.5	97.1	.7	145.1	.8	209.0	.6	261.1	.5	332.1	2.6	388.9	.4
57.1	1.3	99.1	.9	146.0	.7	211.1	.6	265.0	.6	333.1	.9	400.9	.5
58.1	.7	100.1	7.7	147.1	13.0	215.1	1.6	267.0	.4	340.0	.5	402.9	.4
59.2	1.7	101.1	1.7	148.1	1.6	216.0	.6	269.0	.4	341.1	.7	429.0	.7
61.0	.6	102.1	1.0	148.9	1.8	217.1	28.2	281.0	2.4	342.1	.5	430.2	.9
62.9	.4	103.1	9.1	157.0	1.5	218.1	6.7	282.0	1.0	345.1	.4	431.0	.6
64.9	.6	104.1	.8	158.1	.6	219.2	3.0	283.0	.5	346.1	.4	432.2	.5
67.3	.6	105.1	.7	160.9	.5	220.0	.5	284.0	.6	347.1	2.5	444.0	.9
69.1	1.3	113.1	.6	169.1	1.0	221.0	2.1	285.1	.6	348.0	2.7	445.1	5.7
70.0	2.0	114.1	.5	170.1	.9	222.1	.5	286.1	.6	349.0	1.1	446.1	3.7
71.0	.7	115.1	2.2	171.1	1.1	223.0	.4	287.0	.6	355.1	1.8	447.1	2.4
72.1	2.9	116.1	1.7	172.1	1.3	227.9	.6	295.0	.4	356.1	1.6	447.9	.9
73.1	100.0	117.0	2.9	173.1	.5	229.1	.9	299.1	.6	357.1	1.5	455.2	.6
74.1	8.3	118.1	.8	174.0	.5	230.1	2.8	300.1	.8	358.1	1.1	472.1	.5
75.1	10.4	127.0	.6	187.1	1.1	231.1	1.3	312.1	1.9	359.1	.8	514.8	.6
76.1	.8	129.0	4.2	188.1	2.8	232.0	.7	313.2	.6	360.1	.5	518.1	.4
77.1	1.5	130.0	1.2	189.1	2.4	242.1	1.4	314.1	1.2	369.2	.5	778.8	1.1
79.2	.5	131.0	2.0	190.1	.7	243.2	2.8	315.1	.7	370.0	.4	779.5	1.3
81.0	.5	132.0	.8	191.1	1.6	244.1	1.3	316.1	1.0	371.0	.4	780.6	.9
83.1	.5	133.0	3.0	193.0	.8	245.1	4.9	319.1	1.1	372.2	2.1	782.0	.5
84.0	.5	134.0	.7	201.0	.5	246.1	1.3	320.1	.8	373.1	1.3	794.1	6.4
85.1	.4	135.0	.6	203.1	.4	256.1	.6	325.0	.8	374.1	.8	795.4	3.4
86.0	.4	141.0	1.1	204.0	1.0	257.0	1.0	328.0	.5	375.0	.4	795.6	3.3

TABLE 17. Mass spectrum of pH 7 LC Peak-252 and GC Peak-26.63 product

MASS	%	MASS	%	MASS	%	MASS	%
57.1	1.3	103.1	11.9	157.0	1.6	390.9	1.4
58.1	1.5	105.1	1.1	157.9	1.4		
59.2	5.6	114.2	1.2	170.1	1.7		
61.1	1.2	115.1	1.7	174.0	1.2		
69.1	1.7	116.2	1.0	189.2	2.6		
71.1	2.4	117.1	4.6	196.0	1.0		
72.0	2.9	129.0	4.1	203.0	1.1		
73.1	100.0	131.0	3.3	204.0	3.3		
74.1	6.3	133.0	4.7	211.0	4.2		
75.1	12.3	141.0	1.0	217.0	26.6		
77.1	3.6	142.0	3.0	218.1	5.5		
85.0	1.0	143.1	2.5	219.1	4.1		
85.9	1.6	144.1	4.1	230.1	2.6		
89.0	2.3	145.0	1.3	231.1	1.0		
100.1	4.2	147.1	9.0	243.1	1.0		
101.1	3.4	149.1	1.7	259.0	.9		

TABLE 18. Mass spectrum of pH 7 LC Peak-252 and GC Peak 22.13 product.

MASS	%	MASS	%	MASS	%
55.1	1.9	133.0	1.3	312.1	1.4
57.1	1.8	142.0	1.2	316.2	7.8
58.0	2.5	147.1	10.9	317.2	2.0
59.1	2.9	147.9	1.7	385.0	22.1
69.0	1.9	151.0	1.9	386.0	5.1
72.1	3.2	178.0	2.4	387.0	3.2
73.1	100.0	188.1	1.9		
74.1	8.6	203.0	1.4		
75.1	11.3	204.0	4.2		
77.0	13.8	208.0	9.4		
78.2	1.8	223.0	8.9		
101.1	1.3	224.0	2.1		
103.1	2.0	228.0	1.5		
116.1	1.4	266.1	2.3		
117.1	1.9	278.0	1.4		
131.0	1.9	299.1	1.2		

fragmentation pattern for this conclusion. The intensity of this gas chromatographic peak was always small. Varying the amount of LC Peak-252 product silated did not increase the intensity of this GC Peak. It is therefore believed to be an unknown decomposition product due to its low possible molecular weight in comparison to that of xanthosine (284). LC Peak-282 gave the gas chromatogram shown in Figure 101. The mass spectrum (Table 19) for GC Peak-40.13 of Figure 101 gave a possible molecular ion of 512. GC Peak-40.13 was never very intense, although various different conditions were tried. A similar mass spectrum (Table 19) was observed for the oxidation peak Ia product and the oxidation peak IIa product. For these reasons it is thought the mass spectrum is of a decomposition product. The decomposition could have occurred during liquid chromatography, silation, or even the electrolysis. Neither of the products from the two small peaks (LC Peaks 222 and 354) could be silated. There was insufficent sample to perform other analytical methods to determine their identity.

pH 4. At pH 4 potential changes caused only minor alterations in the relative amounts of the various products. Varying the concentration of xanthosine oxidized caused no alteration in the observed products. Oxidation of 1 mM xanthosine (8 mg) at 1.4 V and subsequent lyophilization gave a cream colored residue. This residue was dissolved in two ml of doubly distilled water. Separation of the resultant

TABLE 19. Mass spectrum of pH 7 LC Peak-282 and GC Peak-40.13 product

MASS	%	MASS	%	MASS	%	MASS	%
57.1	7.8	163.0	2.1	263.2	2.5	512.3	21.9
61.1	2.0	177.0	4.5	265.1	2.0	513.3	8.4
73.1	44.3	189.1	2.7	267.1	3.5	514.5	4.3
74.1	4.3	191.2	9.8	281.1	18.0		
75.1	5.9	192.0	2.3	282.1	6.1		
77.1	2.5	193.1	4.9	283.2	3.5		
81.2	2.0	203.0	2.3	295.1	2.0		
96.1	7.8	205.1	2.7	327.1	2.1		
103.0	2.3	207.1	100.0	341.0	2.1		
117.0	2.1	208.1	20.3	349.3	2.7		
119.1	2.1	209.1	15.8	355.1	3.7		
129.0	2.0	219.1	3.5	455.2	23.8		
133.1	10.5	221.1	5.1	456.2	8.2		
147.1	8.2	247.2	8.8	457.4	2.7		
148.1	2.0	248.3	2.7	483.4	4.1		
149.1	6.8	249.2	2.0	497.2	2.0		

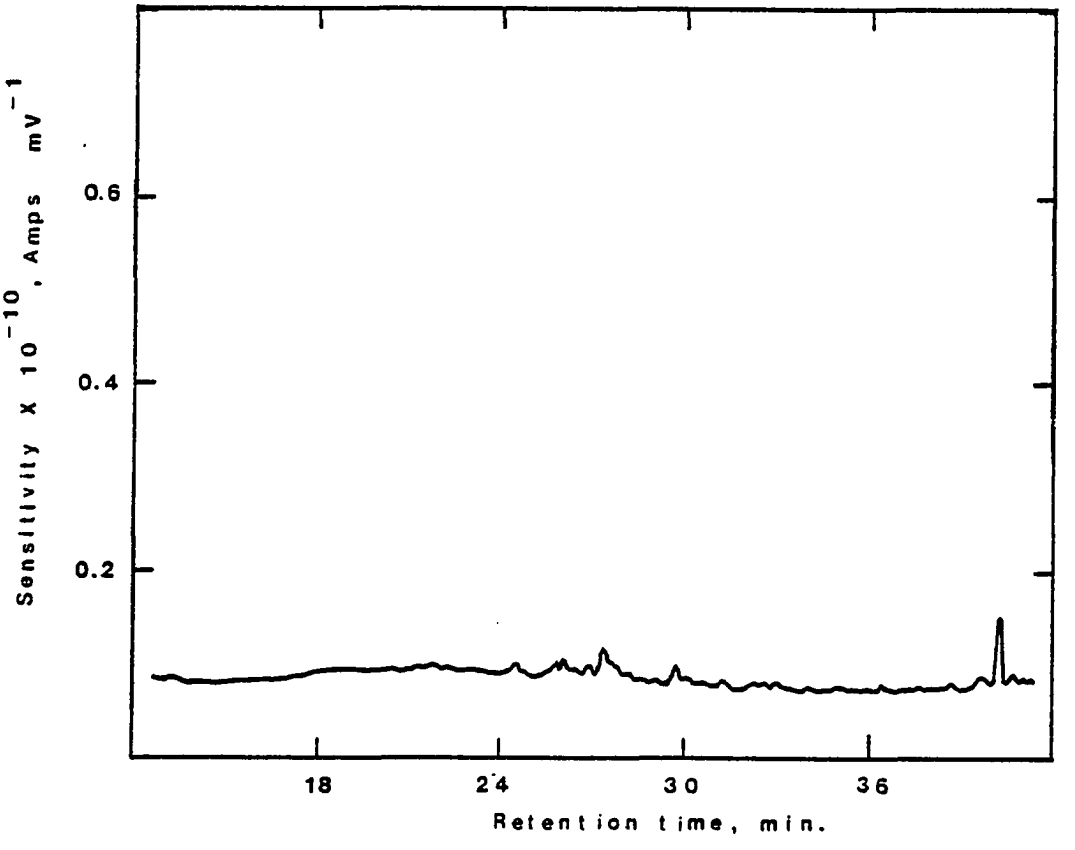

Figure 101. Gas chromatogram of oxidation peak IVa product with retention volume of 282 ml using SE-30 packing (column dimensions, 2 mm x 6 ft). Flow rate 30 mlhr^{-1}. Temperature program: 100°C for 12 min., then raised 6° per min.

solution was achieved by liquid chromatography using Sephadex G-10 (90 cm x 2.5 cm). The flow rate of the eluting solvent (0.001 M HCl) was 30 $mlhr^{-1}$. In Figure 102, the chromatogram obtained is shown. Three prominent peaks (retention volumes 201 ml, 261 ml, and 492 ml) were observed. In addition, three small peaks were obtained (retention volumes 225 ml, 315 ml, and 375 ml). The first large chromatographic peak (LC Peak-201) was due to phosphate from the electrolysis solution.

GC/MS was used to obtain a mass spectrum of the product from LC Peak-261. The gas chromatogram and mass spectrum are shown in Figure 103 and Table 20, respectively. These were found to be identical to those obtained for allantoin-riboside. The i. r. spectrum for this product is also shown in Figure 103. LC Peak-492 was sufficiently volatile to permit direct insertion mass spectroscopy. The mass and i. r. spectra (Figure 104) obtained for this product were compared to those for authentic alloxan and proved to be the same. Phosphate could not be removed from LC Peak-225. Therefore no product analysis could be accomplished on this material. LC Peak-315 product at pH 4 showed the same GC/MS data as LC Peak-282 product at pH 7 (Figure 101 and Table 19). The LC Peak-375 product was insufficiently volatile to permit direct insertion mass spectroscopy. It also would not silate. There was not sufficient material to try to identify this product by other chemical methods.

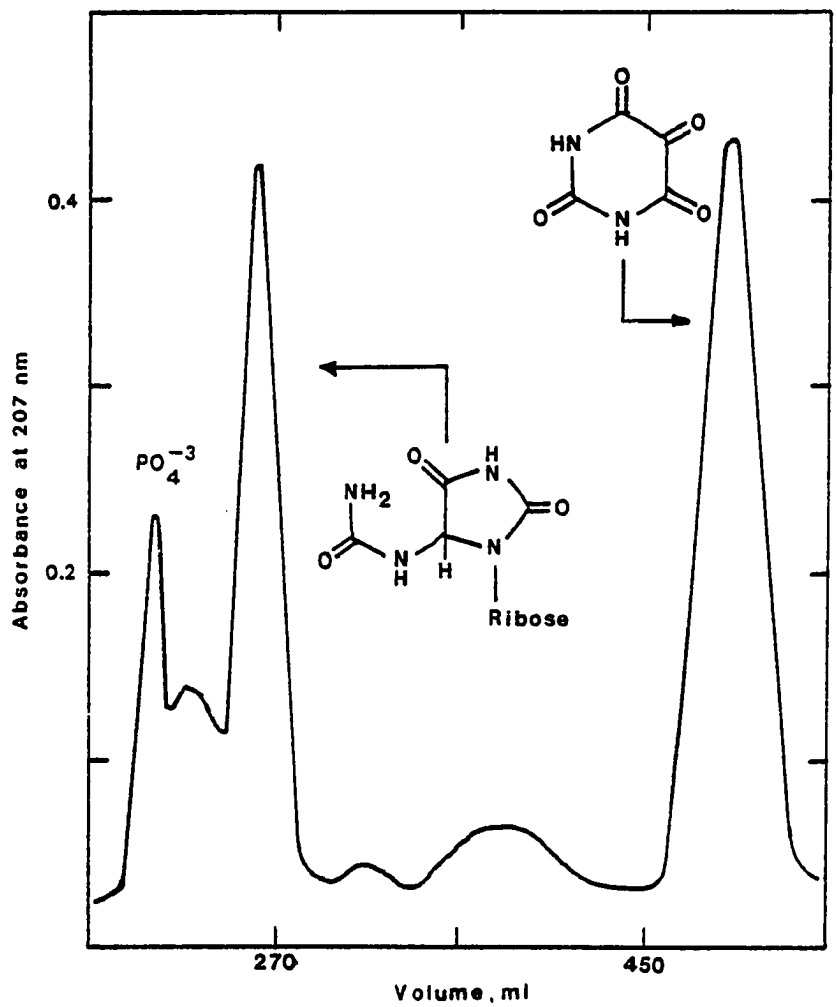

Figure 102. Liquid chromatogram of oxidation products at pH 4 at 1.4 V (peak IVa) using a gel-permeation resin (Sephadex G-10, 90 cm x 2.5 cm). The eluant was 0.001 m$\underline{M}$ HCl. Flow rate 30 $mlhr^{-1}$.

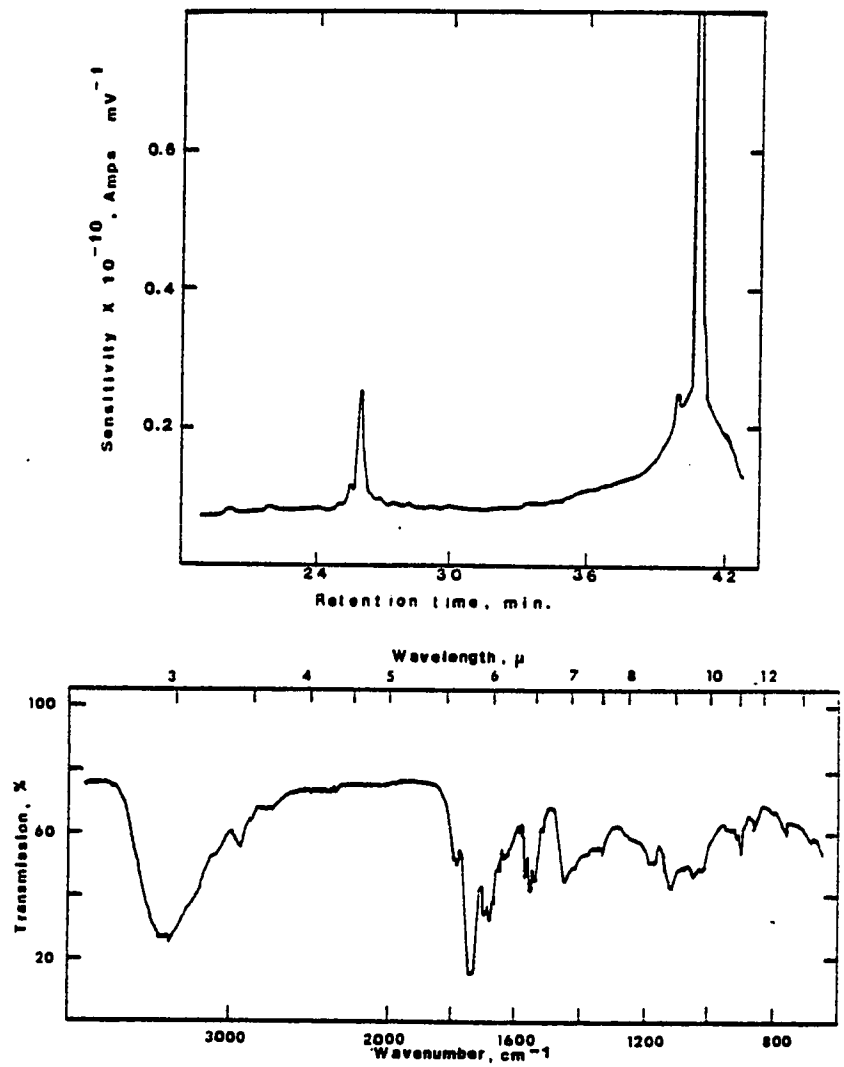

Figure 103. a. Gas chromatogram of pH 4 oxidation peak IVa product with retention volume of 261 ml using SE-30 packing (column dimensions, 2 mm x 6 ft). Flow rate 30 $mlhr^{-1}$. Temperature program: 100°C for 12 min., then raised 6° per min.

b. I. r. spectrum of pH 4 oxidation peak IVa product with retention volume 261 ml. I. r. is of a KBr disc.

TABLE 20. Mass spectrum of pH 4 LC Peak-261 and GC Peak-40.61 product.

MASS	%	MASS	%	MASS	%	MASS	%	MASS	%	MASS	%	MASS	%
53.1	.3	102.1	.7	145.1	.7	190.2	.7	228.2	.2	313.2	.2	375.3	.2
55.2	.6	103.2	9.4	146.1	.6	191.2	.9	229.2	.7	314.2	.5	387.1	.2
56.2	.2	104.2	.7	147.1	14.5	192.1	.2	230.2	1.8	315.2	.6	409.1	.2
57.2	.4	105.2	.6	148.1	2.2	193.1	.3	231.2	1.1	316.2	.6	430.3	.8
58.1	.5	111.2	.3	149.1	2.1	196.0	.2	232.2	.5	317.2	.2	431.2	.5
59.2	1.2	113.1	.8	150.0	.3	198.1	.3	241.2	.3	319.3	.3	432.2	.4
61.1	.4	114.1	.5	153.1	.3	199.1	.4	242.2	.8	328.2	.2	444.3	1.1
69.0	.7	115.2	2.2	154.0	.2	200.2	.3	243.2	2.4	329.2	.6	445.3	6.1
70.1	.9	116.2	2.9	155.1	.4	201.1	.6	244.2	1.2	330.2	10.3	446.3	4.4
71.1	.5	117.1	2.5	156.1	.5	202.2	.2	245.2	2.3	331.2	4.8	447.1	2.8
72.2	3.1	118.2	.4	157.2	1.5	203.2	.4	246.1	.6	332.2	2.2	448.2	1.0
73.1	100.0	119.2	.4	158.1	.6	204.0	.5	247.2	.3	333.2	.8	449.2	.3
74.1	8.7	126.1	.3	159.1	.3	205.2	.5	256.2	.5	345.2	.4	472.3	.2
75.1	6.6	127.1	.7	169.2	1.6	206.2	.2	257.2	.8	347.2	.5	475.1	.2
77.1	.5	128.2	.2	170.1	1.1	207.2	.4	258.1	1.4	348.2	.5	560.3	.5
81.0	.3	129.1	4.4	171.1	2.1	211.1	.2	259.2	3.3	349.2	.2	561.2	.2
84.1	.2	130.0	1.1	172.1	2.3	212.1	.3	260.1	1.0	355.2	.6	607.3	.2
85.1	.4	131.1	2.5	173.1	1.1	213.1	.3	261.1	.5	356.3	1.1	779.3	1.1
86.1	.5	132.1	.5	174.1	1.0	214.1	.4	269.2	.3	357.3	.9	780.3	.6
89.1	.9	133.0	3.7	175.1	.4	215.2	1.1	272.1	.2	358.3	.6	781.2	.5
93.1	.4	134.1	.5	184.1	.2	216.1	.6	273.2	.2	359.2	.8	782.2	.2
97.0	.4	135.1	.3	185.1	.2	217.2	14.2	284.1	.3	360.3	.4	794.4	6.5
98.2	.2	141.1	2.0	186.2	.3	218.2	2.8	285.2	.5	371.2	.3	795.4	3.8
99.1	.9	142.0	1.2	187.2	1.5	219.2	1.1	286.3	.3	372.3	1.4	796.5	2.2
100.1	4.6	143.1	2.3	188.2	5.4	220.1	.3	300.2	.3	373.3	.7	797.4	1.1
101.1	1.7	144.1	.5	189.2	2.6	221.1	.6	312.2	.5	374.3	.6	798.3	.4

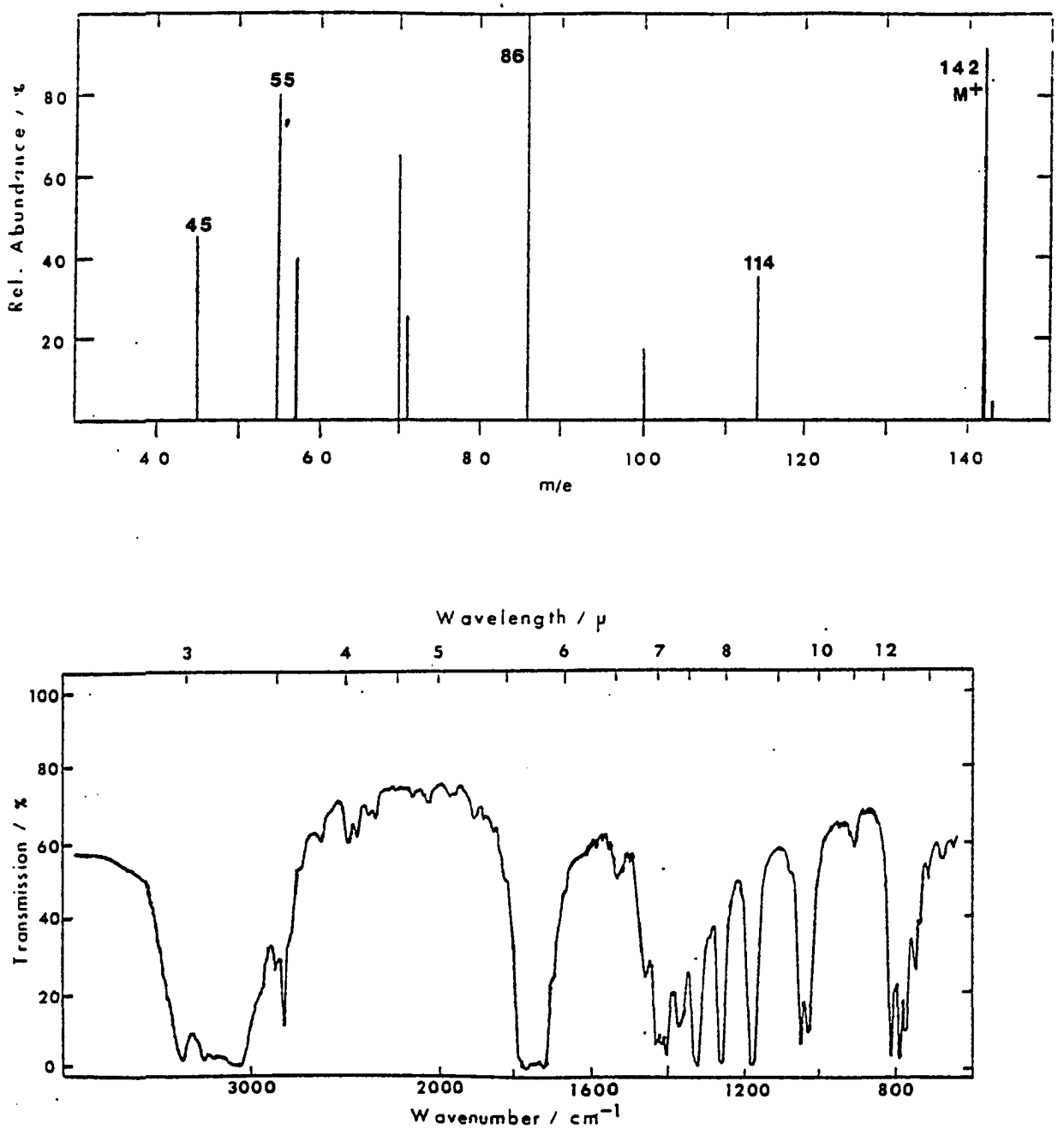

Figure 104. Mass and i. r. spectra of pH 4 oxidation product with retention volume of 492 ml. I. r. is of a KBr disc.

The identification of alloxan as a product implies that urea-riboside should also be a product due to the proposed mechanism (vide infra). Urea-riboside is reported[73,74] to be unstable in neutral and mildly acidic solutions. Therefore it was not detected in any liquid chromatography peaks. Fully silated urea-riboside would have a molecular weight of 624. One of the several "decomposition" GC peaks previously mentioned could be due to urea-riboside.

It should perhaps be stressed, as with the 9-methylxanthine products, that the structures of the xanthosine dimers and allantoin-riboside have not been absolutely confirmed. Independent chemical syntheses or x-ray studies are required.

Reaction Mechanism

Peaks IIIa/IVa. Using voltammetry (Figure 70 and 71) and product analysis, Peak IIIa was shown to be an adsorption prepeak of peak IVa. The same products were obtained from mass electrolysis at potentials corresponding to either oxidation peak.

The mechanism of the electrochemical oxidation of xanthosine (I, Figure 105) at peaks IIIa/IVa (Figure 74) proceeds by an initial $2e^{\ominus}$, $2H^{\oplus}$ oxidation of the $N_7=C_8$ bond to give uric acid-9-riboside (II, Figure 105). Inclusion of $2\ H^{\oplus}$ in the electrochemical process is based on the pH dependency of peak potential shown by peaks IIIa and IVa in Figures 62-65. Uric acid-9-riboside has been shown[72] to be

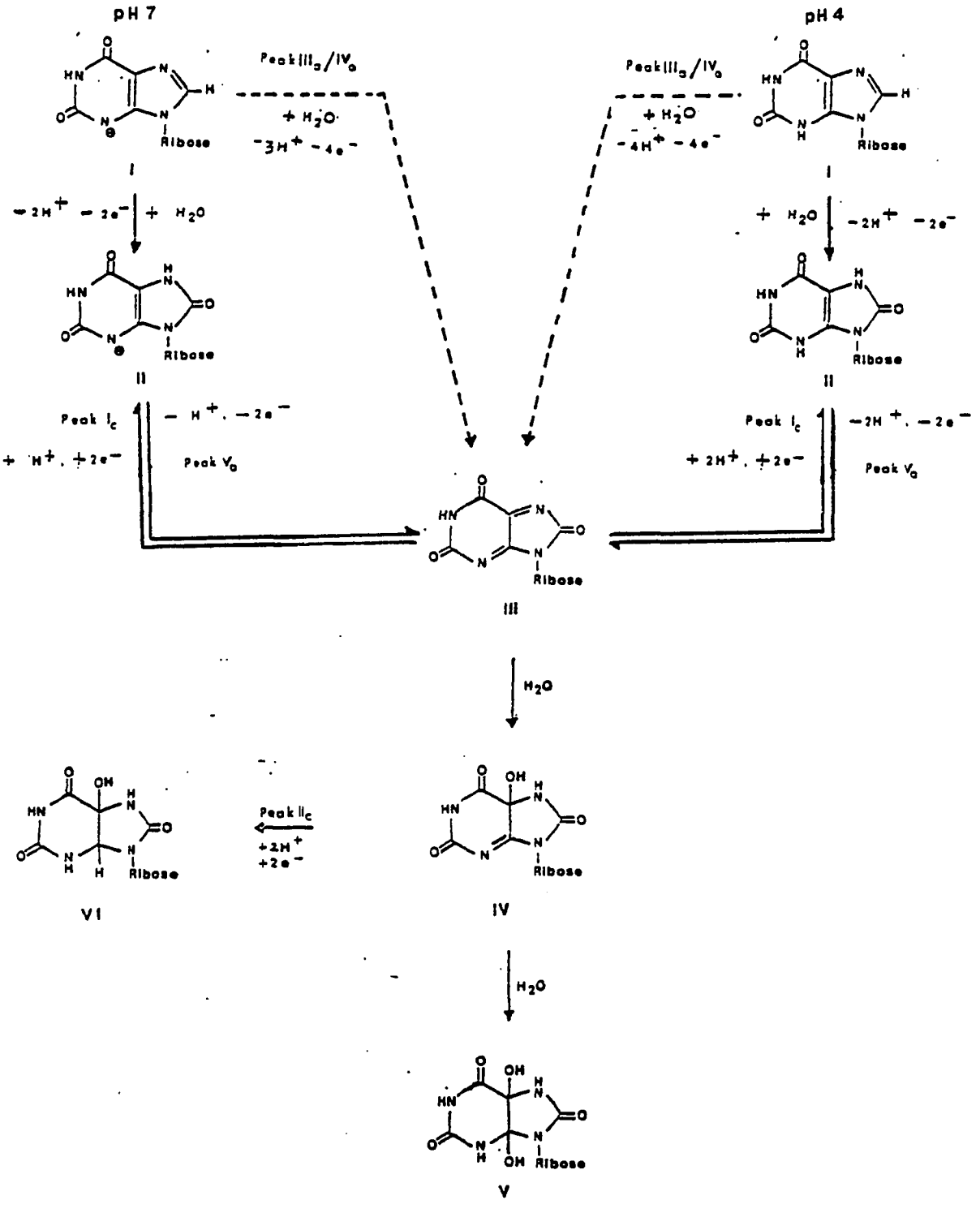

Figure 105. Products and mechanism of the electrochemical oxidation of xanthosine at peaks IIIa/IVa at the PGE.

more readily oxidized than xanthosine. Thus, once formed it is immediately oxidized in a further $2e^{\ominus},2H^{\oplus}$ process (pH 4) or $2e^{\ominus},1H^{\oplus}$ process (pH 7) to uric acid-9-riboside diimine (III, Figure 105). Voltammetric peaks IIIa/IVa (Figure 74) of xanthosine therefore correspond to the $4e^{\ominus},4H^{\oplus}$ (pH 4) or $4e^{\ominus},3H^{\oplus}$ (pH 7) oxidation to the diimine (III, Figure 105). Cathodic peak Ic observed cyclic voltammetrically (Figure 74) is due to reduction of the diimine back to uric acid-9-riboside (III→II, Figure 105). Partial hydration of the diimine gives IV (the imine-alcohol). Thin-layer spectroelectrochemical experiments (vide supra) show the imine-alcohol is responsible for reduction peak IIc. The imine-alcohol is proposed to be electrochemically reduced in a $2e^{\ominus},2H^{\oplus}$ process to VI. Further hydration of the imine-alcohol gives uric acid-9-riboside-4,5-diol (V, Figure 105). Proposed kinetic measurements for this hydration (Figures 91 and 92; Table 15) give a rate constant of ca. 0.0016 s^{-1} at pH 4 and a rate constant of ca. of 0.0051 s^{-1} at pH 8. The diol decomposed by an analogous route as that in Figure 57 for 9-methyluric acid-4,5-diol. However there is the obvious difference of ribose substitution at the N(7) position (Figure 106). At pH 8 according to product analysis, the diol decomposed to allantoin-riboside and at pH 4 to allantoin-riboside and alloxan. The anodic peak (peak Va) observed on the second positive-going sweep of xanthosine is possibly reoxidation of uric acid riboside, formed in the peak Ic process, back to the diimine or probably due to uric acid-9-riboside formed by partial oxidation of

SECONDARY REARRANGEMENT and HYDROLYSIS to ALLANTOIN-RIBOSIDE

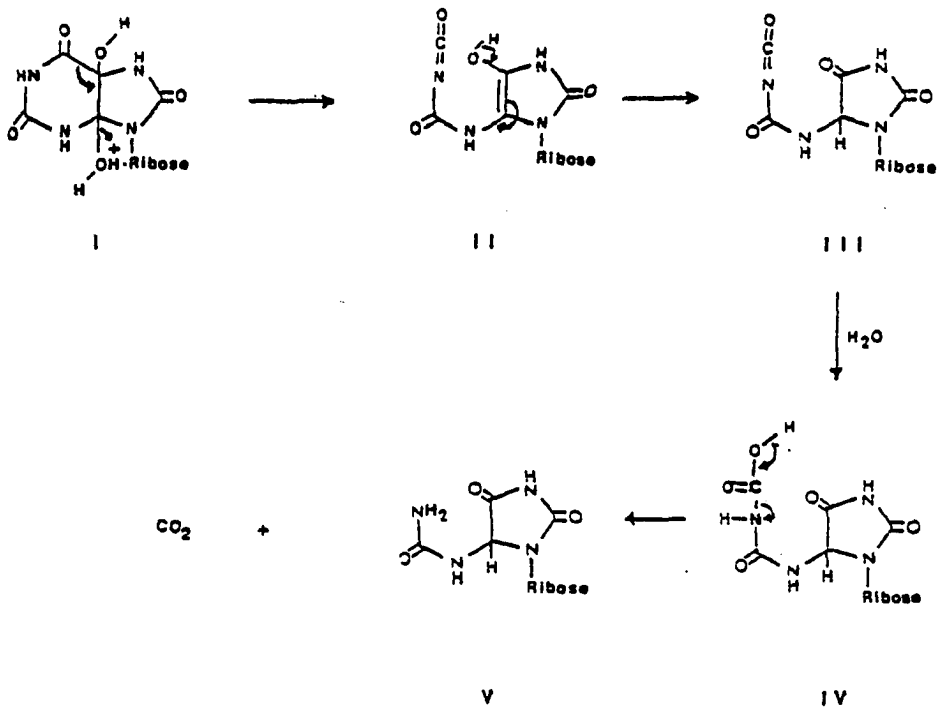

I II III

V IV

SECONDARY REARRANGEMENT to ALLOXAN

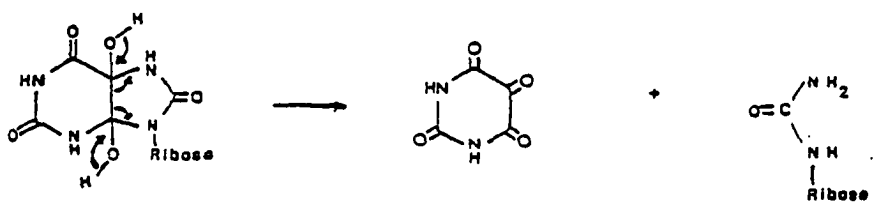

I VI VII

Figure 106. Proposed mechanism for decomposition of uric acid-9-riboside-4,5-diol to allantoin-riboside (V), alloxan (VI), and urea-riboside (VII).

xanthosine under cyclic voltammetry conditions.

Peak Ia. The presence of voltammetric peak Va in the second positive potential sweep during switching potential studies (Figure 75 and 78) of xanthosine in the vicinity of peak Ia indicated that some uric acid-9-riboside and uric acid-9-riboside-4,5-diol are produced. This implies a 4-electron transfer. Peak Ia involves between 1-2 electrons per molecule of xanthosine under voltammetric conditions (vide supra). Potentiostatic n-values show approximately 1 electron is involved in the peak Ia process at both pH 4 and 7. Spectroelectrochemistry of solutions of xanthosine at concentrations greater that 1 mM at pH 7 (Figure 82) showed an absorbance peak at 340 nm. This peak was not observed at pH 4 (Figure 87) or pH 7 at concentrations below 1 mM (Figure 84). To account for the varying electron number, the observed spectroelectrochemisty, and the obtained products (8, 8'-Bi-9-β-D-ribofuranosyl-9H-purine-2,6-(1H,3H)-dione, allantoin-riboside, and alloxan) two oxidative routes must be involved. The proposed mechanism of electrochemical oxidation of xanthosine at oxidation peak Ia is dependent on the pH of the electrolysis solution. At pH 7, the monoanion of xanthosine (I, Figure 107) is initially electrochemically oxidized in a $1e^{\ominus}$ process to give a cation radical (II, Figure 107). This reaction would explain the independence in the Ep vs pH data shown by xanthosine above the pK_a=5.7 (Figures 62-65). The cation radical II subsequently loses a hydrogen at the C-8 position

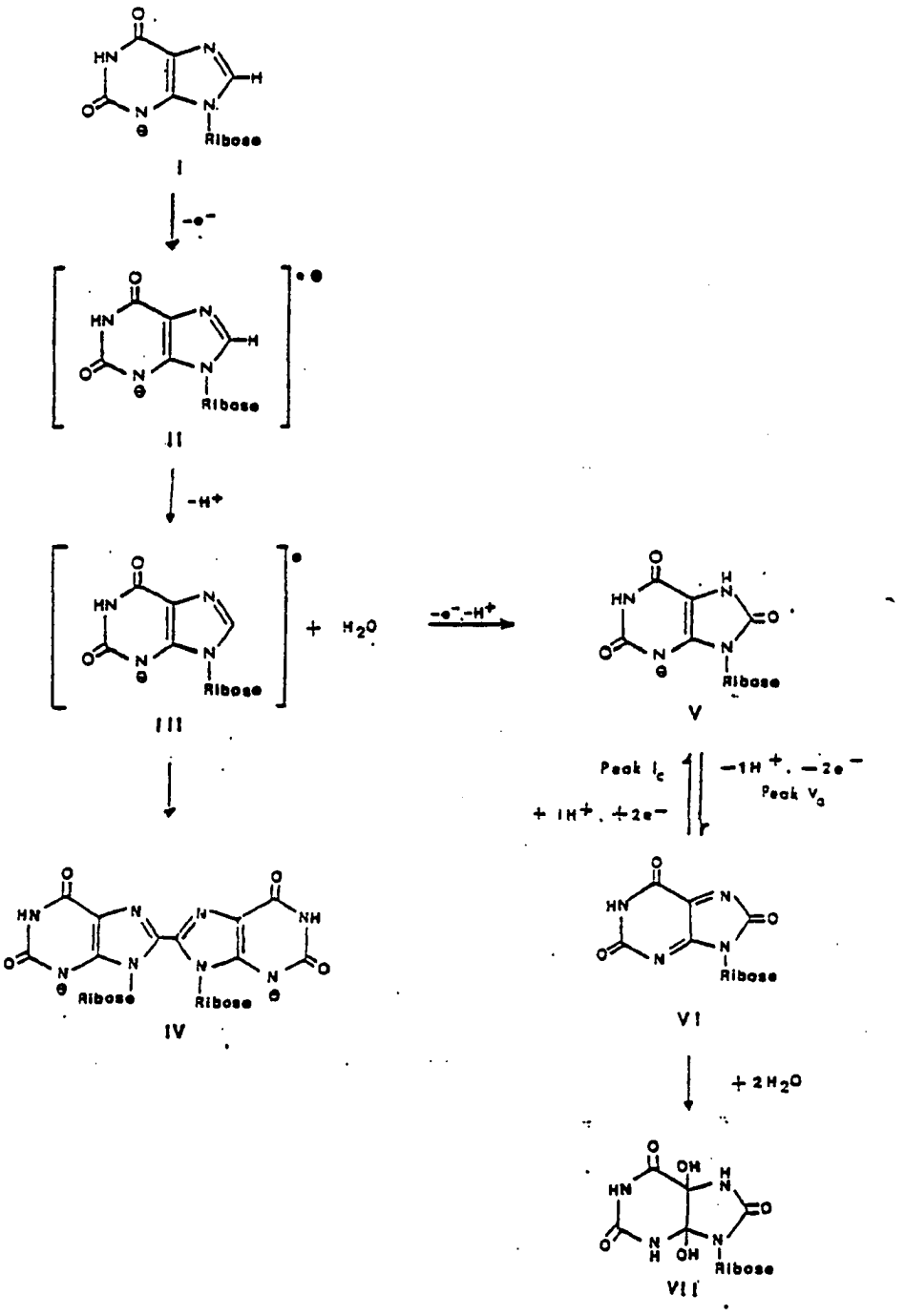

Figure 107. Products and mechanism of the electrochemical oxidation of xanthosine at peak Ia in pH 7 phosphate buffer.

to form a new free radical (III, Figure 107). This can either dimerize to give 8, 8´-Bi-9-β-D-ribofuranosyl-9H-purine-2,6-(1H,3H)-dione (IV, Figure 107) or be further oxidized to uric acid-9-riboside (V, Figure 107) in a further $1e^{\ominus}$, $1H^{\oplus}$ oxidation. Potentiostatic n-values (Table 14) and product analysis (Figure 95) indicated that dimerization is the preferred pathway at ≥1 mM concentrations of xanthosine. Any uric acid-9-riboside (V) formed is immediately oxidized in a $2e^{\ominus}$, $1H^{\oplus}$ process to uric acid-9-riboside-diimine (VI, Figure 107). This diimine hydrates in two stages to give uric acid-9-riboside-4,5-diol (VII, Figure 107). Allantoin-riboside would be to ultimate product formed from the diol in the same manner proposed in Figure 106. The neutral species of xanthosine (I, Figure 108) at pH 4 is electrochemically oxidized in a primary $1e^{\ominus}$, $1H^{\oplus}$ process to give a free radical (II, Figure 108). This mechanism explains the dependency of Ep vs pH displayed by xanthosine below the pK_a = 5.7 (Figures 62-65). The free radical can either dimerize to give 8, 8´-Bi-9-β-D-ribofuranosyl-9H-purine-2,6-(1H,3H)-dione (III, Figure 108) or be further oxidized to uric acid-9-riboside (IV, Figure 108) in a further $1e^{\ominus}$, $1H^{\oplus}$ oxidation. Thin-layer spectroelectrochemistry (no 340 nm absorbance peak, Figure 87) and Product analysis (similar to Figure 102) implies no dimerization occurs. However, voltammetric and potentiostatic (Table 14) n-values indicate some dimerization has occurred. The small potential difference between oxidation peaks Ia and IIa at pH 4

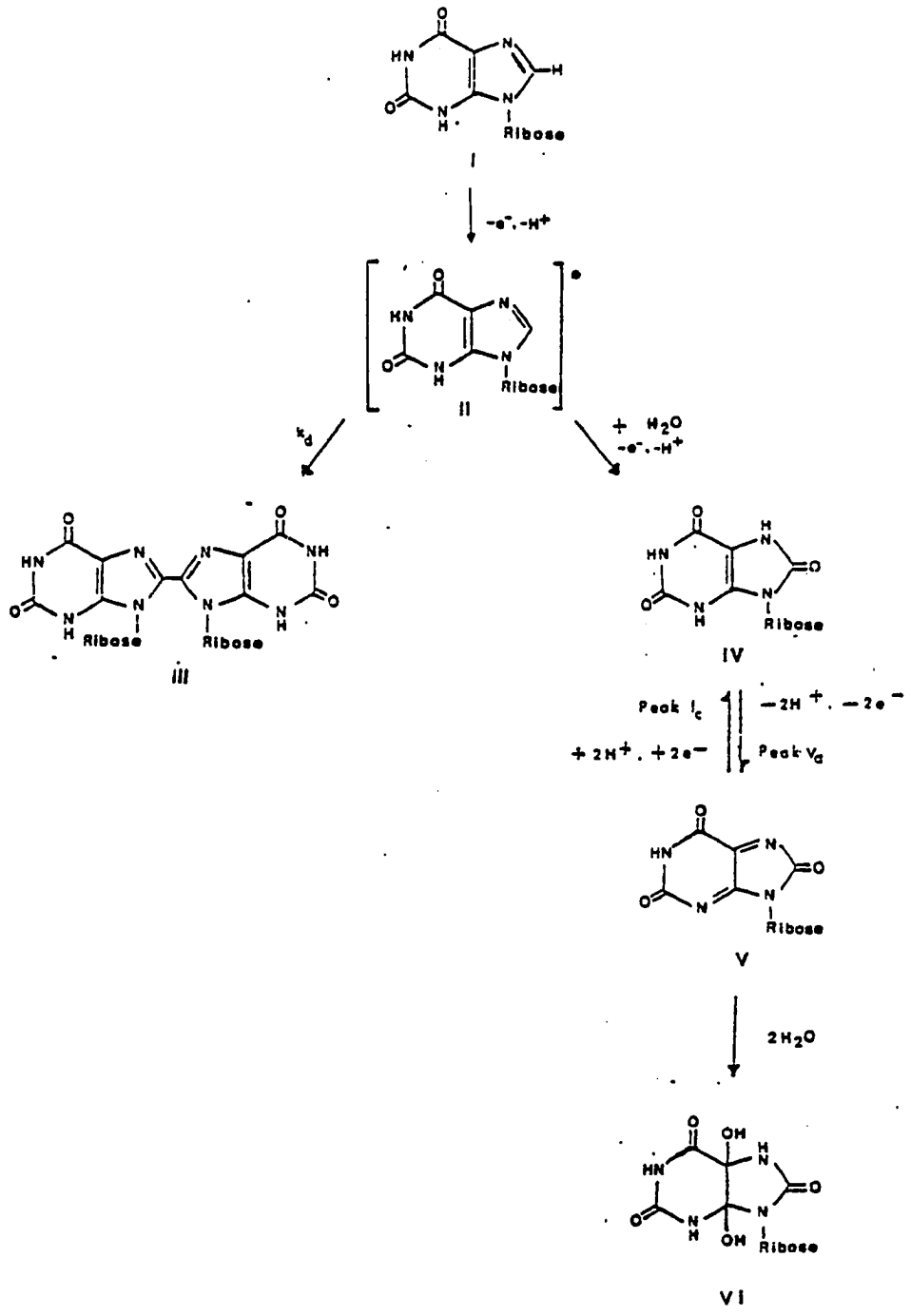

Figure 108. Products and mechanism of the electrochemical oxidation of xanthosine at peak Ia in pH 4 phosphate buffer.

(A, Figure 77) may explain this discrepancy. Any dimer formed is immediately oxidized in the peak IIa process and subsequently decomposes to the observed products (vide infra). The uric acid-9-riboside (IV) formed is very rapidly oxidized in a $2e^{\ominus}$, $2H^{\oplus}$ process to uric acid-9-riboside-diimine (V, Figure 108). This diimine is identical to those in Figures 105, 106, and 107. Therefore, it also hydrates in two steps to give uric acid-9-riboside-4,5-diol (VI, Figure 108). This diol would be expected to readily fragment to the observed products, allantoin-riboside and alloxan.

It is believed dimerization occurs to a larger extent as the concentration increases. This might explain the higher potentiostatic n-values observed at low concentration (Table 14). Also the absence of peak IIa in the voltammetry of 0.5 mM xanthosine (Figures 74 and 77B) implies no dimerization occurs at these low concentrations. However, the increased prominence of oxidation peak IIa in the voltammetry of 1.0 mM and higher concentrations of xanthosine (Figures 71 and 72) indicates dimerization increases with concentration.

Peak IIa. The presence of oxidation peak IIa was shown by voltammetry (Figures 76 and 77) to be concentration dependent. Also, voltammetry performed during coulometry at potentials corresponding to peak Ia (Figure 79) showed the peak height of IIa increased during the initial phase of the electrolysis. These results imply that the peak IIa process is a further oxidation of a high concentration product formed

at peak Ia. Above the pK_a (5.7), the coulometric n-value (Table 13) for the peak Ia/IIa process of xanthosine varied from 2.7 at a concentration of 3.0 mM to 3.1 at a concentration of 0.1 mM. The coulometric n-values at pH 4 varied from 3.2 at 3.0 mM to 3.6 at 0.1 mM. During the course of these coulometric experiments a yellow color developed. This color remained after completion of the electrolysis at higher concentrations (Table 13). At low concentrations the yellow color fades and completely disappears. Potentiostatic n-values also showed a concentration dependency (Table 14). These varied for the peak Ia/IIa process of xanthosine from 1.8 at 3.0 mM to 1.4 at 10.0 mM. To account for the varying electron number and the observed products (8,8´-Bi-9-β-D-ribofuranosyl-9H-purine-2,6-(1H)-dione-3,5-(3H)-diiminylidene (yellow dimer), allantoin-riboside, and alloxan) secondary chemical reactions and oxidations are proposed to be involved. It is proposed the peak Ia process must precede the peak IIa oxidation (vide supra). Under these conditions the peak IIa process involves a further 1 electron (per molecule of xanthosine) oxidation of a high concentration product from peak Ia. Thus a mechanism is proposed where 8,8´-Bi-9-β-D-ribofuranosyl-9H-purine-2,6-(1H,3H)-dione (Ia and Ib, Figure 109) is initially electrochemically oxidized in a $2e^{\ominus}$ process at pH 7 or a $2e^{\ominus}$, $2H^{\oplus}$ process at pH 4 to give 8,8´-Bi-9-β-D-ribofuranosyl-9H-purine-2,6-(1H)-dione-3,5-(3H)-diiminylidene (II, yellow dimer, Figure 109). This reaction scheme would explain the

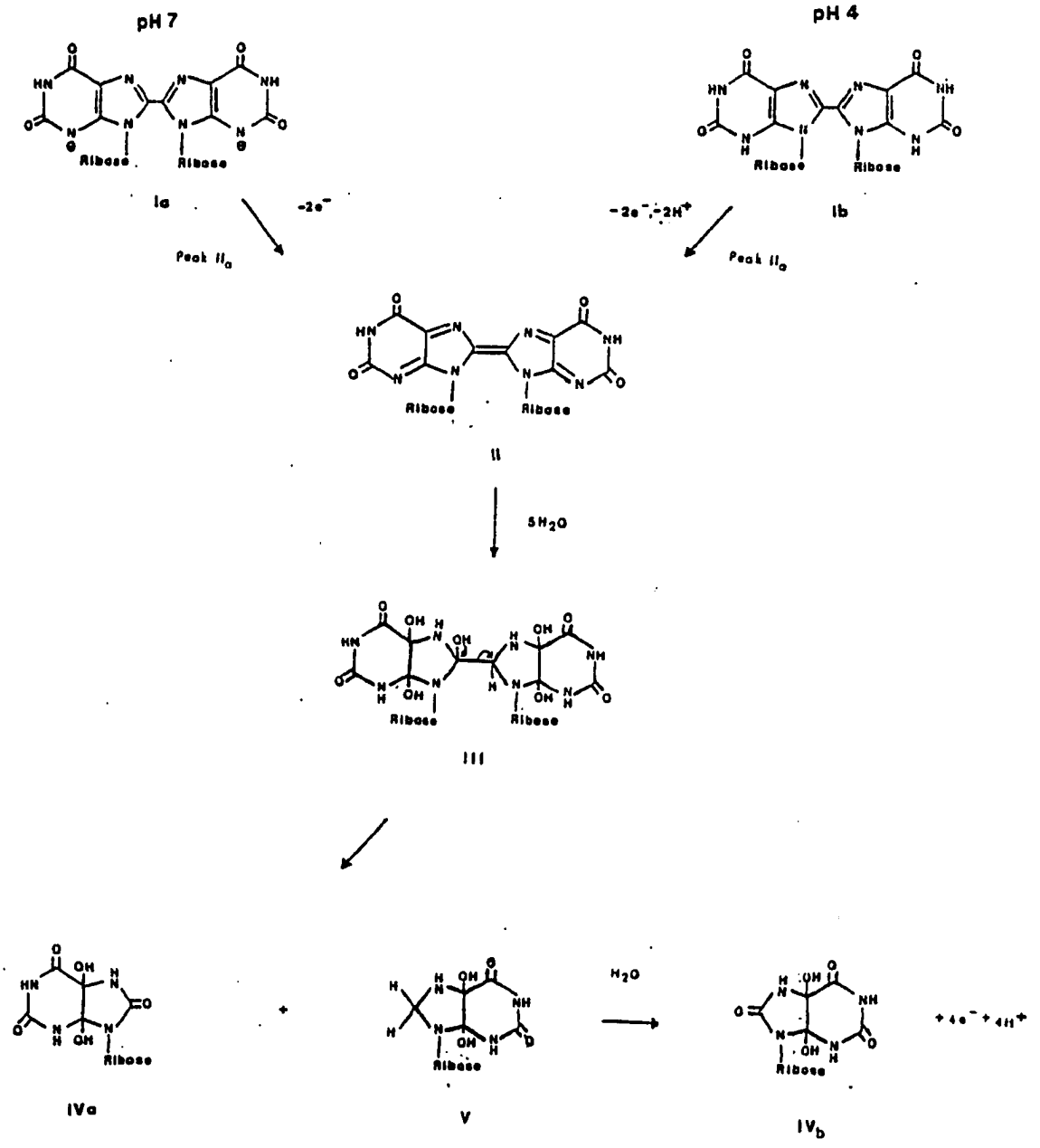

Figure 109. Products and mechanism of electrochemical oxidation at peak IIa of xanthosine.

independence of Ep vs pH above the pK_a (5.7) and the dependency of Ep vs pH below this pK_a shown by xanthosine (Figures 62-65). The yellow dimer (II) with its system of conjugated double bonds would be expected to be readily electrochemically reducible (vide supra). In fact the small reduction peaks observed in cyclic voltammetry of xanthosine (Figures 75 and 78) were shown to be due to the yellow dimer. At pH 7, the yellow dimer was sufficiently stable to permit these voltammetic experiments. However, II decomposes slowly at pH 7 and more quickly at pH 4 perhaps to give structure III (Figure 109). A simple fragmentation of III to uric acid-9-riboside-4,5-diol (IVa, Figure 109) and 8,8-dihydro-uric acid-9-riboside-4,5-diol (V, Figure 109) can be written. Uric acid-9-riboside-4,5-diol (IVb, Figure 109) is also possibly formed as a result of electrochemical or air oxidation of compound V in a $4e^{\ominus}$, $4H^{\oplus}$ process. This diol would be expected to readily fragment in the Figure 106 mechanisms to the observed products, allantoin-riboside and alloxan. The differences in the potentiostatically and coulometrically determined n-values can be explained by the proposed peak IIa mechanism. Potentiostatic experiments are completed in a few seconds. This is insufficient time for compound II (Figure 109) to hydrate to compound V. Therefore, the oxidation of V does not take place. The result is an n-value (Table 14) due to the oxidation of only compound I to the yellow dimer (II, Figure 109). In the case of coulometry,

several hours are required to complete these experiments. This gives sufficient time to produce and oxidize compound V. As a result coulometric n-values (Table 13) imply some or all of compound I (Figure 109) has decomposed to the fragmentation products of uric acid-9-riboside-4,5-diol. The low coulometric n-values for 0.5 mM and 3.0 mM concentrations of xanthosine at pH 7 (Table 13) are due to slower hydration at this pH.

As in the electrochemical oxidation of 9-methylxanthine, it should perhaps be noted that for xanthosine there is insufficient evidence at this time to definitely explain the effect of pH on the yield of products. It is likely that the various decomposition reactions are acid or base catalyzed hence changing the yields and nature of products with pH. The proposed mechanisms are only tentative as several others could be written. However, the basic mechanisms proposed above can be used to account for the electrochemistry and products formed.

Experimental

Chemicals

Xanthosine was obtained from Vega-Fox (Tucson, AZ).

Apparatus.

The apparatus employed has been described in previous chapters.

Procedures.

All procedures were the same as previously described.

Summary

Xanthosine exhibits upto four voltammetric oxidation peaks at the PGE between pH 2-8. Peak Ia is an irreversible $1e^{\ominus}$ oxidation at a pH value above the pK_a (5.7) of the C_8 position to give a radical cation. This radical cation subsequently loses a $H^{\oplus}$ from the C_8 position. Below the pK_a, peak Ia is an irreversible $1e^{\ominus}$, $1H^{\oplus}$ oxidation to give a similar free radical. These radicals can subsequently follow two mechanistic routes. At high concentrations they form 8,8´-Bi-9-β-D-ribofuranosyl-9H-purine-2,6-(1H,3H)-dione. Both radicals at low concentrations are further oxidized in $1e^{\ominus}$, $1H^{\oplus}$ processes to uric acid-9-riboside. Since uric acid-9-riboside[72] is more readily oxidized that xanthosine the former compound is immediately oxidized in a $2e^{\ominus}$, $2H^{\oplus}$ (pH 4) or a $2e^{\ominus}$, $1H^{\oplus}$ (pH 7) process to uric acid-9-riboside-diimine. This diimine hydrates to give uric acid-9-riboside-4,5-diol. The diol readily fragments to the observed products. Oxidation peak IIa is due to further irreversible electrochemical oxidation of 8,8´-Bi-9-β-D-ribofuranosyl-9H-purine-2,6-(1H,3H)-dione in a $2e^{\ominus}$ process above the pK_a (5.7) of a $2e^{\ominus}$, $2H^{\oplus}$ process below the pK_a to form 8,8´-Bi-9-β-D-ribofuranosyl-(H-purine-2,6-(1H)-dione-3,5-(3H)-diiminylidene. This compound is only moderately stable. It hydrates (slowly

at pH 7, more readily at pH 4) and fragments to give uric acid-9-riboside-4,5-diol and 8,8-dihydro-uric acid-9-riboside-4,5-diol. The latter compound is oxidized in a $4e^{\ominus}$, $4H^{\oplus}$ process to uric acid-9-riboside-4,5-diol. This diol fragments to the same products as were formed in the peak Ia mechanism. Oxidation peak IIIa was shown to be an adsorption pre-peak of IVa. Peak IVa is due to irreversible electrochemical oxidation of xanthosine in an overall $4e^{\ominus}$, $3H^{\oplus}$ process above the pK_a(5.7) or a $4e^{\ominus}$, $4H^{\oplus}$ process below the pK_a to give uric acid-9-riboside-diimine. Initially, xanthosine undergoes an irreversible $2e^{\ominus}$, $2H^{\oplus}$ electrooxidation to form uric acid-9-riboside. This latter compound is rapidly oxidized in a $2e^{\ominus}$, $1H^{\oplus}$ process above the pK_a or a $2e^{\ominus}$, $2H^{\oplus}$ process below the pK_a to give uric acid-9-riboside-diimine. This diimine hydrates to form uric acid-9-riboside-4,5-diol. Again, this diol fragments to the products observed in the peaks Ia and IIa processes. The electrochemical products of all four peak processes were examined by u. v., i. r., mass spectrometry, and voltammetry at the PGE. Chemical and electrochemical mechanisms were studied using thin-layer spectroelectrochemistry.

CHAPTER IV

SUMMARY

These investigations were concerned with the effect of substitution at the N-9 position on the electrochemistry of xanthine. The compounds studied were 9-methylxanthine and xanthosine. Xanthosine represents the first investigation from our laboratory concerning the electrooxidation mechanisms and products of a purine nucleoside.

The study of the electrochemical oxidation of 9-methylxanthine was undertaken because this molecule serves as a model for xanthosine. Electrooxidation of 9-methylxanthine at its third and fourth oxidation peaks proceeds in a similar manner to that of xanthine with the obvious methylation difference in the observed products. At the first oxidation peak of 9-methylxanthine a radical is formed. Depending on concentration this radical can either dimerize or be further oxidized to form products similar to those observed from oxidation at the third and fourth oxidation peaks of 9-methylxanthine. The second oxidation peak has been shown to be further oxidation of the dimer formed in the first oxidation peak process to a second moderately stable dimer.

The electrochemical oxidation of xanthosine was shown

to be nearly identical to that of 9-methylxanthine.

These electrooxidations were studied using linear sweep and cyclic voltammetry, controlled potential coulometry, potentiostatic studies, and thin-layer spectroelectrochemistry.

CHAPTER V

REFERENCES

1. E. Fischer, Ber. Dtsch. Chem. Ges., 17, 329(1884).
2. E. Fischer, Ber. Dtsch. Chem. Ges., 30, 558(1897).
3. R. K. Robins, Heterocycl. Compd., 8, 162(1967).
4. A. Albert and D. J. Brown, J. Chem. Soc., 157, 2060(1954).
5. "Properties of Nucleic Acid Derivatives," 5th rev., ed., Calbiochem, Los Angeles, California, 1964.
6. F. Bergmann and S. Dikstein, J. Am. Chem. Soc., 77, 691 (1955).
7. C. H. Willits, J. C. Decius, K. L. Dilte, and B. E. Christiensen, J. Am. Chem. Soc., 77, 2569(1955).
8. M. E. Bolis, Adv. Clin. Chem., 10, 157(1967).
9. W. T. Caraway, Stand. Methods Clin. Chem., 4, 239(1963).
10. Marcet, "An Essay on the Chemical History and Medical Treatment of Calculous Disorder," London, 1817, pp. 95-107 (cited in Robins[3]).
11. Runge, "Neuste phytochemische Entdeckungen," Vol I., p. 144. Berlin, 1820 (cited in Robins[3]).
12. A. Woskresensky, Ann. Chem. Pharm., 41, 125(1942).
13. A. Kossel, Ber. Dtsch. Chem. Ges., 21, 2164(1888).
14. F. G. Mann and J. W. Porter, J. Chem. Soc., p. 751(1945).
15. V. Papesch and E. F. Schroeder, Med. Chem., (N. Y.), 3, 175(1956).

16. L. S. Goodman and A. Gilman, eds., The Pharmacological Basis of Therapeutics, 3rd ed., p. 355, Macmillan, New York, 1967.

17. G. Dryhurst, Electrochemisty of Biological Molecules, Academic Press, New York, 1977, p. 2.

18. J. L. Owens, H. A. Marsh, and G. Dryhurst, J. Electroanal. Chem., 91, 231(1978).

19. M. Z. Wrona, J. L. Owens, and G. Dryhurst, J. Electroanal. Chem., 105, 295(1979).

20. E. Praetorius, Biochim. Biophys. Acta, 2, 602(1948).

21. E. S. Canellakis and P. P. Cohen, J. Biol. Chem., 213, 385(1955).

22. H. R. Mahler in, The Enzymes, 2nd ed., P. D. Boyes, H. Lardy, and K. Myrback (Eds), Vol. 8, Academic Press, New York, pp. 285, 1963.

23. K. G. Paul and Y. Avi-Dor, Acta Chem. Scand., 8, 637(1954).

24. E. S. Canellakis, A. L. Tuttle, and P. P. Cohen, J. Biol. Chem., 213, 397(1955).

25. H. R. Howell and J. B. Wyngaarden, J. Biol. Chem., 235, 3544(1960).

26. M. Griffith, J. Biol. Chem., 197, 399(1952).

27. M. Z. Wrona and G. Dryhurst, Biochim. Biophys. Acta, 570, 371(1979).

28. G. Dryhurst, J. Electrochem. Soc., 119, 1659(1972).

29. B. H. Hansen and G. Dryhurst, J. Electroanal Chem., 30, 407(1971).

30. B. H. Hansen and G. Dryhurst, J. Electroanal Chem., 30, 417(1971).

31. B. H. Hansen and G. Dryhurst, J. Electroanal Chem., 32, 405(1971).

32. F. Bergmann and S. Dikstein, J. Biol. Chem., 223, 765(1956).

33. F. Bergmann, H. Kwientiny, G. Levin, and D. J. Brown, J. Am. Chem. Soc., 82, 598(1960).

34. J. L. Owens, Ph. D. Dissertation, University of Oklahoma.

35. D. Lichtenberg, F. Bergmann, and Z. Neiman, J. Chem. Soc., C, 1676(1971).

36. Jordan, The Nucleic Acids, Vol. 1, E. Chargaff and J. N. Davidson, eds., Academic Press, New York, 1955, p. 447.

37. G. Dryhurst, J. Electrochem. Soc., 116, 1097(1969).

38. R. H. Wopschall and I. Shain, Anal. Chem., 39, 1514(1967).

39. R. A. Osteryoung, G. Laues, and F. C. Anson, J. Electrochem. Soc., 110, 926(1963).

40. C. A. Streuli and W. D. Cooke, Anal. Chem., 26, 963(1954).

41. W. Kemula, Z. Kublik, and A. Axt, Roczniki Chem, 35, 1009 (1961).

42. R. S. Nicholson and I. Shain, Anal Chem, 36, 706(1964).

43. H. Matsuda and Y. Ayabe, Z. Electrochem., 59, 494(1955).

44. P. J. Elving, W. A. Struck, and D. L. Smith, Mises Point Chim. Anal. Org. Pharm. Bromatol., 14, 141(1965).

45. R. W. Murray, W. R. Heimeman, and G. W. O'Dom, Anal. Chem., 39, 1666(1967).

46. R. N. Adams, Electrochemistry at Solid Electrodes, Marcel Dekker, Inc., New York, 1969, p. 23.

47. L. Meites, Polarographic Techniques, 2nd ed., Wiley, New York, 1965, p. 527.

48. J. L. Owens, H. H. Thomas, and G. Dryhurst, Anal. Chim. Acta, 96, 89(1978).

49. F. W. Rollgen and H. R. Schulten, Org. Mass Spectrom., 10, 660(1975).

50. E. Blout and M. Fields, J. Amer. Chem. Soc., 72, 479(1950).

51. H. Goldner, G. Dietz, and E. Carstens, Ann., 692, 134(1966).

52. H. Goldner, G. Dietz, and E. Carstens, Ann., 693, 233(1966).

53. L. Czuchajowski and M. Eckstein, Rocz. Chem, 41, 907(1967).

54. G. Soberon and P. P. Cohen, Arch. Biochem. Biophys., 103, 331(1963).

55. L. F. Cavalieri, J. J. Fox, A. Stone, and N. Change, J. Amer. Chem. Soc., 76, 1119(1954).

56. K. Bowden, E. Braude, E. Jones, and B. Weedon, J. Chem. Soc., 45(1946).

57. R. Silverstein and G. C. Bassler, Spectrometric Identification of Organic Molecules, John Wiley and Sons, Inc., New York, 2nd ed., 1968, p. 160.

58. P. O. P. T s'o, ed., Basic Principles in Nucleic Acid Chemistry, Academic Press, New York, 1974, p. 245-249.

59. G. Dryhurst, unpublished work

60. L. F. Fieser and M. Fieser, Reagents for Organic Synthesis, John Wiley and Sons, Inc., New York, 1967, pp. 159-160.

61. J. J. Lingane and O. L. Davis, J. Biol. Chem., 137, 567 (1941).

62. J. Pinson and J. Armand, Coll. Czech. Chem. Communs., 36, 585(1971).

63. S. Kwee and H. Lund, Acta Chem. Scand., 25, 1813(1971).

64. H. Blitz and E. Topp, Chem. Ber., 46, 1387(1913).

65. R. W. Murray, W. R. Heineman, and G. W. O'Dom, Anal. Chem., 39, 1666(1967).

66. W. R. Heineman, B. J. Norris, and I. F. Goelz, Anal. Chem., 47, 79(1975).

67. R. C. Weast, ed., Handbook of Chemistry and Physics, 52nd ed., Chemical Rubber Co., Cleveland, 1971-72, p. C-205.

68. V. E. Norvell and Gleb Mamantov, Anal. Chem., 49, 1470 (1977).

69. J. W. Strojek, G. A. Gruver, and T. Kuwana, Anal. Chem., 41, 481(1969).

70. M. S. Denton, T. P. DeAngelis, A. M. Yacynych, W. R. Heineman, and T. W. Gilbert, Anal. Chem., 48, 20(1976).

71. H. A. Sober, ed., Handbook of Biochemistry, 2nd ed., Chemical Rubber Co., Cleveland, 1970, p. G-52.

72. B. Janik and P. J. Elving, J. Amer. Chem. Soc., 92, 235 (1970).

73. M. H. Benn and A. S. Jones, Chem. and Ind., 31, 997(1959).

74. M. H. Benn and A. S. Jones, J. Chem. Soc., 163, 3837(1960).